CHEMICOSTRUCTURAL DIVERSITY OF THE BRACHIOPOD SHELL

ALWYN WILLIAMS and MAGGIE CUSACK

[deceased, formerly of University of Glasgow; and University of Glasgow]

INTRODUCTION

Descriptions of the chemicostructure of the brachiopod shell published in Volume 1 of the revised *Treatise on Invertebrate Paleontology, Part H, Brachiopoda* (KAESLER, 1997), were submitted in 1995. They appeared in three chapters with little cross reference for a reason that was valid at the time. The structures of the periostracum and shell of living brachiopods were described in relation to the secreting outer epithelium of the mantle in the chapter on Anatomy (WILLIAMS & others, 1997, p. 9–41). The structures of periostracal casts and recrystallized shells of fossil brachiopods were described in another chapter on Shell Structure (WILLIAMS, 1997, p. 267–320). This segregation was imposed to distinguish paleontological inferences from neontological observations (WILLIAMS, 1997, p. 267). Six of the twelve or so distinctive structures characterizing the brachiopod shell are found in living species, especially the later rhynchonelliforms and craniiforms, and could be broadly identified in Paleozoic antecedents. Yet the shell structures of most extinct groups were evidently the product of secretory regimes that were then difficult to reconcile with living models. Shell biochemistry, which was described in a third chapter (CUSACK, WALTON, & CURRY, 1997, p. 243–264), was even more difficult to integrate into a chemicostructural phylogeny. In 1995, this kind of investigation had been sporadically pursued for only 30 years, and there had been little systematic sampling of the shell biochemistry of extant groups. More importantly, sophisticated techniques showed that the organic constituents of shells degraded rapidly during fossilization into residues that are no longer diagnostic of the original polymers.

Within the last decade, significant advances have been made in chemicostructural research on fossil as well as living shells. The full structural diversity of the mature shell is now better known, and feasible secretory regimes have been proposed to explain extinct fabrics. Ultrastructural and biochemical studies of the paracrystalline relationships between basic biomineral and polymeric units have revealed many processes of calcification, while mineral alignments in fossil shells have been used to identify their degraded, organic substrates and matrices. An unexpected discovery is that the mineral constituents of first-formed and juvenile shells can be different from those secreted during the mature phase of growth. Such profound changes in the ontogeny of secretory regimes were common in early lingulate brachiopods. The trace element and stable isotope contents of the brachiopod shell have also been studied and merit consideration, as do novel structures found in the exoskeletons of such early lingulates and Problematica as *Micrina*.

As a result of these advances, the processes of secretion responsible for the chemicostructural diversity of the living shell can be identified as homologous with regimes that secreted the various skeletal structures of extinct groups. Accordingly, changes in shell structures will be reviewed on assumptions that they reflect the evolution of a small number of secretory regimes that first differentiated in the early Paleozoic. Description of the phylogeny of skeletal chemicostructures, however, has to take into account regimes that were subject to ontogenetic changes. A hiatus in the secretion of juvenile and mature shells of lingulates can be traced throughout the geological record. It seems appropriate, therefore, to compare
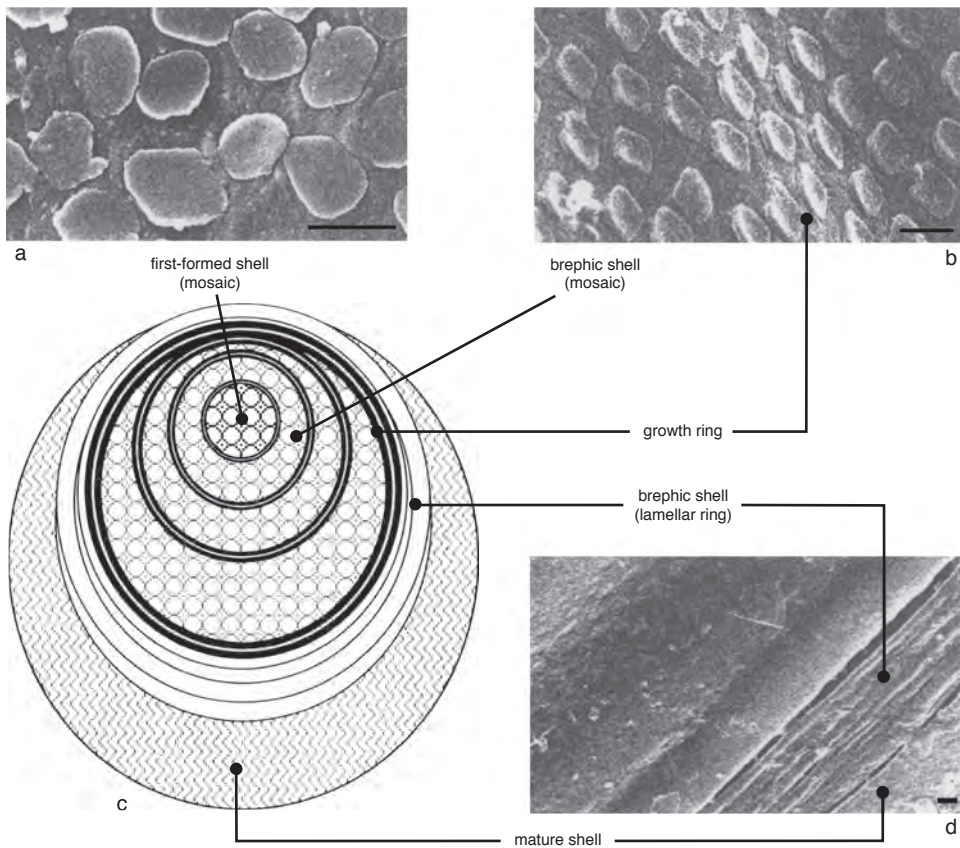
FIG. 1548. Illustration of terminology used to describe mosaic of siliceous tablets and its bounding lamellar ring in living *Discinisca* sp. cf. *tenuis* (SOWERBY). SEMs show disposition of tablets in first-formed and brephic shells and of lamellar ring relative to mosaic and mature shell; scale bars: 1 μm (Williams, 2003).

the chemicostructures of first-formed (and brephic) shells independent of the phylogeny of mature shells.

Finally, a terminology of the skeletal chemicostructures of brachiopods is now well established. A few new terms have been sparingly introduced during the last decade and are defined within the text. Two standardized terms, however, are required to describe the detailed as well as the general aspect of chemicostructures. In this chapter, the term fabric will be used to describe any particular chemicostructural feature as a whole; the term texture is used to describe the arrangement of the constituent parts of a fabric.

JUVENILE SHELL OF BRACHIOPODS

There is much confusion about what constitutes a first-formed, brephic, and juvenile shell (WILLIAMS, 2003). Their usage in this chapter is intended to describe phases in shell growth that are apposite for living and extinct species alike, as illustrated in Figure 1548. The so-called first-formed coat is simultaneously secreted by a collective of epithelial cells when they become differentiated from the ectoderm for such a role. The term is preferred to the embryonic shell of FREEMAN and LUNDELIUS (1999) because embryonic is also used for the vitelline
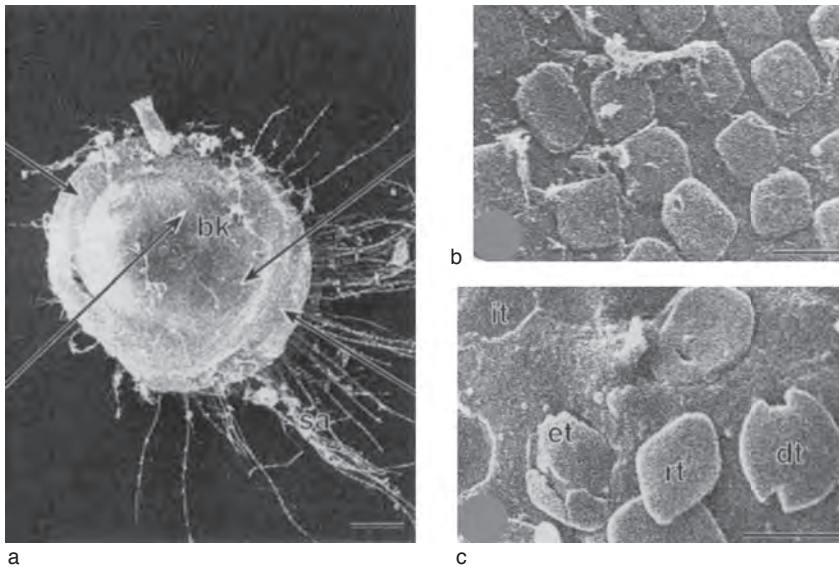
FIG. 1549. SEMs of gold-coated, dorsal surface of untreated, critical-point-dried, newly settled juvenile of *Discinisca* sp. cf. *tenuis; a*, general view showing sites of detailed studies relative to beak (*bk*) and setae (*sa*); scale bar: 100 µm; *b*, orderly, rhombically arranged tablets in midregion of mosaic; scale bar: 1 µm; *c*, mosaic at beak with deformed (*dt*) and rhombic (*rt*) tablets, latter dislodged, another escaping (*et*) from a ruptured, brittle vesicular cover and imprints (*it*); scale bar: 1 µm (Williams, Lüter, & Cusack, 2001).

(fertilization) membrane (WILLIAMS & others, 1997, p. 154). The coat may be an organic sheet as found in living lingulids (the protegulum of YATSU, 1902). It may be an organic sheet (periostracum), internally coated with mineral granules as in living rhynchonellates or craniids, or an organic sheet externally covered with a well-ordered array (mosaic) of mineralized tablets (WILLIAMS, CUSACK, & others, 1998). When mineralized, the coat or mosaic is referred to as the first-formed shell.

The brephic shell is the circular (or arcuate) zone enclosing the first-formed shell. It is secreted incrementally by a growing mantle lobe and may be bounded by a lamellar ring (the halo of CHUANG, 1977) composed of ripplelike folds or concentric lamellae. The mature shell surrounds the brephic shell and is characterized by the development of adult surface features including those that normally distinguish genera and species. In this context, the term juvenile can be used to identify the first-formed and brephic shells together.

The juvenile shells of the crown species of the three brachiopod subphyla differ not only from one another but also, with the possible exception of rhynchonelliforms, from those of their stem groups. The latter are more similar to the juvenile shells of contemporaneous, extinct groups, as will be shown in the text.

DISCINOID JUVENILE SHELLS

The juvenile shell of discinids is mineralized (WILLIAMS, CUSACK, & others, 1998). Thus, nearly all of the juvenile dorsal valve of *Discinisca* sp. cf. *tenuis*, approximately 0.5 mm in diameter, is covered by a single-layered mosaic of siliceous tablets typically arranged rhombically (Fig. 1549–1550). Tablets on the subconical, wrinkled first-formed shell are less well ordered and can vary in shape from rhombic to discoidal, with a mean length of 1 µm; but many are deformed, especially through the lack of secretion of their centers (Fig. 1551). Tablets of the brephic mosaic (Fig. 1552) are larger with a long diagonal averaging

1.54 µm and are overwhelmingly rhombic with rare deformities resulting mainly from conchoidal fracturing. They are well ordered but become more widely spaced and more closely crowded on the sides and in the troughs, respectively, of folds (growth rings). They may also be absent from patches of 50 µm² or more toward the margin.

The thickness of tablets is bimodally distributed at 30–90 nm and 120–210 nm. This distribution accords with tablets being unilamellar and bilamellar, predominantly so on the first-formed shell and toward the mosaic margin respectively. The lamellae are granular and, in bilamellar tablets, are separated by a slotlike cavity up to 70 nm deep. The edges of both lamellae commonly form an unbroken margin that confines the cavity within a tablet (Fig. 1552). Lamellae of degraded tablets have an exaggerated texture of granules that, under the TEM, are resolved as discrete rhombs, approximately 25 nm long diagonally and arranged in rhombic arrays (Fig. 1553a). Further degradation induced by reagents removes the polymeric glue binding the siliceous granules that then tend to aggregate along the frayed edges of tablets. In some parts of the mosaic, however, especially in the first-formed shell, an untreated substrate can also be coated with aggregates. These are likely to be siliceous spherules that had been secreted and dispersed before the formation of tablets.

Tablets are assembled intracellularly in the outer epithelial collective underlying the first-formed shell and in nascent vesicular cells being generated as the outer mantle lobe that secretes the growing margin of the brephic shell (WILLIAMS, LÜTER, & CUSACK, 2001, p. 33; LÜTER, 2004). Each tablet grows within a vesicle (Fig. 1553b), initially by nucleation of siliceous rhombs and their organic coats on the inner surface of the vesicle. Traces of fibrils in the interstices between rhombs, as seen in TEM sections, suggest that the tablet matrix is a water-soluble polymer permeated by fibrous proteins. Further lateral accretion of rhombs complete a vesicular lining of granules that
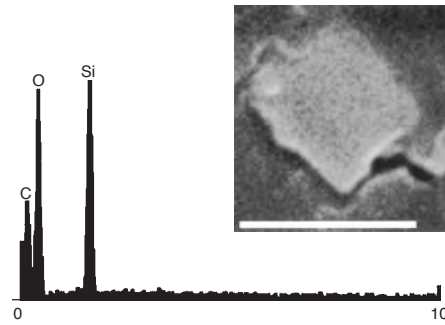

FIG. 1550. EDX spectrum (full scale 300 counts) of a carbon-coated tablet in acetate shown as a top-right inset; scale bar: 1 µm (Williams & others, 1998).

adopt the rhombohedral shape of silica, irrespective of organic constituents. When crystallization is complete, a cavity is normally created in the medial plane, as in an ellipsoidal geode, virtually dividing the tablet into a bilamellar structure. Unilamellar tablets are assumed to have crystallized in a flat vesicle that precludes the development of a medial cavity.
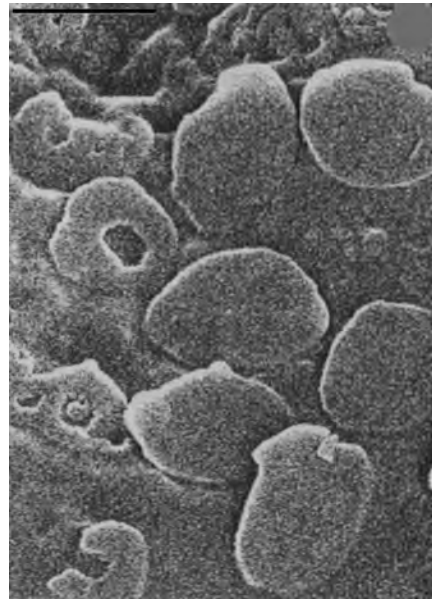

FIG. 1551. SEM of gold-coated, deformed and poorly ordered, overlapping tablets at beak of dorsal valve of settled juvenile *Discinisca* sp. cf. *tenuis* treated with bleach (0.7% by volume) for 18 h; scale bar: 1 µm (Williams, Lüter, & Cusack, 2001).
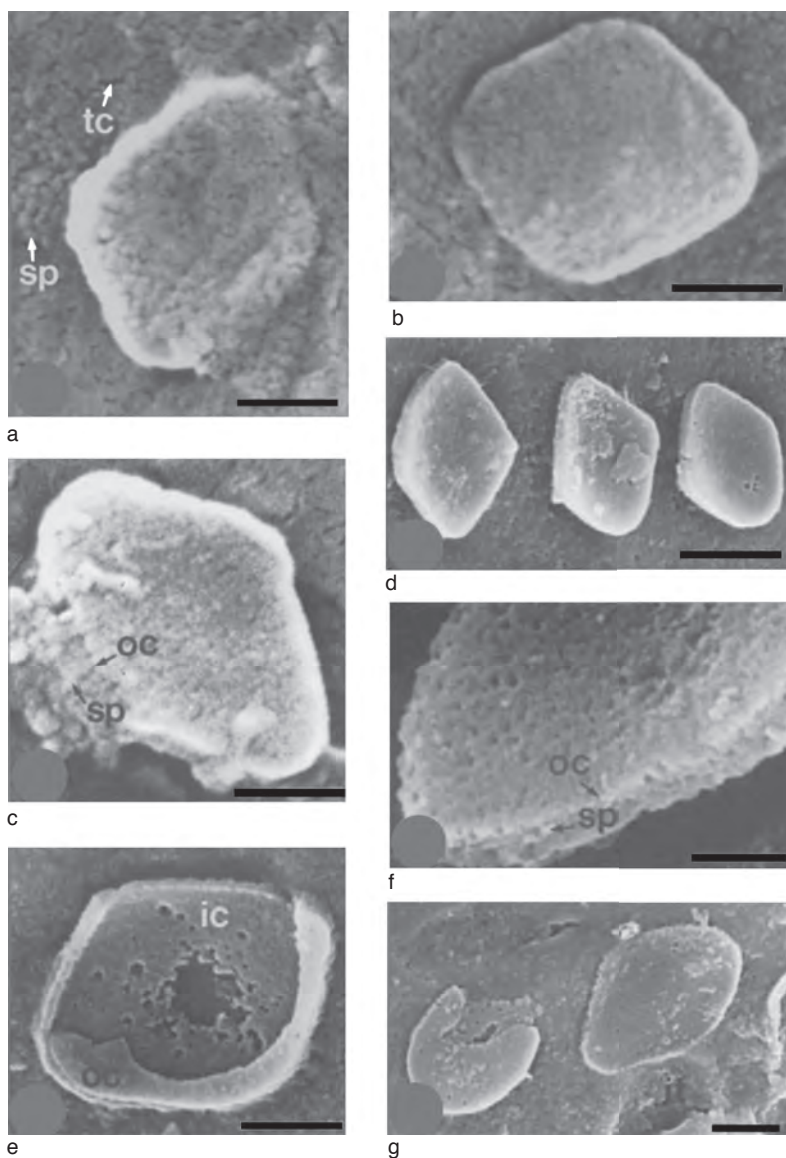
Fig. 1552. SEMs of larval shells of *Discinisca tenuis; a–b,* concave and convex tablets on dried dorsal valves, elevated above tension-cracked (*tc*), spherular (*sp*) primary layer, but also with tension-cracked, spherular coats (view *c*) with concave tablet on dried dorsal valve with coat split near outer edge (*oc*) to expose contents of spherular apatite (*sp*); scale bars: 0.5 μm; *d,* concave tablets on surface of dried dorsal valve displaying well-spaced nature; scale bar: 1 μm; *e–g,* tablets treated with 0.2% bleach, exposing spherular apatite (*sp*) between the outer (*oc*) and inner (*ic*) coats of partly digested tablets; scale bars: 0.5 μm, 200 nm, 0.5 μm (Williams, Cusack, & Buckman, 1998).

The exocytosis of tablets (enclosed in their vesicular coats) to form a monolayer under the external glycocalyx is followed by the secretion of a substrate of chitin and GAGs (glycosaminoglycans). The rheological condi-tion of the substrate is confirmed by the way tablets tend to sink into it. Some tablets may be deeply embedded, while others may be so tilted as to leave lunate imprints on the substrate (Fig. 1549). Tablets are rarely
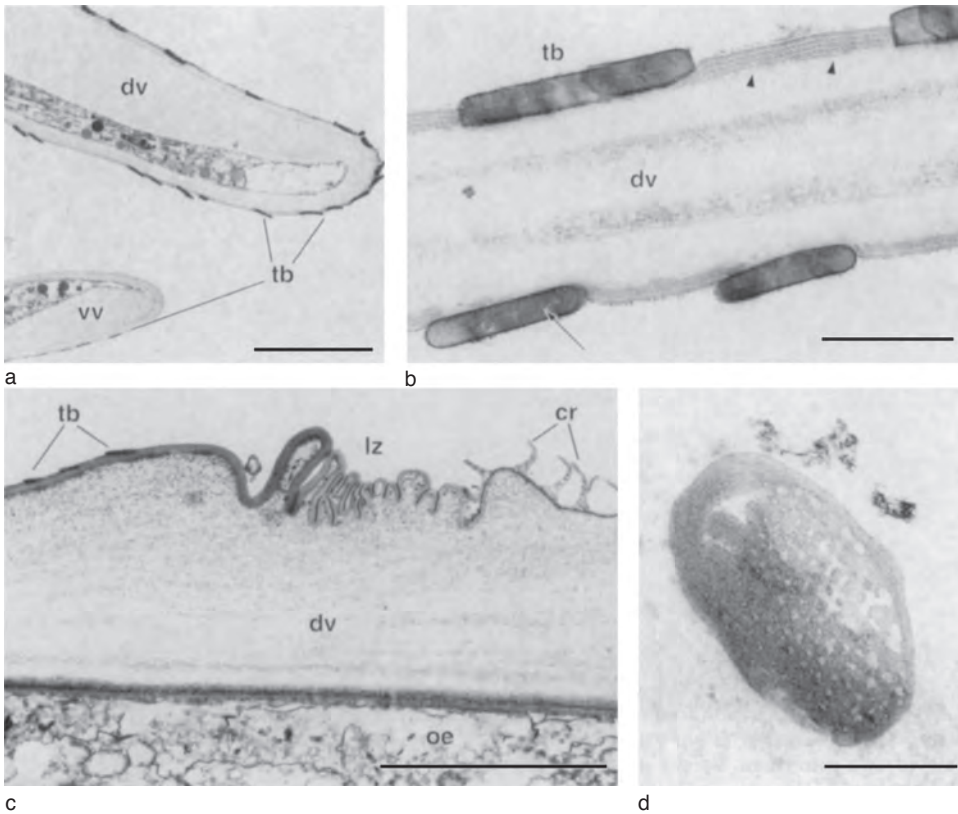
FIG. 1553. TEMs of pelagic and recently settled juveniles of *Discinisca* sp. cf. *tenuis; a–b, d*, free-swimming juvenile; *c*, recently settled juvenile. All specimens fixed and stained; *a,* margin of dorsal (*dv*) and ventral (*vv*) valve with tablets (*tb*) partly embedded in an outer layer correlating with periostracum; scale bar 5 μm; *b*, details of tablets (*tb*) with inner cavity (*arrow*) on dorsal valve (*dv*); note 5 electron-dense sheets of outer periostracal layer (*arrowheads*); scale bar 0.5 μm; *c*, lamellar ring (*lz*) separates mosaic with tablets (*tb*) and mature shell with superstructure of concentric ridges (*cr*); dorsal valve (*dv*) underlain by outer mantle epithelium (*oe*); scale bar: 5 μm; *d*, oblique section through tablet, showing rhombic arrangement of silica granules; scale bar: 0.25 μm (Williams, Lüter, & Cusack, 2001).

preserved on the juvenile surfaces of adult shells because they are dissolved or drift free of their substrate as the glycocalyx cover degrades. Their imprints on polymerized substrates betray their former presence, but even substrates can be abraded or stripped off the living shell by exfoliation, which accounts for the sporadic preservation of mosaic imprints in fossils.

The mosaic is bounded by a tablet-free ring of lamellae, separating it from the mature shell (Fig. 1554–1555). The junction between the lamellar ring and mosaic is sharp, with secretion of tablets ceasing within a zone approximately 5 μm wide,

although cessation is not always simultaneous in the ventral and dorsal valves. The ring is composed of periostracum disposed as up to eight inwardly dipping lamellae that range from asymmetrical or isoclinal folds (Fig. 1554) to discrete sheets (Fig. 1555). The junction between the lamellar ring and the mature shell is also sharp, commonly with signs of rupture probably resulting from postmortem dehydration. The chitinous periostracum of the mature shell is also folded but is ornamented by its distinctive superstructure of concentric ridges composed of pellicular sheets of chitin (Fig. 1555).
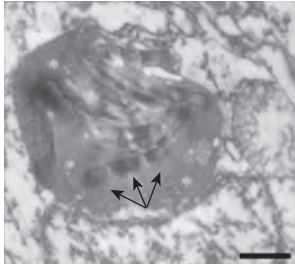
FIG. 1554. Cross section through a tablet-producing cell at hinge of periostracal slot of *Discinisca* sp. cf. *tenuis,* revealing a vesicle containing several siliceous tablets (*arrows*); scale bar: 0.5 μm (Lüter, 2004).

The folds and sheets of the lamellar ring are identical with disturbances affecting the periostracum and primary layer of brachiopods generally. They are caused by rapid retractions and advances of the outer mantle lobe (WILLIAMS, BRUNTON, & MACKINNON, 1997, p. 330). Their development in *Discinisca* coincides with the attachment of the juvenile to its benthic substrate. Yet it does not necessarily follow that these lamellae bordering the mosaic are so-called skeletonized shock waves registering the trauma of settlement, because traces of the lamellar ring have been found in one pelagic specimen but not in a few newly settled juveniles. The vacillations of the outer mantle lobe, as represented by the ring of lamellae, is more probably linked to genotypic as well as phenotypic factors, especially further differentiation of the periostracal slot and both inner and outer mantle lobes (WILLIAMS & others, 1997, p. 14).

The periostracum of the late brephic (lamellar ring) and mature shell is underlain by a layer of sulfated GAGs with some chitin. This succession correlates with the mosaic and its substrate. Both successions are secreted by cytologically similar outer epithelia with tubular microvilli. Despite this similarity, secretion of silica and apatite does not proceed simultaneously during shell growth. Ten young shells, 475–580 μm in diameter, were analyzed by EDX. The analysis of a pelagic juvenile showed that the inherent mineralizing element was Si with no trace of Ca or P (specimen 1 in Fig. 1556). This pelagic juvenile was within the size range for settlement, and tablet secretion
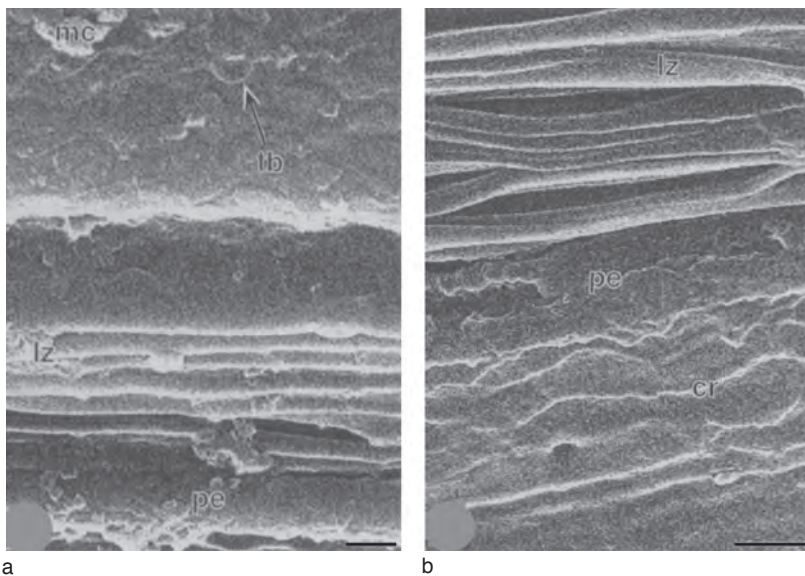

FIG. 1555. SEMs of gold-coated shells of recently settled juveniles of *Discinisca* sp. cf. *tenuis* sonicated for 15 min. in tap water; *a–b*, changes shown from mosaic (*mc*) with tablets (*tb*) outward to lamellar ring (*lz*) and periostracum (*pe*) of mature dorsal valve with its superstructure of concentric ridges (*cr*); scale bars: 1 μm (Williams, Lüter, & Cusack, 2001).
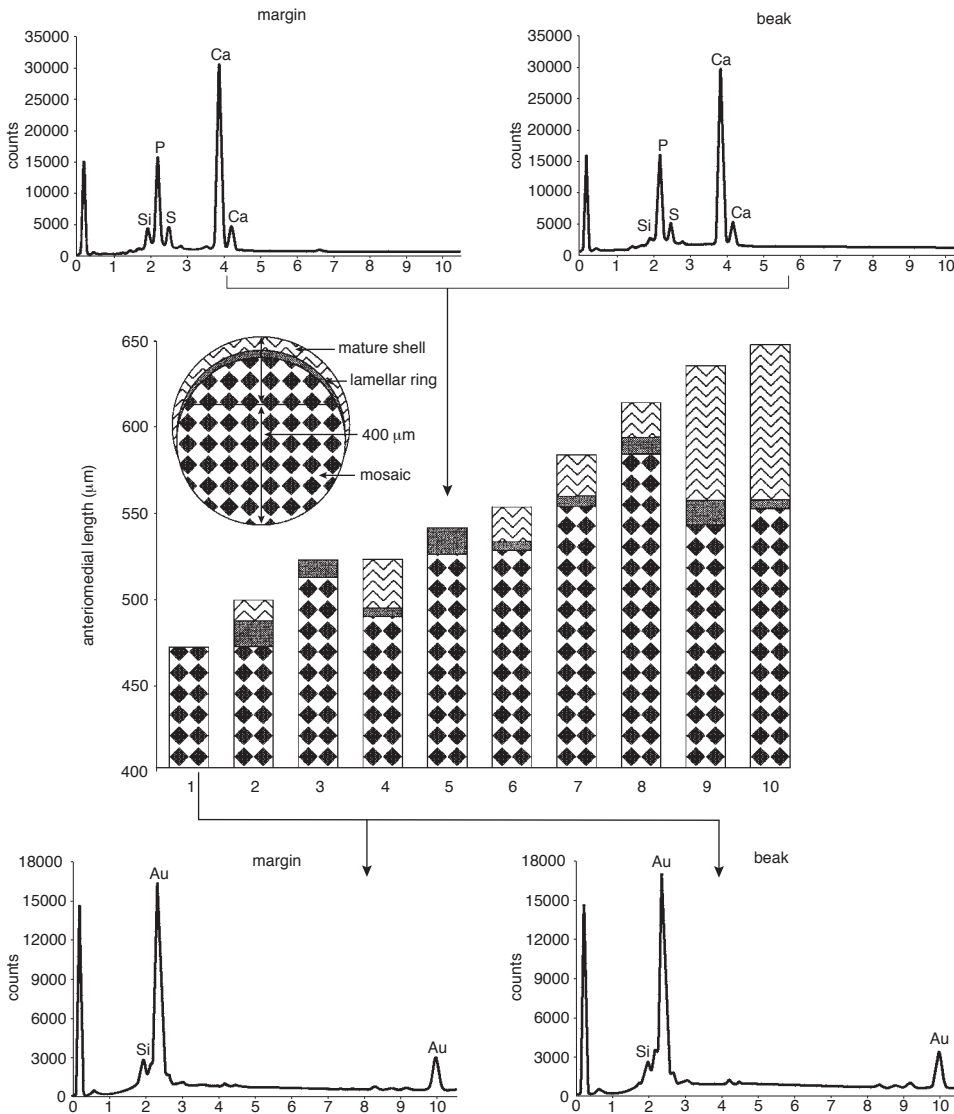
FIG. 1556. Graphical representation of variation in development and sagittal lengths of shell surfaces anteromedially of 400 μm of mosaic on ten smallest dorsal valves of *Discinisca* sp. cf. *tenuis* subjected to EDX analysis. Specimens 1 and 2 were gold coated, the remainder carbon coated; specimen 1, the only pelagic juvenile, was fixed in glutaraldehyde, specimen 2 in Bouin's, and remainder were dried, untreated valves. Spectra of valve margins and beaks of two specimens are shown for pelagic specimen 1 and the settled specimen 5, which was of intermediate length but without mature shell (Williams, Lüter, & Cusack, 2001).

may have ceased already on the concealed inner sides of the incipient outer mantle lobes. In contrast, in settled juveniles less than 50 μm longer (Fig. 1556), where cessation of silica secretion is confirmed by the presence of the lamellar ring, apatite could be traced everywhere from the first-formed shell to the margin. A subsidiary peak of S is also associated with the Ca and P peaks of apatite. It presumably signals the sulfated
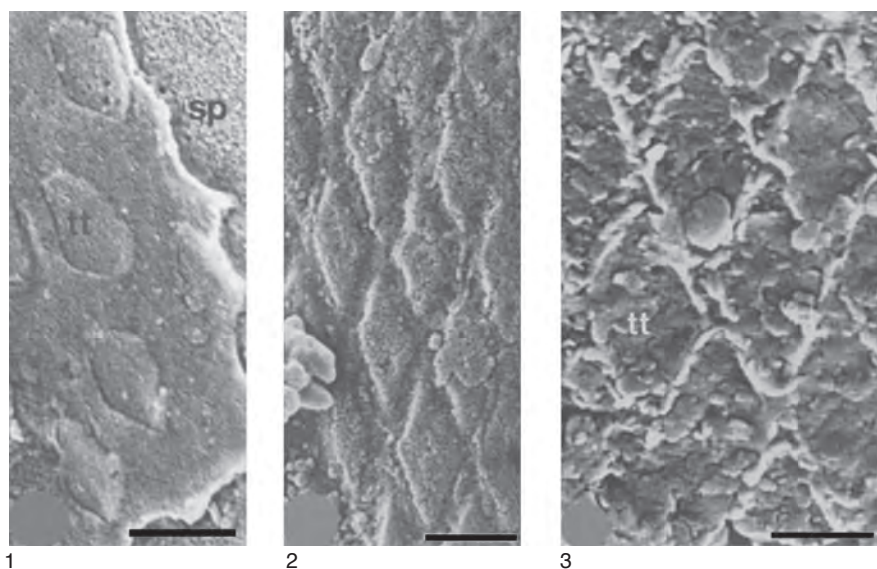
FIG. 1557. SEMs of exteriors of discinid larval shells; *1,* tension-cracked fragment of outermost coat of dried valve of *Discina striata*, bearing imprints of tablets (*tt*) and underlain by primary layer with spherular apatite (*sp*); scale bar: 1 μm; *2*, tablet imprints on tension-cracked, spherular external surface of primary layer of *Pelagodiscus atlanticus*, treated with subtilisin; scale bar: 1 μm; *3*, imprints of tablets (*tt*) on exterior of larval shell of Upper Jurassic *Discina*; scale bar: 1 μm (Williams, Cusack, & Buckman, 1998).

GAGs secreted as the matrix for the initial apatitic aggregates (WILLIAMS, CUSACK, & BUCKMAN, 1998, p. 2,008). Although apatitic secretion begins before the growth of the mature shell (specimen 5 in Fig. 1556), it appears to have a mutually exclusive relationship with the siliceous secretion of the mosaic. By the time an anteromedial arc of mature shell has appeared on the surface of a dorsal valve, even the apatite secreted under the mosaic of the first-formed shell is many times thicker than the overlying layer of siliceous tablets. In the absence of cytological differences, it is assumed that the epithelium generated outside the lamellar ring everywhere loses the capacity to secrete silica. In effect, there is a temporal and spatial hiatus in shell mineralization that precludes chemical interaction between the siliceous and phosphatic regimes. Both regimes operate consecutively within the outer epithelium underlying the mosaic. Yet the phosphatic regime of the mosaic area is not activated until apatite secretion begins under the

lamellar ring (possibly some days after the deposition of the siliceous tablets) and is presumably triggered by a chemical signal from the ring region (WILLIAMS, LÜTER, & CUSACK, 2001, p. 34).

Imprints of mosaics occur on the juvenile shells of living *Discina* and *Pelagodiscus* (Fig. 1557; BALINSKI & HOLMER, 1999, fig. 3Q). *Discina* has been sporadically recorded in post-Paleozoic sediments but tablet imprints are rarely preserved (Fig. 1557) due to exfoliation or abrasion of the juvenile shells. Imprints of siliceous tablets have also been found on some juvenile shells of the Late Devonian *Schizobolus* (BALINSKI & HOLMER, 1999, fig. 3N) and the late Silurian *Opatrilkiella* (Fig. 1558). No mosaic imprints, however, have been found in the oldest discinoids, including the sister group of discinids (WILLIAMS, CUSACK, & others, 1998, p. 2096), the Ordovician orbiculoideids such as *Orbiculoidea* and *Schizotreta*. Species of the latter genera are common, and it can be confidently asserted
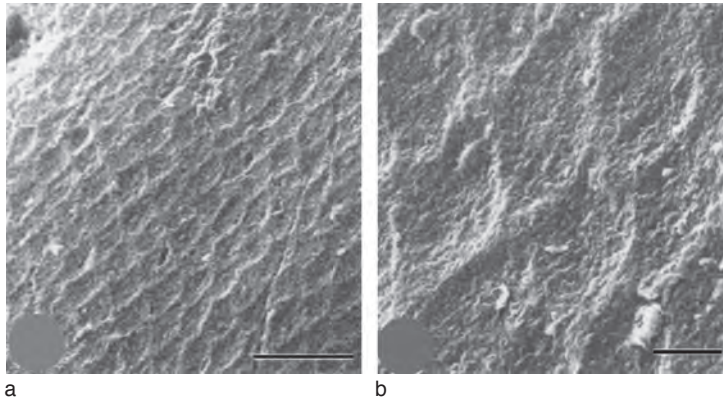
Fig. 1558. SEMs of gold-coated valve surfaces of lingulate shells dissolved out of rock; *Opatrilkiella minuta* Mergl, GLAHM 114648, upper Silurian, Czech Republic; *a*, dorsal valve of juvenile with *b,* details of rhombic imprints; scale bars: 1 µm (Williams, 2003).

that their juvenile shells, which are well delineated by lamellar rings, were devoid of imprints of any kind in contrast to their mature shells.

The development and mode of preservation of the discinoid juvenile shell have been described in detail because they serve as models to explain the origin of micro-ornamentation of many early Paleozoic lingulates. Moreover, the physicochemical constraints imposed when shell secretion involves more than one mineral could have a bearing on how the organophosphatic and organocarbonate brachiopod shells were first differentiated.

ACROTRETIDE JUVENILE SHELL

Imprints made by structures associated with the periostracum or the first-formed cuticle occur on the shells of over 100 of the 250 or so genera assigned to the Lingulata. Only the Siphonotretida lack imprints that ornament the shells of about one-third of the Lingulida and are invariably present on the juvenile shells of the Acrotretida. The imprints of acrotretide mosaics were the first to be discovered and were described in Volume 1 as impressions of vesicular periostracum (Williams, 1997, p. 269–271). They will be discussed before those of lingulides (other than the discinids already described) because they are the best known

and include all distinctive impressions characterizing the lingulates.

Only four distinctive kinds of imprints (Fig. 1559) are known (Williams, 2003). Imprints on a micrometric scale have either flat bases and vertical sides (discoidal or rhombic) or inwardly convex bases with sloping sides (hemispherical). Cylindroid pits on a nanometric scale can also occur in association with the flat-based or hemispherical imprints; they are small-scale versions of semiellipsoidal imprints found on lingulide shells. The subcircular areas bearing these imprints vary in diameter from approximately 150 µm (*Acrotretella*) to 220 µm (*Conotreta*) and occupy the beaks of shells. These areas are free of growth rings and are assumed to be the casts of first-formed shells. They are bounded by one or two growth rings that form a conspicuous, cylindroid ridge (roll) that is interpreted as the brephic shell.

Variations in the shapes and packing of flat-based imprints of acrotretides are exemplified by the mosaic casts of *Opsiconidion* and *Eoconulus*. The first-formed dorsal valve of *Opsiconidion* is wrinkled and raised as a pair of submedial ridges diverging anteriorly, but lacks growth bands (Fig. 1560). It is impressed by subcircular imprints that fade along an irregular boundary in the antero-medial sector of the roll. The imprints,
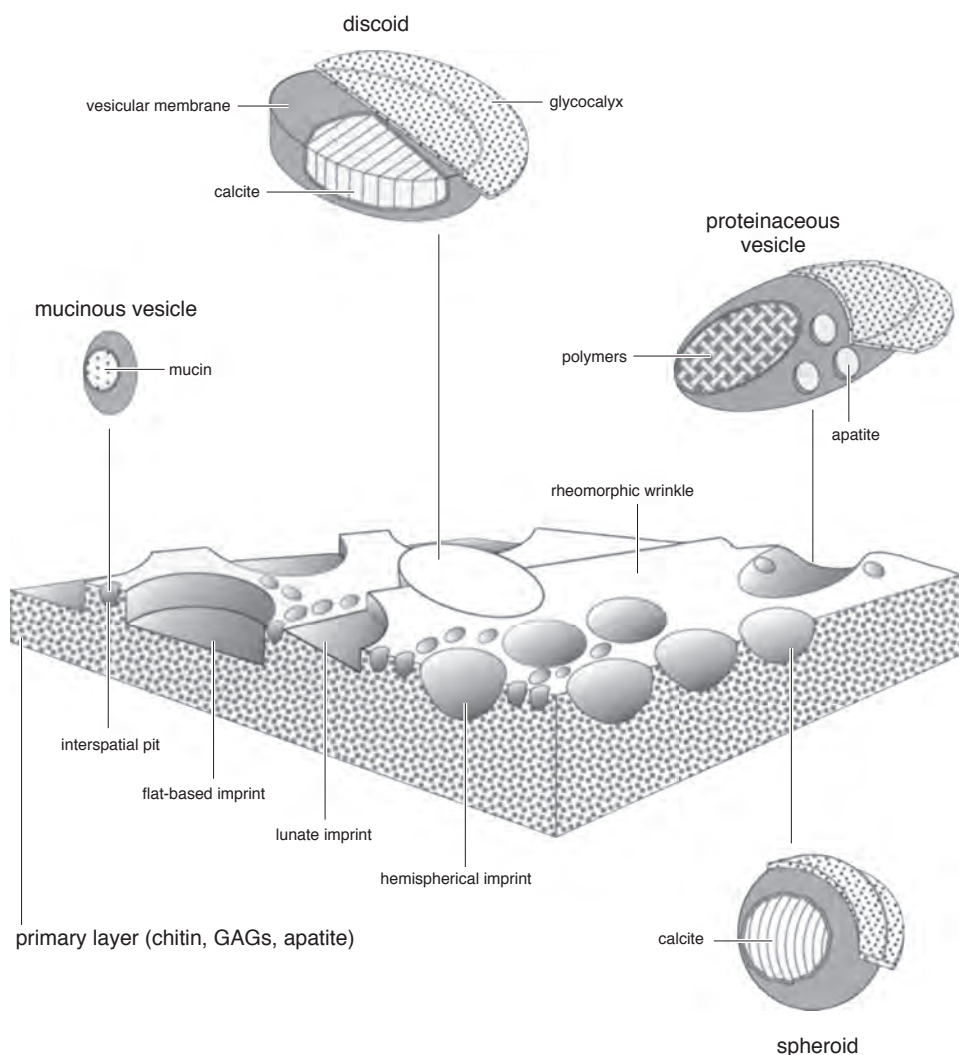
F_{IG}. 1559. Graphical representation of a block section of juvenile acrotretide shell *in vivo* showing disposition of various imprints in primary layer (and first-formed lamina) and assumed chemicostructures of discoids, spheroids, and vesicles making imprints (Williams, 2003).

approximately 4.4 µm in diameter, are essentially arranged in hexagonal, close-packed arrays (Fig. 1560), but there is much overlap. Imprint surfaces are smooth or finely granular, and their vertical walls are up to 500 nm deep. The walls and interspaces between imprints are indented by cylindroid pits (Fig. 1560). In some *Opsiconidion* species, the first-formed shell consists of overlapping clusters of imprints, 2 µm to 7 µm in diameter. The imprints are usually arranged in successions up to five deep with the largest imprint being outermost and the smallest being innermost (Fig. 1560). The smoothly textured imprints may be flat or gently convex inwardly. They are so overcrowded that they amalgamate into chambers, reducing the substrate into flat-topped polygons. The imprints themselves may be pierced by cavities.
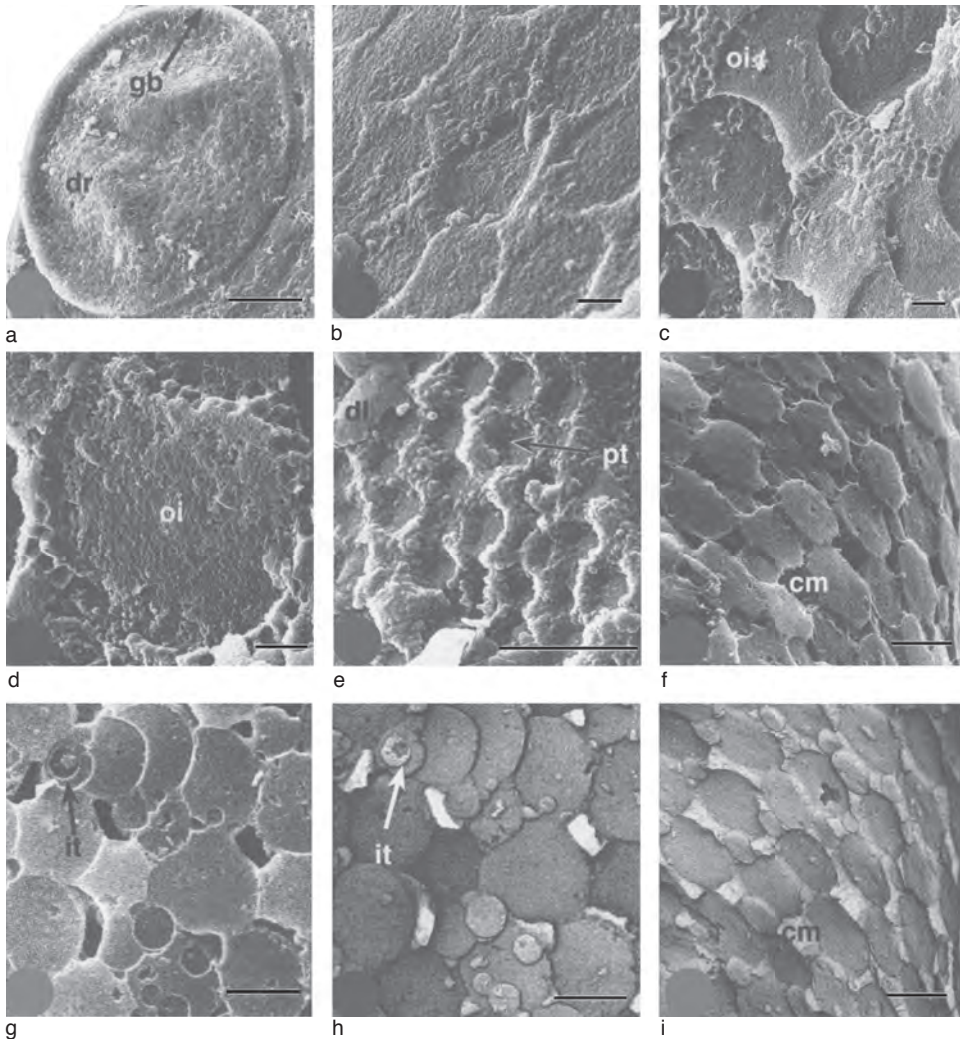
FIG. 1560. SEMs of gold-coated valve surfaces of acrotretide shells dissolved out of rock, various *Opsiconidion* species, upper Silurian, Czech Republic; *a, c–e, O. decessus* MERGL, GLAHM 114649; *b, O. ephemerus* MERGL, GLAHM 114650; *f–i, O. simplex* MERGL, GLAHM 114651; *a,* general view of first-formed dorsal valve bounded by growth band or roll (*gb*) with divergent ridges (*dr*); scale bar: 50 μm; *b,* flat-based elliptical imprints in hexagonal, close-packed array; scale bar: 5 μm; *c–e,* overlapping, flat-based imprints (*oi*) and details of pits (*pt*) in interspaces with dislodged panel (*dl*); scale bars: 1 μm; *f, i,* detail and inverted image of first-formed ventral valve with flat-based chambers (*cm*); scale bars: 5 μm; *g–h,* detail and inverted image of first-formed dorsal valve showing overlapping successions of flat-based circular imprints, some of which (*it*) had been incorporated within the primary layer; scale bars: 5 μm (Williams, 2003).

The flat-based imprints on the dorsal valve of *Eoconulus* (Fig. 1561) are approximately 8 μm in diameter medially, becoming smaller (approximately 6 μm) toward the roll. Their vertical sides may be more than 1 μm high and may be separated from the granular floor by a shallow gutter. The imprints are arranged in hexagonal arrays, and the walls and interspaces between them are flat topped and indented by close-packed, shallow to hemispherical pits, approximately 700 nm in diameter.
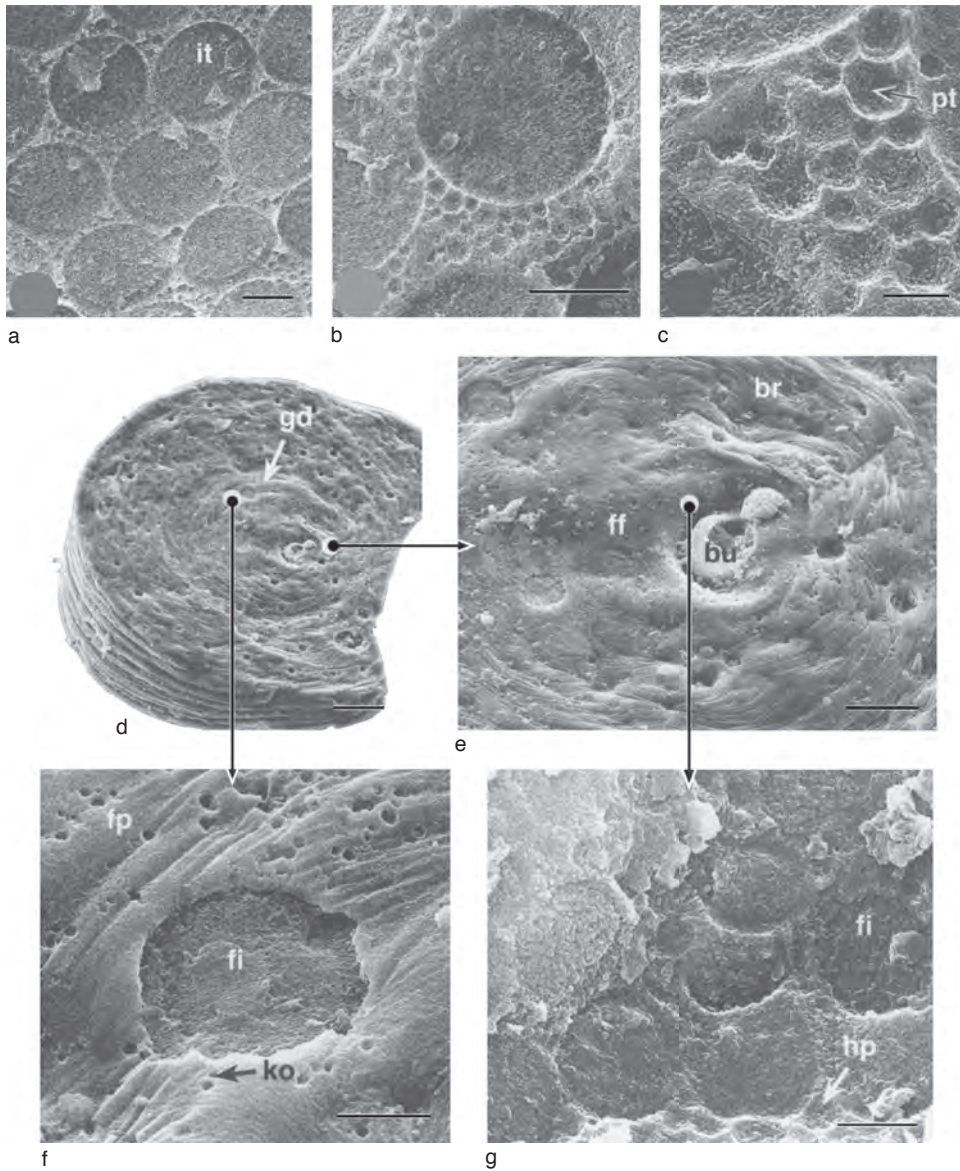
FIG. 1561. SEMs of gold-coated valve surfaces of acrotretide shells dissolved out of rock; *a–c*, *Eoconulus* sp. cf. *semiregularis* BIERNAT, GLAHM 114663, middle Ordovician, Sweden; general view and details of flat-based circular imprints (*it*) and interspaces with close-packed pits, some compound (*pt*); scale bars: 5, 5, and 1 μm respectively; *d–g*, SEMs of encrusting part of ventral valve of *Eoconulus* sp. cf. *semiregularis* BIERNAT, GLAHM 114652, middle Ordovician, Sweden, showing *d*, general disposition and *e*, details of surface features including bulla (*bu*) in first-formed shell (*ff*) with *g*, overlapping, flat-based imprints (*fi*) and small, hemispherical pits (*hp*), surrounded by eccentrically folded brephic zone (*br*) separated by growth disturbance (*gd*) from mature shell with tightly folded drapes (*fp*) perforated by sporadic, flat-based imprints (*fi*) and kiskinoids (*ko*) (view *f*); scale bars: 100, 25, 10, and 2.5 μm in *d–g* respectively (Williams, 2003).

Unlike other acrotretide shells, imprints on the encrusting surface of the ventral valve of *Eoconulus* differ from those of the dorsal valve (Fig. 1561). The juvenile shell, approximately 200 µm in diameter, consists of a vestigial holdfast approximately 25 µm in diameter within a first-formed valve delineated by a tightly folded brephic shell. The wrinkled first-formed shell is variably ornamented by poorly ordered flat-based imprints approximately 3.5 µm in diameter and close-packed hemispherical pits. The mature shell is also eccentrically folded and indented by widely scattered, flat-based circular imprints up to 25 µm in diameter. These imprints must have been made by bodies secreted on a folded periostracum, because they breach the surface without being affected by external folding. Sporadically occurring deep pits appear to have been mechanically excavated like koskinoids (WILLIAMS, 1997, p. 320).

Flat-based imprints are characteristic of the first-formed shells of the biernatiids, eoconulids, scaphelasmatids, torynelasmatids, and many acrotretid genera. Their mean diameters range from 1.4 µm to 4.8 µm, and their floors, which may be gently convex or concave (*Linnarssonella*), are commonly separated from their bounding walls by a gutter approximately 100 nm wide. The imprints of some species (*Conotreta*) are deep (700 nm) relative to their diameter (1.9 µm).

Hemispherical imprints are the most common impressions on lingulate shells. They ornament the first-formed shells of most acrotretids and torynelasmatids and all ephippelasmatids but with some variation. Thus, the hemispherical pits on the first-formed shell of *Numericoma* (Fig. 1562), which range in diameter from 0.7 to 2.7 µm, have smooth linings and are close packed with larger ones surrounded by clusters of smaller ones, giving a bubble-raft appearance (BIERNAT & WILLIAMS, 1970). The walls between contiguous imprints, however, may be as thin as 75 nm without being

rheologically deformed, which precludes structural comparison with bubble rafts. The close-packed hemispherical to semiellipsoidal imprints on the first-formed shell of *Eurytreta* are smaller in mean diameter (1.5 µm) and mostly deep with rare, shallow impressions, possibly representing aborted secretion. The flat-topped walls and interspaces between imprints are indented by roughly bounded pits affected by cleavage. The mean diameters of hemispherical pits of other acrotretides vary from 1.1 µm (*Prototreta*) to 2.6 µm (*Apsotreta*). Pits indenting walls and interspaces are shallow (seldom more than 400 nm). The juvenile shell of *Ceratreta* is ill defined and unusual in two respects. It bears impersistent growth bands, and the small, hemispherical imprints (1.2 µm in diameter) are only sporadically preserved on surfaces apparently unaffected by exfoliation.

LINGULIDE JUVENILE SHELL

Unlike that of living discinids, the first-formed shell of living lingulids is a smooth organic sheet presumably chitinous, as are the discrete brephic valves. BALINSKI (1997), however, has shown that the first-formed shell of Devonian lingulids consists of two discrete, cuplike valves (approximately 90 µm in diameter) ornamented by radial ridges, tubercles, or hemispherical pits (1–3 µm in size). Some compound pits with rounded interspaces or bubble-raft casts characterize Early Devonian species. This evidence that the protegulum is a post-Devonian feature of the lingulid lineage accords with the fact that the first-formed shells of Paleozoic lingulides consist of discrete valves, although pitting is variably developed. There is also variation in the distribution of imprints on shell surfaces. In some groups, imprints are restricted to the juvenile shell; in others, imprints indent the entire shell or, more rarely, the mature shell only.

Lingulides with pitted juvenile shells include the linguloid paterulids and eoobolids and the acrotheloids. The first-formed
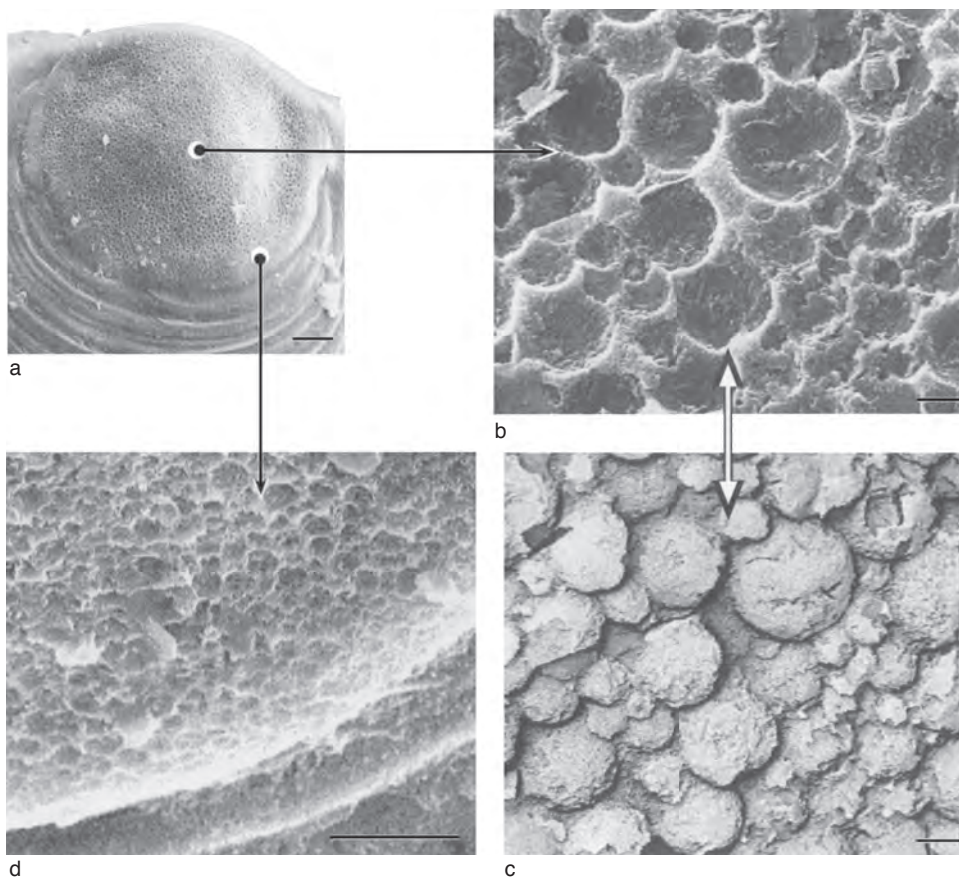
FIG. 1562. SEMs of a first-formed dorsal valve (*a*) and surface details (*b–c*) of *Numericoma perplexa* HOLMER, GLAHM 114661, middle Ordovician, Sweden, showing clustering of smaller, hemispherical imprints around larger ones in cast and inverted image becoming shallower toward bounding roll (*d*); scale bars: 20, 1, 10, and 1 μm respectively (Williams, 2003).

shell of *Paterula*, approximately 60 μm in diameter, is impersistently and arcuately wrinkled, which affects the disposition and distribution of surface imprints (Fig. 1563). The circular, flat-based imprints (2.3 μm in mean diameter) are variably distributed. Groups of closely crowded, overlapping imprints, up to three deep, are scattered among more openly distributed clusters. Some overlapping imprints are presumably casts of bodies that accumulated on top of one another in the substrate. Others forming stacked, incomplete, lunate impressions could have been made by bodies that had been partly separated from the first-formed shell during its wrinkling (a common feature of the juvenile shells of living discinids). The first-formed shell is surrounded by a brephic zone of growth seldom more than 7 μm wide anteromedially. This zone is underlain by stratified laminae of the primary layer and with the bounding mature shell is gently folded into ripples, eccentric to the first-formed shell. The brephic shell surface is indented by close-packed elliptical imprints, although circular imprints also occur. The mature shell is characterized by highly ordered, rhombic impressions with long diameters aligned with the eccentric folding; despite their crystalline aspect, the impressions are surface ornament (WILLIAMS, 2003, p. 71).
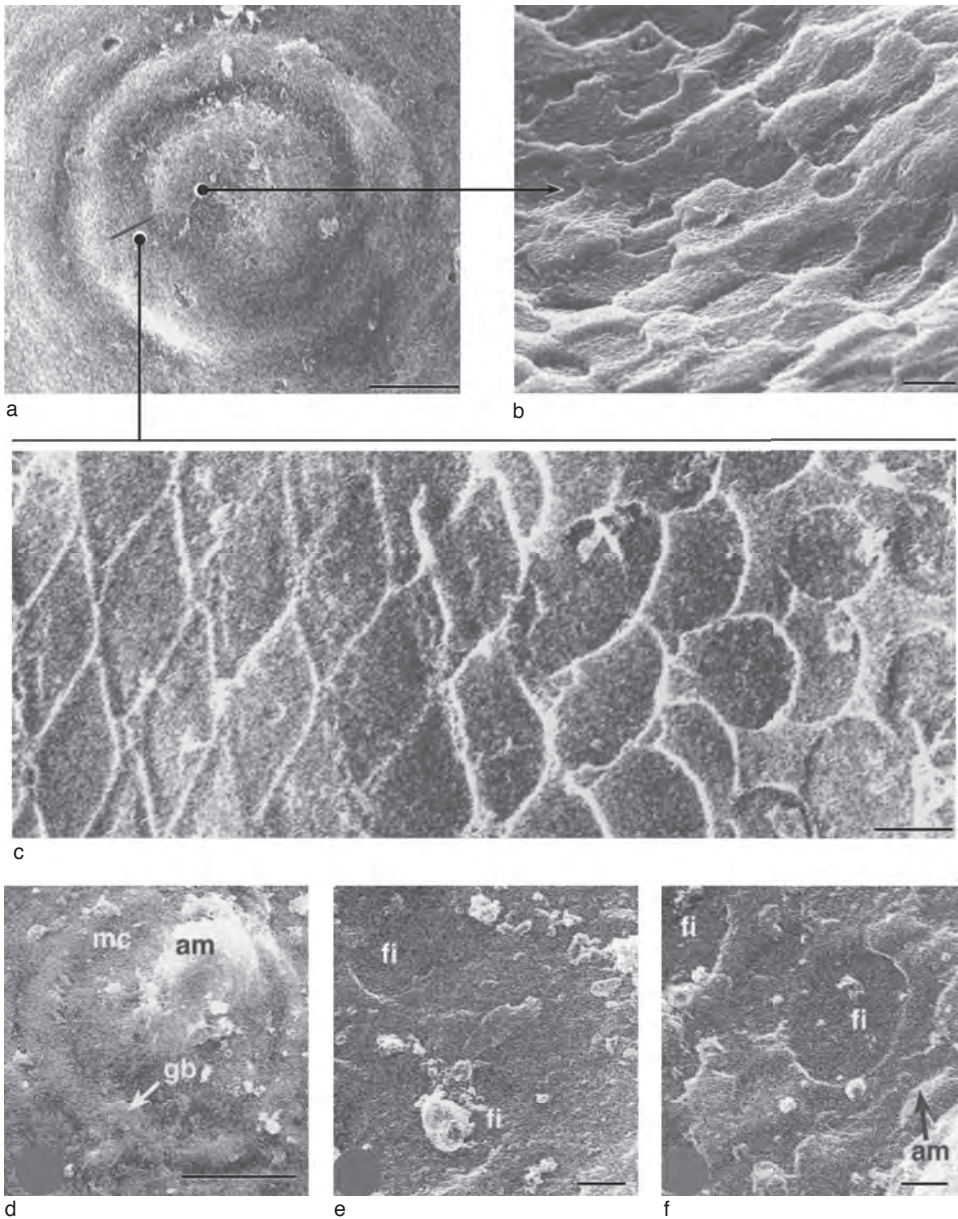
Fɪɢ. 1563. *a–c*, SEMs showing surfaces of juvenile and surrounding mature shell of dorsal valve of *Paterula* sp., GLAHM 114653, middle Ordovician, Sweden; scale bars: 25, 2, and 2 μm; *d–f*, *Paterula* sp., GLAHM 114656, middle Ordovician, Sweden; general view of untreated mudstone cast with adherent apatitic shell (*am*), identified by EDX, of dorsal, first-formed valve with bounding growth band (*gb*) and *e–f*, details of part of mudstone (*mc*), shown in *d*, bearing subcircular, shallow, flat-based imprints (*fi*); scale bars: 50, 1, and 1 μm respectively (Williams, 2003).

Nearly all chemicostructural studies of fossilized apatitic-shelled brachiopods have used specimens dissolved out of rock. This preparation could have affected imprints and any traces of the bodies making them. One sample giving evidence of the fossilized state of undissolved shells has been described (Wɪʟʟɪᴀᴍs, 2003, p. 82). In the dorsal valve
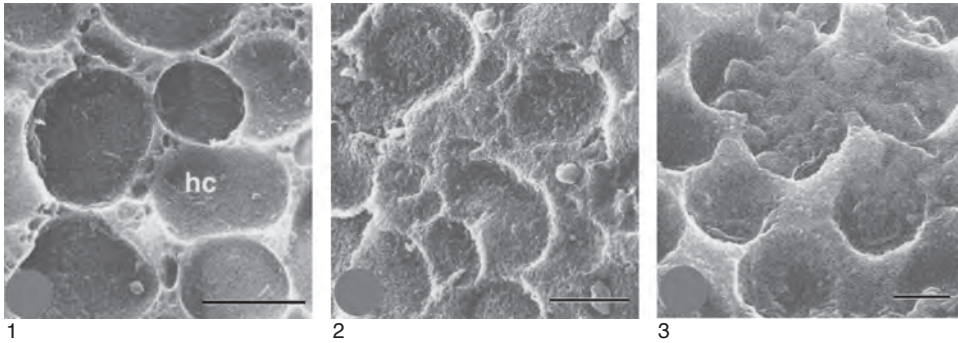
Fig. 1564. SEMs of gold-coated, first-formed dorsal valve surfaces of acrotretide shells dissolved out of rock; *1, Orbithele ceratopygorum* (Brögger), GLAHM 101736, lower Ordovician, Sweden; view of flat-based, circular, and hemicylindroid (*hc*) imprints separated by pitted walls; scale bar: 5 µm; *2, Acrothele coriacea* Linnarsson, GLAHM 101734, middle Ordovician, Sweden; flat-based hemispherical and deformed imprints with fracture section showing compact lamina of first-formed shell; scale bar: 5 µm; *3, Karathele napura* (Kruse), GLAHM 101737, Lower Cambrian, Australia; view of hemispherical imprints; scale bar: 1 mm (Williams, 2003).

of *Paterula* embedded in mudstone, part of the first-formed shell had broken away to expose the interface between the valve exterior and mudstone (Fig. 1563). The mudstone is pitted with shallow, flat-based cavities that could only have been the external counterparts of imprints found on the first-formed shell. Unlike its apatitic primary layer, which was unaffected by diagenesis, the mosaic of the first-formed shell of *Paterula* must, therefore, have been composed of discoidal tablets that degraded mineralogically as well as organically during fossilization.

The juvenile shell of *Eoobolus* is well defined by a lamellar ring and is pitted by sharp-edged hemispherical imprints approximately 1 µm in diameter (Holmer, Popov, & Wrona, 1996).

The spinose juvenile shells of acrotheloids (Fig. 1564) are also well defined by a strong roll. Those of acrothelids (*Orbithele*) are ornamented by large (up to 9 µm in diameter), flat-based to convex (rarely concave)-based imprints. The imprints form hexagonal arrays with rare overlaps and deformed hemicylindroids. The gently rounded walls and interspaces are impressed by deformed hemispherical pits less than 1 µm in diameter. The juvenile shells of botsfordiids (*Karathele*) are indented by

hemispherical pits approximately 1.5 µm in diameter and up to 1 µm deep. The pits are so closely packed as to be separated by knife-edge walls regularly culminating in interspaces indented by shallow depressions.

Apart from the paterulids and eoobolids, when pitting occurs on linguloid juvenile shells, it also indents mature shells as in all zhanatellids. The hemispherical imprints on the juvenile shell of *Rowellella* are alternately arranged in concentric rows. They are seldom more than 3 µm in diameter (compared with approximately 6 µm on the mature shell), and most have been made by spheroids that were rigid relative to a rheological substrate that was commonly deformed by radial drag into chevron folds around the pits (Fig. 1565). In contrast, the first-formed shell of the obolid *Obolus eichwaldii* are indented by large semiellipsoidal imprints arranged in radial rows and bounded by round-topped walls. In the brephic shell, three or so radial rows of concentrically disposed semicylindroids alternate with strips indented by lenticular slots oriented at all angles. The slots bear median ridges, indicating that they are casts of platy, bilamellar bodies. Small hemispheroidal pits sporadically indent the rounded borders separating the semicylindroids (Fig. 1565).
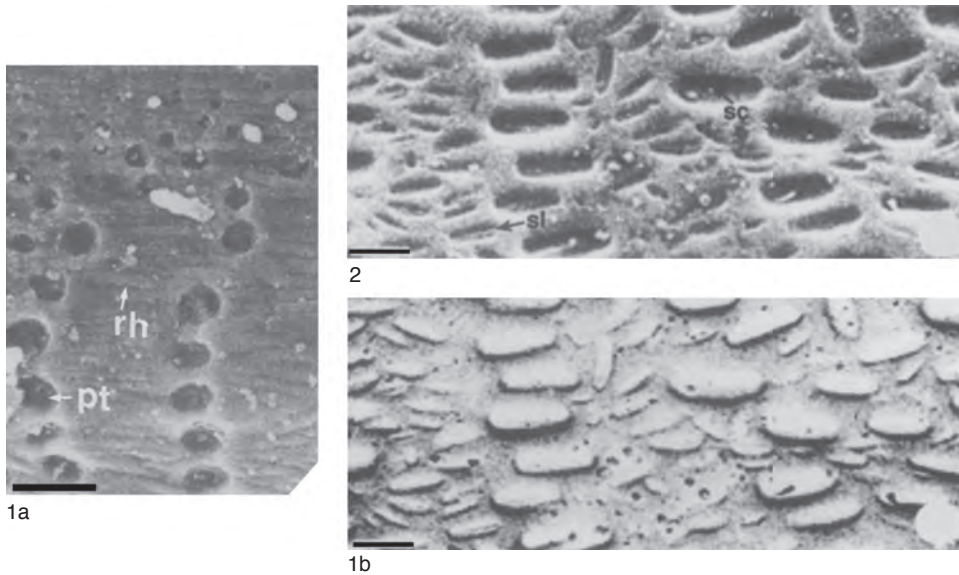
FIG. 1565. Shell exterior of *1, Rowellella rugosa* GORJANSKY, GLAHM 101723, Lower Ordovician; *1a,* initiation and development of radially disposed pits (*pt*) separated by rheomorphic folding (*rh*); scale bar: 10 μm; *1b,* general view; *2,* inverted image of pitted surface of mature shell of *Obolus eichwaldi* MICKWITZ, GLAHM 101451, Cambrian, Russia, showing orientation and inclination of semicylindroid pits (*sc*) and lenticular slots with median clefts (*sl*); scale bars: 5 μm (Cusack, Williams, & Buckman, 1999).

The most distinctive features, however, of linguloid pitted surfaces are the apatitic tablets and discoids still preserved in mature shells of the zhanatellid *Wahwahlingula antiquissima* (Fig. 1566). The borders and sides of the large, hemispherical imprints bear subcircular to prismatic, flat-bottomed imprints, 0.6–1.2 μm in maximum diameter. These imprints are not deformed but tilt into the sides of the larger pits as narrow slots. Some imprints contain closely fitting tablets of apatite, about 100 nm thick. This intimate association suggests that the prismatic to slotlike imprints are casts of apatitic tablets that occur in three or four horizons within the outermost zone of the primary layer (Fig. 1566).

At this juncture, it is relevant to note the nature of the imprints on discinoid orbiculoideids, even though they are restricted to the mature shell. The periodic disposition of the hemispherical imprints in discrete radial arrays on the *Orbiculoidea* shell has previously been interpreted as being determined by the distribution of setae at the mantle margin (WILLIAMS, 1997, p. 272). The pits, which are commonly deformed, average 2.5–3 μm in diameter and are graded in bands bounded by fila (WILLIAMS, CUSACK, & BUCKMAN, 1998, p. 2,022). On the outer side of a filum and extending outwardly for approximately 30 μm, the pits are hexagonally close packed before becoming aligned in radial arrays. The shell surface is seldom free of fine, rheomorphic folds that can occur in swarms in some interfilar surfaces. The pits are evidently hemispherical casts of presumed spheroidal bodies preserved in a rheological substrate. The bodies making the pits were not homogenous but composed of close-packed spheroids (Fig. 1567), which themselves appear to have been aggregates of small vesicles. The toughness of the coats of these composite spheroidal bodies is revealed by the way rheomorphic folds in the substrate can radiate from pits (Fig. 1567) that retained their shape (presumably during dehydration of exposed dead
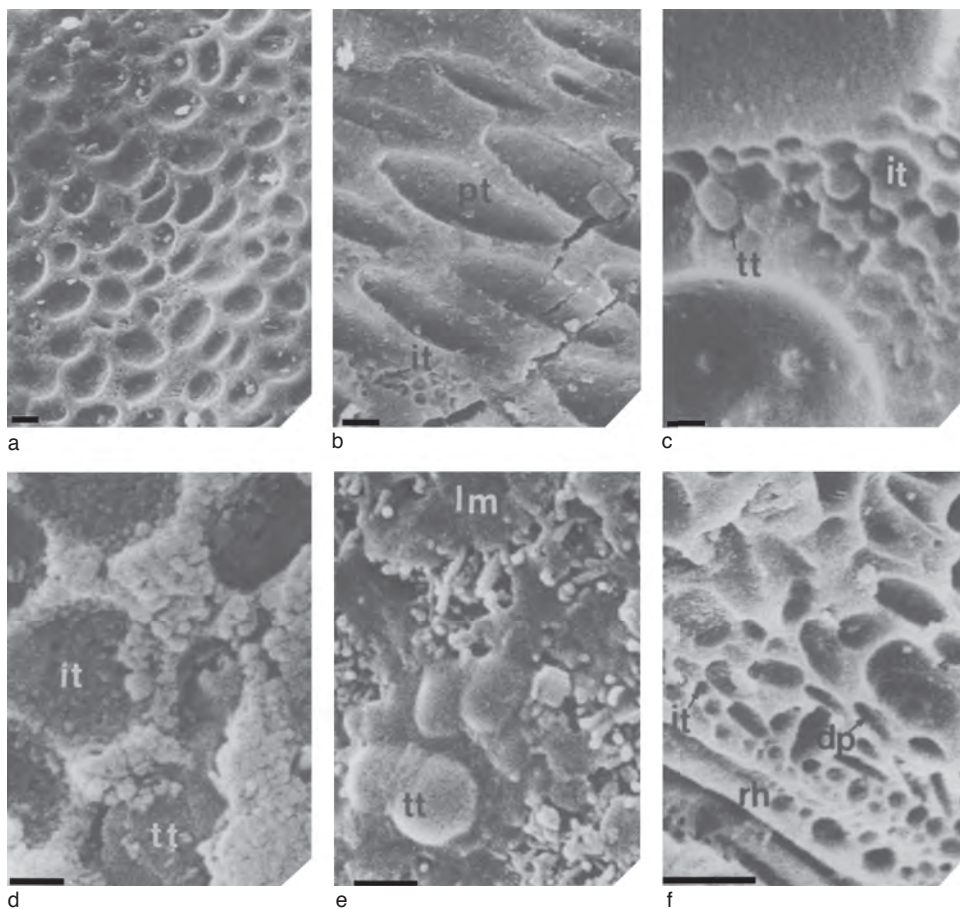
Fig. 1566. Shell exterior of *Lingulella* (?) *antiquissima* (Jeremejew), GLAHM 101691, Upper Cambrian, Russia; *a*, general view of pitted surface between two fila; scale bar: 5 μm; *b*, slotlike pits (*pt*) with long axes concentric with valve margin and casts of tablets (*it*) just beyond boundary of larval shell; scale bar: 2 μm; *c*, detail of borders between contiguous pits showing tablets (*tt*) and their casts (*it*); scale bar: 1 μm; *d*, flat-bottomed subcircular casts (*it*) of tablets (*tt*); scale bar: 500 nm; *e*, tablets (*tt*) within primary layer associated with lithified membranes (*lm*) and apatitic rods and spherules; scale bar: 1 μm; *f, in vivo* repair of damaged part of valve with radial, rheomorphic folding (*rh*) of primary layer with tablet casts (*it*) and deformed pits (*dp*) tracing zone of fusion of torn mantle edge; scale bar: 5 μm (Cusack, Williams, & Buckman, 1999).

shells prior to burial and fossilization). The pits on the mature shells of *Schizotreta*, the oldest orbiculoideid, are also in close-packed bands giving way to radial arrays but, despite being about three times as big as those of *Orbiculoidea*, were not similarly composed of casts of smaller spheroids.

PATERINATE JUVENILE SHELL

The paterinate juvenile shell is well defined by a raised border homologous with the lingulide lamellar ring (Fig. 1568).

Its microtopography is variable, being mainly tuberculate (as in *Micromitra*) but is also indented with hemispherical imprints (*Askepasma*) or is featureless apart from wrinkling (*Dictyonites*).

The tubercles of *Micromitra* are arranged in open hexagonal arrays that become more sporadically distributed before dying out on the brephic growth band. They are hemispherical in the undeformed state, with diameters of 4.5–6 μm and have cores of apatitic spherules (Fig. 1568).

The hexagonally packed imprints of *Askepasma* indent the entire external surface, including the juvenile shell where they differ only in being less regularly distributed as a result of rheomorphic wrinkling (Fig. 1569). The imprints, approximately 7 μm in diameter, are bounded by rounded walls and are very rarely covered by gently convex, striated covers that are possibly phosphatized remnants of an original coat. Eight to thirteen apatitic domes, approximately 600 nm in diameter, are commonly found hexagonally arranged on the hemispherical floors. *In vivo*, the imprints and their substrate acted as an integrated rheological sheet so that the hexagonal arrangement of pits was deformed by changes in shell shape and became shallow or aborted on raised fila.

ORIGIN OF IMPRINTS ON LINGULIFORM JUVENILE SHELLS

Until the discovery of the flat-based impressions made by siliceous tablets on the juvenile shells of living discinids, all imprints on fossil linguliforms were interpreted as having been made by vesicles in the periostracal infrastructure (WILLIAMS, 1997, p. 269). A reappraisal of such imprints, however, suggests that they are the casts of four kinds of superficial, mineralized as well as organic, bodies (WILLIAMS, 2003).
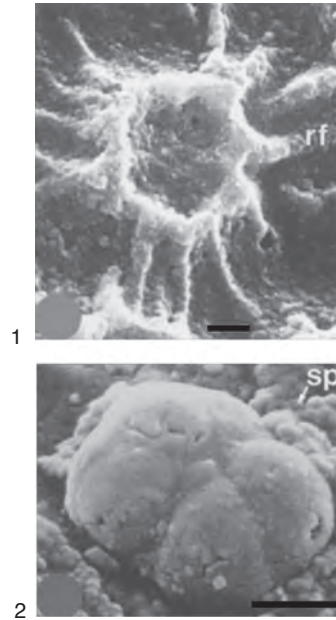

FIG. 1567. *1*, SEMs of pit on shell exterior of Lower Carboniferous *Orbiculoidea nitida,* England, showing composite nature of pit and raised substrate with radiating folds (*rf*); scale bar: 1 μm; *2*, internal view of imprint of composite vesicle in spherular (*sp*) primary layer of *Roemerella*; scale bar: 1 μm (Williams, Cusack, & Buckman, 1998).

Flat-based circular imprints indent the juvenile shells of many acrotretides and lingulide paterulids and acrotheloids. The diameter of imprints tended to vary only
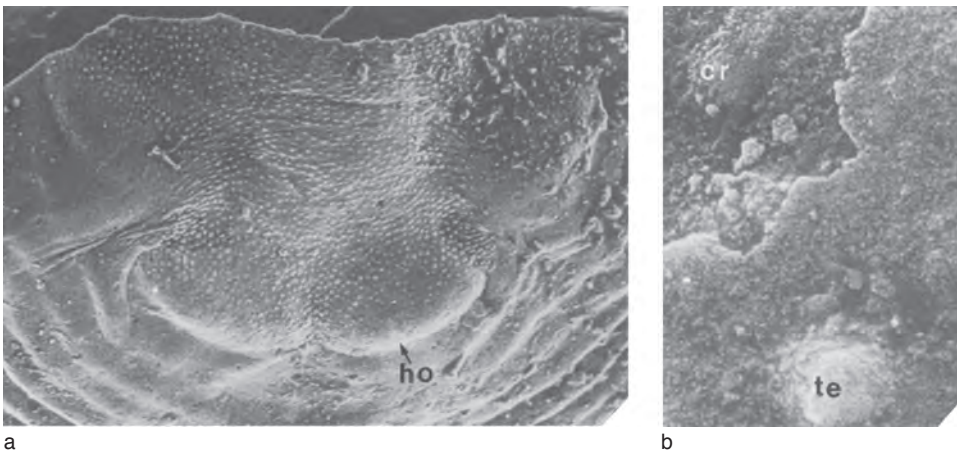

FIG. 1568. *Micromitra* sp. cf. *ornatella* (LINNARSSON), Sosiuk Formation, Middle Cambrian, Turkey; *a,* tuberculate exterior of larval dorsal valve delineated by lobate halo (*ho*), ×180; *b,* detail of exfoliated tubercles (*te*) with solid cores (*cr*), ×4800 (Williams & others, 1998).
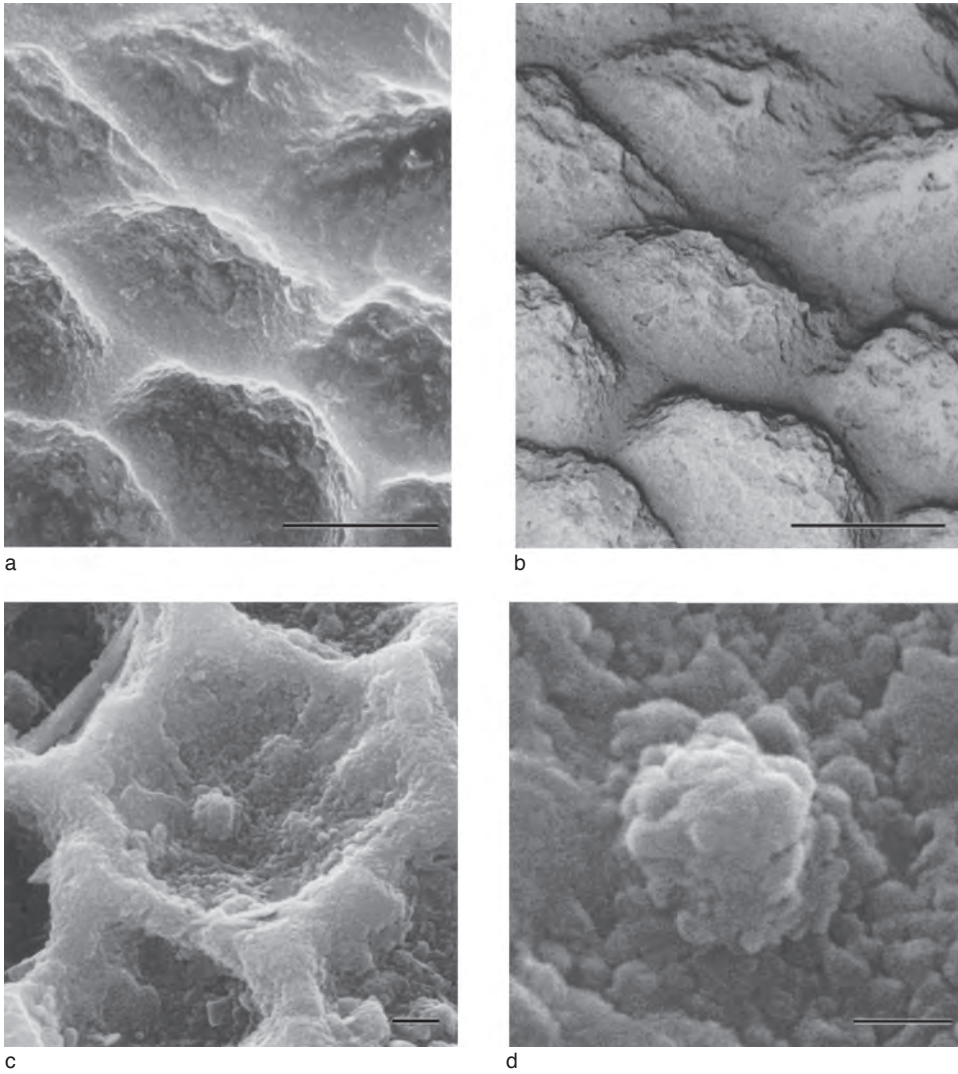
Fig. 1569. Hexagonally packed imprints on external surface of *Askepasma toddense* Laurie, Todd River Dolomite, Australia, Lower Cambrian; *a–b*, general and inverted views; scale bars: 20 μm; *c–d,* view of single imprint with detail of dome composed of spherular apatite; scale bars: 1 μm and 0.5 μm respectively (new).

during shell growth in species but differ significantly among genera. The basic arrangement of imprints is a single-layered, close-packed hexagonal array, although some imprints are disordered as in *Opsiconidion* where they form clustered successions. Notwithstanding these differences

in size and arrangement, evidence favors the imprints as casts of mineralized tablets. The finely textured surfaces of imprints and their constancy of shape suggest that they were membrane-bound discoidal tablets, assembled intracellularly. The chemicostructure of the tablets, as ordered mineral aggre-

gates in an organic matrix, would account for the constant shape and thickness of imprints. The tablets would generally have been up to six times thicker than discinid siliceous rhombs, which would explain the better, more widespread preservation of their imprints.

No remnants of these postulated tablets have yet been found so that their composition is also a conjecture. In that respect, the fact that tablets have never been seen is the prime clue to their likely composition. Three factors militate against the survival of tablets on specimens prepared for ultrastructural studies. The glycocalyx covering mosaics and the membranes enclosing such tablets would have quickly degraded during the life of individuals (as in discinids) thereby facilitating the shedding of tablets during fossilization. Acrotretide and *Paterula* tablets, however, would have been virtually immersed in a rheological primary layer that, on phosphatization, frequently formed flaps over discoidal rims that should have been strong enough to trap some tablets. Of course, tablets would have been prone to degradation during fossilization but that would depend on their mineral composition. In the zhanatellid *Wahwahlingula*, for example, apatitic discoids are preserved within tightly folded imprints of the primary layer. Yet the mosaics of *Opsiconidion* that must have been sporadically stacked in clusters of five or so, deeply embedded in the primary layer of the shell, are now all represented by discoidal cavities beneath superficial imprints. This suggests that the mineral components of *Opsiconidion* tablets decomposed as completely as their organic matrix during fossilization.

Survival of tablets could also have been jeopardized by the way linguliform shells are dissolved out of rock for study. The structures exposed on rock matrix by the partial exfoliation of the first-formed shell of *Paterula* (Fig. 1563) were, therefore, noteworthy. The shallow, flat-based, circular cavities impressed on the mudstone could only have been the imprints of the external surfaces of discoidal tablets. Unlike its apatitic substrate, the primary layer, the mosaic of the first-formed shell of *Paterula* must have been composed of tablets that degraded mineralogically as well as organically during fossilization. The same assumptions can be made about the circular, flat-based cavities indenting the encrusting surface of *Eoconulus* (Fig. 1561). The adhesive periostracum of *Eoconulus* would have acted as a protective coat during fossilization, and the contents of the cavities could have been dissolved during the extraction of specimens of rock matrix.

The mineral components of living brachiopod skeletons consist almost exclusively of calcium fluorapatite (LEGEROS & others, 1985), calcium carbonate as calcite (JOPE, 1965, p. 158), and silica (WILLIAMS, CUSACK, & others, 1998, p. 2095). JOPE (1965) also reported traces of $FePO_4$, $MgCO_3$, and Fe_2O. If one of the three dominant minerals had been the sole inorganic constituent of the inferred tablets imprinted on the shells of acrotretides, acrotheloids, and paterulids, it is most likely to have been calcite (or aragonite; Fig. 1559), because apatitic tablets are still preserved and siliceous tablets still retained their rhombic shape in Paleozoic obolids and discinids respectively.

Apart from differing in shape, hemispherical imprints are also significantly smaller than discoidal ones. Structurally, however, they are similar in being unaffected by rheomorphic changes in the primary layer and were probably made by membrane-bound mineralized spheroids. Discoidal and hemispheroidal imprints are mutually exclusive in acrotretides but occur together in some acrotheloid shells, like that of *Acrothele* (which seems also to have been impressed by proteinaceous vesicles described below). Accordingly, the spheroids are assumed also to have been composed of calcitic granules in a proteinaceous matrix (Fig. 1559).

There are two other kinds of imprints that, being deformable to the same degree as their rheomorphic substrates, were probably made by organic bodies. The small, cylindroid to shallow, basinal depressions indenting the walls and interspaces of significantly larger imprints may coalesce into compound structures. Their lack of rigidity suggests they are casts of mucinous vesicles, secreted simultaneously with larger membrane-bound crystalline or organic structures.

The large (approximately 3–8 µm) pits, indenting the mature as well as the juvenile shell of many lingulides, are variably deformable in a manner suggesting that they are all casts of organic vesicles with differentially thickened bounding membranes. As they were probably an integral part of the periostracal infrastructure, they could have been analogous with the empty vesicles with glycoproteinaceous coats up to 250 nm thick found in the terebratulide periostracum (WILLIAMS & others, 1997, p. 15). The vesicles with thin membranes would have been deformed to the same extent as their rheological substrate (*Wahwahlingula*, *Obolus*), whereas those that retained their original shape (*Rowellella,* orbiculoideids) had thick coats. A repaired valve of *Wahwahlingula* confirmed that exocytosis of such vesicles was confined to the outer mantle lobe, whereas apatitic tablets were secreted immediately beneath the infrastructural boundary of the periostracum (CUSACK, WILLIAMS, & BUCKMAN, 1999, p. 810).

The bodies that made the hemispherical imprints on the shells of such paterinates as *Askepasma* were also deformable and presumably organic in composition. They were, however, indented by pits represented by apatitic domelike casts, commonly arranged hexagonally on the floors and sides of imprints. The bodies are, therefore, unlikely to have been vesicles, but were possibly thornlike chitinous structures anchored within the imprints by fibrillar tissue occupying the pits.

CRANIIFORM JUVENILE SHELLS

Information about the chemicostructure of the juvenile shell of living craniiforms is meager and concerned exclusively with the dorsal valve of the lecithotrophic *Novocrania*. The first-formed dorsal valve is simultaneously secreted as a complete cover, approximately 100 µm in diameter, by an epithelial collective differentiated six days after fertilization (NIELSEN, 1991, p. 15; Fig. 1570). The rudimentary periostracum is little more than a cuticular film because a granular and platy calcitic coat is discernible below this substrate (NIELSEN, 1991, fig. 15B). By the eighth day after fertilization, when the dorsal valve is more than approximately 200 µm in diameter, a radially ribbed, brephic shell has been secreted holoperipherally around the first-formed shell (NIELSEN, 1991, fig. 15C). This differentiation of the juvenile dorsal valve of living *Novocrania* accords with that found on well-preserved beaks of more mature valves. The diameter of the juvenile valve is variable (up to 300 µm), and the first-formed and brephic parts are not always clearly distinguishable (Fig. 1571). The calcitic units secreted on the rudimentary periostracum of the first-formed valve are granular aggregates and rhombs 90–190 nm in size, while those of the brephic valve are finely laminar on a nanometric scale. Some of the radial ribbing figured by NIELSEN (Fig. 1570) represents the edges of laminae; others could be the beginning of slats found in the primary layer (CUSACK & WILLIAMS, 2001a, p. 882).

The several phases of recrystallization that affected most pre-Cenozoic craniids have obliterated the fine structure of juvenile shells preserved at the beaks of dorsal valves but not their micromorphology. Thus, FREEMAN and LUNDELIUS (1999) have argued
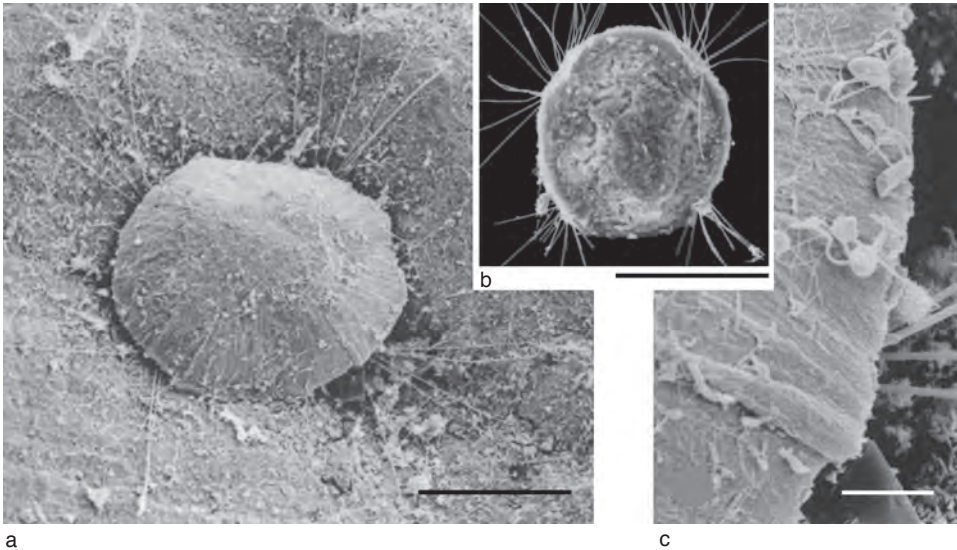
Fɪɢ. 1570. Metamorphosis of larva of *Crania*; *a*, brachial valve has reached periphery of body and pushed larval setae to sides; *b*, juvenile about three days after settling; *c*, detail of valve edge; scale bars 100 μm, 100 μm, and 10 μm respectively (Nielsen, 1991).

that the onset of growth banding (comparable with the lamellar ring) indicates that craniids were variably planktotrophic as late as the Tertiary. These aspects of fossilization characterize the juvenile shells of the Ordovician, free-lying *Orthisocrania,* which with *Pseudocrania* is assumed to represent the sister group of the contemporaneous attached craniid, *Petrocrania*. Both juvenile valves of *Orthisocrania* are delineated by growth banding as convex semiellipsoids up to 700 μm or so long (Fig. 1572). They are recrystallized but with hints of stratified lamination on their sides. The surface of one juvenile ventral valve is indented by a narrow imprint suggesting that the shell had been temporarily attached to a cylindroid substrate, presumably by cementation, as there are no traces of a pedicle opening.

Otherwise, the juvenile shell of the earliest known craniids was similar to those of living species.

RHYNCHONELLIFORM JUVENILE SHELLS

Knowledge of the development of the first-formed shell of living rhynchonelliforms is limited to studies by Sᴛʀɪᴄᴋᴇʀ and Rᴇᴇᴅ (1985a, 1985b) of lecithotrophic juveniles of *Terebratalia*. The first-formed shell (the protegulum of Sᴛʀɪᴄᴋᴇʀ & Rᴇᴇᴅ) is secreted within the first day after metamorphosis. It consists of a nonhinged, bivalve structure with the ventral valve approximately 160 μm wide (Sᴛʀɪᴄᴋᴇʀ & Rᴇᴇᴅ, 1985b, p. 299). Each valve, which is wrinkled and lacks growth banding, is secreted simultaneously by the epithelial collective and consists
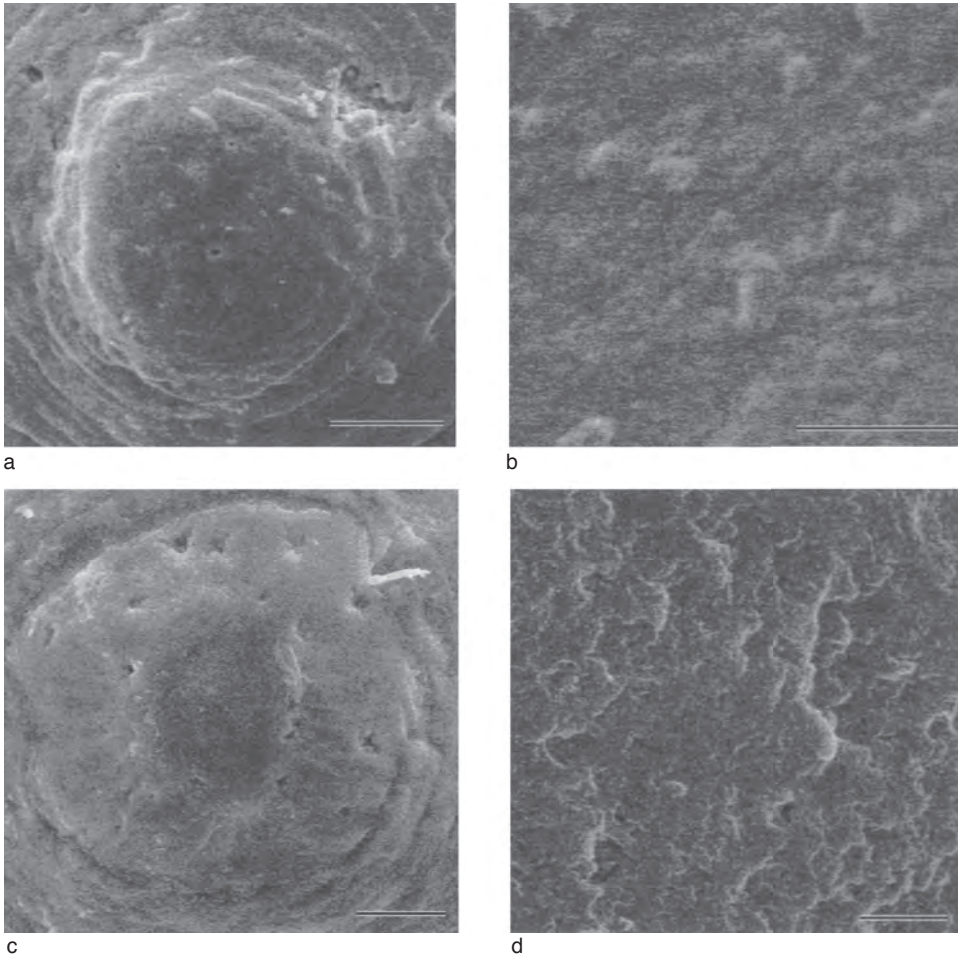
Fig. 1571. Two juvenile dorsal valves of Recent *Novocrania anomala* (Müller), Oban, Scotland; *a–b,* poorly differentiated but well-preserved valve with textural detail of granular aggregates and rhombs of first-formed valve; scale bars: 100 μm and 0.5 μm respectively; *c–d,* well-differentiated first-formed and brephic shell with traces of radial ribbing and textural detail of finely laminar brephic shell; scale bars: 50 μm and 1 μm respectively (new).

of a rudimentary periostracum devoid of superstructures, which acts as a substrate for a coat of granules approximately 100 nm in size aggregating into monolayers of spherules and rhombs (Fig. 1573). The coat is calcitic (Stricker & Reed, 1985b; Fig. 1574). Valve surfaces are indented by close-packed, circular, shallow depressions approximately 1 μm in diameter (Stricker & Reed, 1985a, p. 266). Their origin is unknown as dimpling by dehydration on such a well-ordered scale is unlikely. They

may be casts of mucinous droplets accumulating between a transient glycocalyx and the polymerizing periostracal rudiment.

An interesting aspect of the studies by Stricker and Reed (1985a, 1985b) is the abrupt change identified by them in the secretion of the brephic shell. On the fourth day after metamorphosis, secretion of the first-formed shell is followed abruptly by the deposition of the primary and secondary layers of the brephic shell, which "occurs more or less simultaneously throughout the
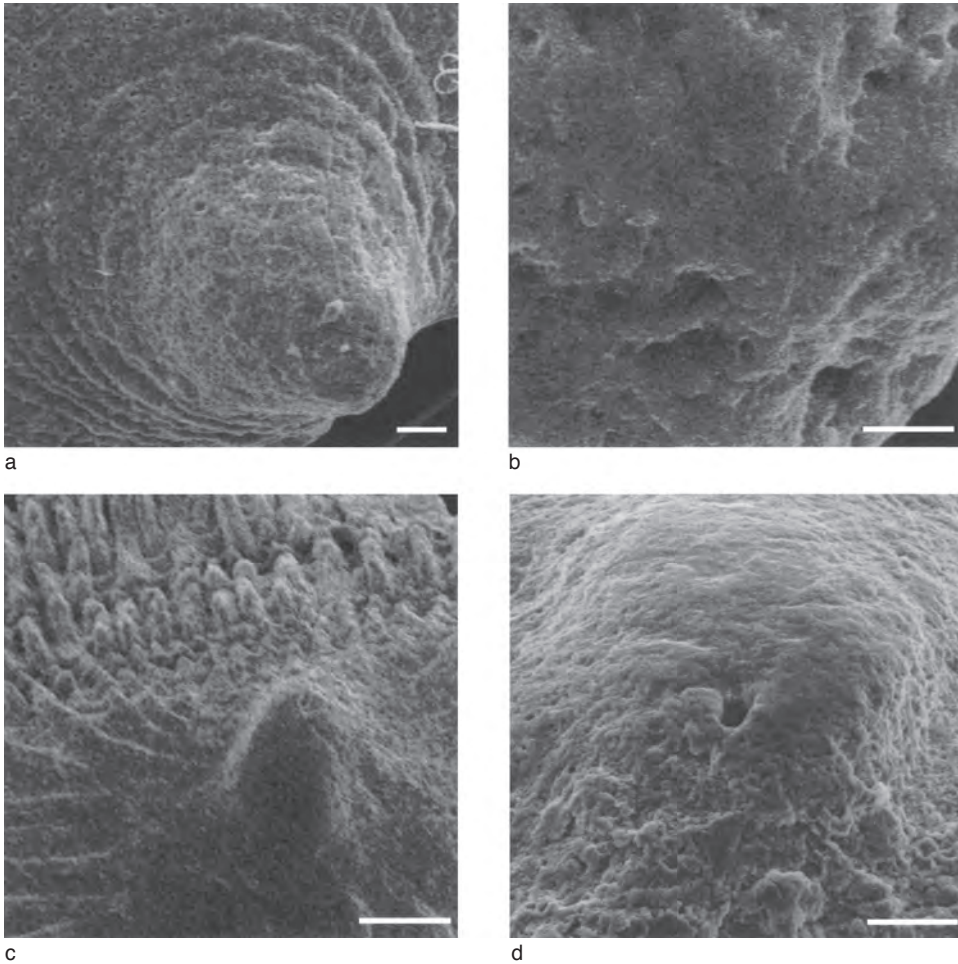
Fig. 1572. Juvenile shell of *Orthisocrania depressa* (von Eichwald), Ordovician, Grjazno Formation, St. Petersburg, Russia, lower Caradoc; *a–b,* juvenile ventral valve with surface detail of first-formed shell; scale bars: 100 μm and 25 μm respectively; *c–d,* juvenile dorsal valve with surface detail of first-formed shell; scale bars: 500 μm and 100 μm respectively (new).

epithelium" (Stricker & Reed, 1985a, p. 270) underlying the first-formed shell. Such a change is comparable with that affecting the secretory regime in the ontogeny of living discinids.

No microornament has been found on the first-formed shells of a sample of other living species, including another terebratulide (*Terebratulina*), a rhynchonellide (*Notosaria*), and a thecideide. Given the biological and ecological range of this sample, it is unlikely that the absence of pits is due to exfoliation or some such factor. Carbonate substrates do

serve as casting materials, as is confirmed by the presence of sporadic, shallow depressions less than a micron in diameter preserved on the mature shells of the rhynchonellide *Frieleia* and presumably made by mucinous vesicles within the periostracal infrastructure. Accordingly, the pits on the first-formed shell of *Terebratalia* could be a generic feature.

The first-formed shells of extinct rhynchonelliforms are likely to have been secreted by planktotrophic larvae (Freeman & Lundelius, 2005. Their surface features are poorly known but no microscopic imprints on them
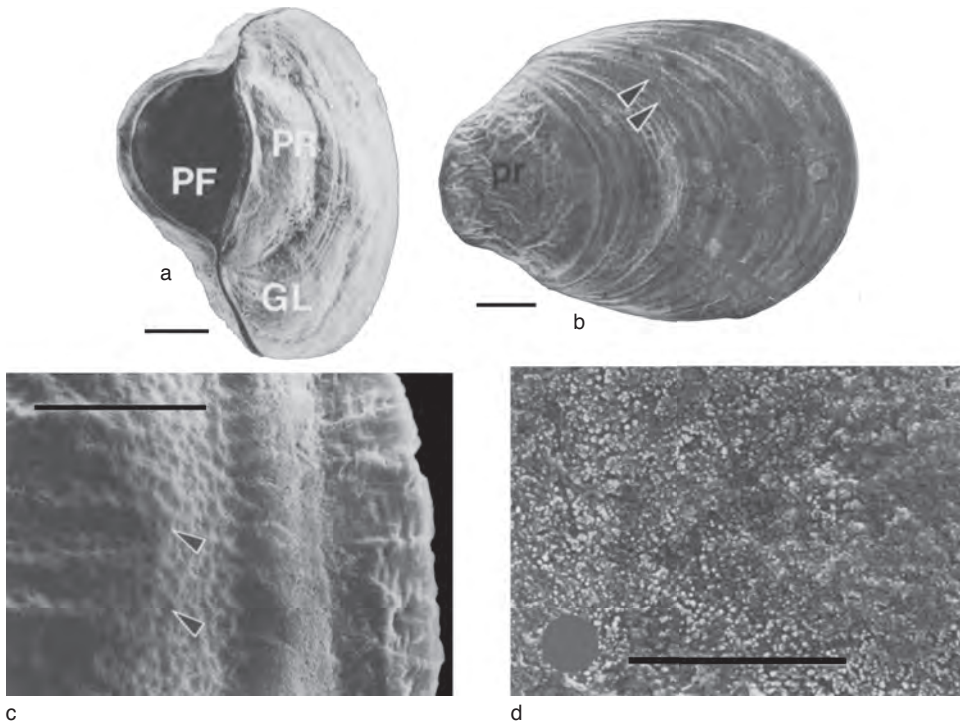
FIG. 1573. SEM of posterior end of juvenile *Terebratalia transversa* shell at *a,* 11 days postmetamorphosis; protegulum (*PR*) is visible at posterior end of shell, and concentrically arranged growth lines (*GL*) occur anterior to protegulum; posterior fenestration (*PF*) between two valves represents hole through which pedicle protrudes; scale bar: 50 μm (Stricker & Reed, 1985b); *b,* external surface of juvenile shell at 23 days postmetamorphosis; note protegulum at posterior end of shell; *double arrowheads* mark concentrically arranged growth lines resulting from periodic accretions of juvenile shell material; scale bar: 50 μm; *c,* outer surface of protegulum with numerous small indentations (*arrowheads*); scale bar: 10 μm; *d,* inner surface of protegulum at 1 day postmetamorphosis; scale bar: 5 μm (Stricker & Reed, 1985a).

have been reported, and it is unlikely that any inherent differences in their fabric would have survived fossilization.

DIVERSITY OF THE BRACHIOPOD JUVENILE SHELL

A comparative study of the juvenile shell throughout brachiopod phylogeny reveals a chemicostructural and micromorphological diversity that has always been greater in the organophosphatic linguliforms than in the organocarbonate craniiforms and rhynchonelliforms. In contrast, the progression of shell secretion during ontogeny seems to be the same, at least in living lingulates and rhynchonellates, with a discontinuity in the deposition of juvenile and mature skeletal successions. Several assumptions on the

evolution of brachiopod secretory regimes can be drawn from these ontogenetic and phylogenetic differences. They are best presented by comparing skeletal successions with a standard secretory regime (Fig. 1575) with the rudimentary periostracum or cuticle as a reference layer separating superstructural and infrastructural features (WILLIAMS & others, 1997, p. 16).

Most of the diversity of the juvenile linguliform shell is related to the development of various superstructural features. The protegulum and siliceous tablets of living lingulids and discinids respectively are secreted with the glycocalyx serving as a substrate. The folded protegulum represents the first-formed lingulid shell. It follows therefore that the brephic shell is the pair of discrete
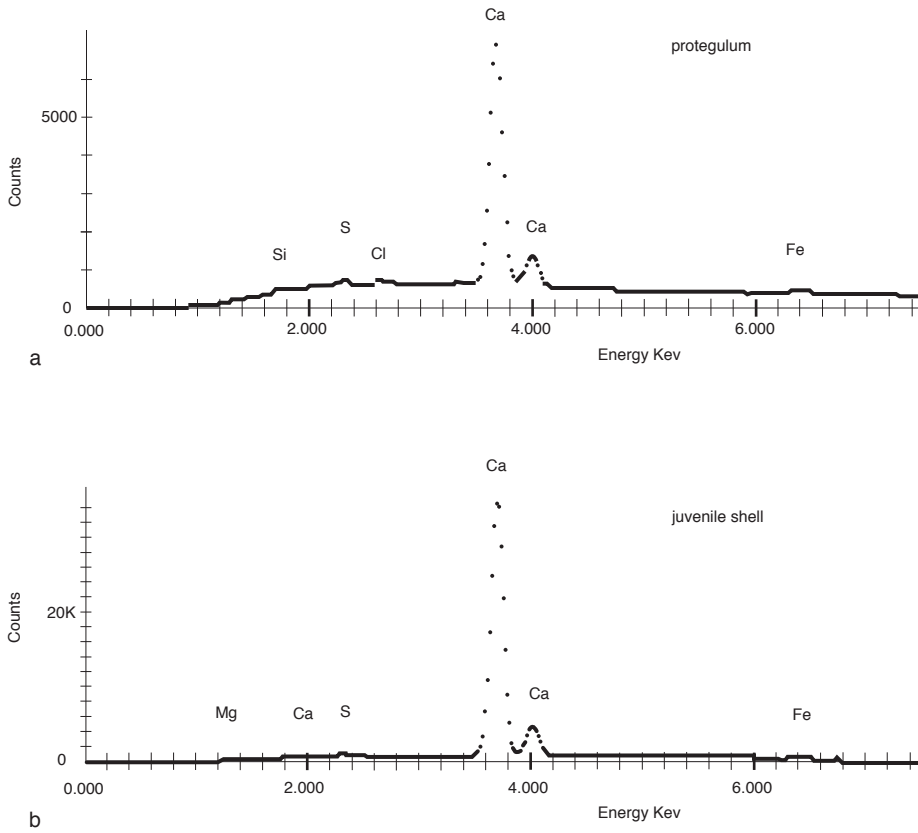
Fig. 1574. Qualitative electron microprobe analysis of elemental composition of protegulum (*a*) and a 23-day-old juvenile shell (*b*); *Ca,* calcium; *Cl,* chlorine; *Fe,* iron; *Mg,* magnesium; *Si,* silicon; *S,* sulfur; *Counts,* total counts detected during a 10 min. accumulation; *Energy Kev,* energy of X-ray (Stricker & Reed, 1985b).

valves secreted beneath and beyond the protegulum to the bounding lamellar ring. These valves appear to be composed largely, if not entirely, of a periostracal cuticle; but further study is needed to determine whether the onset of apatitic secretion coincides with the initial growth of the mature shell. If it does, the primary layer of the mature shell is the first mineralized lamination within the skeletal succession of living lingulids. This was not necessarily so in Paleozoic lingulids and many other extinct linguloids, which lacked protegula (Balinski, 1997) but had discrete, mineralized juvenile valves *ab initio*. It is therefore possible that these juvenile shells had an infrastructural apatitic layer that ceased being secreted in post-Paleozoic lingulids. The assumption is in accord with

evidence that since the Carboniferous, the shell of *Lingula* (*s.l.*) has been undergoing a decalcification of its skeletal secretory regime (Emig, 1990; Cusack & Williams, 1996, p. 48). The juvenile parts of Paleozoic linguloid shells are rarely preserved, however, which suggests that they were not mineralized. In effect, linguloid juvenile shells have always been the same as those of living discinids except for the absence of superstructural mosaics in most species. This is the preferred assumption.

The development of mosaics in juvenile shells has an ambiguous role in postulating linguliform phylogeny based on shell structure. Mosaics have always consisted of a single layer of mineralized tablets (including spheroids) secreted on transient glycocalyces
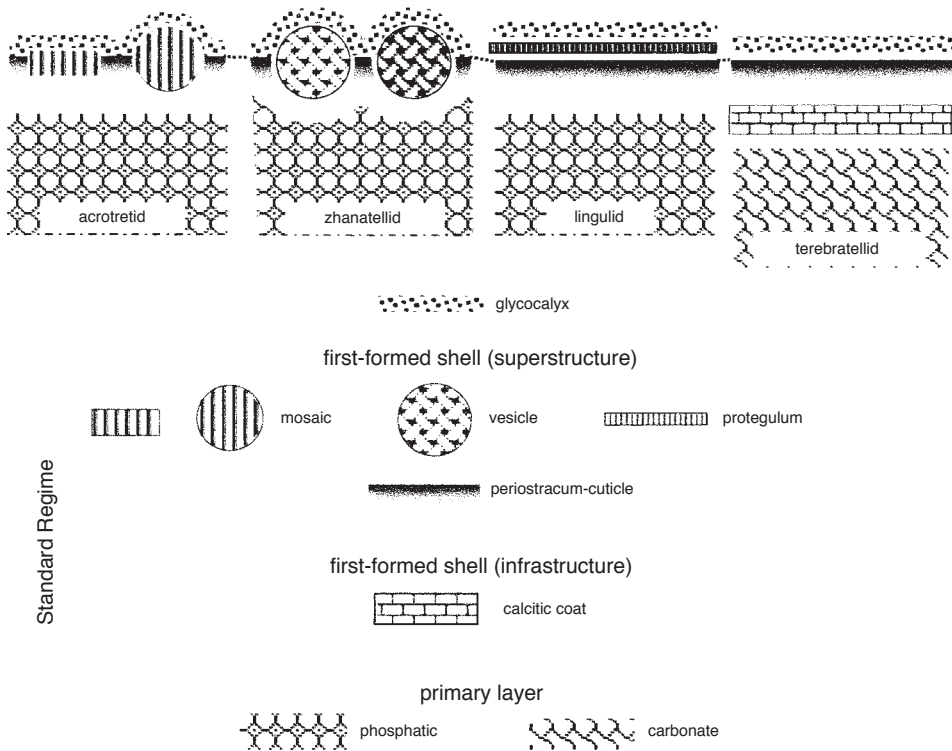
F<small>IG</small>. 1575. Graphical representation of full range of superstructures and infrastructures of brachiopod juvenile shell (standard secretory regime) as secreted relative to a correlated periostracal or cuticular base in four main types of successions (new).

and cemented together by penecontemporaneous exudations of a polymerizing periostracal cuticle as in living discinids. Yet there are two disconcerting aspects to such an extraordinary juvenile, superstructural, secretory regime. The tablets have varied in composition for they are demonstrably siliceous (discinids) and apatitic (arguably infrastructural in zhanatelids) but were inferentially calcitic in acrotretides and some lingulides. Morever, even if the mosaics of lingulide acrotheloids are plesiomorphously linked with those of acrotretides, the inferred calcitic mosaics of linguloid paterulids and siliceous mosaics of discinids were secreted by independently activated regimes.

Homoplasy also obscures relationships among lingulides with vesicular imprints. Apart from evidence that vesicles originally differed at least in the thickness and rigidity of their coats, their imprints on mature parts of shells indicate that they were constituents of fully developed periostraca and had been secreted by the vesicular cells of the outer mantle lobes (as in the zhanatellid, *Wahwahlingula*). According to this interpretation, the collective responsible for the secretion of a vesicular juvenile shell would have been cytologically homologous with those in the mature outer mantle lobe. It is, therefore, a moot point whether juvenile vesicles were secreted with the periostracum acting as a penecontemporaneous cement. We prefer this interpretation (Fig. 1572) and assume that such shells were nodular *in vivo*.

The deformable imprints of paterinates are unique among the Brachiopoda. They are unlikely to have been made by vesicles, but the conjecture (see p. 2418 herein) that they accommodated thornlike structures

with basal pits occupied by fibrils is just one of several possible interpretations.

The infrastructural secretion of the first-formed shells of living craniids and terebratulides is not in phase with the superstructural secretion of lingulate mosaics (Fig. 1575). Secretion of mosaics continues during growth of the brephic shell of discinids until the planktotrophic larvae settle. Secretion of the infrastructural first-formed shell does not continue during the brephic shell growth of craniids and terebratulides but ceases as the lecithotrophic larvae settle. Accordingly it seems that the partition of shell secretion during ontogeny into two distinct regimes coincides with a change from a planktonic to a benthic mode of life. There then remains the possibility that chemicostructural differences between juvenile and mature shells reflect different functions of the respective mineralized covers during mobile and sedentary modes of life.

MATURE SHELL OF BRACHIOPODS
INTRODUCTION

The mature brachiopod shell is that part of the integument secreted by the mantle, a fold of epithelium that is first differentiated during brephic growth. The fold is marginally indented by a circumferential periostracal groove separating the outer, skeleton-secreting and inner, ciliated, epithelial sheets (WILLIAMS & others, 1997, p. 9). The outer epithelium secretes the periostracum, which is succeeded inwardly by the mineralized primary, secondary, and rare tertiary layers (WILLIAMS, 1997, p. 267). The diversity of mantle and shells has been extensively described in Volume 1. New data include: a more precise correlation of periostracal successions; a better understanding of the basic, mineral units of organophosphatic and organocarbonate shells, especially unit aggregation in relation to associated organic constituents; and a clearer picture of the origin and evolution of many shell textures. Apart from the ever-present periostracum and primary mineralized layer, there are

three fabrics of the secondary mineralized shell to be considered: organophosphatic stratiform, organocarbonate tabular laminar, and organocarbonate fibrous. They will be reviewed in that order.

PERIOSTRACUM

The term periostracum has always been used for the outermost coat of the brachiopod shell, which can be up to 100 μm thick and is entirely organic in most species (WILLIAMS & others, 1997, p. 12). The organic constituents are varied and universally include polysaccharides and proteins according to standard staining techniques. β-chitin, however, has a restricted distribution. It is identifiable by Pyrolysis MS in the periostraca of living linguliforms, but there are no traces of it in the periostraca (or even the shells) of representative living craniiforms and rhynchonelliforms (WILLIAMS, LÜTER, & CUSACK, 2001).

The periostracum may also be multilayered, and confusion can arise when attempting to correlate different periostracal successions. Confusion is minimized by recognizing a bilamellar or electron-dense sheet separating superstructural and infrastructural features as a datum horizon (periostracal substratum). The substratum, up to 20 nm or so thick, is always present, being the first constituent of the periostracum to be secreted. It serves therefore as a substrate for both superstructural and infrastructural features. Recent studies of the tripartite periostracum of living lingulides have shown that it has a dual origin. The concentric, scalloped ridges forming the superstructure of the discinid periostracum (Fig. 1576f) consists of up to 100 or more, well-ordered fibrillar sheets disposed almost parallel with the periostracal substratum (WILLIAMS & others, 1997, p. 102; Fig. 1576a–c). The ridges, which are separated from one another by flat zones of several sheets, are commonly corrugated into dark and light strips approximately 80 nm wide and orthogonal to the substratum. The origin of this superstructure is revealed at and near the junction between

the outer, nonciliated inner epithelium and the inner, vesicular epithelium of the inner and outer mantle lobes respectively (Fig. 1576a–b). Here fibrils, probably chitinous, are spun out from the inner epithelium and fabricated by microvilli into sheets that are constantly applied to the substratum, originating as a secretory product of the vesicular cells at the hinge (Fig. 1576b, 1576d–e). The sheets are fashioned into concentric ridges by rhythmic contractions of the microvilli. This dual system of secretion also accounts for the formation of the pellicle that is loosely connected to the substratum of lingulids. In *Glottidia*, for example, the pellicle is a compacted sheet of fibrils secreted by the microvilli of the inner epithelium and exceptionally bears imprints of the microvillous tips (Fig. 1577). In effect, the superstructures of mature periostraca of all brachiopods are secreted by nonciliated epithelium of the inner mantle lobe and the periostracal substratum and infrastructures by the lobate or vesicular cells of the outer mantle lobe. This dual system of secretion is at variance with the correlation of periostracal successions shown in figure 9 of Volume 1 (Williams & others, 1997, p. 16; an amended version is given herein (Fig. 1578).

Evidence for a dual secretion of the periostracum also helps to clarify the sources of imprints on both juvenile and mature shell surfaces of some lingulides (like zhanatellids) and paterinates (*Askepasma*). Assuming that the juvenile cuticle correlates with the periostracal substratum, the vesicles that made such imprints could not have been secreted by an inner epithelial collective overlying the juvenile shell and must have been infrastructural in origin.

ORGANOPHOSPHATIC SHELL

In Volume 1, the stratiform nature of the organophosphatic shell was described, as were its basic constituents, granular fluorapatite in diverse aggregations, and various intercrystalline and paracrystalline polymers, notably proteins, GAGs, and β-chitin. Emphasis was given to reconciling previous chemicostructural studies that had described and interpreted the stratiform, laminar successions in conflicting ways. The rheological properties of the primary layer were characterized. The rhythmic nature of most of the laminar sets of the secondary layer was clarified, and a standard terminology was proposed, based on the laminar successions of the living *Lingula* shell. Several fabrics were also described, including those of extinct groups. More recent investigations have afforded not only new information in all these different fields but also a feasible phylogeny for the more important fabrics. Such advances are described below, first with respect to the rheological properties of the primary layer and the canaliculate system characterizing most lingulates. This is followed by a review of new data on the fabrication of the basic constituents, especially in baculate, virgose, and columnar laminar sets, before dealing with the more problematic fabrics.

The primary layer is the initial coat of biominerals laid down on the periostracum as a foundation for the more elaborate fabrics of the secondary shell. Its rheological properties are such that the layer can be deformed by concentric folds (fila) and lamellose extensions without developing planes of disruption within the secondary layer. These surface ornamentations are common features of linguliforms, and their development

---

Fig. 1576. Secretion, structure, and morphology of mature periostracum of Recent *Discinisca* sp. cf. *tenuis* (Sowerby), Swakopmund, Namibia; scalloped ridges (*sr*) constituting superstructure (view *f*) consist of fibrillar sheets (views *a–c*) secreted by microvilli (*ms*) of inner epithelium (*ie*) (views *a, d–e*) on periostracal substratum (*pe*) (view *c*) that originates as a secreted layer of vesicular cells (*vr*) at hinge of inner and outer mantle lobes (views *a–b*); scale bars: 300 nm, 200 nm, 100 nm, 200 nm, 100 nm, and 1 µm (new).
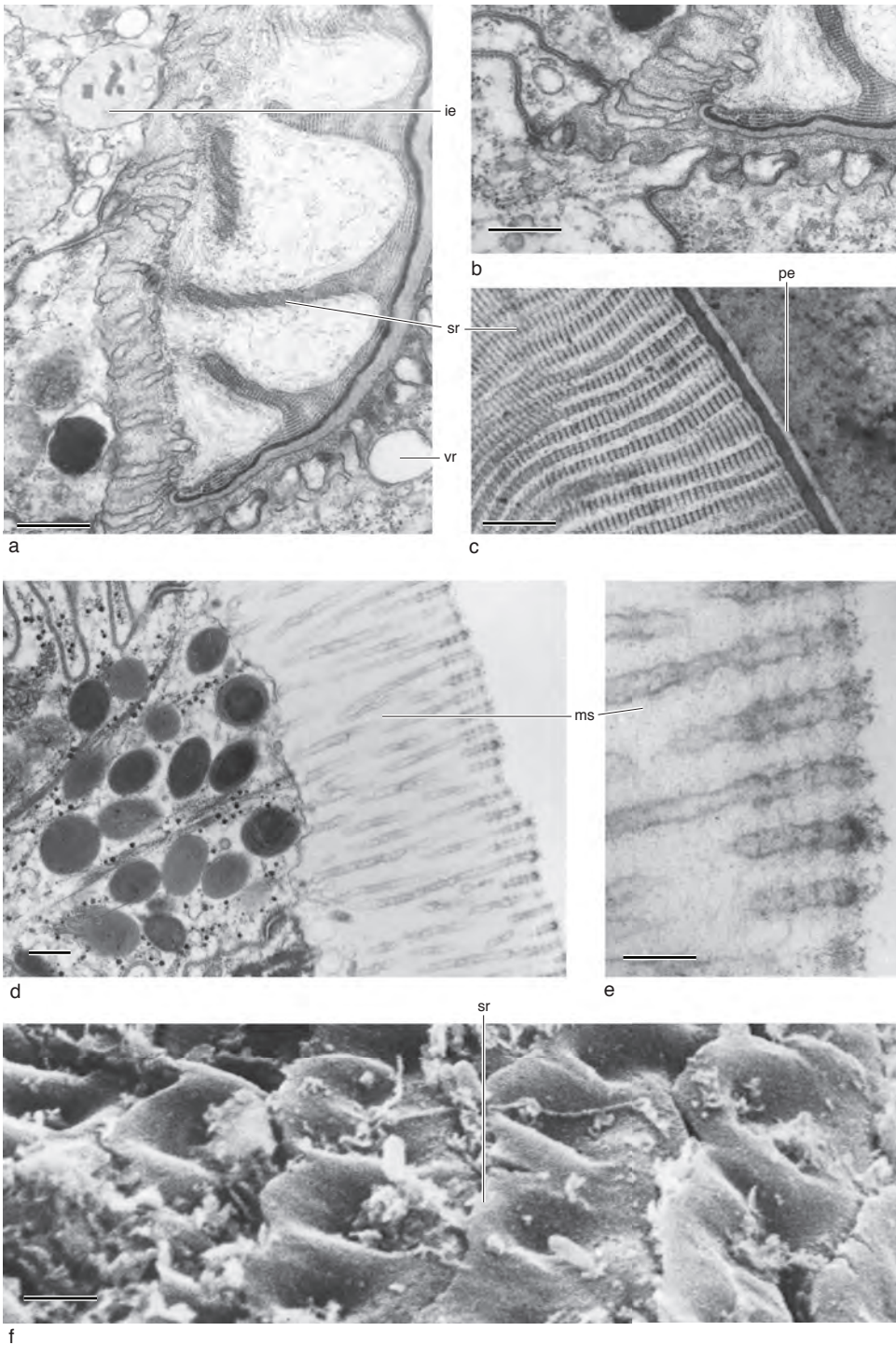
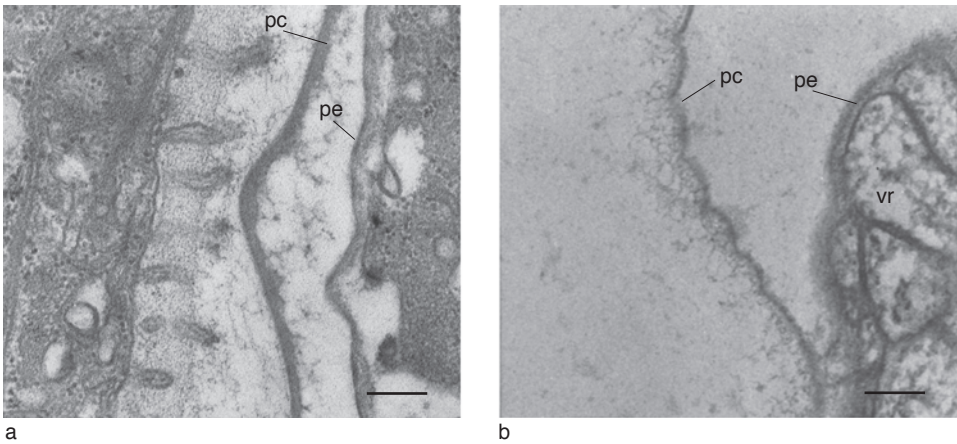FIG. 1576. *For explanation, see facing page.*

FIG. 1577. Two TEM sections of near proximal sectors of periostracal groove of *Glottidia pyramidata* (STIMPSON) (see fig. 7 in WILLIAMS & others, 1997) showing *a,* pellicle (*pc*), bearing imprints of secreting microvilli of inner epithelium (*pe*) in *b,* in relation to periostracal substratum (*pe*) secreted by vesicular cells (*vr*); scale bars: 100 nm (new).

has been studied in *Discinisca* (WILLIAMS, CUSACK, & BRUNTON, 1998, p. 2016).

Lamellae, which may extend for several millimeters beyond the curvature of a valve, are composed of periostracum and primary and outermost secondary layers. On the outer surface of a lamella, a periostracum and primary layer form folds induced by variations in the disposition of the outer mantle lobe and in the rate of shell secretion.
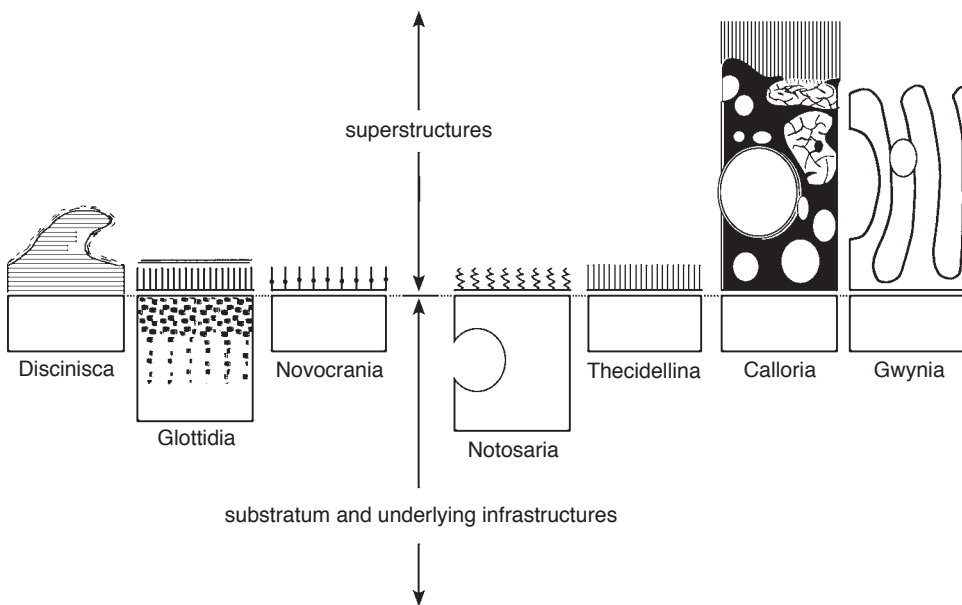

FIG. 1578. Amended version of figure 9 in WILLIAMS and others (1997) showing various stylized brachiopod periostracae correlated in relation to periostracal substrata (*thickened lines*) that serve as a substrate for organic structures secreted by inner epithelium (superstructures) and lobate and vesicular cells of outer mantle lobes (infrastructures) (adapted from Williams & others, 1997).

Immediately internal of a fold (Fig. 1579), a sequence of stratified laminae of the outermost secondary layer splits into two, which diverges within the core of the fold to form a wedge with the primary layer coating its outer face. The wedge is filled by an organic mesh with apatitic spherules deposited by an inframarginal band of the outer mantle lobe simultaneously with the secretion of periostracum and primary layer at the tip of the lobe. This same secretory regime gave rise to even the most conspicuous fila, such as those of *Schizotreta* (see Fig. 1596).

Several folds may develop before a lamellar extension is terminated. The termination is marked by a sudden retraction of the mantle so that no periostracum nor primary layer is deposited along the ledge or on the inner surface of a lamella; and their secretion begins again only when they form the outer coat of the next lamella (Fig. 1579). This process of accelerated forward growth terminated by sudden retraction of the outer mantle lobe is similar to that giving rise to lamellae in organocarbonate-shelled brachiopods (WILLIAMS, 1971, p. 61), although no proteinaceous coats covering the inner surfaces of the *Discinisca* lamellae have yet been found.

CANALS

Canals, originating within the primary layer or at its interface with the secondary layer (WILLIAMS, BRUNTON, & MACKINNON, 1997, p. 343) and orthogonally disposed to lamination, permeate the shells of living lingulids (WILLIAMS, CUSACK, & MACKAY, 1994, p. 251) and discinids (WILLIAMS, CUSACK, & BRUNTON, 1998, p. 2013–2015). The two canal systems differ in detail but grow in the same way and are homologous so that the better known discinid canal system can be taken as typical, at least of the lingulides.

In *Discinisca* (WILLIAMS, CUSACK, & BRUNTON, 1998), the canals, being approximately 350 nm in diameter, are densely distributed and frequently branch into parallel sets coalescing inwardly, with
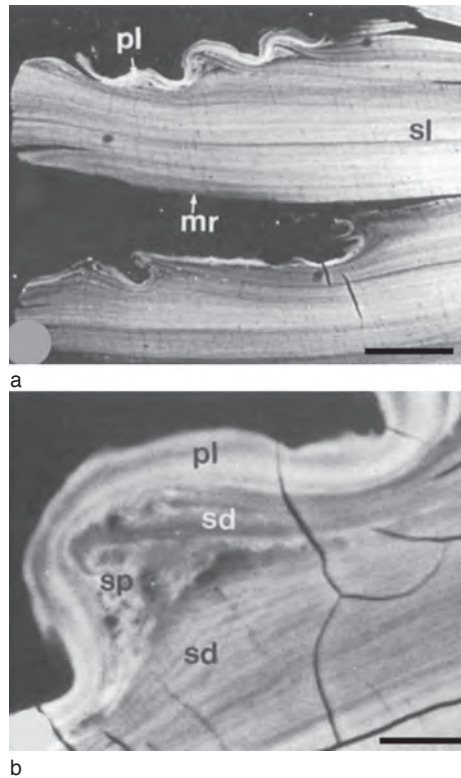
a

b

FIG. 1579. Back-scattered electron micrographs of polished vertical resin-impregnated section, treated with bleach, showing concentric lamellae on shell surface of *Discinisca lamellosa; a,* general view of two lamellae with rheomorphic folding of periostracum and primary layer (*pl*) relative to secondary layer (*sl*) and trace of mantle retraction (*mr*); scale bar: 50 μm; *b*, detail of rheomorphic fold showing continuity of periostracum and primary layer (*pl*), divergence of stratified laminae (*sd*) at steep outer face of fold and infill of spherular apatite in organic mesh (*sp*); scale bar: 10 μm (Williams, Cusack, & Buckman, 1998).

approximately 20 apertures per 100^2 μm of a dorsal interior. The canals are enmeshed in a chitinous and proteinaceous matrix. Galleries and chambers containing GAGs (Fig. 1580) with apatitic concretions are commonly enlarged around groups of canals. In *Discina* the wall and contents of a canal are secreted simultaneously with the laminar succession perforated by it. They are extruded from the same site on the apical plasmalemma and can usually be traced through several laminar sets in a vertical section (Fig. 1581).
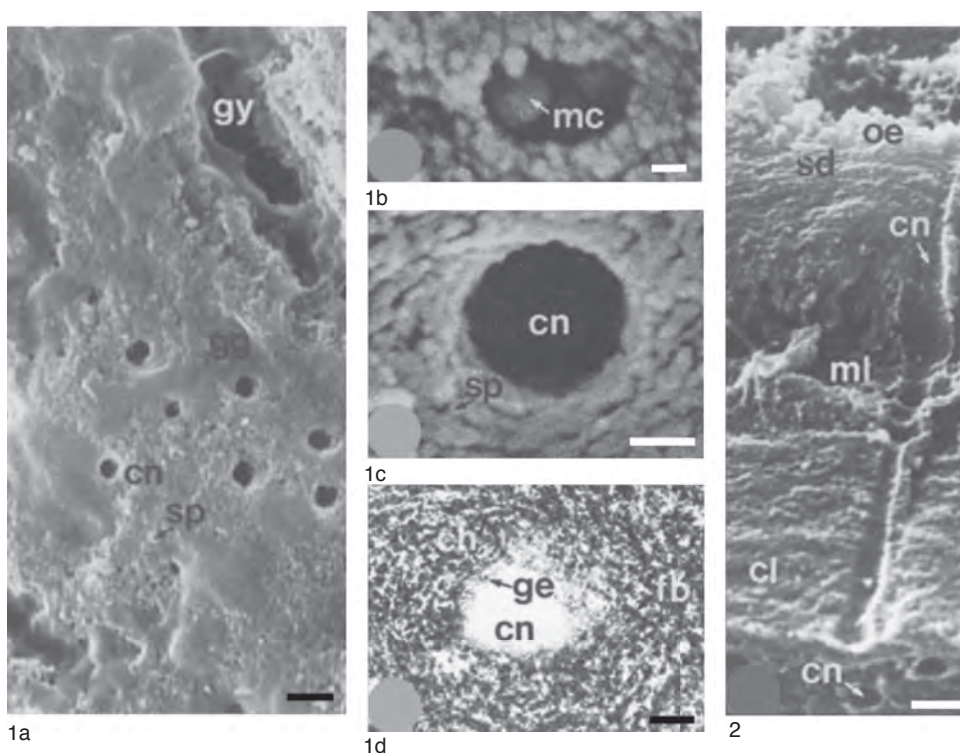
Fig. 1580. Scanning (*1a–c, 2*) and transmission (*1d*) electron micrographs of sections and interiors of *Discinisca tenuis* (*1a–d*) and *Discina striata* (*2*); *1a*, internal surface of spherular apatite (*sp*) and GAGs (*gg*) showing canal openings (*cn*) and galleries (*gy*), treated with buffer; scale bar: 1 µm; *1b*, detail of partly exposed chamber with mosaics (*mc*) in critical-point-dried vertical fracture section; scale bar: 200 nm; *1c–d*, cross sections of canals (*cn*) on internal surface treated with subtilisin and in demineralized rubbly lamina showing spherules (*sp*) and granules (*ge*) of apatite associated with electron-dense and electron-lucent fibrils that are assumed to be actin (*fb*) and chitin (*cn*) respectively; scale bars: 200 nm, 100 nm; *2*, critical-point-dried vertical fracture section of a succession of compact (*cl*), membranous (*ml*), and stratified (*sd*) laminae, secreted by outer epithelium (*oe*) and penetrated by a canal (*cn*); scale bar: 1 µm (Williams, Cusack, & Buckman, 1998).

The site of origin is marked by a lens of electron-dense fibrils and granules with a glycogen-rich cytosol immediately beneath the apical plasmalemma and its overlying recumbent tubular extensions that may be up to five deep. Tubules secreting the shell contain electron-lucent particles and fibrils. They show no signs of having been deflected by growing canal columns, suggesting that they are more or less permanently arranged into a flexible ring about the secretory site of a canal.

A typical canal has two structural aspects dependent on the composition of the surrounding laminae (Fig. 1580). In miner-alized laminae, a canal is relatively narrow with a diameter of approximately 200 nm. Externally its membranous wall bears apatitic spherules and internally fibrils and rare spherules. The contents of a canal are also membrane bound and divided into unequal segments by perforated, transverse partitions (compare the partitions in *Lingula;* WILLIAMS & others, 1997, fig. 38, p. 44). In a predomi-nately organic lamina, a canal rapidly widens in diameter to 750 nm or more (Fig. 1580). Its wall consists internally of hoops less than 100 nm wide and may bear rare apatitic spherules. The hoops comprise alternating bands of electron-lucent and darker, beaded

lineations and are presumably chitinous. The external surface of the wall supports a dense mesh and more rare strands, presumably chitinous and proteinaceous, linking canals as in *Lingula* (WILLIAMS & others, 1997, fig. 21.1, p. 28).

The inferred function of the homologous canal systems permeating the shell of living lingulids and discinids has to be compatible with several aspects of their origin and growth. These include the following: the initiation of canals on the outer surface of the outer mantle lobe and their persistence throughout shell growth; the synthesis of annulated canal walls from persistent electron-dense, fibrous lenses just proximal of apical plasmalemmas of the outer epithelium; and the secretion of the canal system simultaneously with proteinaceous and chitinous networks of fibrils pervading the shell (Fig. 1582).

These criteria suggest that canals serve as vertical struts interconnecting with proteinaceous and chitinous nets to form an organic scaffolding in support of the stratiform successions of the shell. Indeed, laminar support seems to be the only feasible function. Unlike the large, papillose evaginations (caeca) of the mantle into the calcitic shells of punctate brachiopods, which serve as storage centers, no distinctively stored compounds have been found in canals. Only sporadic traces of shell constituents, degraded vesicular membranes, and myelin figures, periodically sealed by transverse membranes, have been identified. In structural terms, therefore, this canaliculate framework is to the organically rich lingulide shell what the cytoskeleton is to the cell.

In living lingulids, apatitic spherules seldom adhere to canal walls and do not aggregate into a mineralized coat (Fig. 1583). Consequently, traces of canals are rarely found in fossil lingulides except as perforations of compact laminae (Fig. 1584). The columnar fabric of some early linguloids and most acrotretides is possibly a mineralized canal system, but whether it is homologous
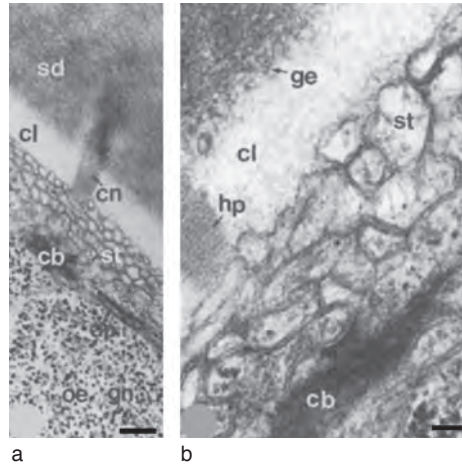

FIG. 1581. Transmission micrographs of canals in shells of *Discinisca tenuis; a,* demineralized section of integument showing relationship of a canal (*cn*) to a succession of stratified (*sd*) and compact (*cl*) laminae, secreting tubular extensions (*st*) of apical plasmalemma (*ap*) of outer epithelium (*oe*) rich in glycogen (*gn*) and electron-dense fibrillar source (*cb*) of canal; scale bar:1 μm; *b,* detail of a hooped lining (*hp*) of a canal in relationship to a compact lamina (*cl*) with proteinaceous coated granules (*ge*), a zone of tubular extensions of apical plasmalemma (*st*) and its source (*cb*); scale bar: 100 nm (Williams, Cusack, & Buckman, 1998).

with the canaliculate framework of lingulides will be considered later.

BACULATE AND VIRGOSE SECONDARY LAYERS

The chemicostructure of living lingulid shells has been adopted as a standard for organophosphatic brachiopods because it includes two of the five main fabrics and most of the textures of the linguliforms as a whole. The textures and fabrics, identified in Figure 1585, are defined in Volume 1 (WILLIAMS & others, 1997, p. 24–32) but rhythmic sets (recurrent laminar sequences) as well as baculate and virgose fabrics require further consideration.

The laminar sets of the secondary shell of lingulids and discinids are rhythmically disposed (e.g., the four identified in Fig. 1585). Rhythms are frequently complicated by the repeated secretion of a lamina(e) or
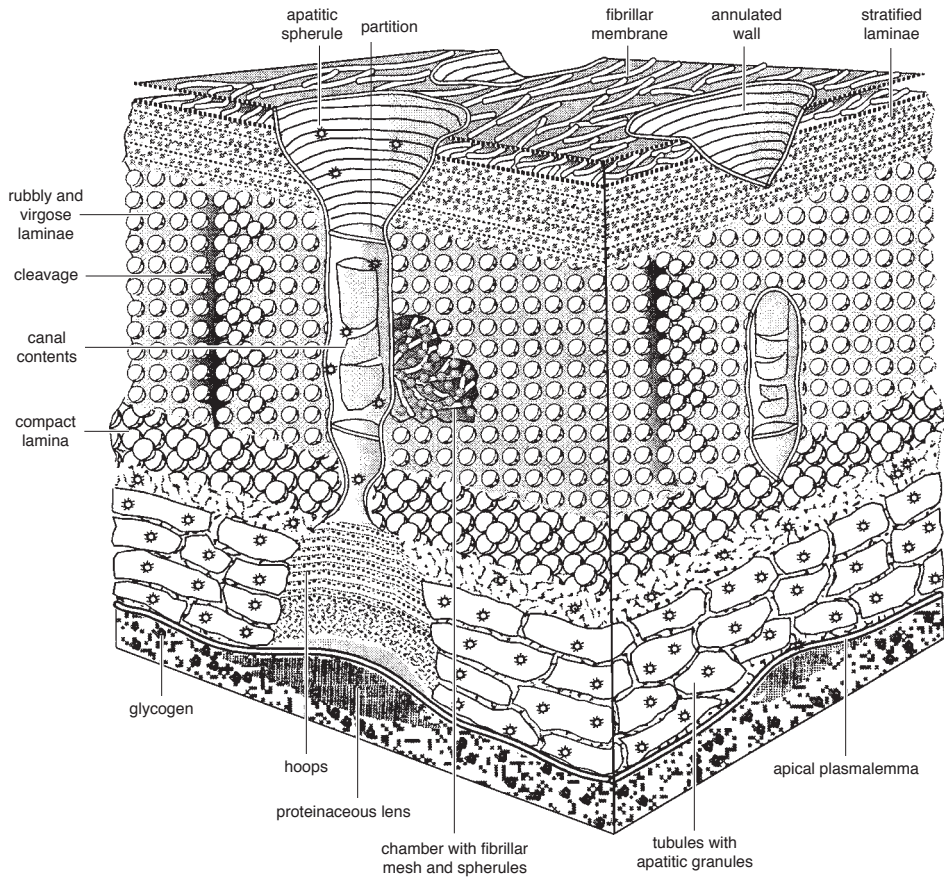
Fig. 1582. Stylized representation, at various magnifications, of secretion of discinid and lingulid canals and main structural changes affecting them in different kinds of lamination (Williams, Cusack, & Buckman, 1998).

by the omission of a lamina(e) characterizing the full cyclical suite. There is also ambiguity on how best to define a rhythm. The convention has been to identify the onset of a rhythm as the base of a graded sequence, which is in sharp contact with a different deposit, normally the same as the top of the graded sequence. In living lingulides, the sharpest interface is between a predominantly organic or membranous lamina and an apatitic, compact lamina. In *Lingula*, such a rhythmic sequence begins with a compact lamina grading inwardly into an increasing organic sequence containing botryoids and rods of apatite (virgose fabric), terminating in a membranous lamina that acts as the substrate for the succeeding rhythmic succession.

The rhythm of *Glottidia* is similar to that of *Lingula*, assuming that the baculate laminae of *Glottidia* are correlatives of the botryoidal, rubbly, and virgose laminae of *Lingula*. In the medial part of a valve, the typical rhythm begins with a compact lamina permeated by canals. The compact lamina grades inwardly into a baculate zone that may become gradually less biomineralized inwardly or more abruptly terminated by membranes serving as a substrate for the compact lamina of the succeeding rhythmic set. This rhythm is also characteristic of the highly inclined baculate sets toward the valve margin. The grading of baculate sets may be interrupted by sheets, presumably β-chitin, that are coated with granular apatite to form stratified lamination. The growth of baculi
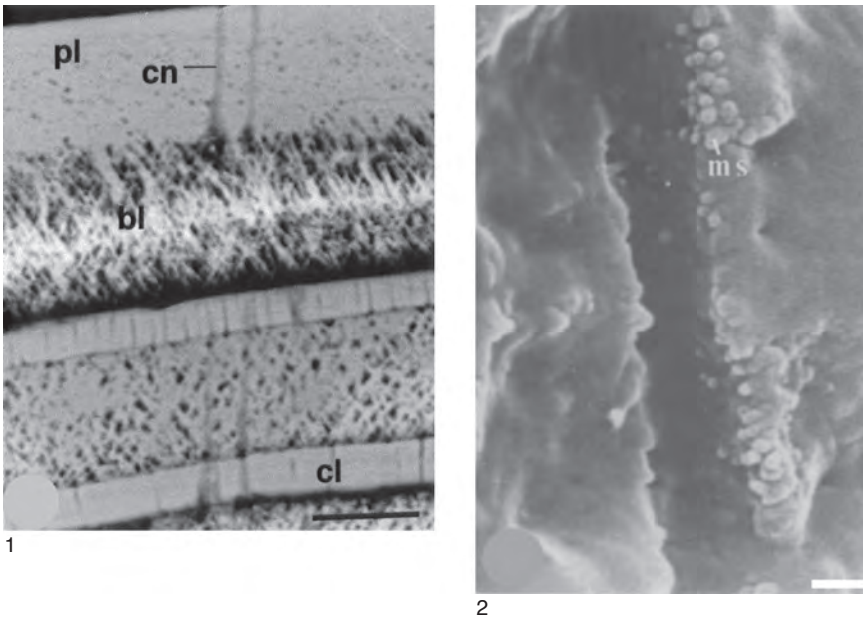
FIG. 1583. *1*, Back-scattered electron micrograph of polished transverse section of dorsal valve of Recent *Glottidia palmeri* DALL digested by subtilisin. Electron back-scatter image shows distribution of apatite (*white*) and organic (*grey* to *black*) constituents with primary layer (*pl*) to top and secondary graded baculate sets including compact (*cl*) and baculate (*bl*) laminae traversed by canals (*cn*); scale bar: 25 µm (Williams & Cusack, 1999); *2*, SEM of gold-coated vertical posteromedian section of valve of shell of *Lingula anatina*, digested with endoproteinase Glu-C, revealing canal wall studded with mosaics (*ms*) in botryoidal lamina; scale bar: 0.5 µm (Williams, Cusack, & Mackay, 1994).

can also be aborted into short rods similar to the virgose lamination of *Lingula,* and even reversals of the cycle can occur. Overall, however, the sets are asymmetrical for they almost invariably grade from biomineral-rich to organic-rich laminae (and only rarely vice versa).

In discinids, on the other hand, the dominant rhythm is the reverse with a wholly (or mainly) organic sequence grading inwardly through a baculate lamina into a compact lamina, abruptly succeeded by a membranous lamina marking the base of the succeeding rhythmic sequence.

Although laminar diversity has been described in Volume 1, two textural aspects of the secondary shell merit comment. Ellipsoids up to 1 µm long and 150 nm thick and disposed parallel with lamellar boundaries are confirmed as basic spherular aggregates of the secondary shell. They are mostly featureless, but degradation reveals outlines of apatitic spherules arranged linearly (Fig.

1586a). As these ellipsoids are scarcely digested by subtilisin, it is assumed that their coats (capsules) are not exclusively proteinaceous. Moreover, ellipsoidal capsules of other *Lingula* shells are degraded by bleach to reveal linear arrangements of apatitic spherules (Fig. 1586b). This differentially induced degradation suggests that capsules are composed predominantly of a polysaccharide like β-chitin or some other constituent of GAGs (WILLIAMS & others, 2000a, p. 1003). This texture is also found in discinids where spherules normally aggregate in hexagonal, close-packed arrangements (Fig. 1587). Aggregates, however, may also interlock like platy jigsaws or more rarely form ellipsoids with capsules (Fig. 1587; WILLIAMS, CUSACK, & BRUNTON, 1998, p. 2008).

The other textural detail especially relevant in assessing the effects of fossilization is cleavage, which is a common texture of shells of living species (WILLIAMS, CUSACK,
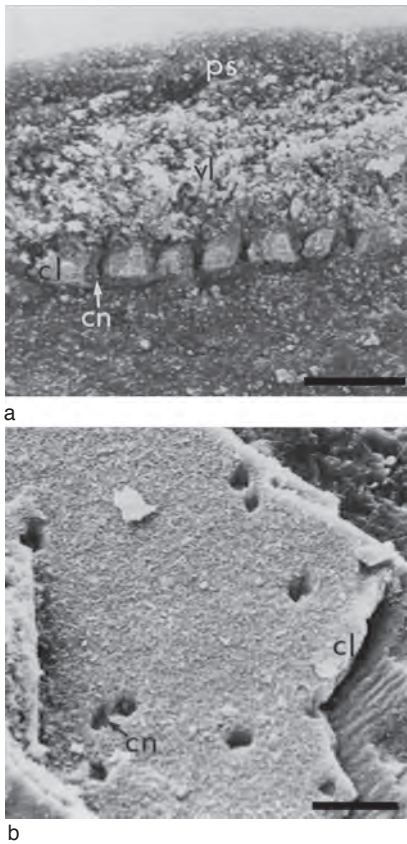
FIG. 1584. SEMs of gold-coated fracture sections of valves of *Lingula squamiformis,* Calderwood, Scotland; *a*, compact lamina (*cl*) perforated by canals (*cn*) and underlying standard outer succession of primary layer (*ps*) and virgose lamina (*vl*); scale bar: 5 μm; *b*, external surface of compact lamina (*cl*) perforated by canals (*cn*); scale bar: 10 μm (Cusack & Williams, 1996).

& BRUNTON, 1998, p. 2009). In fracture sections of discinids, for example, vertical cleavage can affect successions of compact and rubbly laminae (Fig. 1588). The cleavage appears to be related to the distribution of GAGs that are impersistent and sheetlike in the former and more pervasive and bulky in the latter laminae. The thicker compact lamina is more highly and obliquely cleaved, with successive sets of cleavage planes opening in opposite directions. In that part of the succession where the lamina becomes rubbly, a coarser, vertical cleavage predominates. Evidently dehydration of GAGs has an important role in inducing planes of weakness that probably influence the cleavage patterns of fossilized lingulides.

BACULATE LAMINATION

Baculate lamination is preeminently characteristic of lingulides, but the arrangement and structural constituents of baculi in the shells of living lingulids and discinids are different. In the lingulid *Glottidia pyramidata* the secondary shell contains lenses of baculate sets up to 25 μm or so thick. A lens is normally bounded by membranes of protein and β-chitin (Fig. 1589) and contains apatitic ovoids that tend to be linearly organized into baculi up to 750 nm in diameter but commonly more than 10 μm long. Pinacoidal plates orthogonally aligned by epitaxy or screw dislocation can also form baculi (Fig. 1589). The baculi are usually inclined at about 60° to the bounding surface but range in disposition from the vertical to the near horizontal. As aggregates of spherular apatite, the ovoids and ellipsoids are homologues of the spheroidal botryoids of *Lingula* (WILLIAMS & others, 1997), but in addition to their different shape, the *Glottidia* ellipsoids are normally indented at their poles by depressions approximately 30 nm in diameter that may represent traces of axial organic threads. The baculi as well as discrete apatitic spherules and ellipsoids are immersed in GAGs and enmeshed in organic strands that form an intricate web arising from the organic coats of canals and the bounding membranes of β-chitin (Fig. 1590). The fibrous web is structurally and functionally akin to the cytosol framework, and the polymer has been identified as an actinlike protein (CUSACK & WILLIAMS, 1996, p. 47). The web, however, resists digestion by proteinase-K and subtilisin, raising the possibility that it is mainly chitinous. The membranes may also serve as substrates for compact laminae composed of tightly packed, spherular aggregates up to several micrometers thick.

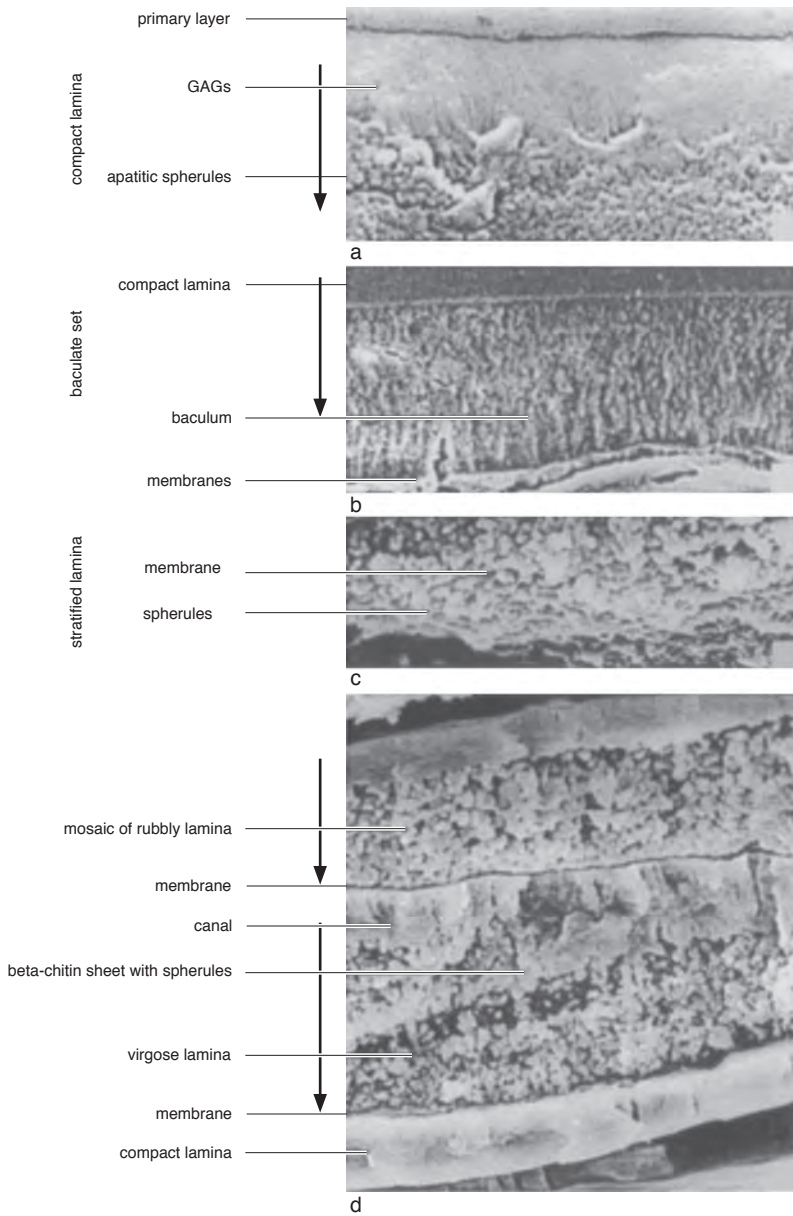A transverse section of the midregion of a mature dorsal valve of *G. palmeri* shows

Fig. 1585. Montage of SEMs of shell of *Glottidia pyramidata* (Stimpson) showing principal lingulide microfabrics; *a*, fracture section treated with phosphate buffer (100 mM, pH7), ×18,000; *b*, polished section of valve mounted in London resin, ×700; *c–d*, fracture sections digested in subtilisin (50 μM in phosphate buffer, 100 mM, pH7), ×3000, ×2000 respectively (Cusack, Williams, & Buckman, 1999).

the full differentiation of the *Glottidia* succession (Fig. 1591). The primary layer is underlain by approximately 20 μm of stratified laminae grading inwardly into a baculate zone. The first-formed baculate sets in the posteromedial region are like gently concave saucers with tapered rims. With further shell growth, outwardly successive baculate sets become more steeply inclined so that in the marginal transverse section
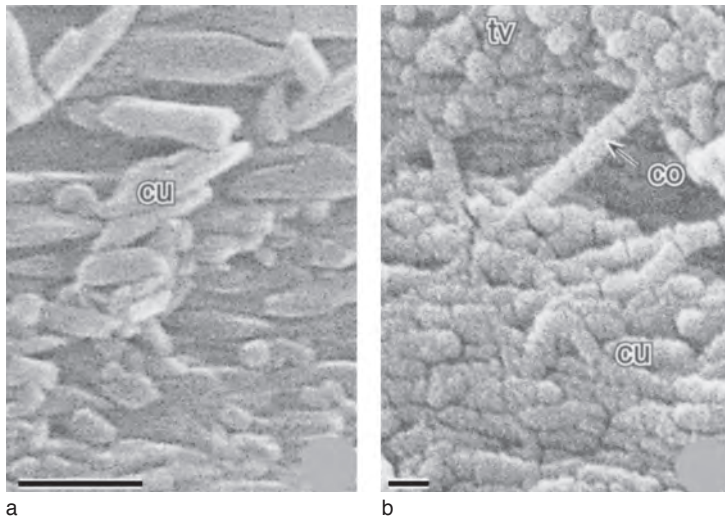
FIG. 1586. *a*, SEMs of scissor-cut, vertical sections of *Lingula parva* SMITH, West Africa, ZB 1533, digested in subtilisin. Detail of walled laminae showing capsules (*cu*) of apatitic spherules, dislodged by enzymic digestion; scale bar: 0.5 μm; *b*, SEM of vertical fracture section of *Lingula anatina* LAMARCK, Japan, digested in subtilisin. Detail of compact laminae showing linear arrangement of capsules (*cu*) composed of spherules with sporadically cross-striated collagen (*co*) and succeeding layer of capsules in transverse sections (*tv*); scale bar: 0.1 μm (Williams & others, 2000).

of a valve they appear as sigmoidal strips between the increasingly diverging zone of primary and stratified secondary shell and an internal zone of compact apatite.

The internal zone is composed of apatite pervaded by canals orthogonal to the inner surface and is a condensed succession of compact laminae alternating with thin to
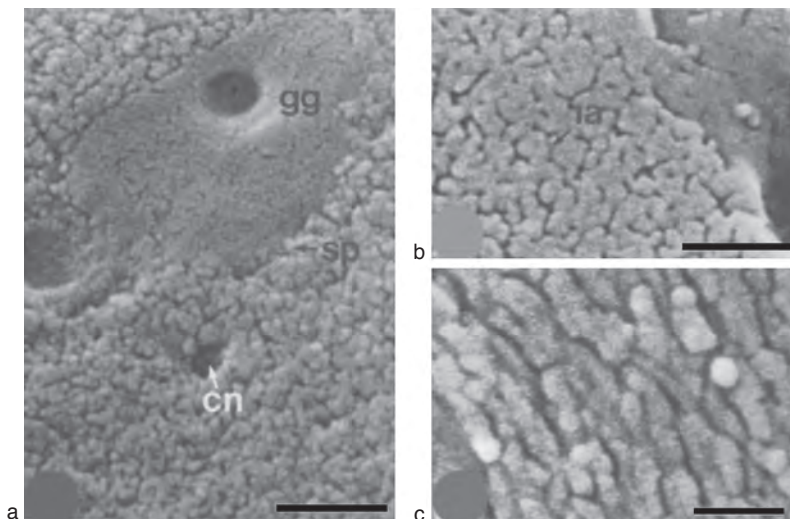

FIG. 1587. SEMs of structural components of shell of *Discinisca tenuis; a–b*, gold-coated internal surfaces treated with buffer, showing spherular (*sp*) and interlocking (*ia*) apatite, canals (*cn*), and GAGs (*gg*); scale bars: 0.5 μm; *c*, internal surface treated with proteinase-K showing rods of spherular apatite; scale bar: 250 nm (Williams, Cusack, & Buckman, 1998).
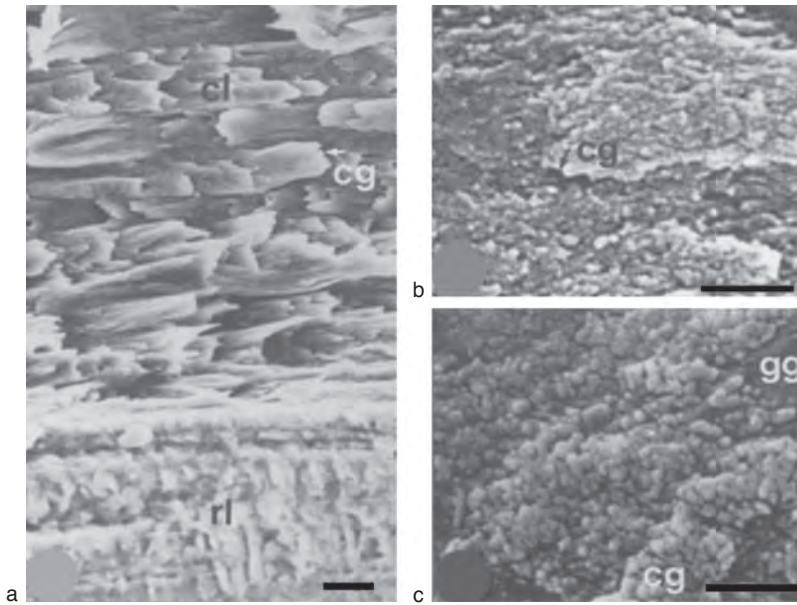
FIG. 1588. *a–c,* SEMs of secondary layer of shell of *Discinisca tenuis; a,* vertical fracture section treated with subtilisin and showing effects of distribution of GAGs on cleavage (*cg*) in compact laminae (*cl*); rubbly laminae (*rl*); *b–c,* enlarged; GAGs (*gg*); cleavage (*cg*) scale bars: 10 μm, 0.5 μm, 0.5 mm respectively (Williams, Cusack, & Buckman, 1998).

impersistently lenticular intercalations with a high organic content (Fig. 1591; CUSACK, WILLIAMS, & BUCKMAN, 1999, p. 818). This zone has been identified as the inner zone in the shell of living discinids (IWATA, 1982, p. 960) and as a tertiary layer in fossil linguloids (HOLMER, 1989, p. 33). The intercalations within the internal zone, however, sporadically swell into baculate lenses. They and their bounding compact laminae are evidently the more medial correlatives of the overlying baculate sets. The internal zone is, therefore, as much a part of the secondary layer as the baculate sets and the stratified laminae underlying the primary layer.

Toward the valve margin the increasing inclination of baculate sets relative to the primary and outer secondary layers is an expression of allometric growth (Fig. 1591). At the margin of a mature valve, especially laterally where the vertical components of the growth vector become increasingly important, baculate sets may be inclined by as much as 60° to the external layer of primary and stratified secondary shell. The

space within this outwardly facing baculate front and the inwardly curling marginal fold of periostracum and primary shell (Fig. 1591) contains the outer mantle lobe (and the periostracal lobe). The entire lobe, which is shaped rather like a rounded prism up to several hundred micrometers wide, contains the protractor muscle system responsible for the protrusion of setae. The lingulid outer lobe is unique among living brachiopods; and highly inclined secondary lamination at the shell margins of fossils is indicative of the *in vivo* presence of this kind of lobe.

The baculate shell structure of extinct linguloids is typified by that of the oldest known group, the obolids. A transverse section of the margin and midregion of a dorsal valve of *Obolus apollonis* showed a homogeneously, apatitic primary layer, underlain by a secondary layer composed of baculate sets (Fig. 1592). The sets were disposed as a succession of inwardly concave plates with swollen margins up to 80 μm thick. The plates were virtually separated from one another by gaps as wide
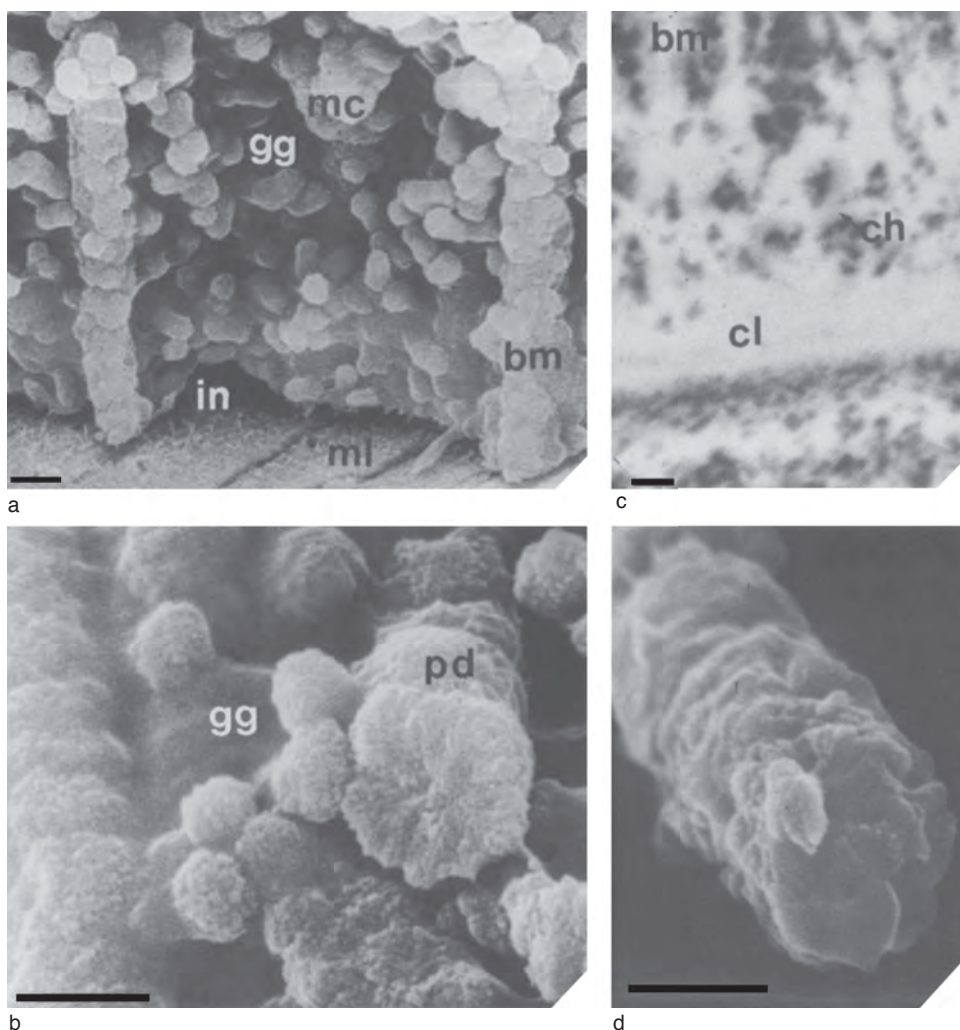
FIG. 1589. *a–b, Glottidia pyramidata*, Recent, Florida; views of baculate laminae exposed in fracture sections of body platforms of valves digested by subtilisin; *a*, baculi (*bm*) traversing mats of β-chitin coated with GAGs (*gg*) and apatitic mosaics (*mc*) at termination of a baculate set marked by interface (*in*) with a membranous lamina (*ml*) of β-chitin bearing proteinaceous strands; scale bar: 1 μm; *b*, detail of baculi showing pinacoidal epitaxis (*pd*) and mosaics associated with β-chitin mat with GAGs (*gg*); scale bar: 1 μm; *c*, detailed view in back-scattered electron micrograph of a carbon-coated, polished section of ventral valve of *Glottidia pyramidata* (STIMPSON), Recent, Florida, showing a succession of asymmetrical baculate sets underlying primary layer, with a compact lamina (*cl*) grading inwardly into trellised baculi (*bm*) transgressing apatitic-coated sheets of β-chitin (*ch*); scale bar: 5 μm; *d*, *Glottidia palmeri* (DALL), Recent, California; view of a fracture section of body platform of a dorsal valve digested in subtilisin showing detail of baculi with spirally stacked pinacoids; scale bar: 200 nm (Cusack, Williams, & Buckman, 1999).

as 500 nm, presumably the former sites of degraded membranous laminae. Eight such plates, varying in total thickness from 220 μm medially to 360 μm marginally, were composed of 27 baculate sets. The baculate sets were most fully developed marginally as inwardly tapering wedges, overlying one another en échelon and inclined at 10°–20° to the external surface. In this marginal zone, the sets were traversed by regularly disposed
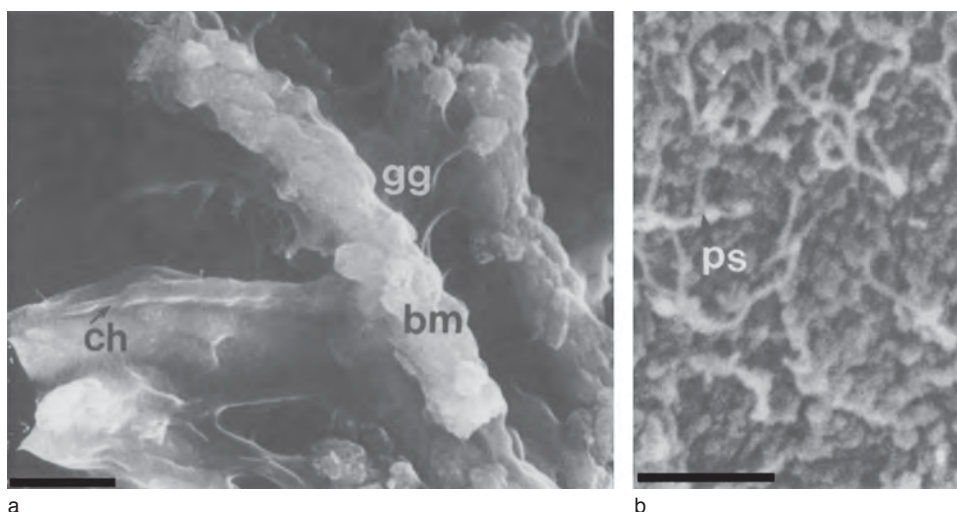
FIG. 1590. *Glottidia palmeri*, Recent, California; *a*, view of fracture section of body platform of dorsal valve digested in subtilisin with details of baculi (*bm*) transgressing β-chitin sheets (*ch*) and GAGs (*gg*); scale bar: 200 nm; *b,* anterior detail of internal surface of valve of *Glottidia pyramidata*, digested in proteinase-K, revealing proteinaceous network (*ps*) supporting apatitic spherules and mosaics; scale bar: 500 nm (Cusack, Williams, & Buckman, 1999).

trellises of baculi subtended between compact laminae (Fig. 1593). Contiguous pairs of compact laminae were separated by a break in continuity that probably represents a recrystallized, mainly organic sheet. The baculi had been recrystallized into aggregates of prismatic apatite (spherular mosaics are more prevalent in *O. transversa*). Medially, the gaps between the plates merged and the horizontally disposed sets became much thinner, mainly through the reduction of the baculate zones to a rubbly or virgose texture (Fig. 1592).

The biomineralized succession of the baculate sets of *Obolus* differs significantly from that of *Glottidia* and living discinids in being symmetrical about its medial plane with the rhythm of compact-baculate-compact laminae at the shell margins reducing to compact-virgose (or rubbly) compact laminae in midregion. The baculate sets of *Obolus* also differ in disposition from those of *Glottidia* in being uniformly gently inclined even at the shell margins. This attitude is not only an allometric consequence of the saucer shape of *Obolus* valves but also probably an indication that the marginal

lobes of the obolid mantle were less intricate than those of living lingulids and more like those of discinids in lacking a periostracal lobe.

Recent chemicostructural studies of the shells of living and extinct discinoids (WILLIAMS, CUSACK, & BRUNTON, 1998; WILLIAMS, CUSACK, & others, 1998; WILLIAMS & others, 2000a) have enlarged and clarified the information on discinid baculation in Volume 1 (WILLIAMS & others, 1997, p. 26–27). The stratiform succession of the *Discinisca* shell serves as a living model, while that of the Ordovician *Schizotreta* is typical of the Paleozoic orbiculoideid sister group of the derived discinids.

In *Discinisca*, the dominant sequence in the secondary layer consists of alternations of compact and rubbly laminae with baculate lamination restricted to the outer secondary layer within the body platform (and septum) of mature ventral valves. Here, baculi occur in rhythmic sets and are typically subtended between rubbly or compact laminae (Fig. 1594). The inner boundary of such a set may be a succession of spherular-coated membranes or a compact
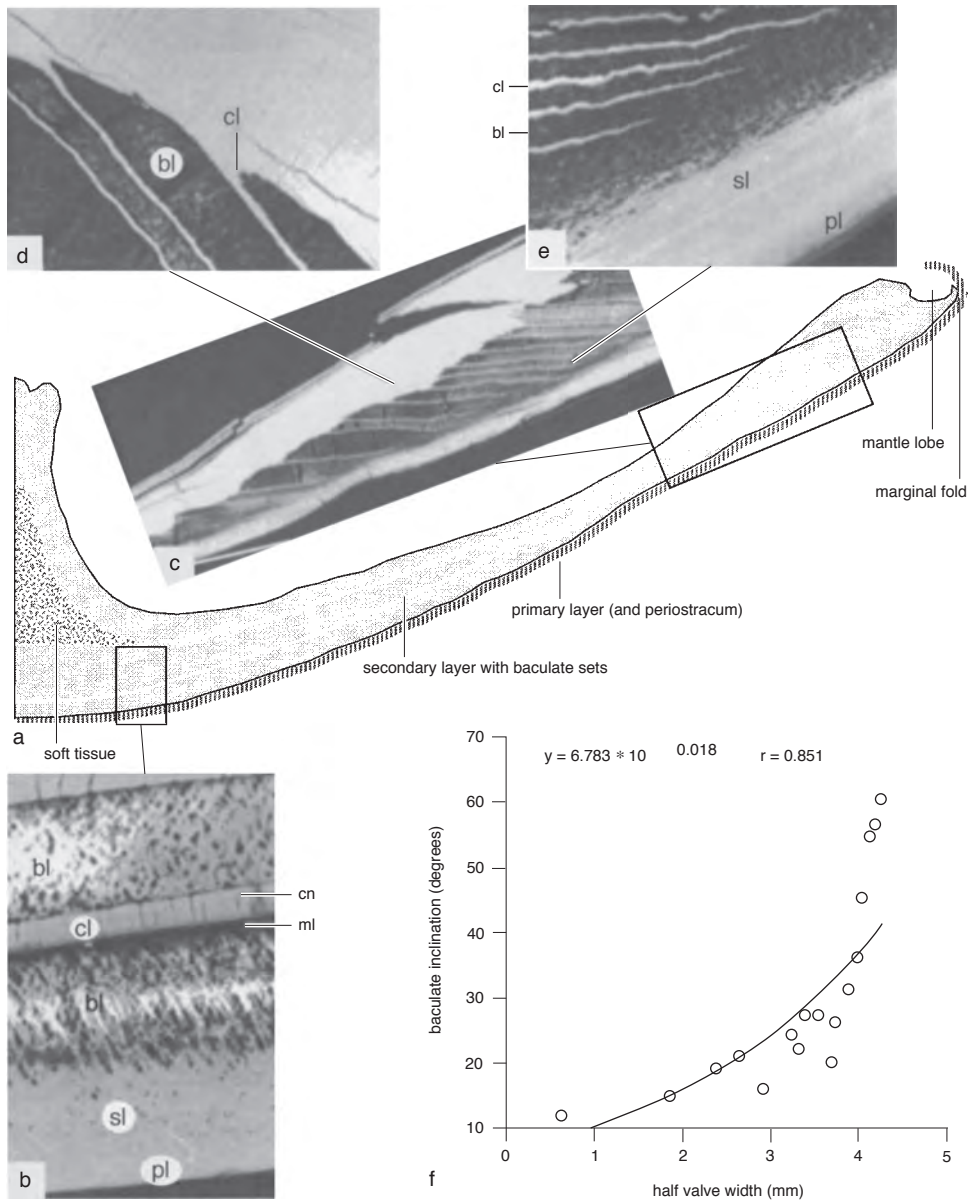
Fig. 1591. *a–f,* Montage of back-scattered electron micrographs of left half of polished posteriomedian transverse section (*a*) of dorsal valve of *Glottidia palmeri* DALL, Recent, California, showing distribution of apatitic (*white*) and organic (*black*) constituents in main stratiform features of shell; baculate laminae (*bl*), compact laminae (*cl*), canals (*cn*), primary layer (*pl*), membranous laminae (*ml*), and stratified laminae (*sl*); *b,* ×600, *c,* ×100, *d,* ×800, *e,* ×1700; *f,* graph in bottom righthand corner shows allometric increase in inclination of baculate laminae to shell surface from midregion to margin of valve (Cusack, Williams, & Buckman, 1999).
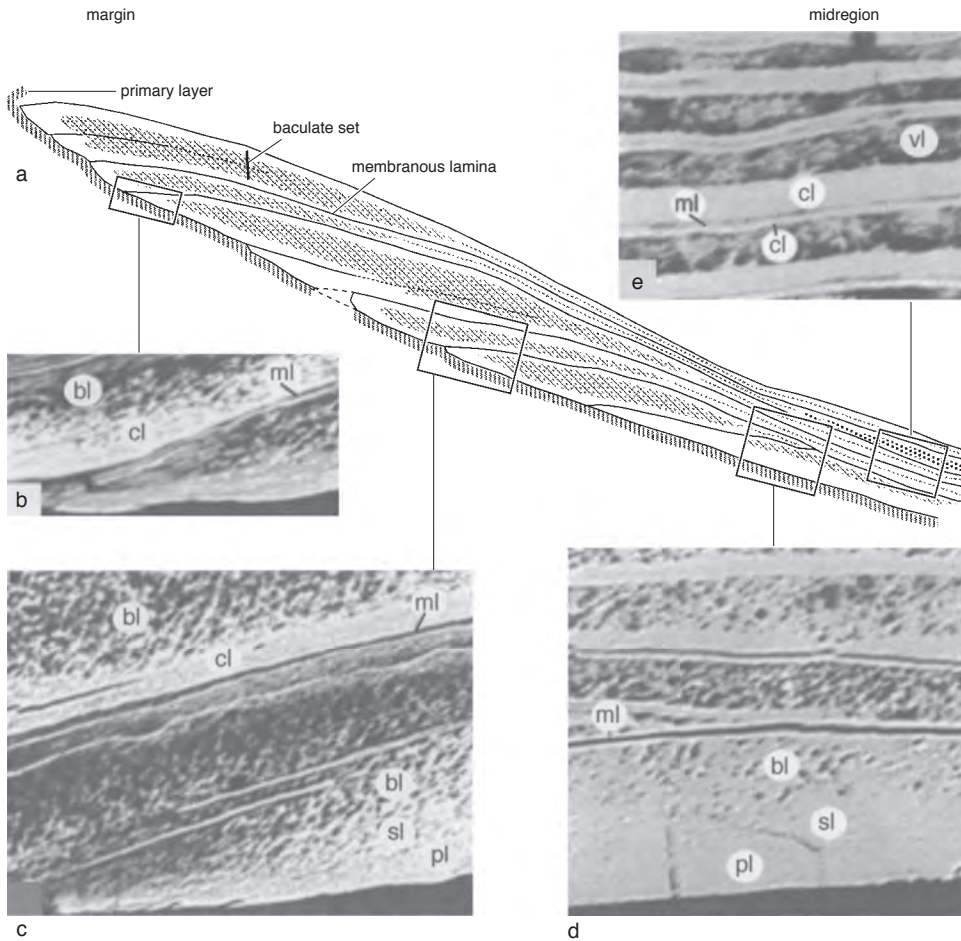
FIG. 1592. *a–e,* Montage of back-scattered electron micrographs of right side of polished posteromedian transverse section (*a*) of dorsal valve of *Obolus apollonis* EICHWALD, GLAHM 101670, Cambrian, Russia, showing distribution of apatitic (*white*) and organic (*black*) constituents in main stratiform features of shell; baculate laminae (*bl*), compact laminae (*cl*), membranous laminae (*ml*), primary layer (*pl*), stratified laminae (*sl*), and virgose laminae (*vl*); *b,* ×500, *c,* ×470, *d,* ×520, *e,* ×1800 (Cusack, Williams, & Buckman, 1999).

lamina with apatitic spherules aggregated into cylindroids at the interface. The outer boundary is commonly a less well defined transition with a high organic content. Individual baculi are 150–250 nm thick and may exceed 5 µm in length. They are unbranched and disposed vertically or at angles of approximately 60° to the substrates to form a three-dimensional trelliswork that,

in the living shell, is supported by the all-pervasive GAGs. In dead shells the removal or shrinkage of GAGs by enzymic digestion or dehydration usually causes a partial collapse of the biomineralized framework and the fragmentation of baculi.

Baculate morphology is variable. The granular surfaces of most baculi, especially those held in place by radiating strands 90
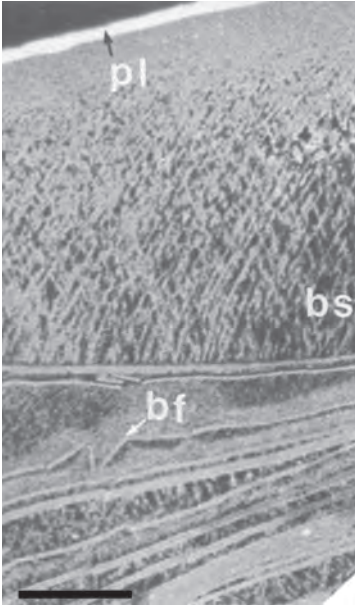
FIG. 1593. Back-scattered electron micrograph of carbon-coated, polished section of dorsal valve of *Obolus apollonis* EICHWALD, GLAHM 101667, Upper Cambrian, Russia, showing succession of baculate symmetrical sets (*bs*) succeeding primary layer (*pl*) with brittle fracture of compact laminae (*bf*); scale bar: 50 μm (Cusack, Williams, & Buckman, 1999).

nm or so thick, are studded with mosaics and cylindroids of spherular apatite (Fig. 1595). Some baculi, however, mainly consist of stacked pinacoids that grow in relation to fine horizontal meshes. Both strands and meshes are exposed when the GAGs matrix of baculate laminae is digested in proteinase-K or subtilisin. In contrast, transverse sections of broken baculi digested by these enzymes have hollow cores, about one-third the dimension of a rod or cores plugged by subcentral spherules. Transverse sections of broken baculi treated with buffered solutions, however, do not have hollow cores, only depressions within clusters of spherules. In both enzymically digested and buffered laminae, some baculi are closed by narrow rounded tips of spherules and are interpreted as having been terminated during laminar secretion. This differential digestion of the organic constituents of baculate laminae suggests that baculi have

axial proteinaceous strands and that the protease-resistant strands and meshes are chitinous. Similar strands and meshes also support mosaics and short rods of spherular apatite in virgose laminae and are likewise assumed to be chitinous.

The baculate sets of fossil discinids and the Paleozoic *Orbiculoidea* are the same as those of living species. The baculate sets of *Schizotreta*, the earliest known orbiculoideid, the sister group of discinids, however, are similar to those of such early linguloids as *Obolus*, as are those of the discinoid trematids (WILLIAMS, CUSACK, & BRUNTON, 1998).

The secondary lamination of *Schizotreta* is dominated by baculate sets secreted at differing rates medially and marginally (Fig. 1596). *In vivo*, a set was composed of an outer membrane(s) succeeded inwardly by a compact lamina grading into a baculate zone capped by a second compact lamina. Although these laminae are now recrystallized, their original ultrastructure can be discerned. Thus, membranes are represented by a break in succession or a layer(s) of spherules; compact laminae by apatitic prisms and rare pinacoids with *c*-axes orthogonal to the set; and baculate laminae by spaces of variable thickness criss-crossed by trellised rods. In submedial successions, where they are well developed, baculi are approximately 500 nm thick. They consist of either irregularly stacked pinacoids or better-ordered prisms with *c*-axes parallel to baculum length. Both types have been found with central indentations suggestive of a nonmineralized core.

Medially, a baculate set is seldom more than a few microns thick, and the middle mineralized zones may be rubbly to virgose rather than baculate. The relatively slow secretion of the succession is confirmed by repeated imprints of hexagonally packed epithelial cells on the inner surfaces of compact laminae. Marginally toward the external shell surface where periodic development of concentric folds (fila) could only have been effected by accelerations in shell secretion, successions of enlarged baculate sets trace the advance of outer laminar lobes
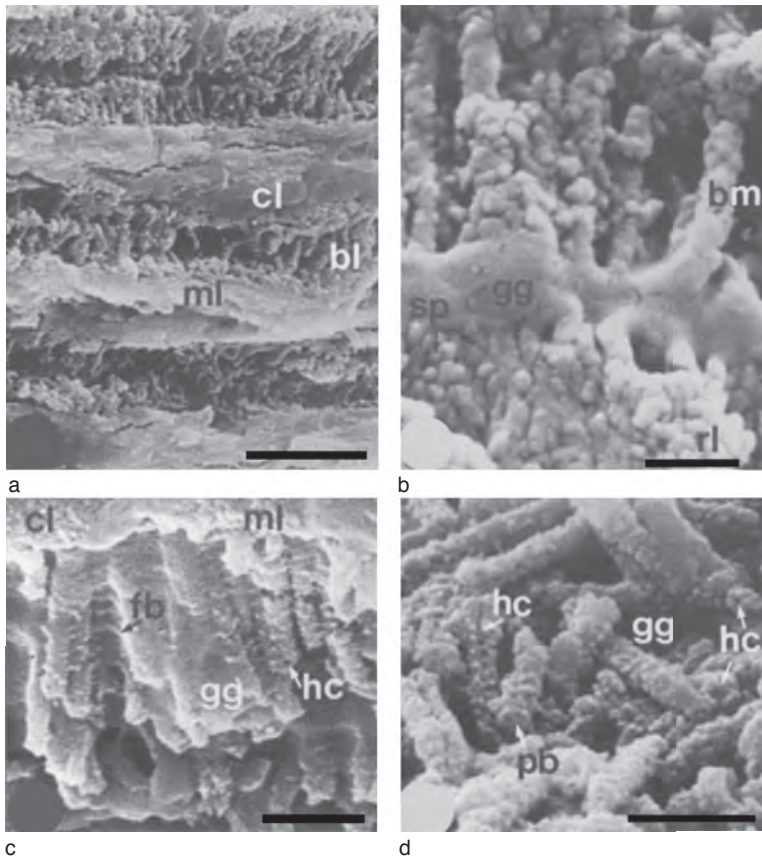
FIG. 1594. SEMs of baculate lamination in vertical fracture sections of secondary layer of *Discinisca lamellosa* (*a–c*) and *D. tenuis* (*d*); all sections treated with subtilisin; *a*, succession of baculate laminae (*bl*) in relation to compact (*cl*) and membranous (*ml*) laminae; scale bar: 5 μm; *b*, baculi (*bm*) some with hollow cores, spherules (*sp*) embedded in GAGs (*gg*) and interconnected by actin strands, succeeded by rubbly laminae (*rl*); scale bar: 0.5 μm; *c*, baculi with hollow cores (*hc*), embedded in GAGs (*gg*) and interconnected by actin strands (*fb*), succeeding compact (*cl*) and membranous (*ml*) laminae; scale bar 1 μm; *d*, broken baculi with some GAGs (*gg*) showing hollow cores (*hc*) and plugged baculi (*pb*); scale bar: 1 μm (Williams, Cusack, & Buckman, 1998).

relative to the main spread of the mantle. A filum would have been secreted by an outwardly deflected outer mantle lobe. The splayed membranes within the filum would have originated from an older membranous sequence secreted posteromedially of the filum. This inwardly located membranous sequence would have served as an axis about which the deflected outer mantle lobe rotated during secretion of the filum. The most striking aspect of a filum growing in this way is the five- or six-fold increase in the cumulative thickness of the baculate and rubbly laminae at its core. In life these wedgelike laminar sets would have consisted mainly of GAGs.

VIRGOSE LAMINATION

The shell structure of living *Lingula* is texturally similar to that of *Glottidia* except for the absence of baculate lamination, which is replaced by sets of a variety of apatitic structures suspended in GAGs. These sets were initially identified as rod and plate (WILLIAMS, CUSACK, & MACKAY, 1994, p. 246) in recognition of the apparent dominant habit of their apatitic aggregates. In the Carboniferous *Lingula squamiformis*,
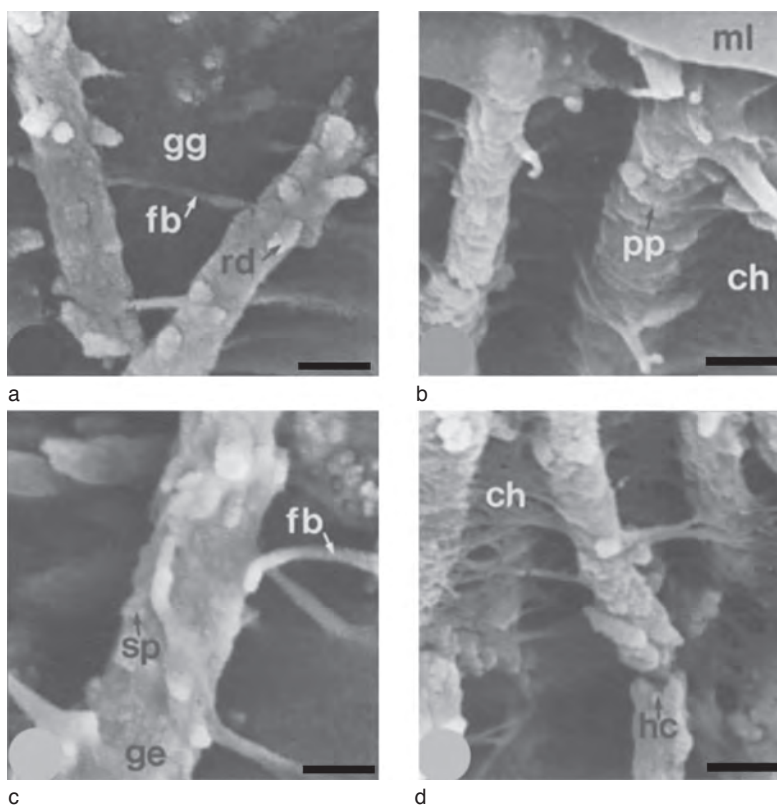
FIG. 1595. *a–d,* SEMs of membranes (*ml*) and baculi in vertical fracture sections of ventral valve of *Discinisca tenuis* treated with subtilisin. Baculi in GAGs (*gg*), composed of pinacoidal plates (*pp*) associated with nets of anastomosing fibrils identified as chitin (*ch*) or of granular (*ge*) spherules (*sp*) and rods simulating prisms (*rd*) associated with actin strands (*fb*) and some broken baculi with hollow cores (*hc*); *a, b,* and *d,* scale bars: 150 nm; *c,* scale bar: 100 nm (Williams, Cusack, & Buckman, 1998).

this fabric, which characterizes the stratiform succession (Fig. 1597), includes laths, plates, mosaics, botryoids, and especially cylindroids up to 1.7 µm long and approximately 250 nm thick (the virgose fabric of CUSACK & WILLIAMS, 1996, p. 40). The cylindroids are randomly stacked, but transverse fractures of some rods bear central depressions. The possibility that the rods had axial organic strands is strengthened by the fact that some may be sinuous, while others, rarely grouped in incipient trellises, are attached to bounding compact laminae (Fig. 1598). In effect, the virgose fabric of Carboniferous *Lingula* appears to represent a degenerate baculate fabric.

Recent comparative studies of the shell structure of living *Lingula* species (WILLIAMS & others, 2000a) have confirmed the prevalence of the virgose fabric and the invariable presence in it of bundles of equal-sized rods of apatitic spherules (fascicles) as displayed in the shell of *Lingula parva*.

A fascicle is an assemblage of several pods, each up to 500 nm long and 150 nm wide and containing three or four strings of beadlike, apatitic spherules that are exposed when the coats of pods are degraded by bleach. The pods are tightly adherent at one end of the aggregate (Fig. 1599), where they are normally attached to an organic strand(s) and splay outward at the other end, where
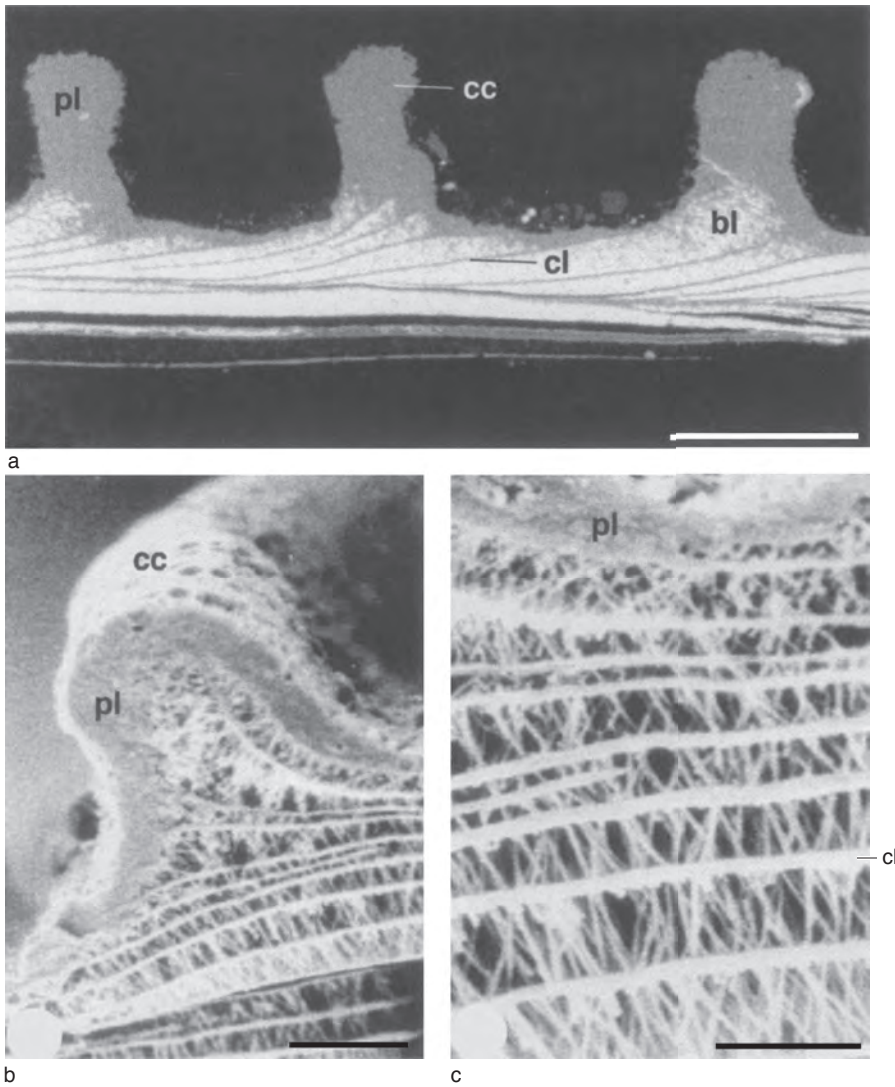
FIG. 1596. SEMs of vertical fracture sections of shell of *Schizotreta corrugata*; *a,* back-scattered SEM of polished vertical section showing distribution of baculate (*bl*) and compact (*cl*) laminae relative to variably thick primary layer (*pl*), forming concentric corrugations (*cc*) on valve surfaces; scale bar: 100 μm; *b–c,* view and detail of baculate sets of corrugations (*cl*) in relation to primary layer (*pl*); scale bars: 25 μm, 10 μm (Williams & Cusack, 1999).

their coats are more readily degradable. Fascicles may occur singly but are commonly attached at their adherent ends either in diametrically opposed pairs or in petaloid groups of four to six fascicles (Fig. 1600).

Toward the top of a fully developed virgose set in the shell of *L. parva*, single and compound fascicles, ellipsoids, and mosaics form discrete botryoidal masses, about one micrometer or so in size, suspended in GAGs (Fig. 1599). The botryoids, which are held in place by a framework of vertical and horizontal branching strands, are roughly aligned alternately. Spherulites are also suspended in GAGs and consist of closely packed pods that radiate from centers of attachment to vertical organic strands (Fig. 1599); the pods are organically coated strings of apatitic
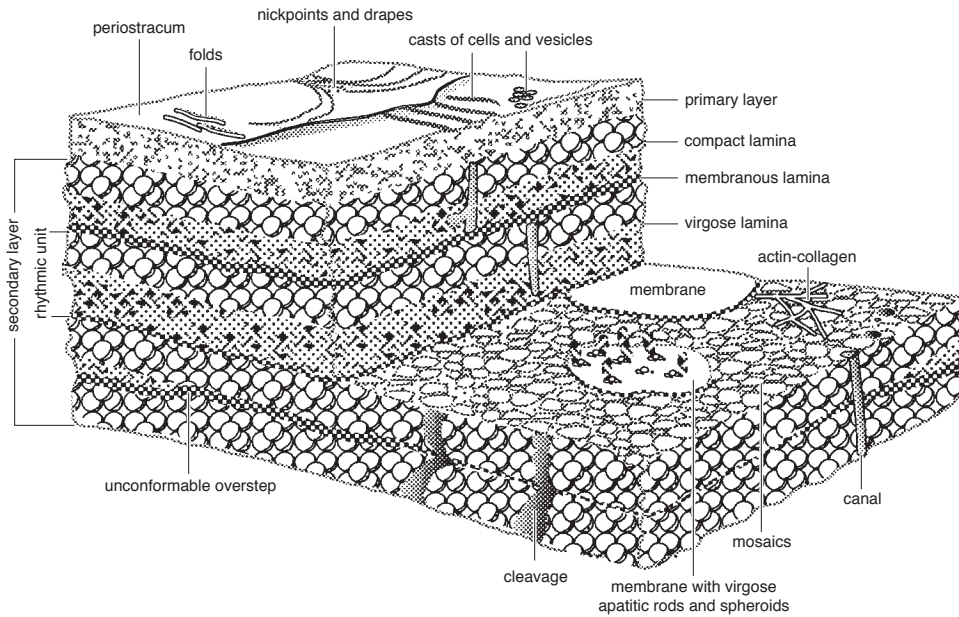
FIG. 1597. Diagrammatic reconstruction of laminar succession in midregion of mature, living valve of *Lingula squamiformis,* Lower Carboniferous, Scotland (Cusack & Williams, 1996).

spherules. Both botryoids and spherulites are not only held in place by the framework of strands but are also enmeshed in a finer organic network of threads (Fig. 1599). Both strands and threads have previously been identified based on their ultrastructural characteristics as collagen (WILLIAMS, CUSACK, & MACKAY, 1994, p. 240) and actin, respectively (CUSACK & WILLIAMS, 1996, p. 47). They have also been identified as β-chitin (WILLIAMS, CUSACK, & BRUNTON, 1998, p. 2011), but this glucosamine-rich constituent (IIJIMA & others, 1991), which imposes a linearity on the apatitic components of the shell, is more likely to be present as membranes and capsules.

Seven samples of the shell structure of other *Lingula* from the Pacific and Indian Oceans did not differ significantly from that of the Japanese *L. anatina,* which incidentally includes fascicles (see WILLIAMS, 1997, p. 279, fig. 237.2). A typical rhythmic unit of the secondary layer of these samples consisted of a compact (or stratified) lamina succeeded

by botryoidal or walled laminae grading into a virgose lamina capped by a membrane(s). In contrast to their close packing in compact laminae, apatitic spherules were commonly encapsulated in succeeding laminae. The general parallelism of capsulated spherules, as seen in surface view and section, suggests some epitaxial control during the secretion of apatite and β-chitin. Virgose laminar sets were found in all samples, with ovoidal capsules and fascicles being especially prominent (Fig. 1600).

The geological range of lingulid shells with virgose lamination is poorly known. Fascicles are abundantly developed (Fig. 1601) in the virgose laminar sets of the Lower Cretaceous *Credolingula* (SMIRNOVA & USHATINSKAYA, 2001). A recrystallized bundle of rods has also been tentatively identified as a fascicle in the shell of the Carboniferous *L. squamiformis* (Fig. 1598); but even if the identification is correct, the structure must have been rarely developed in the shells of this species.
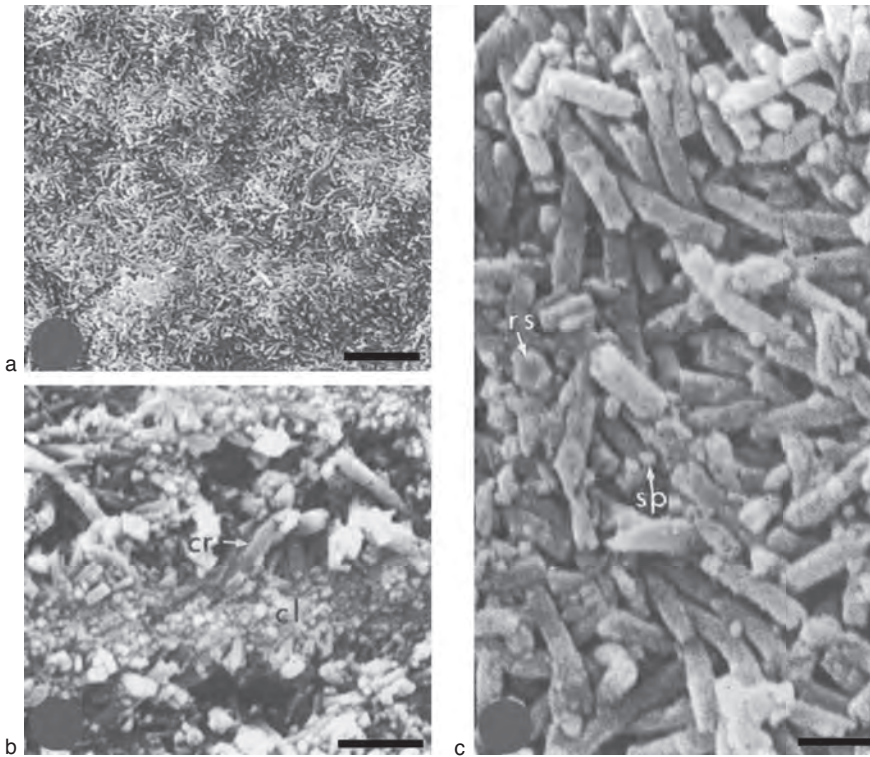
Fig. 1598. SEMs of various gold-coated surfaces of valves of *L. squamiformis,* Kinghorn; *a, c,* external view and detail of a virgose lamina with rods distributed as low mounds separated by shallow troughs reflecting microtopography of secreting plasmalemmas of outer epithelium; ringlike arrangement (*rs*) of spherules seen in transverse sections of some rods and scattered isolated spherules (*sp*); scale bars: 5 μm, 500 nm; *b,* vertical fracture section of compact lamina (*cl*) developed between two thin laminae of rods, some of which are curved (*cr*); scale bar: 1 μm (Cusack & Williams, 1999).

SECRETION OF BACULATE AND VIRGOSE LAMINAR SETS

The secretion of a baculate set has yet to be fully understood. There are at least two ways of secreting baculi to form a three-dimensional trellis. A baculate set is essentially a closed lenticular structure with a roof and floor of membranous or compact laminae enclosing a chamber containing a baculate trellis, secured by chitinous and proteinaceous strands within a GAGs matrix. Most baculi have organic cores; others are composed of pinacoidal stacks or ellipsoidal or linear aggregates of spherules. It is therefore possible that the contents of a chamber are initially secreted as an assortment of baculate components dispersed in GAGs. Differential polymerization within

the GAGs chamber would then give rise to chitinous and proteinaceous strands. Some strands would serve as axes for the aggregation of apatitic spherular coats; others would become guy strands for wholly mineralized baculi growing by linear accretion.

This sequence of polymerization, aggregation, and accretion does not, however, account for the trellised arrangement of baculi. Such a well-ordered crystalline configuration appears to be controlled by the tubular apical plasmalemmas of the outer epithelium (WILLIAMS & others, 1997, p. 26–27). In this mode of secretion, the components of a baculate set would be assembled incrementally and extracellularly with continuously secreted GAGs acting as an extrapallial fluid during polymerization of fibrous strands and the aggregation of
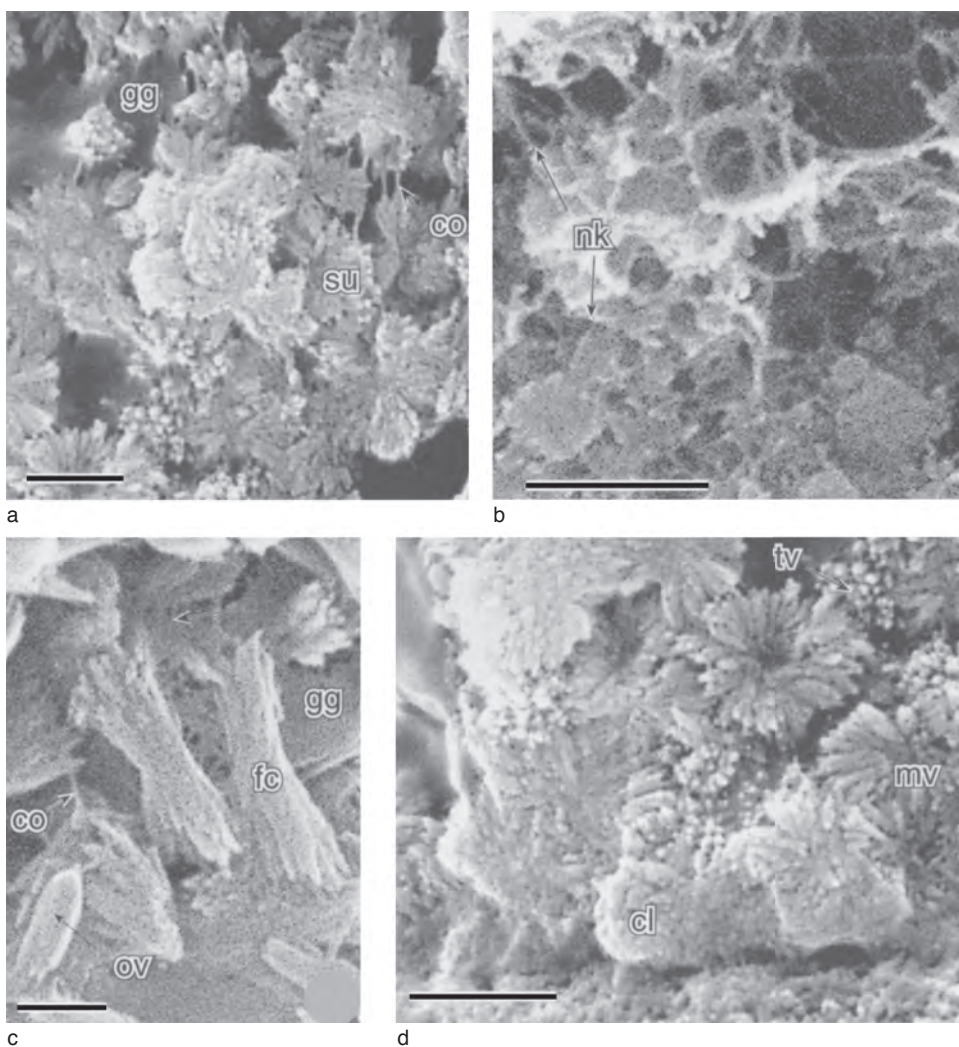
FIG. 1599. SEMs of scissor-cut, vertical sections of *Lingula parva* SMITH, West Africa, ZB 1533, digested in subtilisin; *a,* general view of spherulites (*su*) suspended in GAGs (*gg*) by a collagenous framework (*co*) with *d,* details of spherulites immediately succeeding a compact lamina (*cl*), and tangential (*tv*) and midsection (*mv*) views of spherulites with radiating rods; scale bars: 1 μm; *b,* detail of network of actin-related threads (*nk*) associated with botryoids; scale bar: 0.5 μm; *c,* detail of paired fascicles (*fc*) associated with ovoidal capsules (*ov*), GAGs (*gg*), and collagenous strands (*co*); scale bar: 0.5 μm (Williams & others, 2000).

apatitic granules. The flexibility of tubular plasmalemmas can form tilted surfaces on the tops and along the sides of tubes, with arrays of tops tending to secrete planar structures and the sides high-angled linear bodies (Fig. 1602). Once initiated, the pattern is envisaged as being repeated laterally with the linear bodies (baculi) lengthening inwardly by apical accretion within the thickening layer of GAGs. In effect, baculate trellises could owe their disposition to the flexibility of tubular plasmalemmas and their growth to the polymerization and accretion of organic and mineral constituents after those constituents had been exocytosed with GAGs.
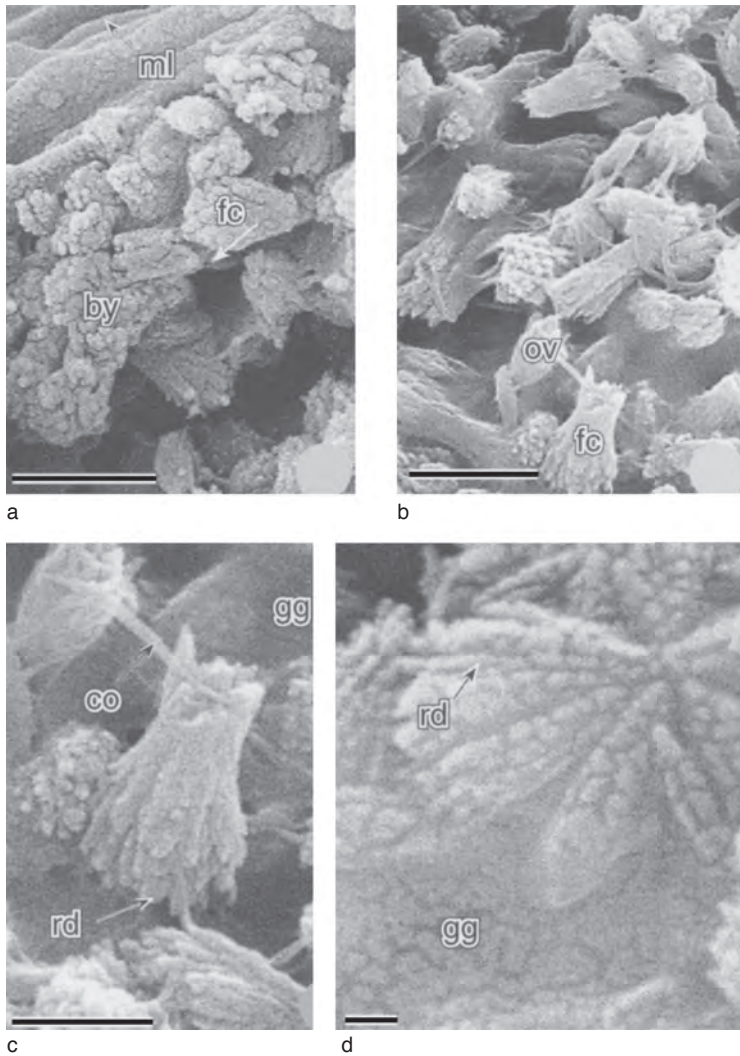
F<small>IG</small>. 1600. SEMs of scissor-cut, vertical sections of *Lingula*; sections treated with bleach; *a, Lingula* sp., Moluccas, NMWZ. 1999. 046.6; view of underside of membranes (*ml*) with GAGs speckled with apatitic spherules showing adherent botryoids (*by*) and fascicles (*fc*) of outer virgose lamina; scale bar: 1 µm; *b–c,* general view and detail of virgose lamina of *Lingula* sp., Western Australia, NMWZ. 1999. 046.8, showing fascicles (*fc*) composed of spherular rods (*rd*), suspended with ovoids (*ov*) in GAGs (*gg*) with connecting strands of collagen (*co*); scale bars: 1 and 0.5 µm respectively; *d, Lingula* sp., Yemen, NMWZ. 1999. 046.1-3; detail of flat-lying, petaloid group of fascicles that are part of an accretionary botryoid, showing disposition of apatitic spherules composing individual rods (*rd*) of fascicles embedded in tension-cracked GAGs (*gg*); scale bar: 0.1 µm (Williams & others, 2000).

A flexible tubular plasmalemma, however, cannot be solely responsible for the growth of baculate trellises. It is also characteristic of the integument of *Lingula*, which is chemicostructurally related to that of *Glottidia* except for the absence of baculate laminae.

In a typical rhythmic sequence in the *Lingula* secondary shell, baculi are replaced by spheroidal, ellipsoidal, and fascicular bodies. No axial canals have been seen in these bodies, and it is assumed that a specific fibrous protein, absent from the *Lingula* shell, serves
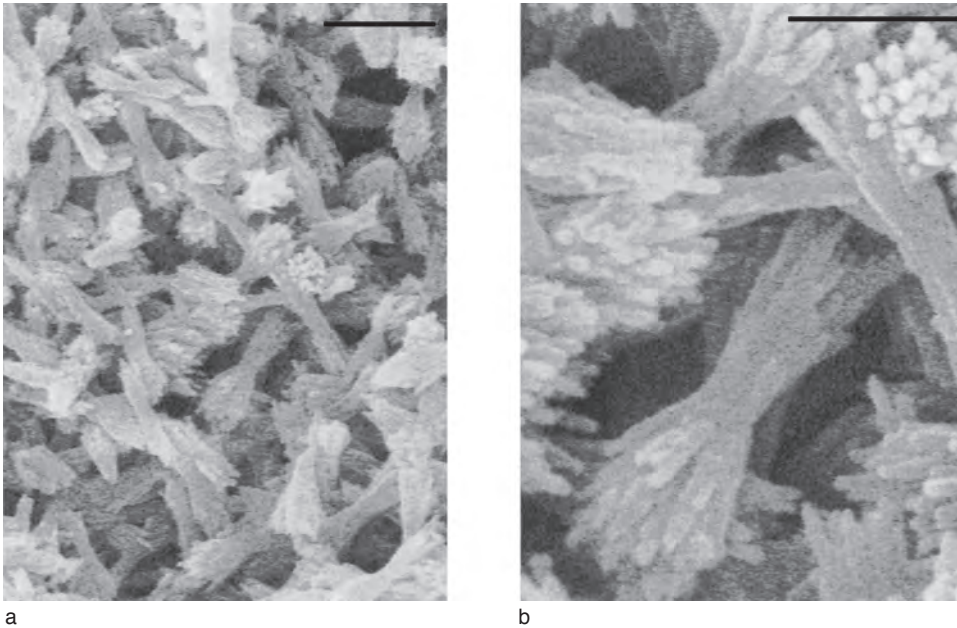
a

b

FIG. 1601. *a,* General view and *b,* detail of fracture section of virgose laminar set in shell of Lower Cretaceous *Credolingula olfevieri* SMIRNOVA, showing fascicles, principal components of virgose fabric; scale bars: 2 μm and 1 μm respectively (new).

as the axis of a baculum. The nature of virgose lamination in the Carboniferous *Lingula squamiformis* shells seems to support this interpretation with sporadic traces of aborted baculate growths on the compact laminae bounding virgose chambers.

The derivation of virgose lamination from baculate sets, however, involved more chemicostructural transformations than the loss of proteinaceous strands. The virgose lamination, possibly of *L. squamiformis* and certainly of *Credolingula* shells, is
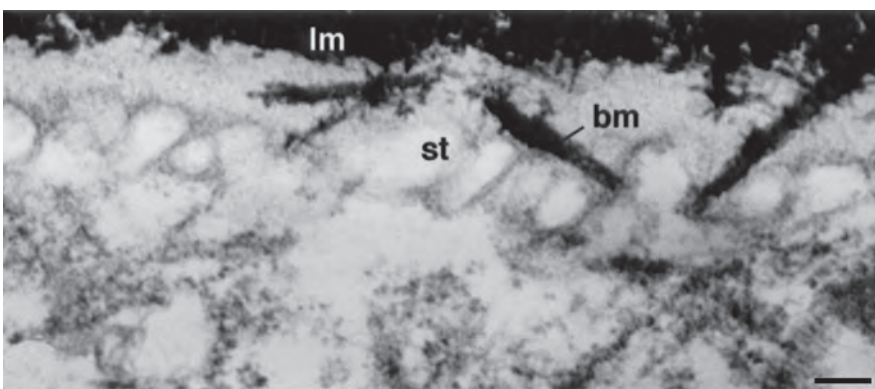

FIG. 1602. TEM of shell and associated outer epithelium of a dorsal valve of Recent *Discina striata*, stained with aqueous solution of lead citrate and uranyl acetate. Tubules (*st*) in relation to baculi (*bm*) accreting beneath a lamina (*lm*) with high organic content; scale bar: 100 nm (Williams & Cusack, 1999).
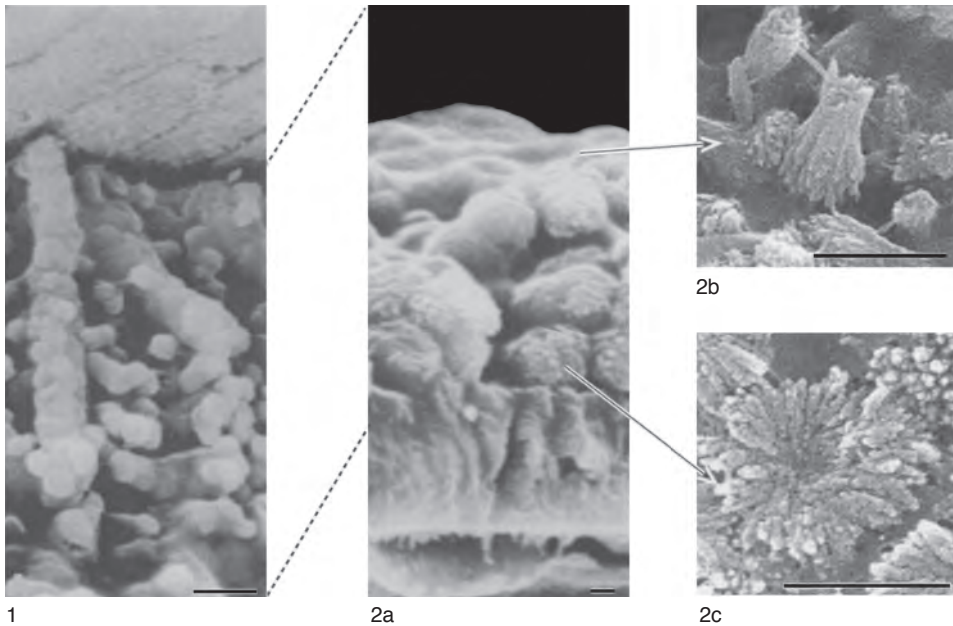
Fig. 1603. Laminar sets in shells of living lingulids: *1*, baculate set of *Glottidia* with baculi and ellipsoids in GAGs subtended between top of compact lamina (below) and membrane with actinlike threads underlying another compact lamina (above); *2a*, virgose set of *Lingula* with membrane (below) succeeded by compact lamina and botryoids in GAGs that have been completely removed toward top; *2b*, fascicles in a collagenous framework within GAGs zone in upper part of a set in *L.* sp. cf. *anatina*; *2c*, spherules in place of botryoids in *L. parva*; scale bars: 1 µm (Williams & others, 2000).

characterized by fascicles, a novel kind of aggregation. The invariable presence of fascicles in such fossil and all living species is noteworthy in two respects. Fascicles are virtually constant in shape with their constituent pods, approximately 500 nm long. They are also flat lying on open frameworks of collagenous strands and may occur at several horizons in a GAGs matrix. These characteristics suggest that fascicles are assembled intracellularly as bundles of linearly arranged apatitic spherules encapsulated in chitinoproteinaceous coats. They are probably secreted as diametrically opposed pairs that fracture easily in midregion during polymerization and dehydration of virgose sets. Spherulites, which so far have been found only in *L. parva*, are also probably assembled intracellularly. A correlation of the principal apatitic aggregates of baculate and virgose laminar sets is given in Figure 1603.

COLUMNAR AND CAMERATE SECONDARY LAYERS

The columnar and camerate fabric of acrotretide brachiopods has been extensively described (HOLMER, 1989; WILLIAMS & HOLMER, 1992), and its main features are summarized in Volume 1 (WILLIAMS, 1997, p. 281–282). Recent research on this fabric includes the discovery of homologous structures in the stem-group brachiopod *Mickwitzia* and in some Cambrian lingulides. The most relevant aspects of acrotretide shell structure leading to these discoveries merit a brief review.

The laminar sets of the acrotretide shell are distinctively stacked like shallow, asymmetric saucers with thickened margins that are wedgelike in section and up to five times thicker than the posteromedial centers of the sets. The relatively smooth columns pervading the secondary shell can be traced
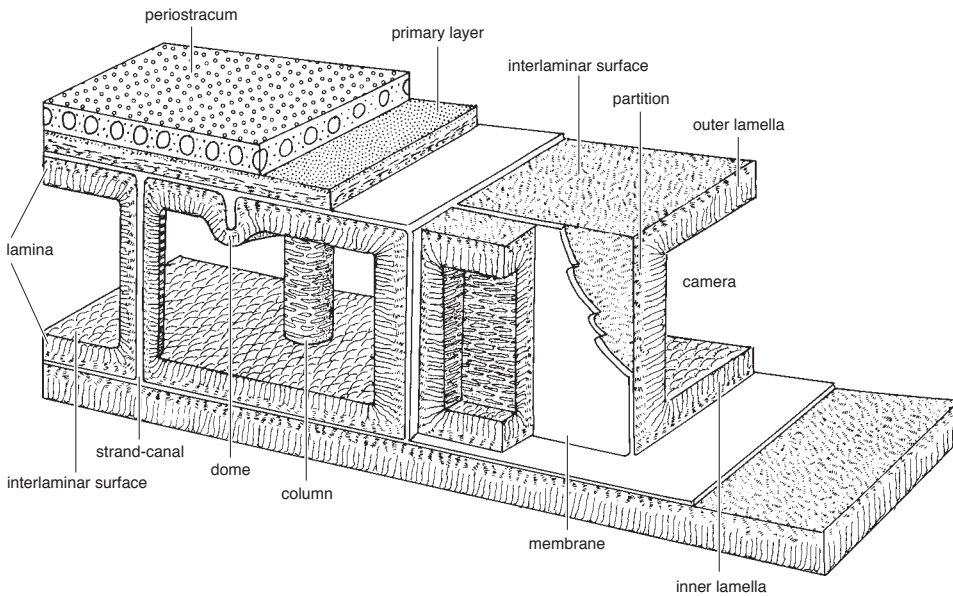
Fig. 1604. Composite diagram showing inferred relationships among various biomineral and morphological components of shell of living acrotretoids (Holmer & Williams, 1992).

through several sets for 30 µm or more; and although they range in diameter from 1.5 to 5 µm (average 2.3 µm), they are much less variable within a laminar set (Fig. 1604). The columns have axial canals, approximately 500 nm in diameter, which are commonly preserved as perforations in contiguous, interlaminar surfaces separating sets and occupied by membranes *in vivo* (Williams & Holmer, 1992, pl. 4,5). Associated domes that are interpreted as aborted columns have a similar range of diameters and are composed of curved overlapping plates with sporadic central depressions (Williams & Holmer, 1992, pl. 5,5). An interesting aspect of the acrotretide shell (Fig. 1604) is that although the structure in many species is columnar, in others it is camerate (*Scaphelasma*), while both fabrics characterize different laminar sets in some acrotretids (Holmer, 1989, p. 54). This differential development of fabric suggests changes in the specificity of calcifying proteins as well as the secretion of interconnected organic partitions from intercellular pathways that replicate the boxlike

shapes of outer epithelial cells (Williams & Holmer, 1992, p. 684). As in living lingulides, the sets of compact laminae containing columns or partitions would initially have been filled with apatitic spherules dispersed in GAGs. As the GAGs degraded, the apatite would have aggregated on the membranous partitions or on orthogonal strands (or canal walls), dependent on the nature of the ambient calcifying protein.

Recent studies show that mineralized columns with axial canals also developed in *Mickwitzia*, the presumed stem-group brachiopod (Holmer, Skovsted, & Williams, 2002), and in halkieriids like *Micrina*, the postulated sister group of the phylum (Williams & Holmer, 2002). The laminar sets of *Mickwitzia* contain two kinds of columnar structures (Holmer, Skovsted, & Williams, 2002, p. 878), as do those of acrotretides (Fig. 1605), differing only in their larger average diameter (5.5 µm). The one like the acrotretide column is composed of concentric layers that normally did not fill the core; the other kind, feasibly homologous with acrotretide domes composed of
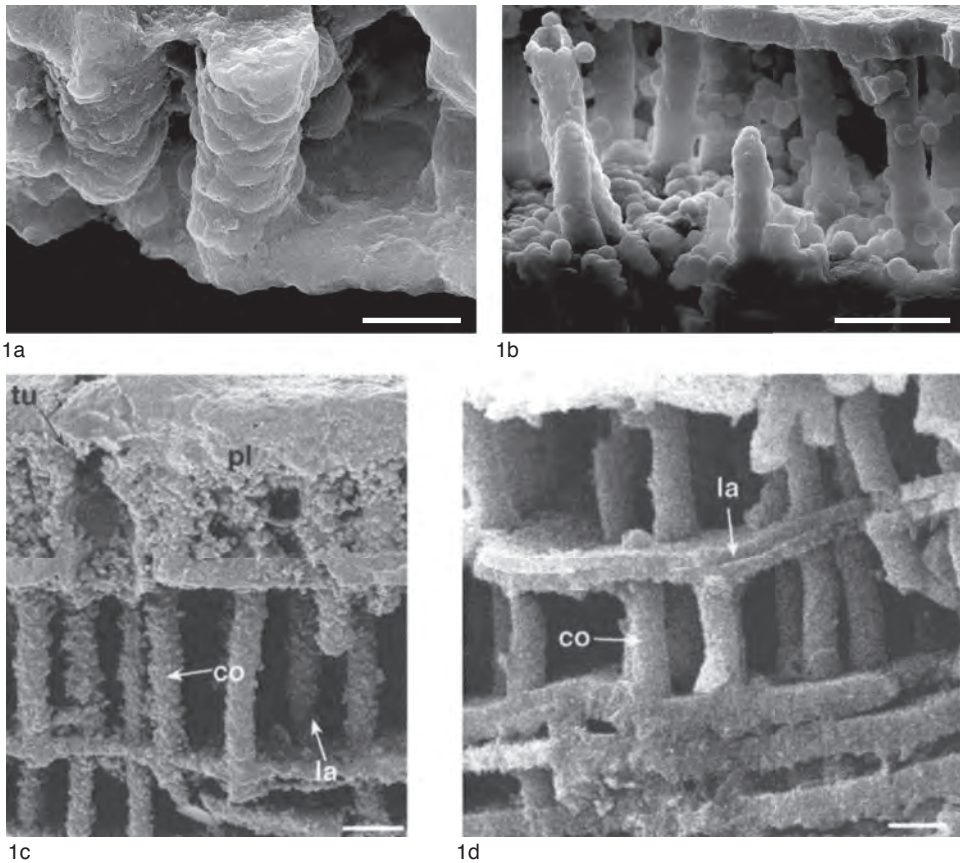
FIG. 1605. *a–b,* SEMs of gold-coated columnar structures of *Mickwitzia* sp. cf. *occidens* WALCOTT, Lower Cambrian; scale bars: 5 and 15 μm (new); *c–d*, SEMs of vertical fractures of shells for *Mickwitzia*, MGUH 26280 and *Prototreta*, GLAHM 14900, showing disposition of columns (*co*) relative to laminae (*la*) and primary layer (*pl*) and external surface in *Mickwitzia*, which is perforated by apertures of tubes (*tu*) with one longitudinal section; scale bars: 10 μm and 5 μm respectively (Holmer & others, 2002).

overlapping plates, consists of vertically stacked discoidal plates (Fig. 1605).

The presence of axial canals in columns and the relative smoothness and constant thickness of columnar walls in any one set have suggested two possible modes of growth. One assumes that mineralized columns were secreted within tubular organic coats by papillose extensions of outer epithelium that were continually entrapped axially by inwardly thickening apatitic walls (HOLMER, SKOVSTED, & WILLIAMS, 2002, p. 878). If that had been so, however, columns and not just canal perforations would have breached interlaminar spaces (compare WILLIAMS & HOLMER, 1992, pl. 4,5). The other assumption, which is preferred, is that the apatite of columns and domes aggregated on a chitino-proteinaceous framework morphologically like the lingulide canaliculate system but with a calcifying protein component(s) that promoted apatitic accretion (except in inter-laminar spaces where membranes occurred *in vivo*). Certainly, the columnar and camerate fabrics must have owed their individuality to at least two mutually exclusive calcifying protein species that controlled the aggregation of apatite within the chambers of the GAGs of the acrotretide laminar sets. The columns and domes of the secondary shell of
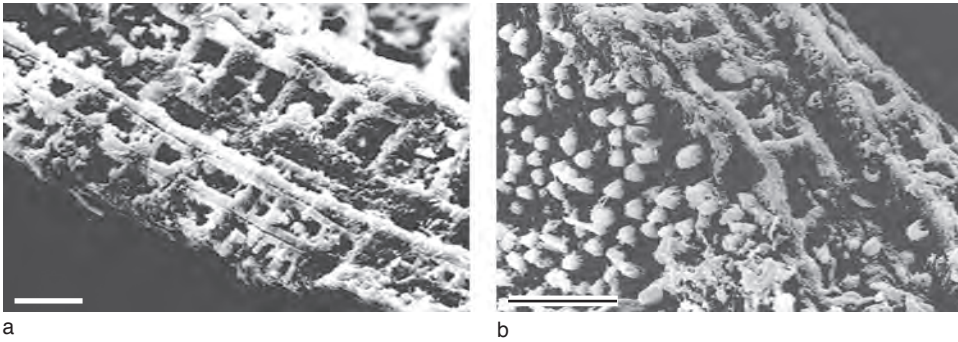
FIG. 1606. *a,* Fracture section of shell of Lower Cambrian *Lingulellotreta* sp., Kazakstan, showing *b,* columnar lamination with domes on an inner surface of a lamina; scale bars: 5 µm (new).

Lingulellotreta (Fig. 1606), with an average diameter of 2.6 µm, are homologous with those of the acrotretide columnar fabric (CUSACK, WILLIAMS, & BUCKMAN, 1999, p. 830). The identification is significant in that the genus is among the oldest recorded lingulides (from the Botomian of the Lower Cambrian; other lingulellotretid genera are baculate; L. E. Popov, personal communication, June 2003). The laminar sets of the secondary shell of the Lower Cambrian

FIG. 1607. SEM of gold-coated fracture section of valve of *Micrina etheridgei,* GLAHM 114748; fracture section view of canals (*cn*) orthogonal to laminar successions (*ls*) relative to internal tube (*tu*) of tubular network; scale bar: 50 µm (Williams & Holmer, 2002).

halkieriid *Micrina* (WILLIAMS & HOLMER, 2002) are also perforated orthogonally by columns with axial canals (Fig. 1607), which appear to be homologous with the acrotretide columnar fabric. In contrast, the differentiation of cell imprints on the interiors of the obolid *Experilingula* into discrete, hexagonal to rectangular concave pieces (Fig. 1608) are unlikely to be homologues of the acrotretide camerate fabric. These pieces can occur on a sequence of at least three compact laminae; but they are not connected to one another by partitions, only by baculi (CUSACK, WILLIAMS, & BUCKMAN, 1999, p. 826).

OTHER LINGULIFORM SHELLS

The shells of the Lower Paleozoic lingulate siphonotretides, the paterinates, and the lingulide eoobolids are also stratiform. Their primary layers were orthodoxly rheological *in vivo,* albeit with bizarre rheomorphic features like the siphonotretide spines (WILLIAMS, HOLMER, & CUSACK, 2004), the paterinide asymmetric folds and basins (WILLIAMS, POPOV, & others, 1998), and the eoobolid asymmetric nodules (see Fig. 1615). Their secondary layers are basically laminar in fabric with little textural elaboration.

In Volume 1 (WILLIAMS, 1997, p. 279), the paterinate secondary shell was described as a laminar succession composed of close-packed hexagonal columns, approximately 8 µm in diameter, that had survived recrystallization
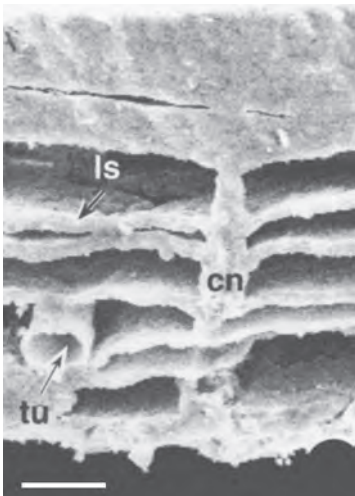
only in *Cryptotreta* (Popov & Ushatinskaya, 1987). A more recent study has interpreted the *Cryptotreta* fabric as a succession of predominately organic, stratified laminae with a rhythmic unit of a few micrometers. Each unit bears the imprints of epithelial cells, which simulate hexagonal columns (Fig. 1609–1610). Rare lenticular chambers within the secondary layer contain walls and needles of apatite (with clays) that were presumably filled with GAGs and dispersed apatite in the living state (Williams, Popov, & others, 1998, p. 232).

The hexagonal imprint succession of the *Cryptotreta* secondary shell is not characteristic of other paterinates. It is not unique, however, being sporadically developed, for example, in contemporaneous *Lingulella* (Curry & Williams, 1983); and similar outer epithelial imprints occur on the internal surfaces of stratified laminae underlying posterolateral muscle scars of *Paterina* (Fig. 1611). The persistence of such imprints is attributed to the much higher membranous content of cryptotretid stratified lamination. Paterinid lamination is coarser, with the mineralized component tending to be compact to rubbly in texture (Fig. 1611).

Although the shell of the siphonotretides is stratiform with the usual rheomorphic primary layer and a simple laminar secondary layer, the basic apatitic constituents are different from other linguliforms. They are prismatic laths up to 60 nm or so long with some tablets and basal pinacoids. These components form monolayers stacked like stratified laminae. The laths may be well ordered, like cross-bladed arrays, but they are normally recrystallized to form a platy lamination (Fig. 1612). This platy lamination is randomly separated into nonlinear rhythmic sets by variably developed lenticular chambers up to 50 µm high (Fig. 1613). The chambers contain clusters of laths aggregating into ovoids, plates, and spherulites embedded in a mesh of nanometric-sized acicular apatite (Fig. 1613). A vertical view of the contents of a chamber shows laths

Fig. 1608. View of internal surface of *Experilingula divulgata* Konreva & Popov, Upper Cambrian, Kazakhstan, showing discrete concave pieces of laminae, each secreted by outer epithelial cell and simulating camerate laminations; scale bar: 10 µm (new).

arising from highly inclined apatitic plates delineating depressions that presumably accommodated extensions of the apical plasmalemma (Fig. 1614). The platy lamination characterizing the secondary shell of siphonotretides resembles the stratified lamination of other lingulates. The principal basic unit, however, is a lath, not a granular spherule. Moreover, although laths are stacked in monolayers, they may be well ordered but are differently oriented in successive laminae. These differences have chemicostructural implications including: a different calcifying protein that promoted prismatic rather than spherular accretion of apatite; polymeric substrates that facilitated prismatic growths; and a relatively loose attachment of the secreting epithelium to the thickening shell, unlike the close attachment that would have been effected in contemporaneous lingulates by canaliculate frames (lingulides) and apatitic columns (acrotretides). Lenticular cavities with apatitic deposits, sporadically distributed within the
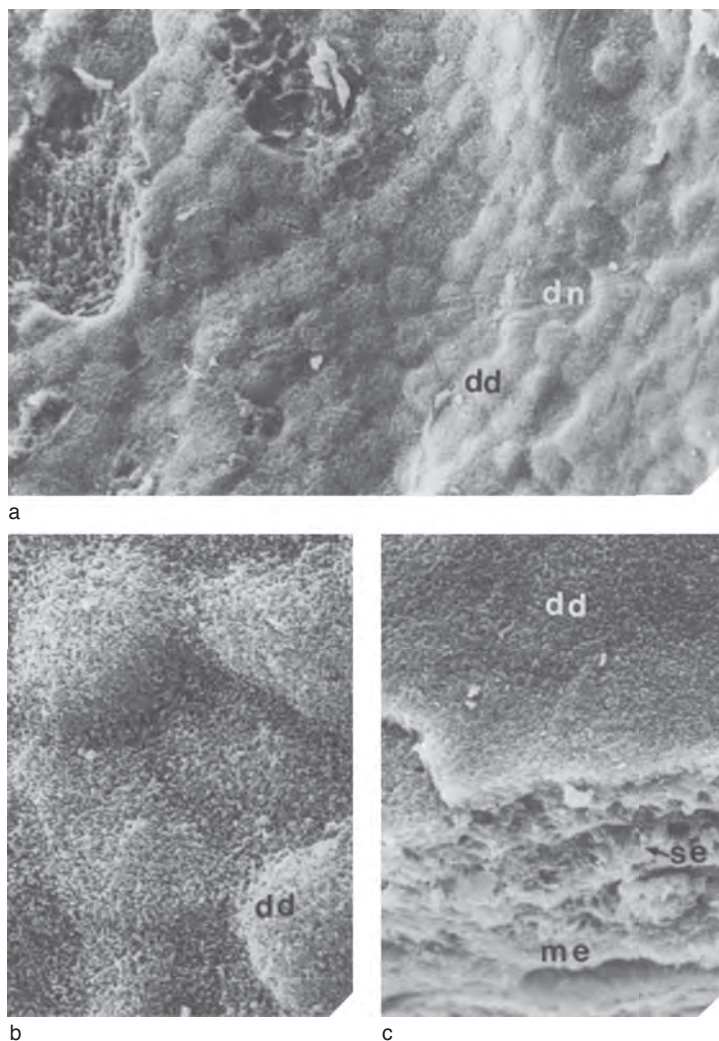
Fig. 1609. *a–b. Cryptotreta undosa* (Linnarsson), Lower Cambrian, Kalmarsund Sandstone, Sweden; general and detailed views of external, subperiostracal surface of undulating lamina with low domes (*dd*) and few relatively depressed areas (*dn*), ×680, ×2800; *c, Cryptotreta undosa* (Linnarsson), Lower Cambrian, Kalmarsund Sandstone; fracture section showing external surface with low domes (*dd*) underlain by stratified laminae of lithified membranes (*me*) and spherules (*se*), ×2000 (Williams, Popov, & others, 1998).

secondary layer, probably originated *in vivo* as localized exudations of excessive quantities of GAGs with dispersed apatitic granules. During fossilization the GAGs would have dehydrated and degraded to leave behind residual apatitic aggregates mainly as meshes of prismatic rods and laths.

The secondary fabric of *Eoobolus* has been described as virgose and precursory to bacula-

tion (Cusack, Williams, & Buckman, 1999, p. 835). Well-preserved shells of *E. pristinus* from Greenland, however, reveal that the fabric of their stratiform successions is unlike those of other lingulides. The primary and secondary layers are separated by a break in succession about 1 μm thick (Fig. 1615b). The break is periodically sealed at inclined junctions marking the lamellose grooves on
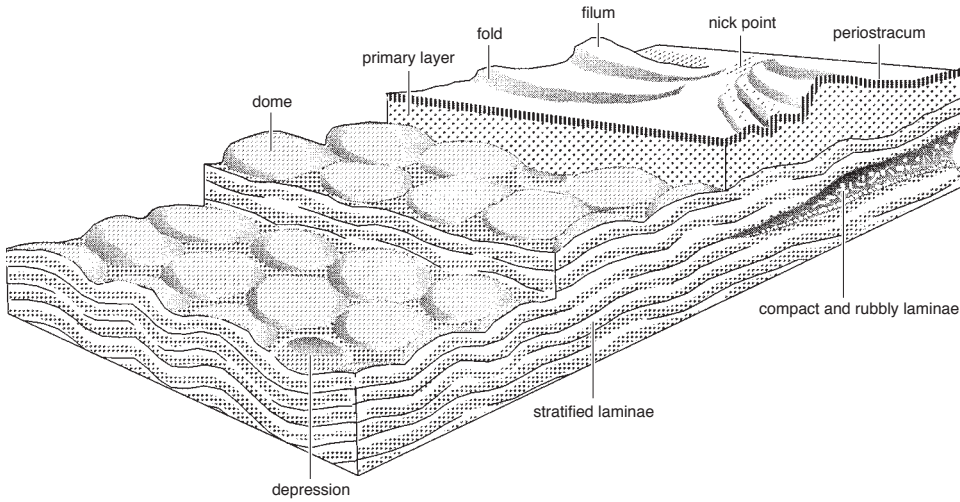
FIG. 1610. Diagrammatic representation of inferred shell structure of cryptotretid paterinates (Williams, Popov, & others, 1998).

the shell surface (Fig. 1615a). The stratified lamination of the secondary layer includes horizontal chambers with widely spaced laminar partitions (Fig. 1615b–c). The chambers are lined by unordered, low stacks and mounds of prismatic tablets of apatite up to 2 µm in size (Fig. 1615d). The fabric has been recrystallized but is neither virgose nor incipiently baculate. Presumably the tablets bear some resemblance to the microstructures that crystallized within the GAGs chambers of the eoobolid living shell.
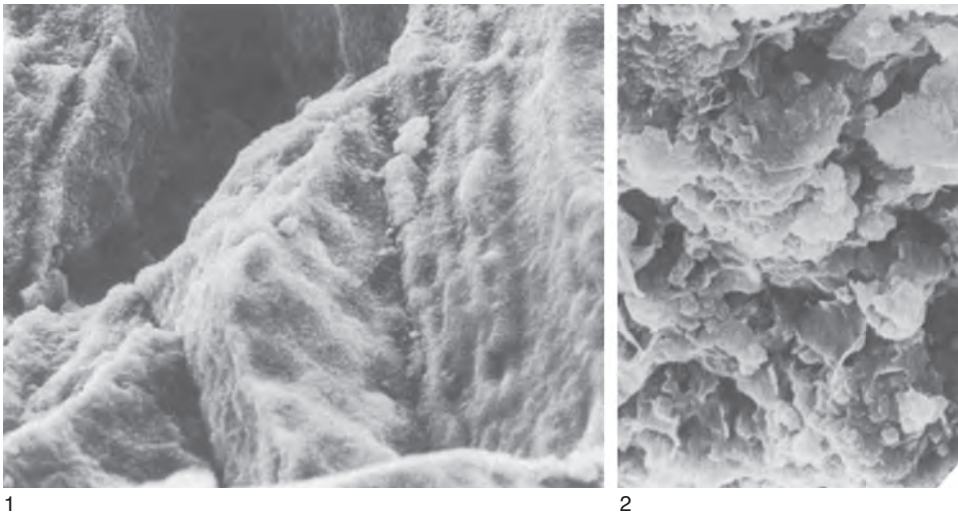
FIG. 1611. *Paterina*? sp., Lower Cambrian, Flinders Range, Australia; *1*, general view of succession of stratified laminae in posteromedian fracture section of mature dorsal valve with exposed internal surfaces bearing hexagonal, close-packed depressions, ×1050; *2*, *Dictyonites perforata* COOPER, Middle Ordovician, Pratt Ferry Formation, Alabama; fracture section of another bounding wall composed of stratified laminae, ×3000 (Williams, Popov, & others, 1998).

Fig. 1612. SEMs of gold-coated fracture sections of valves of *Siphonotreta unguiculata* (*a, c*, GLAHM 1147891; *b*, Br 135730); *a,* basic units of secondary layer, consisting of prismatic laths and minor pinacoidal plates, arranged in monolayers (*ml*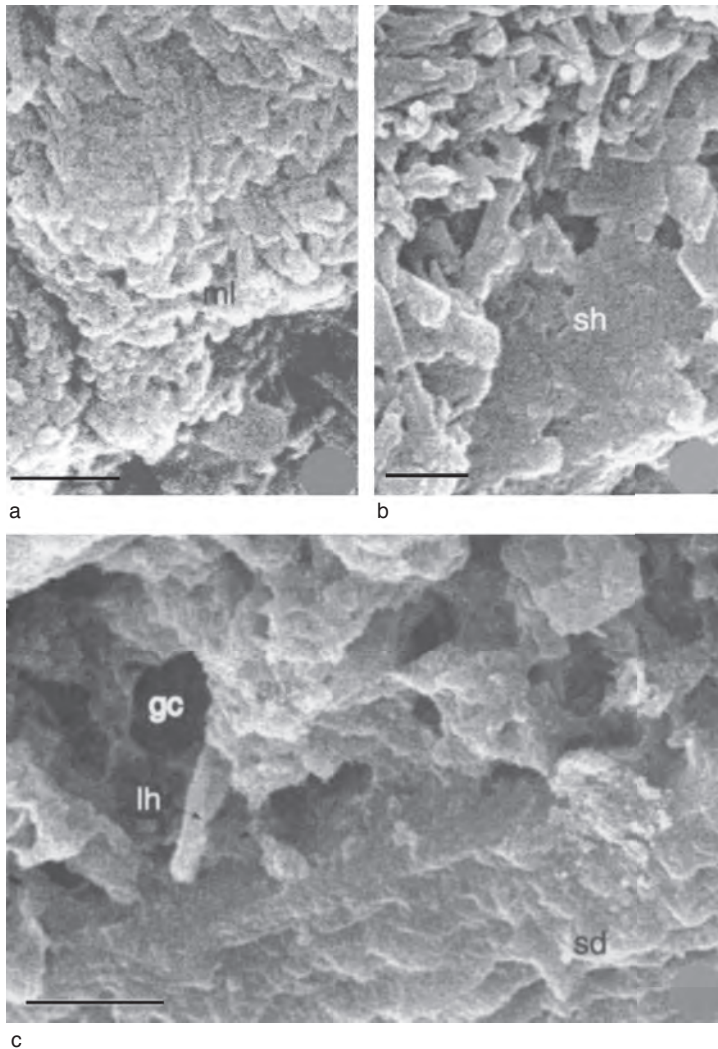) that usually recrystallized (view *b*) into platy laminae (*sh*), occasionally in a cross-bladed arrangement; scale bars: 0.5 µm; *c,* constituents of GAGs chambers (*gc*), floored by stratified laminae (*sd*), consisting of laths (*lh*); scale bar: 5 µm (Williams, Holmer, & Cusack, 2004).

The eoobolids are lingulide-like morphologically, including a pitted juvenile shell. Their relatively simple secondary shell succession is assumed to be a short-lived variant of the linguloid baculate fabric and not homologous with that of either the siphonotretides or the paterinates.

ORGANOPHOSPHATIC SHELL OF
MICRINA

The problematic *Micrina* consists of a pair of bilaterally symmetrical (sellate and mitral) sclerites that have been interpreted as homologues (WILLIAMS & HOLMER, 2002) of the dorsal shells of *Halkieria* (CONWAY-MORRIS
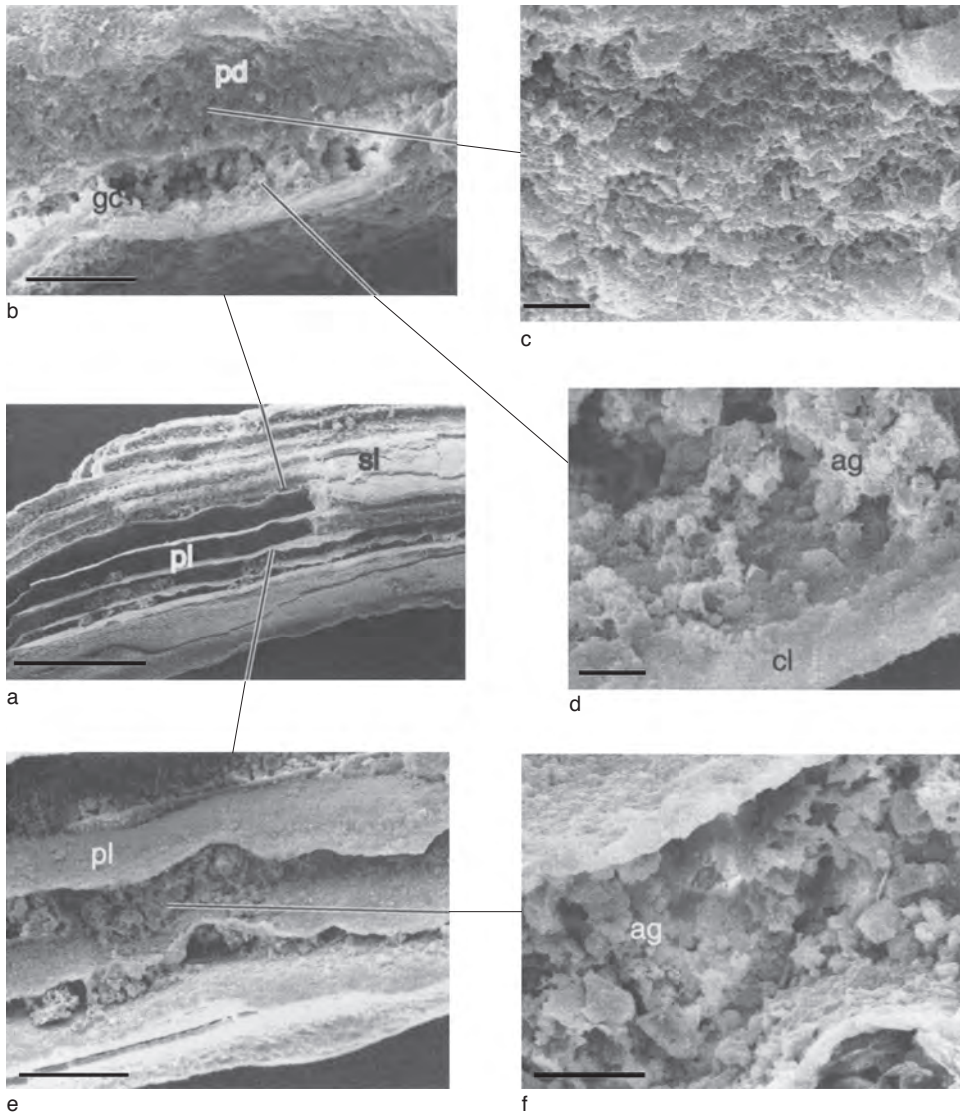
FIG. 1613. Internal view (*a*) and details of part of a mature margin of a dorsal valve (GLAHM 114792a) of *Siphonotreta unguiculata* with lamellae composed of primary shell (*pl*), secreted by a retractable outer mantle fold, interleaved with secondary shell (*sl*); *b*, presumed GAGs chamber (*gc*) within a stratiform succession (views *b–c*) of platy laminae (*pd*), partly compacted and cleaved (*cl*) as in *d* and containing apatitic aggregates (*ag*; view *d*); *e*, rheomorphically folded lamellae (*pl*) that enclosed GAGs chambers (view *f*) with apatitic aggregates (*ag*): scale bars: 1 mm, 50 µm, 5 µm, 5 µm, 200 µm, and 50 µm respectively (Williams, Holmer, & Cusack, 2004).

& PEEL, 1995). The stock has been identified as the sister group of the brachiopods mainly because the apatitic laminar shell of *Micrina* is virtually indistinguishable in structure from the organophosphatic stratiform shells of linguliform brachiopods (WILLIAMS &

HOLMER, 2002). This skeletal homology has gained credence from the discovery that the shell structure of *Mickwitzia*, a stem-group brachiopod, is essentially an acrotretide columnar fabric perforated by the setigerous tubes of *Micrina* (HOLMER, SKOVSTED, &
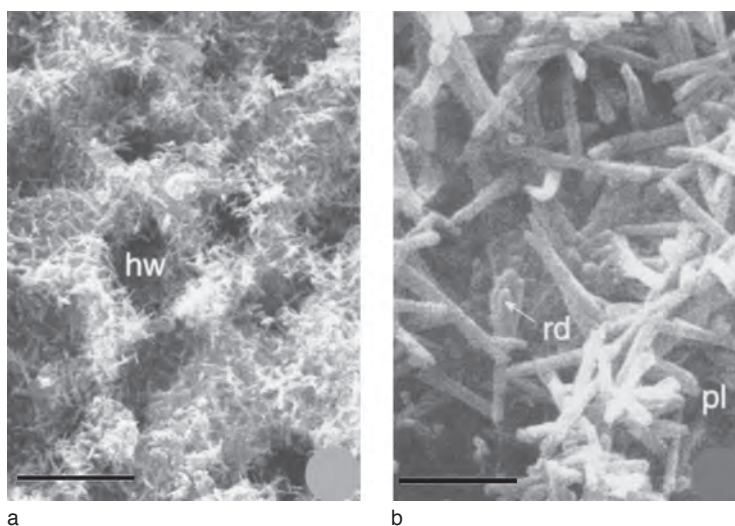
Fig. 1614. SEMs of gold-coated surfaces and fracture sections of *Siphonobolus uralensis*, GLAHM 114780; *a–b*, views of fractured edge and interior of GAGs chamber of mature valve showing mesh of rods (*rd*), laths, and plates (*pl*) indented by hollows (*hw*); scale bars: 5 μm and 1 μm respectively (Williams, Holmer, & Cusack, 2004).

Williams, 2002), which will be described later. The prospect that the fine structure of the *Micrina* sclerites could have been an ancestral brachiopod fabric has prompted this description, in linguliform terminology, of *Micrina* lamination.

The rheomorphic primary layer of *Micrina* sclerites typically consists of mono-layers of platy apatite. The basic aggregates of the secondary layer are also monolayers that amalgamate into compacted, strati-fied laminae approximately 7 μm thick (Fig. 1616). Laminae delineate chambers that, when contiguous, are usually sepa-rated by empty slots or sutured interfaces. The chambers are the dominant structures of the *Micrina* secondary layer, but only their disposition in the mitral sclerite will be described (Fig. 1617). In the medial, abdeltoid zone of the sclerite, where the shell may be less than 100 μm thick, several discrete laminar successions are disposed more or less parallel to the external surface of the sclerite. Each discrete succession is divided medially by slots or impersistent sutures, presumably the sites of degraded membranes that served as substrates for oppositely thickening laminae. Each pair

of laminae thicken toward each other to define the medial part of a chamber and are separated by a space diverging toward the sclerite margin. Here they unite into a lobe to enclose the marginal part of the chamber, which may be up to five times thicker than the medial space. In effect, a complete chamber is like an eccentric, thick-rimmed, shallow saucer enclosed by a pair of platy laminae continuous at the rim. The laminar sets enclosing chambers are arranged in a stack of increasingly larger saucers, a disposition that is virtually the same as that of columnar and baculate laminar sets in lingulate brachiopods. The chambers contain sporadically distributed clusters of crystalline bodies, mostly spherulites but also prisms and fascicles of lath or prisms of apatite (Fig. 1618). These clusters are common in the thickened margins of cham-bers where they are fused to the last-formed surfaces of the bounding laminae; they also aggregate around the tubes running through the chambers. As in lingulates, the cham-bers were probably filled with GAGs and dispersed apatitic granules *in vivo*. Indeed the main differences between the *Micrina* and lingulate shells are textural. In *Micrina*,
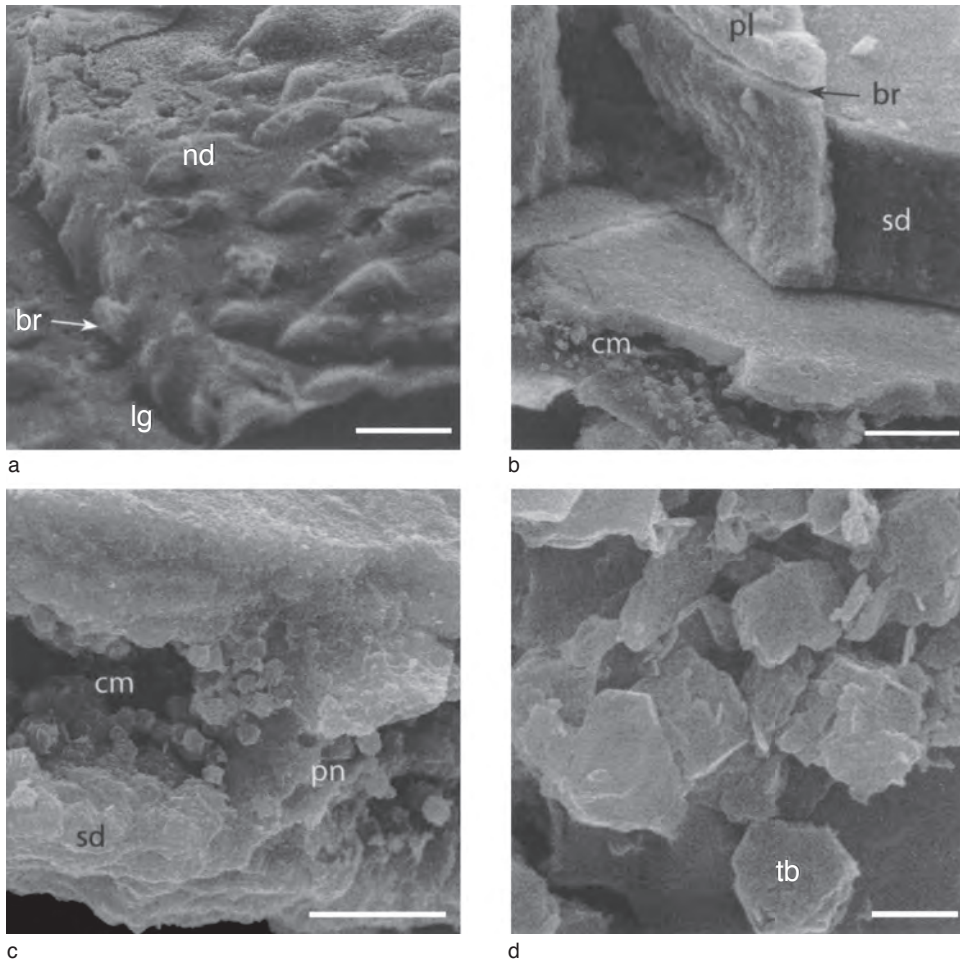
FIG. 1615. Surface ornamentation and shell structure of *Eoobolus pristinus* (POULSEN), Lower Cambrian, northeastern Greenland; *a*, oblique view of shell surface showing nodular ornamentation (*nd*) and a break (*br*) within a lamellar groove (*lg*); *b*, stratiform succession of shell with break (*br*) separating primary layer (*pl*) from secondary layer consisting of stratified laminae (*sd*) with chamber (*cm*); *c*, chamber (*cm*) within stratified laminar succession (*sd*) bounded by laminar partition (*pn*) with *d,* detail of apatitic prismatic tablets (*tb*) lining chamber; scale bars: 20 μm, 20 μm, 10 μm, and 1 μm respectively (new).

laminae are platy (not granular), and the apatitic aggregates in the chamber are spherulitic (not spherular). Such differences suggest that the calcifying proteins responsible for the mineralization of the *Micrina* sclerites were not the same as those controlling the development of the lingulate shell, despite the similarity of skeletal architecture.

ORGANOPHOSPHATIC TUBES

The shells of the lingulate siphonotretides and of *Micrina* and *Mickwitzia*, the postulated sister and stem groups respectively of the Brachiopoda, are pervaded by organophosphatic tubes that grew independently of lamination. The tubes are assumed to have given rise to mineralized surface features or
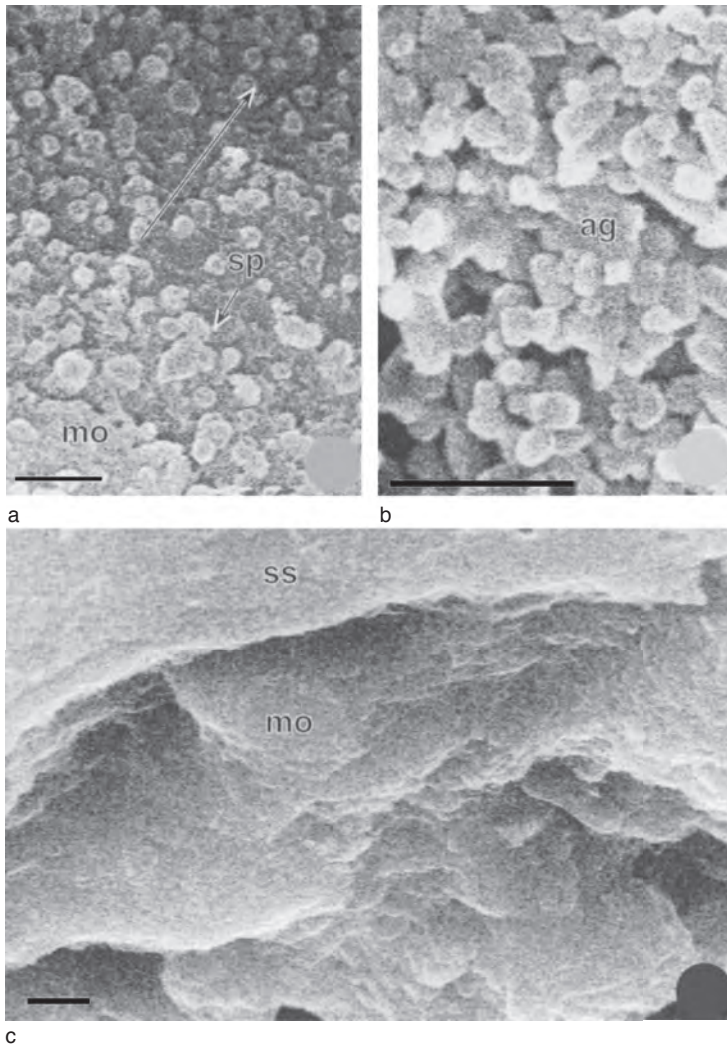
Fig. 1616. SEMs of gold-coated surfaces of mitral sclerites of *Micrina etheridgei*; *a*, GLAHM 114738, *b*, GLAHM 114744, *c*, GLAHM 114742; *a–b*, details of laminar surfaces showing pinacoids and prisms of apatite forming variably aggregated (*ag*) monolayers (*mo*) of tablets and discoids, facing directions of crystallographic steps (*sp*) indicated by *arrows*; scale bars: 1 and 0.5 mm respectively; *c*, platy monolayers (*mo*) of primary layer at margin of young sclerite as seen in oblique fracture, beneath external surface (*ss*); scale bar: 1 mm (Williams & Holmer, 2002).

to have contained setae; and a description of them is relevant to our understanding of brachiopod phylogeny as well as shell growth.

Except for *Schizambon*, the shells of all siphonotretides are perforated by unbranched canals, 20 to 80 or so µm in diameter, disposed orthogonally to lamination and leading to pits and spines ornamenting shell surfaces. Both pits and spines in similar offset patterns characterize postjuvenile shells. Pits are the sole ornamentation of a few siphonotretides, such as *Helmersenia*. On the more mature surface of most siphonotretides, however, pits are replaced by spines as in *Siphonotreta*.

The canals are differentiated at the shell margin as holes with sharp edges perforating
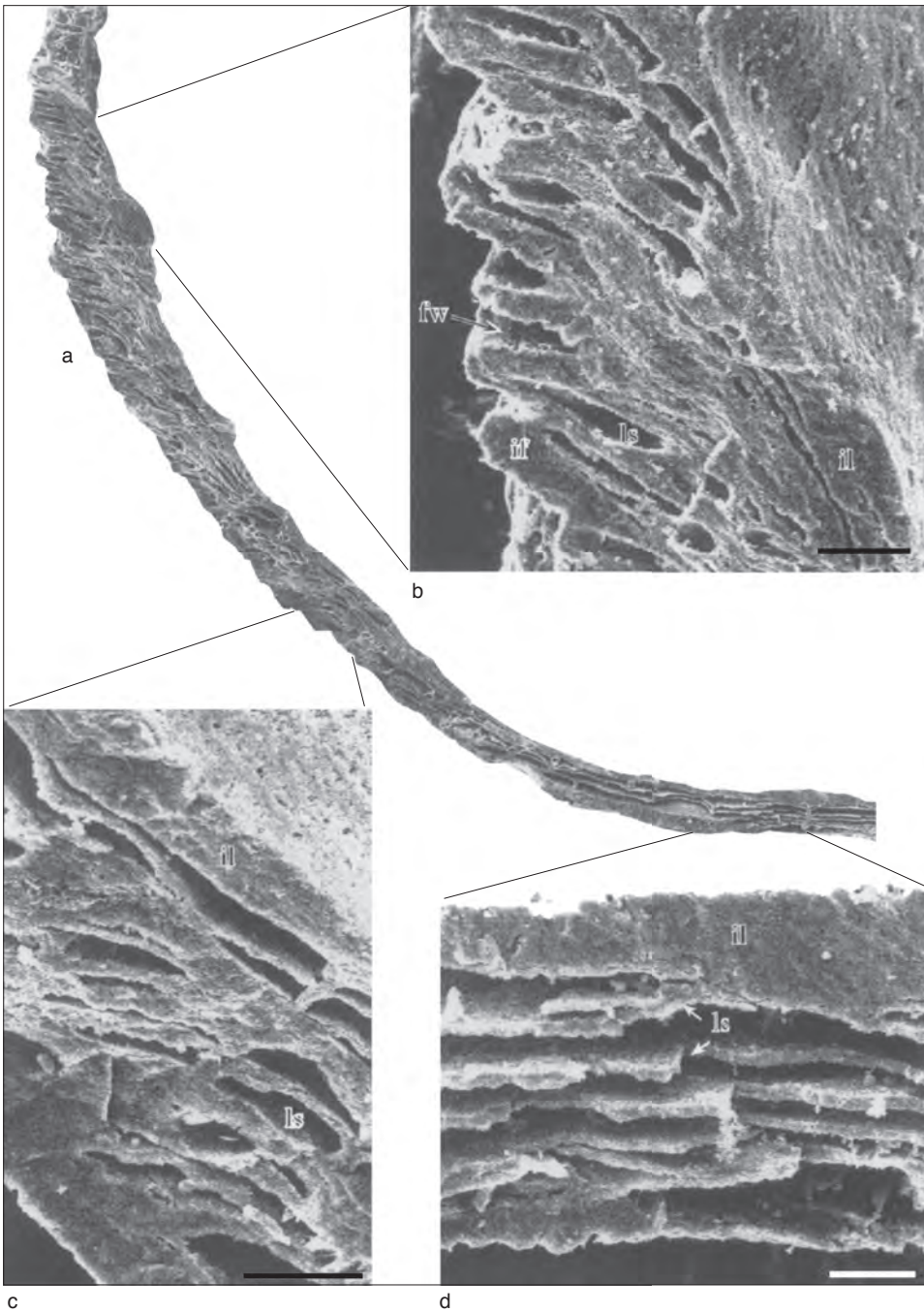
FIG. 1617. *a–d,* Half of transverse fracture section of mature mitral sclerite of *Micrina* (GLAHM 114738) showing progressive tilting of spherulitic laminar sets (*ls*) toward margin, relative to internal lamina (*il*) composed of bases of sets; furrows (*fw*); and chambers of sets with apatitic infills (*if*); scale bars: 100 μm (*b–c*) and 50 μm (*d*) (Williams & Holmer, 2002).
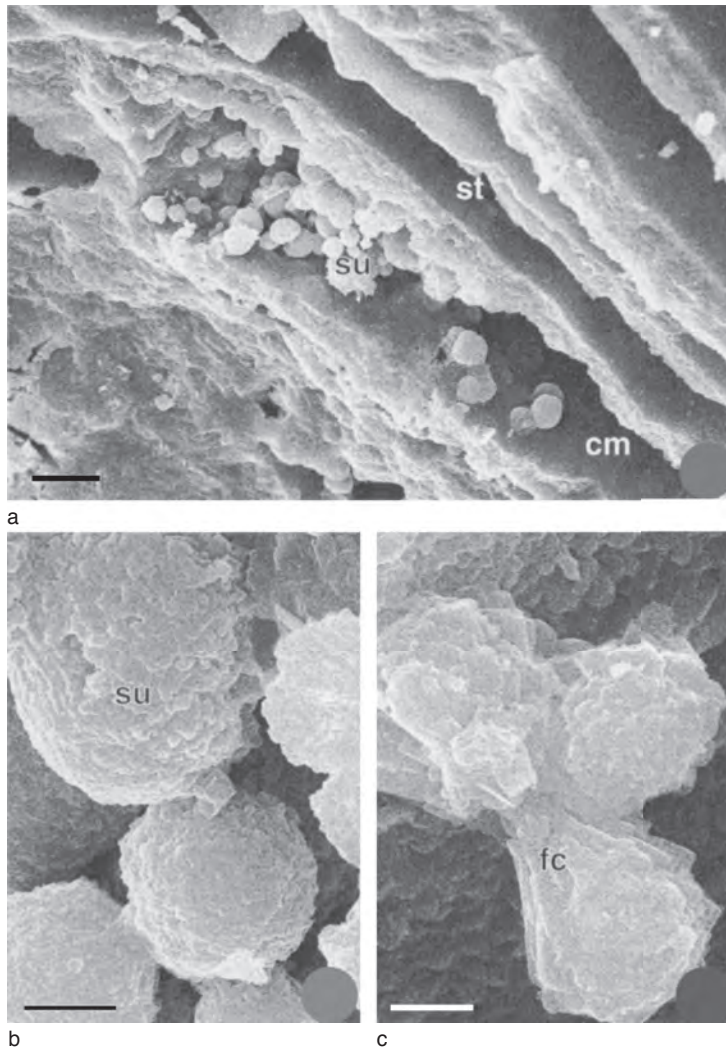
FIG. 1618. SEMs of gold-coated surfaces and fracture sections of mitral sclerites of *Micrina etheridgei*: *a–b*, GLAHM 114738; *c*, GLAHM 114746; *a*, transverse fracture section of laminar succession showing slots (*st*) between sets and spherulites (*su*) adhering to both walls of chamber (*cm*); scale bar: 20 μm; *b–c*, spatitic crystalline bodies in chambers of laminar sets, as platy spherulites (*su*) and prismatic fascicles (*fc*); scale bars: 2 and 1 μm respectively (Williams & Holmer, 2002).

the outer primary layer and are big enough to have been occupied by collectives of up to ten cells (Fig. 1619). Such collectives would have been generated as part of the outer mantle lobe but independently of surrounding vesicular cells. Each collective (acanthoblast of WILLIAMS, HOLMER, & CUSACK, 2004, p. 1333) would have been coated by a membrane that served as an organic coat ensheathing acanthoblasts

in canals lacking mineralized walls as in *Helmersenia* (Fig. 1620) or as a substrate for apatitic canal walls like those penetrating the shell of *Siphonotreta* (Fig. 1621). The canal walls are best seen at the external surface where they emerge as spinal bases (Fig. 1622). The wall, being up to 10 μm thick, is normally recrystallized but traces of laminar stratification concentric to the axis can occur. The axial cavity, occupied
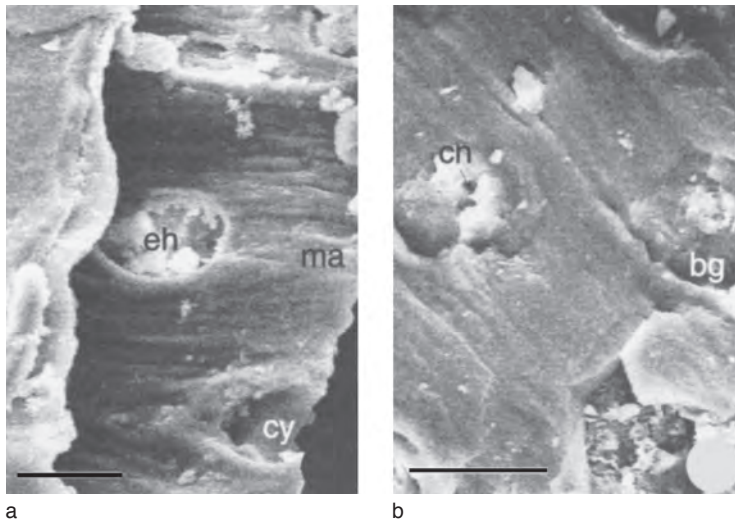
FIG. 1619. SEMs of gold-coated surfaces of valves of *Siphonotreta unguiculata*; *a,* internal view of margin (*ma*) of lamella showing elliptical holes (*eh*) with canopy (*cy*) within a slip stream of grooves orthogonal to margin; scale bar: 50 μm; *b,* internal laminar surface near margin of valve showing structural distinctiveness of penetrating spines with bounding walls (*bg*) and canals (*cn*); scale bar: 100 μm (Williams, Holmer, & Cusack, 2004).

by an acanthoblast in life, may be 30 μm in diameter but can be virtually closed by centripetally secreted apatite. The canal walls with their outer membranous coats retained their structural identity within the thickening shell as seen in fracture sections (Fig. 1621) and especially where they emerge as bosses and pillars within chambers that would have been filled with GAGs and apatitic aggregates *in vivo* (Fig. 1621). Both bosses and pillars normally have axial canals; coarse growth banding commonly gives pillars a crudely stacked appearance.

At the shell surface of *Helmersenia*, the canals are continuous with funnel-shaped antechambers with subcircular rims (Fig. 1620). The rim is broken anteroradially by a roughened, tongue-shaped depression. Within the rim, there is a ring composed of ledges of stratified laminae, some of which may extend centrally to form a concave sheet that may have been perforated in the living state. The morphology and textures of antechambers suggest that *in vivo* they contained degradable thornlike tubercles composed largely of chitin (Fig. 1620; WILLIAMS, HOLMER, & CUSACK, 2004, p. 1332).

The pits on the immature shell of *Siphonotreta* are not differentially structured like those of *Helmersenia* and were probably capped by simple, apatitic canopies or phosphatized membranes (compare those of *Acanthambonia,* Fig. 1623) that would have covered part of the acanthoblast occupying the membrane-lined pit. In later stages of shell growth this part of the acanthoblast would have started growing anteroradially and secreting apatitic laminae on its membranous coat to form a spine.

Spines vary in length and thickness (Fig. 1624). They may be several millimeters long but are seldom preserved intact, while their basal diameters average 80 μm. Although they originate in an offset pattern, they can be densely distributed, especially at the margins of mature shells (Fig. 1624). A typical spine has all the characteristics of a rheological body (Fig. 1622). Long creases deform the base while shorter, transverse ones indent the spinal surface away from the shell. Swellings also occur, as do growth bands and disruptions that dislodge segments. Spines are composed of at least one layer of apatite forming the bounding
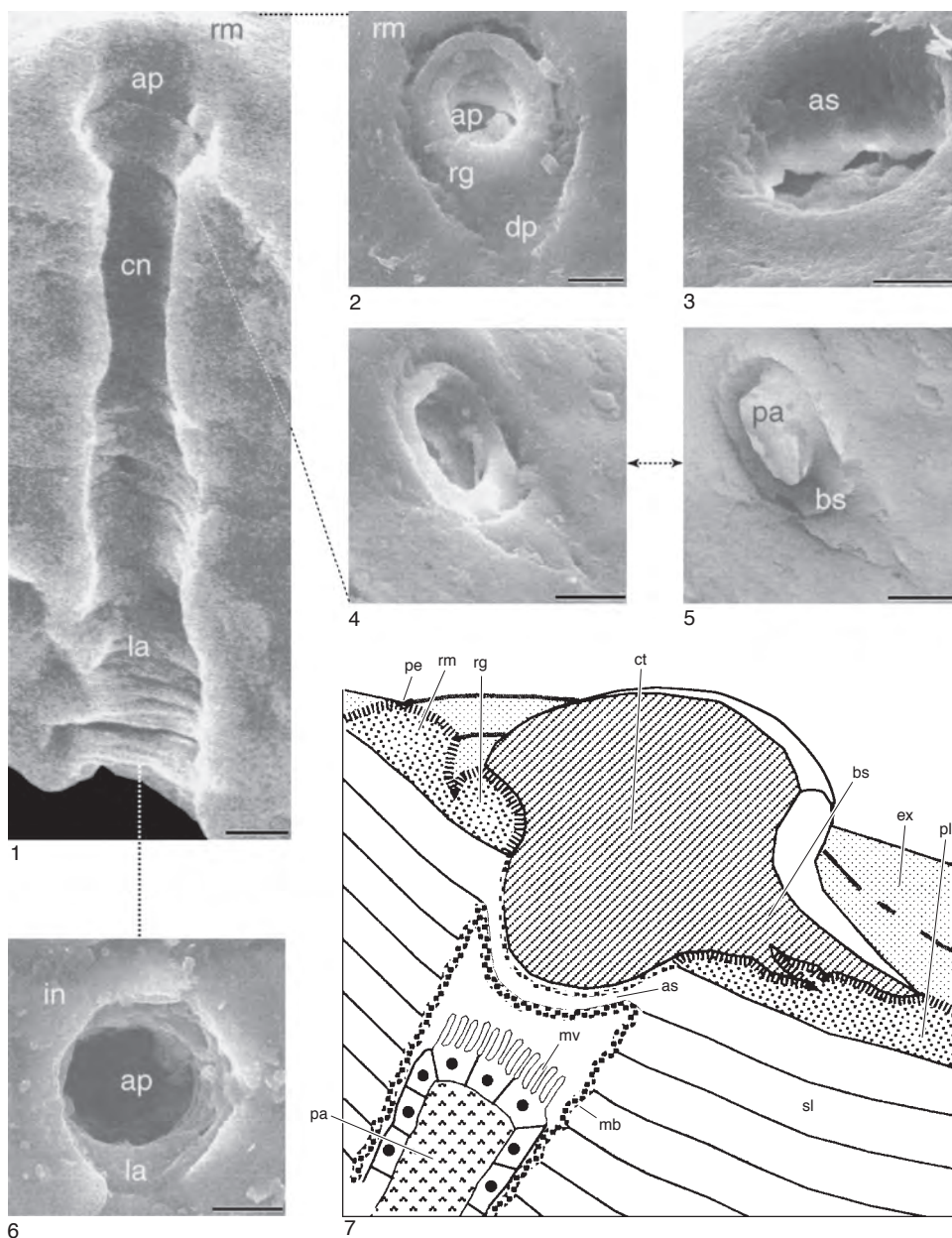
FIG. 1620. Various features of canals of *Helmersenia* (*1–6*) with diagrammatic reconstruction of distal parts of canal in living stage (*7*); *1,* vertical section through canal (*cn*) showing laminar ledges (*la*) forming wall with aperture (*ap*) and raised posterior rim (*rm*) at shell surface and internal (*in*) aperture (*6*) delineated by laminar ledges (*la*), GLAHM 114789; *2–3,* two external apertures (*ap*) in vertical and oblique views (GLAHM 114790, 114801) showing rims (*rm*), ring (*rg*), apatitic sheet (*as*), and anteroradial, tonguelike depression (*dp*); *4,* oblique view of external aperture, with inverted image (*5*) showing disposition of assumed papilla (*pa*) and basal chitinous sheets (*bs*) (GLAHM 114801); *7,* assumed components of canal in living shell with external (*ex*) periostracum (*pe*), rim (*rm*), and ring (*rg*) of primary layer (*pl*) with surface aperture, bounded by concave apatitic sheet (*as*), containing a chitinous (possibly with dispersed apatite) tubercle (*ct*) with basal sheets (*bs*) anteroradially and canal perforating secondary laminar layer (*sl*), lined with membrane (*mb*), and containing microvillous (*mv*) papilla (*pa*); scale bars: 10 μm (Williams, Holmer, & Cusack, 2004).

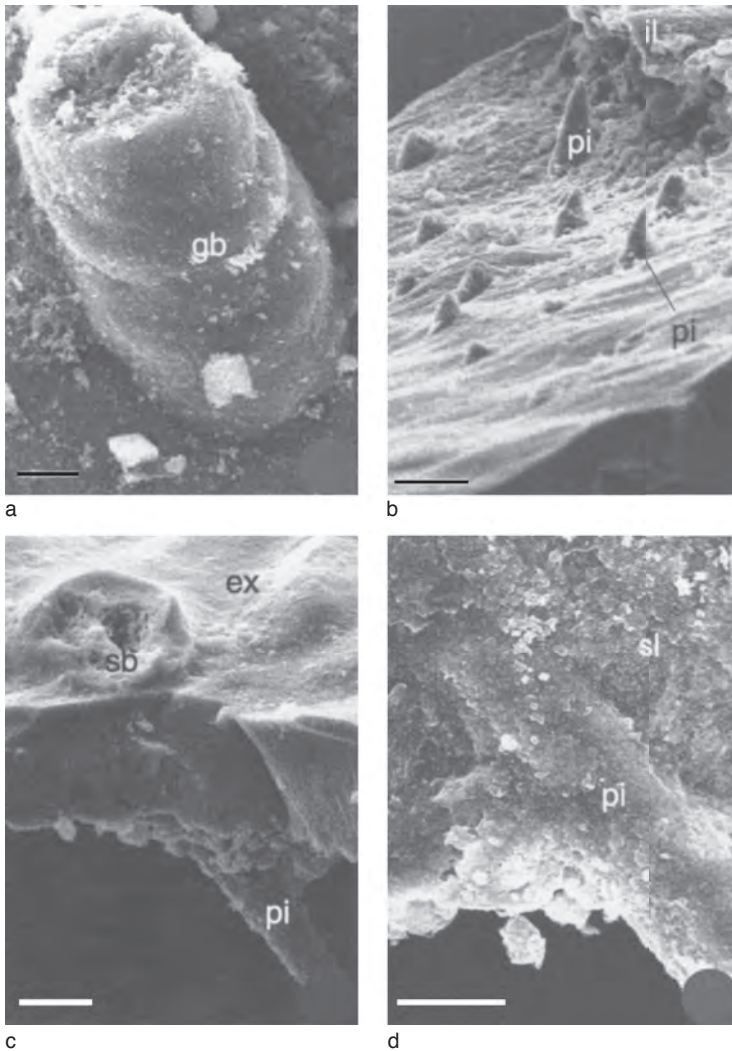FIG. 1621. SEMs of gold-coated fracture sections and surfaces of *Siphonotreta unguiculata*; *a–b*, views of valve interiors showing bands of valve floors delineated by ridges (*il*) corresponding to external lamellae and containing arrays of pillars (*pi*) that may be growth-banded (*gb*) and terminated within a GAGs chamber; scale bars: 10 μm and 100 μm respectively; *c–d*, fracture sections showing penetration of recrystallized shells (*sl*) by pillars (*pi*) to connect with spinal base (*sb*) at valve exterior (*ex*); scale bars: 50 μm and 20 μm respectively (Williams, Holmer, & Cusack, 2004).

wall to an axial canal, which is variably constricted by an additional inner laminar layer(s).

The stresses set up by the differential growth of a spine and its supporting strip of shell, exceptionally delineated by grooves (Fig. 1622), gave rise to transverse folds around the spinal base at the surface and caused the forward bend of the spinal pillar within GAG chambers of the secondary layer. Such strains account for the boomerang shape of a spine, its canal wall, and internal pillar, all secreted by an acanthoblast (Fig. 1625).

The preeminent canal system of *Micrina* consists of a regular network of mineralized tubes that open at the external surfaces of both sclerites. On surfaces that grew radially
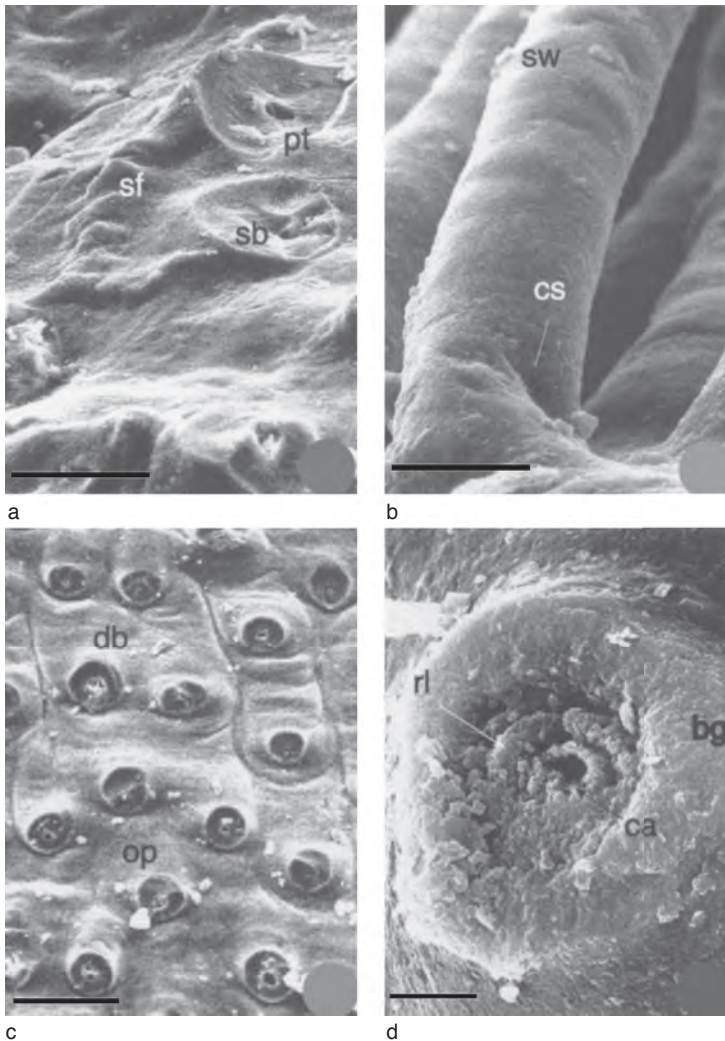
FIG. 1622. SEMs of gold-coated surfaces of valves of *Siphonotreta unguiculata*; *a–b*, conchoidally fractured spinal bases (*sb*) and pits (*pt*) with axial canals in relation to scalloped fila (*sf*) and views of creases (*cs*) at bases of spines with growth banding, sporadic swellings (*sw*); scale bars: 100 μm and 50 μm; *c*, spinal bases in offset (*op*) and dichotomous (*db*) arrangements, each delineated by a groove and contained between posterior transverse folds; scale bar: 200 μm; *d*, transverse section of large spine near its base, showing bounding wall (*bg*), a secondary layer of rubbly apatitic aggregates (*rl*), and tubular wall of compacted apatite (*ca*) delineating axial canal; scale bar: 10 μm (Williams, Holmer, & Cusack, 2004).

at a steady rate, the funnel-shaped openings are spaced concentrically, approximately 100 μm apart, and in alternating arcs (Fig. 1626). In zones where radial growth was slower, as at the sclerite margins, openings and tubes tend to crowd together (Fig. 1627). The tubes, circular to elliptical in cross section, extend throughout most, if not all, of the laminar secondary layer. They are disposed orthogonal to the external surface in the apical region (Fig. 1627) but become increasingly inclined marginally where they may lie virtually subparallel with laminar sets (Fig. 1627) and in line with hemicylindroid imprints extending beyond their funnels (Fig. 1625). The external surface
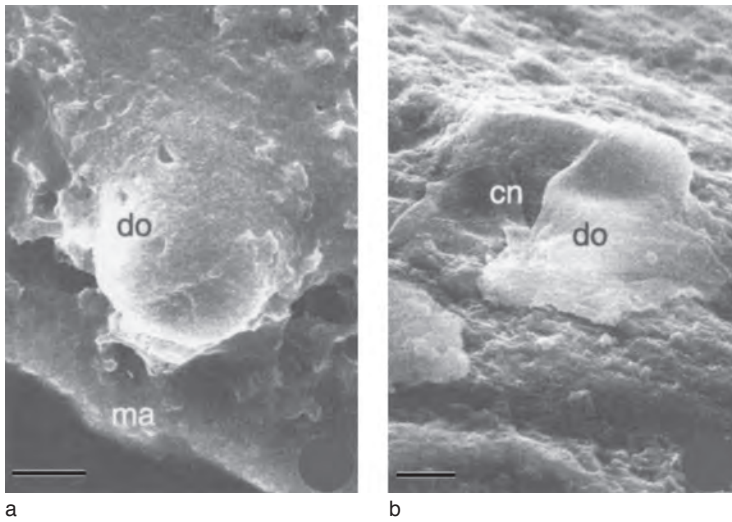
Fig. 1623. SEMs of gold-coated surfaces of *Acanthambonia delicatula* (GLAHM 114794, 114787). Surfaces of immature valves showing partial domes (*do*) that served as spinal joints at external surface, near valve margin (*ma*), and in oblique view with exposed canal opening (*cn*); scale bars: 10 μm and 25 μm respectively (Williams, Holmer, & Cusack, 2005).

of a tube is typically smooth with sporadic accretions of spherulites, laths, and prisms. The tube wall is approximately 4.5 μm thick and is composed of stratified laminae lying parallel with the surface. The tube interior is striated by alternating grooves and ridges parallel with the long axis. The ridges, up to 800 nm wide, are composed of flat-lying, well-ordered discoidal to subhexagonal tablets (Fig. 1628). Each tube consists of three elements: a superficial, funnel-shaped opening separated from the internal hollow, striated tube by an outwardly concave, perforated plate(s) (Fig. 1628). The funnel is typically approximately 10 μm deep with smooth, gently curved surfaces covering horizontally disposed stratified laminae of the primary layer. Its inner boundary is a sharply jagged rim separating it from an antechamber approximately 10 μm deep, with smooth, bulging walls. The inner boundary of the antechamber is a smooth ledge, below which is an outwardly concave apical plate (Fig. 1627) that, when complete, is indented by three oval imprints.

The structure and function of these mineralized tubes and their components in the living state have been interpreted as follows (Fig. 1629). The structures and impressions associated with funnels are consistent with their having contained organic rods that were disposed at high angles in the medial regions but tangentially toward the margins of mature sclerites. The cuticle of such a rod could have been continuous with the periostracum covering the sclerite along the jagged inner edge of the funnel. The base of the rod would have consisted of a disk occupying the antechamber, and, below the inner ledge, a hemisphere with three bosses that fitted into oval depressions or perforations in the outwardly concave plate that could have been little more than a phosphatized membrane. Because the apatitic tubes carrying the canals were secreted independently of laminar sets, they would have been deposited within a cylindroid organic coat that determined the diameter of the tube *ab initio*. The grooves striating the inner surface of the tube walls are consistent in size and disposition with there being casts of microvilli. This ensemble of external organic rods (interpreted as setae) occupying funnels and postulated microvillous cells occupying striated tubes suggests that the cell collectives were setoblasts. That being so, the setal rods and their bases
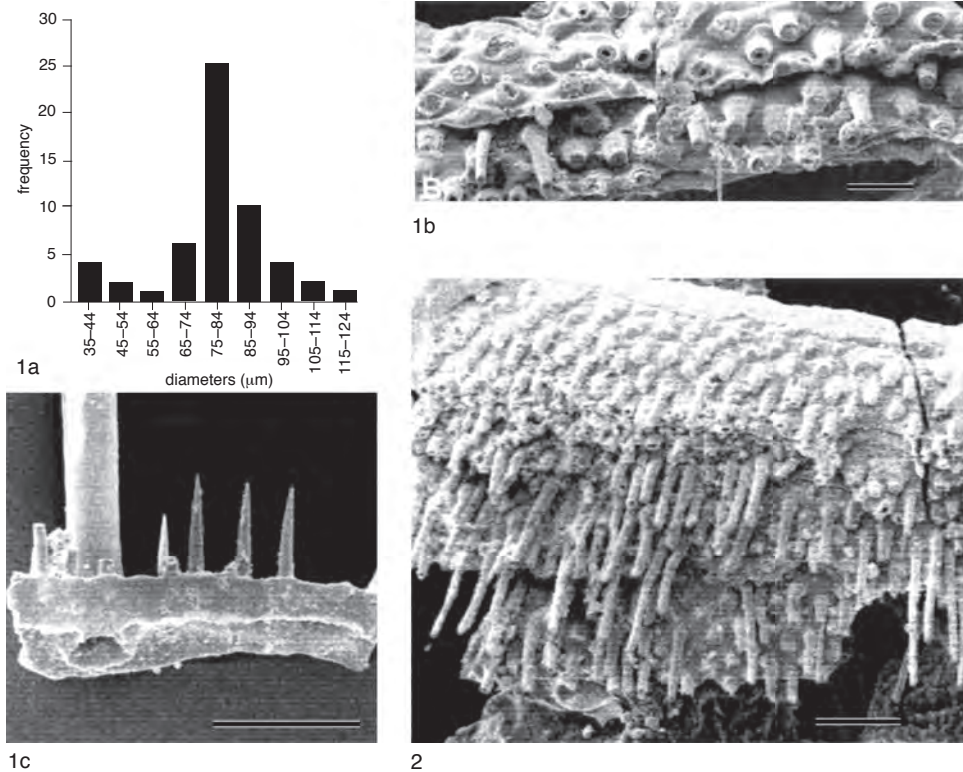
FIG. 1624. Variation in size and distribution of siphonotretide spines; *1a,* range of diameters of 55 spinal bases (mean 80.2 µm) on fragment (*1b*) of *Siphonotreta unguiculata* (GLAHM 114782a, b) bearing two lamellae; scale bar: 200 µm; *1c,* external view of a segment of mature shell of *S. unguiculata* (GLAHM 114781), showing crowded arrays of spines of varying diameter in contrast to differentiated large and small spines of *2, Eosiphonotreta verrucosa*, GLAHM 114798; scale bars: 0.5 mm (Williams, Holmer, & Cusack, 2005).

would have been chitinous and presumably mobile, possibly with fibrillar strands connecting the setal bosses to setoblasts that, however, would usually have been sealed off from the mantle during later sclerite growth (WILLIAMS & HOLMER, 2002).

The columnar shell of the stem-group brachiopod *Mickwitzia* (HOLMER, SKOVSTED, & WILLIAMS, 2002) is also pervaded by hollow tubes approximately 8 µm thick that grew independently of lamination. They are generally disposed orthogonal to the shell surface where they open as smooth rounded apertures. Some tubes are inclined, especially those perforating the ventral pseudointerarea, where they lie more or less in the plane of the pseudointerarea, the external surface of which is frequently indented by semicy-

lindrical depressions immediately distal of the apertures. Striations parallel with their long axes have been found in some of these tubes (Fig. 1630), which are regarded as homologous with those of *Micrina*. The lack of elaborate devices such as antechambers beneath their surface apertures suggests that any setae occupying the apertures would not have been permanent features of the living shell.

EVOLUTION OF THE MATURE ORGANOPHOSPHATIC SHELL

The evolution of the mature linguliform shell is reflected mainly in the diverse fabrics of the secondary layer. The chemicostructure
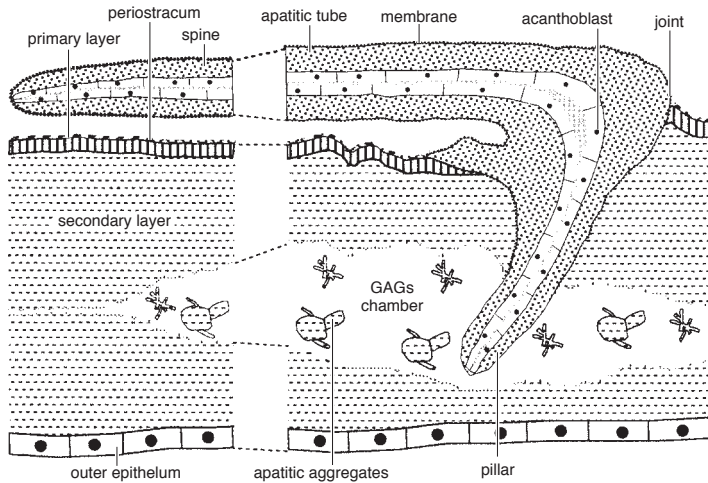
FIG. 1625. Diagrammatic section of *in vivo* siphonotretid integument showing relationship between membrane-bound spine secreted by inferred acanthoblast and stratiform shell secreted by outer epithelium. Reconstruction assumes acanthoblast has been sealed off from outer epithelium and its proximal apatitic tube (pillar) ends with GAGs chamber within secondary layer of shell; forward growth of membrane, showing as substrate for apatitic or GAGs secretion is assumed to have been by intussusception (Williams, Holmer, & Cusack, 2004).

of fossil as well as living shells indicates that the primary layer has always been a rheological coat composed of protein-coated apatite in GAGs; and only superficial rheomorphic and ornamental features survive fossilization. In contrast, six distinctive, long-lasting fabrics with significant textural variations characterize the linguliform secondary shell. Five of these fabrics were fully developed in Cambrian species. Their relationships have been phylogenetically analyzed (Fig. 1631; Table 32–33) on the assumption that all were derived from the secondary shell fabric of a stem-group brachiopod, like *Mickwitzia*, in phase with basic transformations of early brachiopod anatomy.

As shown in Figure 1631, both the columnar and baculate fabrics characterize the short-lived linguloid *Lingulellotreta* (L. E. Popov, personal communication, 2003). The older, columnar fabric is present in the shell of *Micrina*, the assumed sister group of the brachiopod phylum, and is as strongly developed in *Mickwitzia* as in acrotretides. There is no obvious chemicostructural relationship between the columnar and baculate fabrics. The apatite of columns probably aggregated on a chitinoproteinaceous frame

disposed orthogonally to lamination, while baculi assembled in living lingulides as interconnected accretionary, apatitic rods with impersistent axial strands.

The columnar fabric, however, is feasibly a mineralized version of the lingulide caniculate system, which is fabricated independently of baculi. The organic cores of columns would have been a framework similar to the caniculate system in dimensions and disposition. Admittedly, aggregates of apatitic spherules do occasionally adhere to the chitinoproteinaceous walls of canals in living *Lingula* (Fig. 1583), although the sporadic and differential nature of their accretion would preclude their accumulation as solid apatitic columns of uniform thickness. Canals that pass through the baculate fabric of *Glottidia* and living discinids, however, are free of the apatitic spherules that aggregate into baculi (Fig. 1583), as are the organic cores of columns in interlaminar spaces. If both organic frames are homologous, however, the lingulide canaliculate system could have been derived from the columnar fabric by the loss of the calcifying protein dedicated to effecting columnar accretion. In
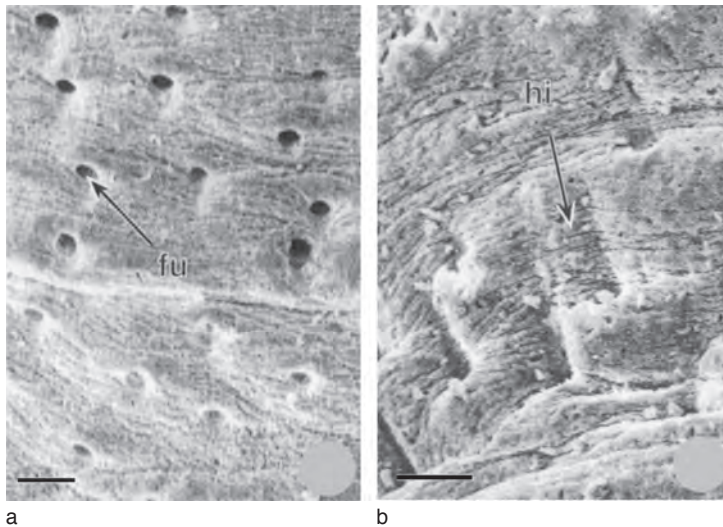
FIG. 1626. SEMs of gold-coated surfaces of mitral sclerites of *Micrina etheridgei; a,* GLAHM 114749; *b,* GLAHM 114741; surface views of funnels (*fu*) of tubular network disposed more or less orthogonally and alternately (*a*) and obliquely (*b*) where they are associated with hemicylindroid imprints (*hi*) indented on rheomorphic folds of external surfaces; scale bars: 100 μm (Williams & Holmer, 2002).

short, the substitution of a calcifying protein promoting baculation for one that effected columnar accretion would have transformed an ancient fabric into another that survives today.

The camerate texture of some acrotretides was also probably mediated by a novel calcifying protein that replaced, or was mutually exclusive with, the protein(s) responsible for the columnar fabric. The first sign of the
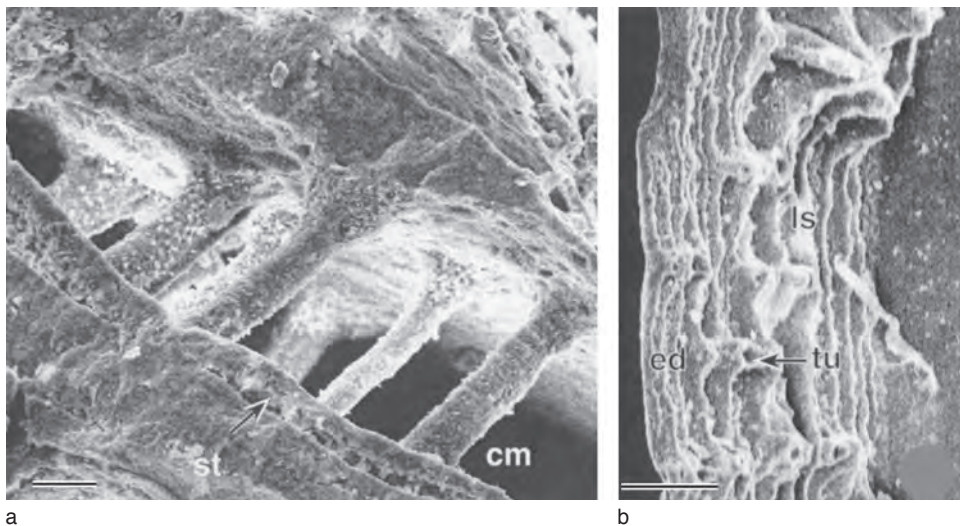
FIG. 1627. SEMs of gold-coated surfaces and fracture sections of sellate sclerites of *Micrina etheridgei; a,* tubes traversing a chamber (*cm*) of laminar set delineated by slots (*st*), with coatings of spherulitic apatite, GLAHM 114750; scale bar: 20 μm; *b,* exfoliated laminar sets (*ls*) at margin (*ed*) of mature sellate sclerite showing crowding together of near horizontal tubes (*tu*), GLAHM 114751; scale bar: 20 μm (Williams & Holmer, 2002).
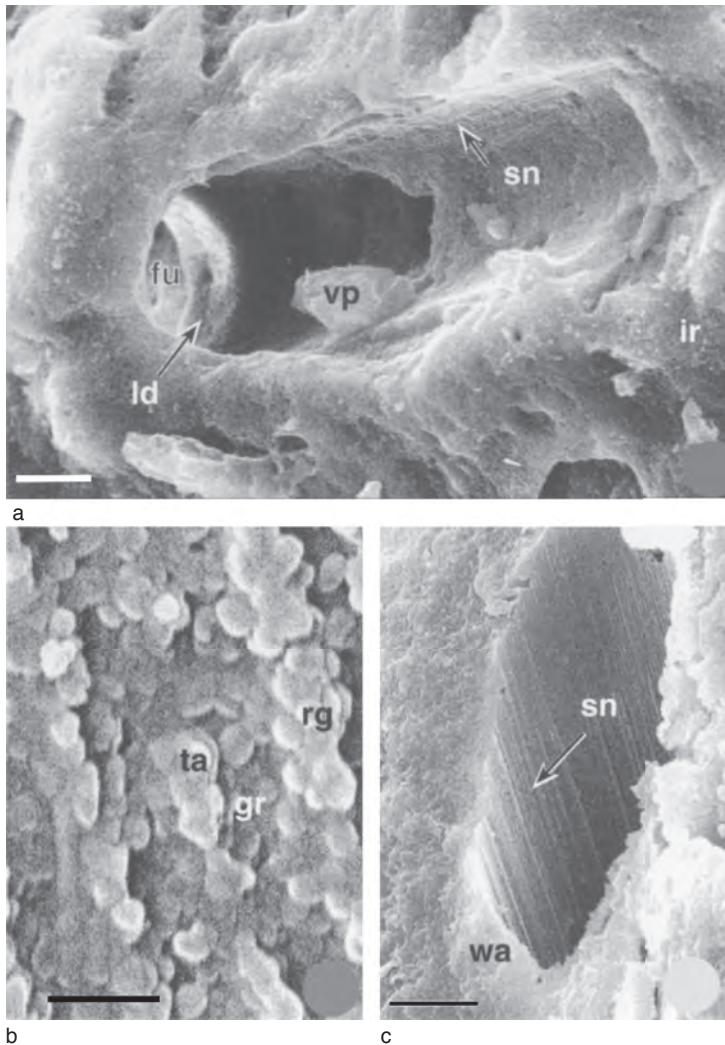
Fig. 1628. SEMs of gold-coated surfaces and fracture sections of mitral sclerites of *Micrina etheridgei*; *a,* general view of slightly inclined tube opening to interior (*ir*) and revealing striations (*sn*) on tube wall, remains of concave plate (*vp*), ledge (*ld*) leading to antechamber and funnel (*fu*); scale bar: 10 μm; *b,* details of tube consisting of grooves (*gr*) and ridges (*rg*) composed of tablets (*ta*), running parallel with tube axis; scale bar: 5 μm; *c,* rheomorphically deformed tube with wall (*wa*) bearing striations (*sn*); scale bar: 5 μm (Williams & Holmer, 2002).

linguloid virgose fabric, which was no later than the Carboniferous, is like a disordered baculation, especially in the way fascicles resemble crossed baculi. Fascicles of living *Lingula*, however, are probably assembled intracellularly and are likely to have originated as a chemicostructural novelty in place of baculate lamination.

In the phylogeny of Figure 1631, the paterinates and the siphonotretides are shown as the most derived linguliforms, but their relationships are open to question. Their defining synapomorphy, a stratiform shell with poorly defined GAGs chambers, confirms that the paterinate and siphonotretide shells are neither columnar nor

F‌IG. 1629. Graphical reconstruction of proximal part of seta and associated setoblast assumed to have occupied funnel-like opening leading into apatitic tube penetrating stratiform shell of *Micrina* sclerite (Williams & Holmer, 2002).

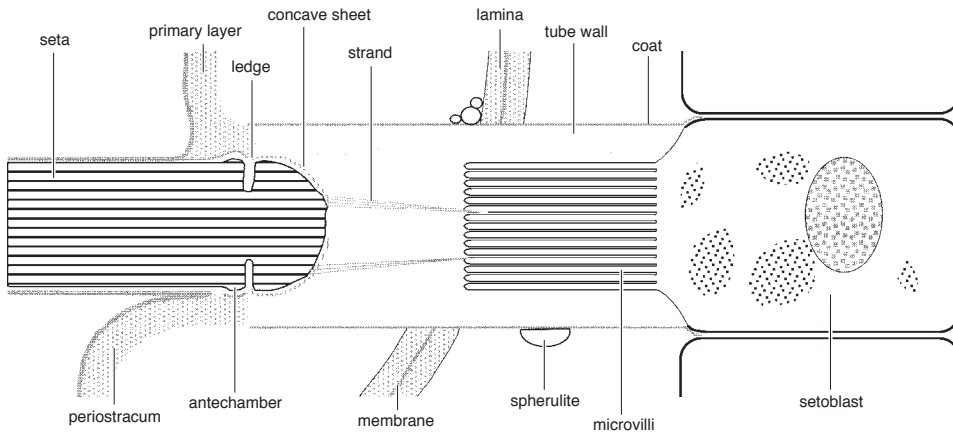baculate and apparently lacked a canaliculate system. Even so, the difference between the acicular and granular nature of their basic apatitic constituents suggests that the similarity of their shell fabrics was due to convergence. The two groups certainly differ from one another as well as other linguliforms in other features. The acanthoblastic spines and tubes of siphonotretides are an apomorphy that developed independently of the setigerous tubes. The most striking differences, however, are those paterinate features that are shared with rhynchonelliforms, including the adductor-diductor muscle system, the development of mantle gonadal sacs, and the fused posterior mantle lobes (W‌ILLIAMS, P‌OPOV, & others, 1998).

ORGANOCARBONATE, TABULAR LAMINAR SHELL

The descriptions in Volume 1 (W‌ILLIAMS & others, 1997, p. 22–23; W‌ILLIAMS, 1997, p. 284–286) of the secretion and structure of organocarbonate, tabular laminar shells were based almost exclusively on investigations by S‌CHUMANN (1970) and W‌ILLIAMS and W‌RIGHT (1970). These studies established that the secondary shell of living craniids, consisting of rhombs of calcite interleaved with glycoproteinaceous membranes, grows spirally with the membranes serving as substrates for calcitic tablets that enlarge and multiply by screw dislocation. The fabric of the secondary layer of extinct craniiforms was also shown to be laminar and different from that of the radially prismatic primary layer that characterizes living species (W‌ILLIAMS & W‌RIGHT, 1970). Since 1997, research has concentrated on the organic constituents of the shell following the discovery that intracrystalline proteins with calcium-binding properties could be extracted from the shell of living *Novocrania* and that calcitic rhombohedra could be sectorally pitted by bleach (B‌ROWN, 1998). By these procedures, the sites of proteins distinguished by their molecular weight have been identified on the secondary (W‌ILLIAMS, C‌USACK, & B‌ROWN, 1999) and primary (C‌USACK & W‌ILLIAMS, 2001a) layers of the shell of living *Novocrania*. Moreover, by comparing organic residues from and the textures of craniid shells of different geological ages, it has been possible to estimate the extent of protein degradation and skeletal recrystallization during fossilization (C‌USACK & W‌ILLIAMS, 2001b).

CHEMICOSTRUCTURE OF THE *NOVOCRANIA* SHELL

The fabric of the dorsal valve of living *Novocrania* differs from that of the ventral valve, especially in the development of the
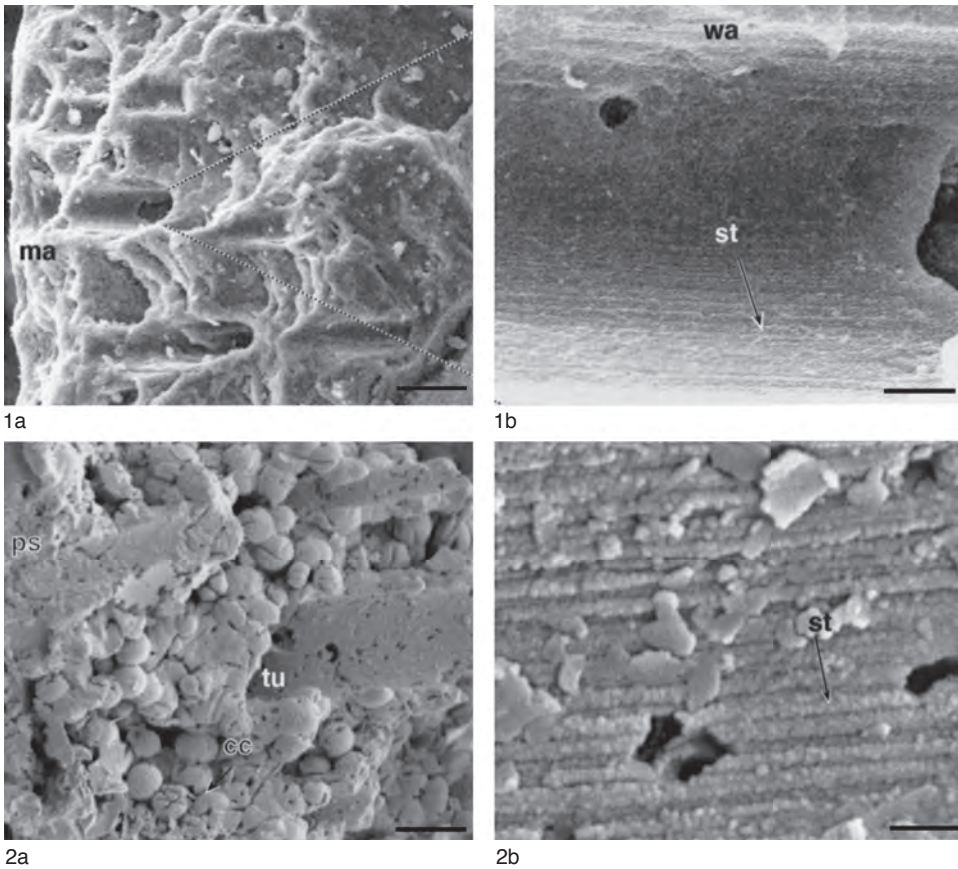
Fig. 1630. General views and details, under SEM, of setigerous tubes at margin (*ma*) of mitral sclerite of *1, Micrina* (GLAHM 114751) and on poorly preserved ventral pseudointeraea (*ps*) of *2, Mickwitzia* (MGUH 26279); tubes (*tu*) with laminar walls (*wa*), intact or fragmented with adhering phosphatized capsules of cocci (*cc*), are striated (*st*); scale bars from left to right: 10 μm and 5 μm in *Micrina*; 10 μm and 1 μm in *Mickwitzia* (Holmer, Skovsted, & Williams, 2002).

secondary layer. The chemicostructure of this layer will be described first because the spatial relationships of its organic and mineral components are the key to the growth of the shell as a whole. Irrespective of fabric differences, however, all mineralized structures are composed of spheroidal or rhombohedral granules of calcite approximately 30 nm in size, which are revealed by degrading the organic constituents and are assumed to be coated with a water-soluble protein (Williams, Cusack, & Brown, 1999). The organic constituents, on the other hand, vary in configuration as well as composition, as

shown by plasma etching and bleach and enzymic treatment.

The secondary layer thickens and spreads by the spiral growth of calcitic laminae, through right- and left-handed screw dislocations of rhombohedra interleaving with glycoproteinaceous membranes that serve as substrates for the mineralized components of the secondary layer (Williams, 1970; Williams & Wright, 1970).

The interlaminar membranes consist of an electron-dense mesh containing close-packed, electron light vesicles approximately 20 nm in diameter (Fig. 1632b). The membranes may terminate abruptly
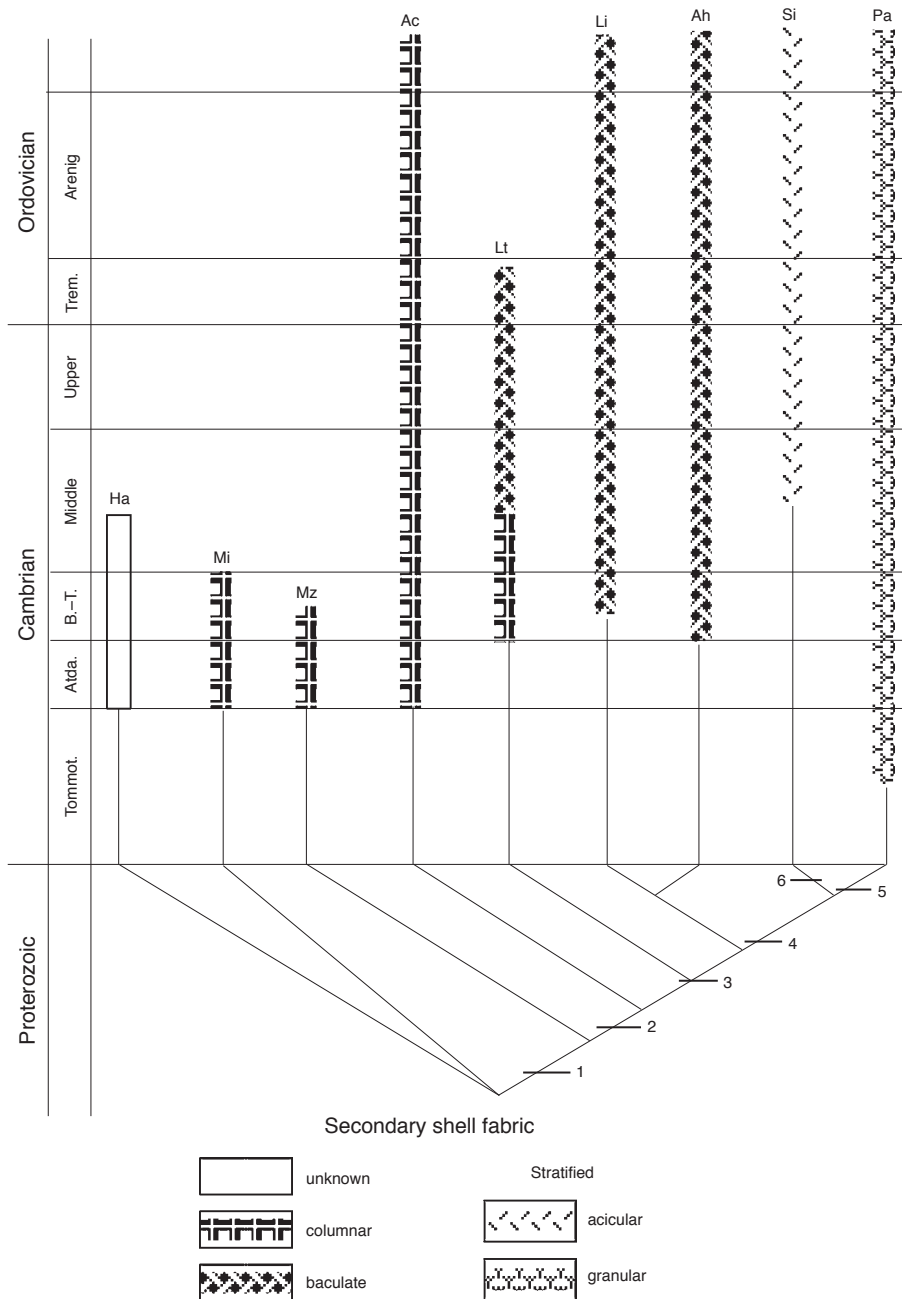
FIG. 1631. Chart showing evolution of main fabrics of secondary shells of Cambro-Ordovician linguliforms with *Halkieria* (*Ha*) and the presumed halkieriid *Micrina* (*Mi*) as sister groups. The linguliform groups are: stem-group *Mickwitzia* (*Mz*), acrotretides represented by *Prototreta* (*Ac*), linguloid *Lingulellotreta* (*Lt*), linguloid *Obolus* (*Li*), acrotheloid *Acrothele* (*Ah*), siphonotretide *Siphonotreta* (*Si*), and the paterinate *Paterina* (*Pa*). The cladogram, which is not to geological time scale, is a 50% majority-rule consensus of 6 trees generated by a PAUP heuristic search (10 stepwise additions) of 11 character states (Table 32) and matrix (Table 33) of 9 named taxa; numbered transformations are: *1,* development of brachipod body plan (characters 1–5 of Table 32); *2,* loss of setigerous tubes; *3,* change from columnar to baculate fabric; *4,* loss of baculi and well-defined GAGs chambers; *5,* development of adductor or diductor muscle systems (and other rhynchonelliform features); *6,* development of nonsetigerous tubes (new).

TABLE 32. List of 11 character states used in the cladogram of Figure 1631 to illustrate a possible origin of the diverse fabrics of the mature secondary shell of early linguliforms (new).

Body plan
1. Bilaterally symmetrical body	segmented (0), unsegmented (1)
2. Disposition of body	straight (0), folded on transverse axis (1)
3. Valves (sclerites)	separated (0), conjoined (1)
4. Valve margins	not apposed (0), apposed (1)
5. Pedicle	absent (0), present (1)

Shell structure and morphology
6. GAGs chambers	poorly defined (0), well developed marginally (1)
7. Columnar lamination	absent (0), present (1)
8. Baculate lamination	absent (0), present (1)
9. Setigerous tubes	absent (0), present (1), other tubes (2)
10. Pedicle opening	absent (0), at ventral beak (1), within ventral valve (2), between valves (3)
11. Muscles operating valves	unknown (0), obliques (1), diductors (2)

or branch at acute angles or in near-vertical steps (Fig. 1632a). Membranes immediately succeeding stepped zones are commonly fragmented. The membranes are differentially digested in enzymes but comprehensively degraded by plasma etching and bleach. All treatments permanently or transiently reveal fibrous networks that presumably support the vesicles (WILLIAMS, CUSACK, & BROWN, 1999). The most common interlaminar polymer extracted from the membranes is a calcium-binding 44 kDa protein with high levels of aspartic acid–asparagine, glutamic acid–glutamine, and serine (BROWN, 1998). The protein also occurs within calcitic laminae.

The basic structural unit of the mineralized secondary layer is a tabular rhombohedron, (10.4), that lies in the plane of the laminar succession and may exceed 5 µm diagonally. Faces sharing edges with the (10.4) face form steps that are seldom more than 300 nm high (Fig. 1633). Their indices can be used to distinguish edges shared with the (10.4) face. Up to four other minor steps are variably developed with edges parallel with the diagonals of the (10.4) face, and they too can be identified by general indices as shown in Figure 1633. The rhombohedra composing a lamina are separated from one another by sutures that sporadically enclose polygonal windows revealing inliers of older, outer laminae. Epitaxial alignment between and within laminae is localized but can

extend through at least ten laminae. Rhombohedra enlarge by spiral or planar growth on interlaminar membranes and are found at all stages of accretion, virtually from nucleation on the internal surface of the valve. Despite their chemicocrystallographic homogeneity, rhombohedra are morphologically distinguishable as monolayered plates and multilayered tablets with different patterns of growth and macromolecular adsorption (Fig. 1634).

Plates occur discretely but more usually as foundations for tablet growth. They may be as small as approximately 150 nm in the long diagonal (Fig. 1635b–c) with (0k.1) steps, roughened by rhombohedral kinks generally developing in larger plates (Fig. 1635d). Plates are essentially flexible monolayers of spherular granules arranged in mosaics or

TABLE 33. Matrix of 11 characters described in Table 32 and 9 designated taxa (new).

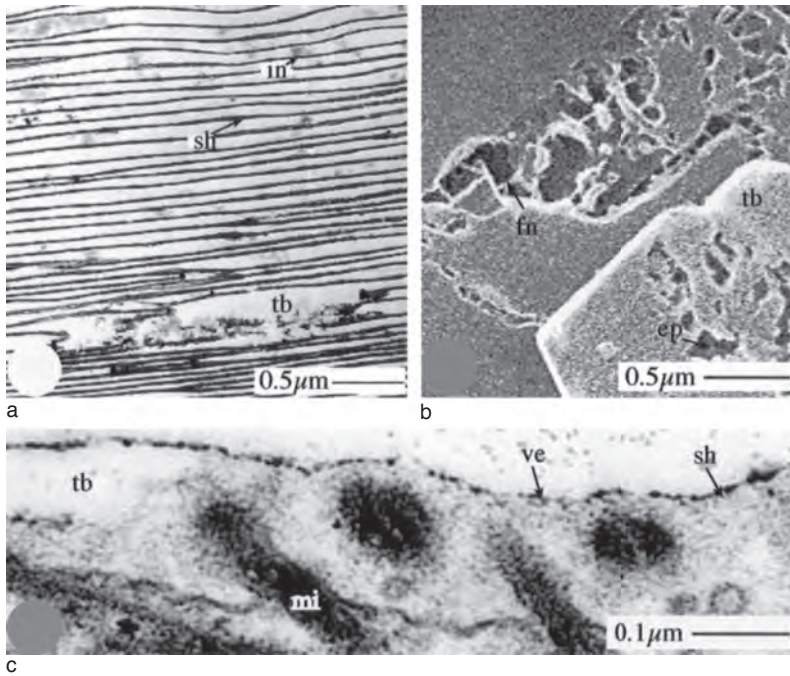|	[11 12345678901]
Halkieria	00000?00?00
Micrina	00000110100
Obolus	11111101011
Prototreta	11111110011
Paterina	11111000032
Acrothele	11111101011
Siphonotreta	11111000221
Mickwitzia	1111111011?
Lingulellotreta	11111111011

Fig. 1632. *Novocrania anomala; a,* integument*; b,* SEM of internal surface treated with 10% bleach for 1 h with etch pits (*ep*) in a tablet (*tb*) and revealing a fibrous network (*fn*) in substrate; *c,* TEM section of decalcified integument, stained with aqueous uranyl acetate and aqueous lead citrate showing electron-dense meshes with electron-light vesicles (*ve*) as sheets (*sh*) originating from microvilli (*mi*) of apical plasmalemma and disrupted above a tablet (*tb*), and as infills (*in*) between laminae in view *a* (Williams, Cusack, & Brown, 1999).

zoned in growth bands approximately 30 nm wide. Their surfaces are either flat or centrally depressed, where granules are more dispersed (Fig. 1635b–c).

Tablets consist of up to eight layers of granular mosaics that, like plates, accrete by planar or, more commonly, spiral growth (Fig. 1636a–b). Degraded surfaces are variably zoned parallel to the edges of tablet faces around flat granular or depressed proteinaceous centers (Fig. 1636a). Rough (0k.1) steps are usually well developed in larger tablets, and the triangular sectors of growth they subtend with the rhombohedral centers may be sharply delineated (Fig. 1636a). Rough (h⁻0.1) steps, when developed, are short and remain so during growth, as is shown by their generation of banding in parallel strips (Fig. 1635d).

Just within the surface edge of a tablet, mosaics of granules may give way to bands of rhombohedra approximately 40 nm long (Fig. 1636c). The bands are the foundations of commonly occurring ramparts up to 600 nm high (Fig. 1636b). Ramparts are composed of rhombohedral aggregates or granules in bands parallel to the edges of tablets (Fig. 1636d). They accrete centripetally as well as vertically and may coalesce to cover organic infills of the central depression (Fig. 1636d).

Differential etching of the surfaces and steps of plates and tablets exposes the relief of the calcite and excavates sites of organic concentrations. The effects are generally more evident on underlying laminae exposed by degradation of organic substrates than on biomineralized surfaces being secreted at death (Fig. 1637d). This suggests that, in addition to some protein doping in the later stages of laminar formation, many organocalcitic microstructures are highly degradable in the living state and can even be destroyed by autolysis.
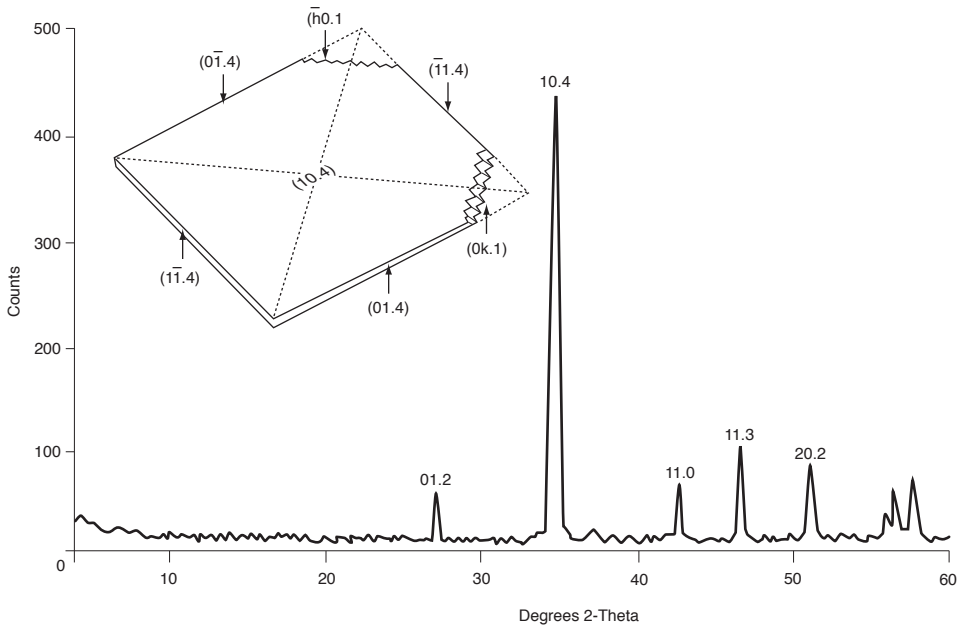
Fig. 1633. X-ray diffraction profile showing frequencies of principal crystal faces in calcite of dorsal valve of *Novocrania anomala* (Müller); inset illustrates rhombohedral indices used in this chapter (Cusack & Williams, 2001).

The simplest etched features are slits or narrow clefts extending between the centers and the acute-angled corners of rhombohedral plates parallel to the long diagonal (Fig. 1638). Growth bands are not dislocated by the kinked sides of clefts that end centrally in a granular mosaic less than 500 nm in diameter. Opposite clefts in flat plates are aligned with each other and arise from a common center; but those in spirally growing plates are sinistrally and dextrally displaced, as are their separate centers in clockwise and anticlockwise spirals respectively (Fig. 1638b). These shifts are presumably a function of rhombohedral distortion by spiral growth. The removal of narrow strips of plates along their long diagonals by enzymes confirms that granules within these zones are invested in a protein that had been adsorbed at the junctions of the (01.4) ^(11.4) and (10.4)^(01.4) steps, virtually from plate inception.

Surface etching of tablets by induced degradation is restricted to triangular zones (Fig. 1637a, 1638a) with bases at or just within the (0k.1) steps and apices, subtending angles up to 70° at central depressions. The sides of excavated (0k.1) sectors are more or less parallel with (10.4) edges but are commonly unequally developed, with one side forming a step and the other a break in slope; both are kinked by rhombohedral cleavage. Degraded sites vary from hillocks to labyrinthine walls or parallel ridges (Fig. 1637c). Deeply etched residues usually rest on basal plates and are aligned with rhombohedral cleavage. Ramparts can grow on the surfaces of tablets with etched (0k.1) sectors. Their subsequent centripetal growth can result in ledges coalescing inwardly to enclose organic infills in the central depressions of tablets (Fig. 1636d, 1637b). Such intralaminar deposits are really part of the organic interlaminar component of the secondary shell.

Degradation of laminae underlying the internal surface of a shell exposes plates and tablets coalesced within mosaics or concentric bands of granules with sutures sporadically enlarged by rhombohedral etch pits
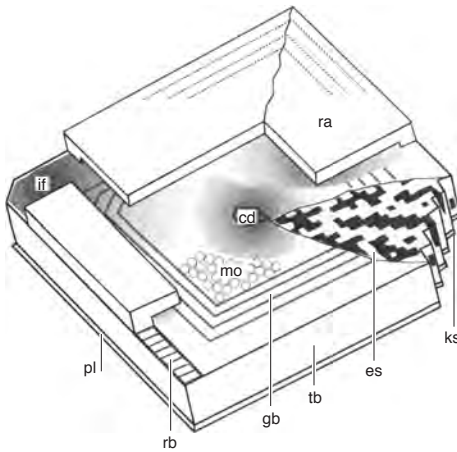
FIG. 1634. Crystallographic and chemicostructural terminology of secondary shell of *N. anomala*. Stylized etched tablet (*tb*) on plate (*pl*) with banded (*gb*), centrally depressed (*cd*), internal surface composed of granular mosaic (*mo*), coated with proteinaceous infill, 44 kDa (*if*) partly covered by ramparts (*ra*) accreting on foundation of banded rhombohedra (*rb*); etched (0k.l) sector (*es*) with ridges and hillocks delineating sites doped by 60 kDa protein along kinked steps (*ks*) (Williams, Cusack, & Brown, 1999).

(Fig. 1637c). Etched (0k.1) sectors in various stages of development and degradation occur together with rare rhombohedral and subtriangular faces that have been differentially etched into rhombohedral grilles or slats, parallel to a (10.4) edge (Fig. 1637d). These structures appear to result from adsorption of abnormal quantities of protein along the cleavage.

Induced degradation of laminae by enzymic digestion confirms that organic residues removed from excavated sites are predominantly proteinaceous. In addition to forming coats enclosing discrete calcitic granules, protein also occurs as infills along sutures and within rhombohedral tablets. These infills are the electron-dense structures subtended between membranes that are seen as particles in some sites of dissolved tablets (Fig. 1632a). This protein is assumed to be the electron-dense mesh of interlaminar organic sheets, secreted with vesicles by microvilli. It has been identified as the 44

kDa protein extracted from both laminae and membranous interleaves.

Tablets are doped with proteins in at least two ways. Centripetal growth of the top granular layers or ramparts can trap organic residues coating medial depressions of tablets. This is the main process for incorporating the 44 kDa protein within tablets. The other sites of doping are (0k.1) sectors. They vary from slits in plates representing kinks along the long diagonal to wide sectors in tablets characterized by strongly developed, kinked (0k.1) steps. Along slits, the protein is secreted as kinked strands at the lengthening junction between the growing $(1\bar{1}.4)$ and $(0\bar{1}.4)$ steps. In sectors, it forms strands aligned with cleavage with offsets enclosing granules so that degradation exposes calcitic ridges and hillocks and releases detached granular aggregates. Accretion of the protein can be periodic with repeated, sustained doping of the kinks in the (0k.1) steps to form more or less continuous organic bands many nanometers thick and parallel with the sector base. Secretion can be terminated within the base of a sector but such protein-free bands appear to be sites for rampart growth. The protein also forms sheets interleaved with granular monolayers; both constituents are restricted to (0k.1) sectors. The sectoral restriction in the secretion of this fibrous protein suggests that it is the exclusively intralaminar, glycosylated 60 kDa protein (BROWN, 1998). Sporadically preserved strands in etched sectors and sutures (Fig. 1632b) may be remnants of this proteinaceous network. The assumed distribution of the two dominant proteins doping calcitic tablets are shown diagrammatically in Figure 1634.

The primary, mineralized layer of the dorsal valve of *Novocrania* differs from the secondary layer in three respects. Although the mineralized components are also calcitic laminae, they expand peripherally, not by spiral growth, but along radial vectors. Moreover, these laminae are not interleaved with glycoproteinaceous membranes. Calcitic
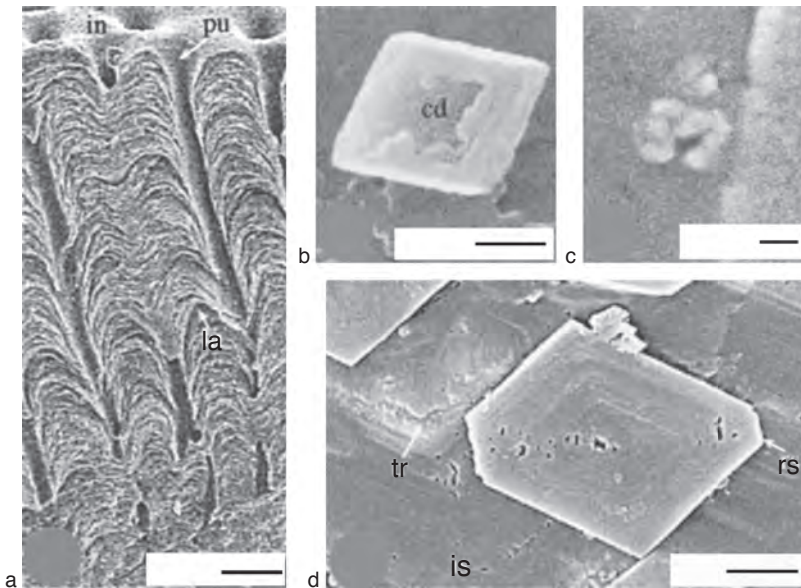
FIG. 1635. SEM views of internal surfaces and fracture sections of secondary shell of dorsal valves of *Novocrania anomala*; *a, c,* digested by proteinase-K in phosphate buffer; *b,* treated with 10% bleach by volume for 6 h; *d,* treated with Hepes buffer; *a,* fracture section showing disposition of laminae (*la*) relative to internal surface (*in*) and punctae (*pu*), *b–c,* immature and newly formed, granular rhombohedral plates with central depressions (*cd*); *d,* growth-banded plate with sparse etch pits along long diagonal between rough steps (0k.l) (*rs*) on interlaminar substrate (*is*) raised by tilted tablet (*tr*) (Williams, Cusack, & Brown, 1999).

structures are invested in, or associated with, an organic matrix that is not degraded by protease enzymes only by bleach and is presumably a polysaccharide. Finally, the pustules described below do not develop in the primary layer. The boundary between the primary and secondary layers is accordingly well defined in section and on the valve floor where the three-fold succession of the primary layer is exposed as three concentric zones (Fig. 1639).

At the margin of the mature valve, granular monolayers approximately 25 nm thick form a succession of 50 or more sheets in which the granules are generally arranged linearly parallel with the ($\bar{h}$0.1) planes (Fig. 1640a–b). This lineation is strongly developed in inwardly succeeding laminae that overlap one another like tiles (Fig. 1640c). Steps of (10.4) rhombohedra form growing edges of these laminae, which, in the degraded state, are divided into strips

(slats). As this alignment is predominantly that of grills within the secondary layer, it is assumed that the primary laminae are also doped between slats by the fibrous 60 kDa protein. In the inwardly succeeding laminae, nearer the boundary with the secondary layer, hemicylindroid to flat-topped projections are commonly secreted as spines to virtually discrete laths of laminae (Fig. 1641a–b) with growing edges formed of (10.4) steps subtending rhombohedral angles. The spines are commonly banded at acute angles to their lath bases, indicating incremental forward growth by the secretion of monolayers of granular calcite. An amorphous organic residue persists in the spaces between spines when treated with proteinase-K, suggesting that such infills are polysaccharidal. Laminar successions, peripheral to the secondary layer, are normally composed of membranes interspersed with rhombohedral plates, fretted
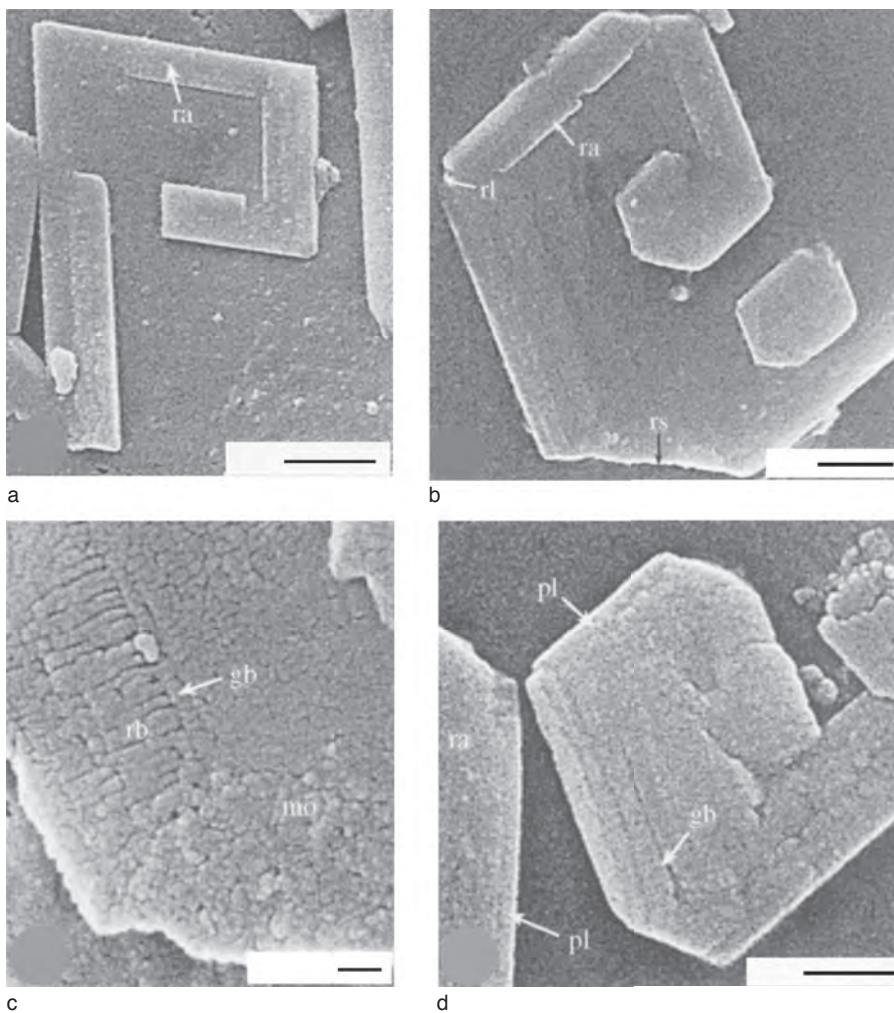
FIG. 1636. SEM views of internal surfaces and fracture sections of secondary shell of dorsal valves of *Novocrania anomala; a*, treated with 10% bleach for 6 h, *b, d*, digested by proteinase-K in phosphate buffer; *c*, treated with Hepes buffer; *a*, spiral tablet system with centripetally growing ramparts (*ra*) elevated above interlaminar substrate; *b*, clockwise spiral tablet system with centripetally growing rampart (*ra*) and (0k.l) and ($\overline{h}$0.l) rough steps (*rs*) and (*rl*) respectively; *c*, corner of tablet with growth banding (*gb*), bands of larger rhombohedra (*rh*) parallel with (01.4) step and granular mosaic (*mo*) within rough (0k.l) step; *d*, tablets on plates (*pl*) with growth-banded (*gb*) ramparts (*ra*) covering central depression (Williams, Cusack, & Brown, 1999).

or fragmented by bleach (Fig. 1642c–d) and also with some protein doping along the long diagonals revealed by digestion with proteinase-K. This succession is structurally preliminary to the spirally growing rhombohedra interleaved with glycoproteinaceous membranes of the secondary layer.

The weakly developed ventral valve of *Novocrania* is composed only of primary layer that occurs mainly as a thickened, finely nodular marginal ring (CUSACK & WILLIAMS, 2001a, p. 886) with a coarsely tuberculate outer face. The peripheral periostracal strip is coated by a monolayer of calcitic gran-
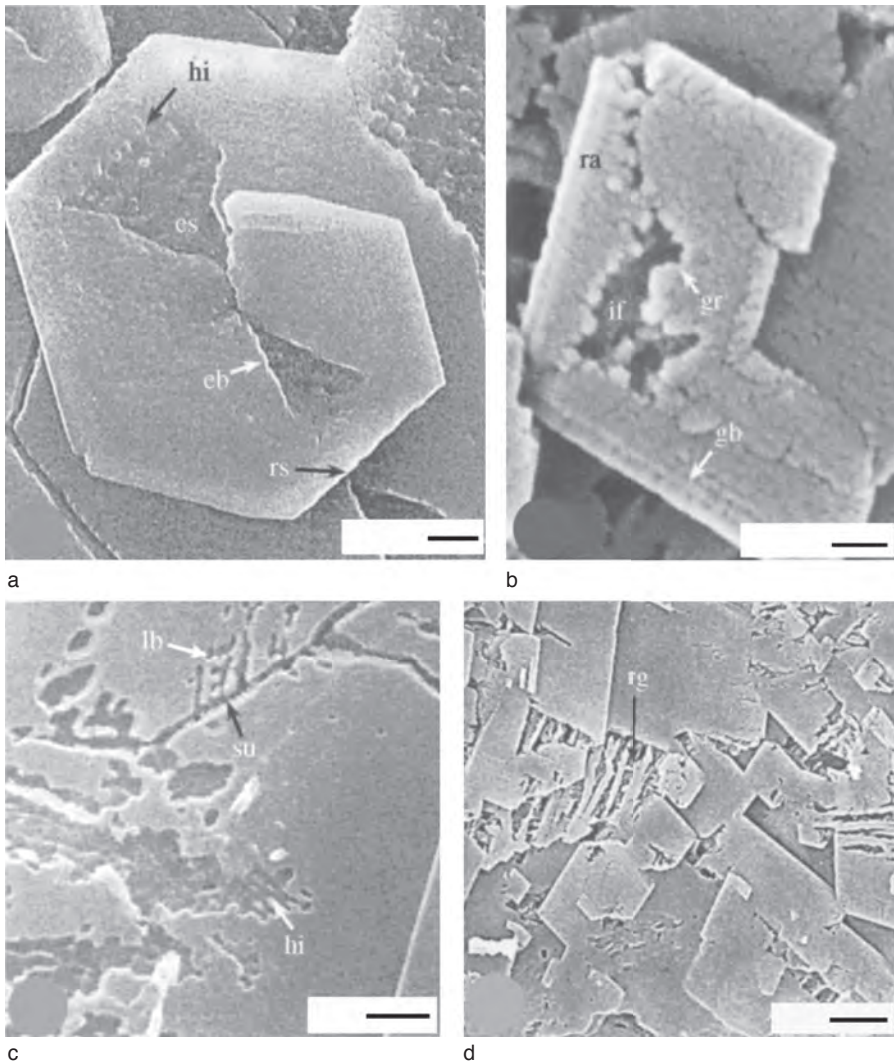
Fɪɢ. 1637. SEM views of internal surfaces of secondary shell of dorsal valves of *Novocrania anomala; a, c,* treated with bleach (10% and 20% v/v respectively) for 6 h; *b, d,* digested by proteinase-K buffered by Hepes; *a,* etched sectors (*es*) within, or delineating, rough (0k.l) edges (*rs*), bounded by etched, kinked steps (*eb*) parallel with (1$\overline{1}$.4) and (01.4) edges and containing hillocks (*hi*) and granular sheets respectively; *b,* tablets, twinned on (0k.l) plane (?) with infill centers (*if*) revealed by degradation of centripetally grown, granular (*gr*) cover of banded (*gb*) ramparts (*ra*); *c,* laminar etching along sutures (*su*) with rhombohedral labyrinths (*lb*), ridges, and hillocks (*hi*); *d,* rhombohedral grilles (*rg*) in laminar substrates (Williams, Cusack, & Brown, 1999).

ules that form spherular and cylindroid aggregates (Fig. 1642a–c). The granules are coated with polysaccharide, traces of which survive degradation, while rare pinacoidal plates of calcite are presumably exocytosed in the completed state (Fig. 1642b–c). The boundary between the periostracal strip and the inner, nodular zone is relatively sharp, although nascent nodules can form on the periostracal calcitic coat. A nodule may be initiated as a cluster of discrete columns of rhombohedra that serve as the core of an
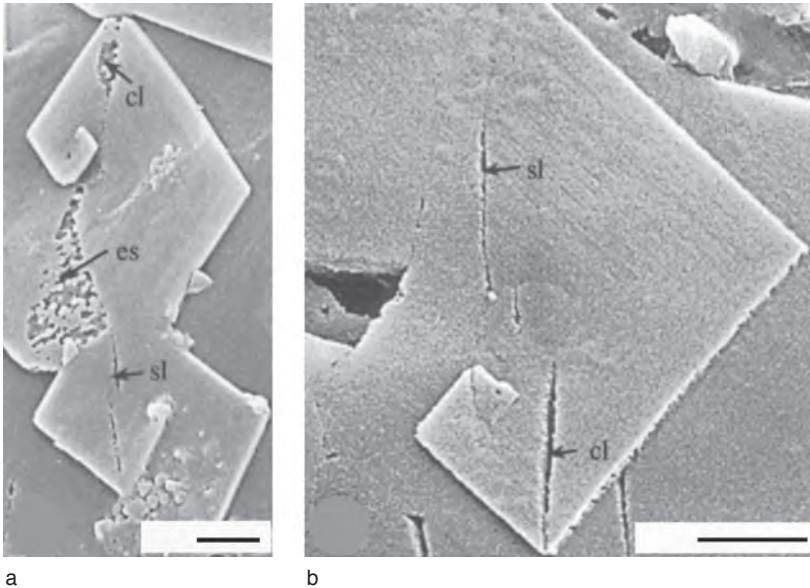
a   b

FIG. 1638. SEM views of internal surfaces of secondary shell of dorsal valves of *Novocrania anomala* digested by proteinase-K buffered by *a,* phosphate and *b,* Hepes, revealing slits (*sl*), clefts (*cl*), and etched (0k.l) sectors (*es*) in spirally growing plates and tablets (Williams, Cusack, & Brown, 1999).

assemblage of overlapping plates penetrated by cylindroid cavities approximately 100 nm in diameter. The full assemblage is a low semiellipsoid up to 10 μm in long diameter (Fig. 1642d–e). The nodules tend to be well ordered in close-packed rays or radial columns. When untreated the zone is coated with polysaccharide.

The tubercles on the outer face of the marginal ring form inwardly inclined projections approximately 150 μm long (Fig. 1642a), and their surfaces are nodular. Toward the crest of the marginal rim, the tips of the tubercles become flat topped and are composed of vestiges of nodules, broken granular plates and slats, spherules and GAGs, a fabric that is characteristic of resorption (Fig. 1643b). The superficial features of the shell underlying the mantle and body cavities are variable, for they include pustules, cleft cysts, and slats (CUSACK & WILLIAMS, 2001a, p. 888). The basic calcitic constituents of the succession, however, are rhombohedral plates with linearly arranged granules that also aggregate into spherules and tablets; laths,

composed of such aggregates, commonly change directions through a laminar succession as in composite structures (Fig. 1644). Treatment with bleach or enzymes did not expose proteinaceous concentrations as slots or pitted sectors within the laminar successions.

The chemicostructural succession of the ventral valve suggests that the valve consists exclusively of a primary layer. The regular size and distribution of nodules are reminiscent of cellular imprints, suggesting that each nodule is secreted by an outer epithelial cell. This differential secretion is characteristic of the retractable outer lobe and adjacent mantle, which is probably attached to the flat-topped tubercles by myofibrillar bundles.

The recently studied pustules on the internal surface of the secondary layer of *Novocrania* (CUSACK & WILLIAMS, 2001a, p. 880–883) are noteworthy as similar features are the internal expressions of pseudopunctation that characterize many strophomenates (WILLIAMS, 1997, p. 305–312). The pustules, which are grouped approximately 30–50
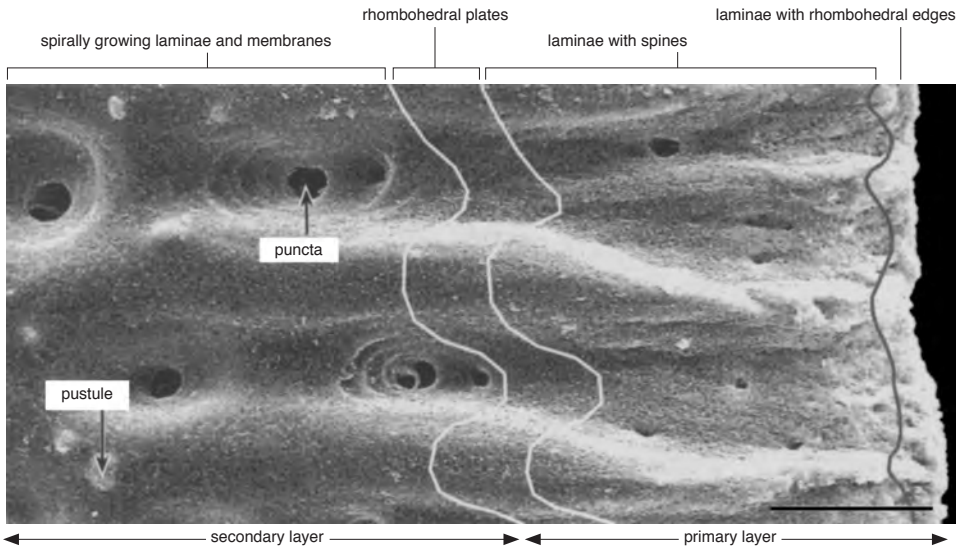
FIG. 1639. Various structural features characterizing surfaces of primary and secondary layers of dorsal valve of *Novocrania anomala* (MÜLLER); scale bar: 50 µm (Cusack & Williams, 2001).

µm apart around openings of punctae, are more or less hemispherical with bases 5–7 µm in diameter (Fig. 1645a–b). They are not superficial features because they can be traced within sections as cylindroid inward deflections of laminae (Fig. 1644a,c). These cylindroid cores may be impregnated with an amorphous tension-cracked, organic residue (Fig. 1644a–b) that is degraded by bleach but not by protease enzymes and is presumably a mucous polysaccharide secreted by specialized epithelial cells. The mucus is sporadically distributed as a plug along the core and invades deflected laminae bounding a pustule. The plugs contain laminar fragments as well as clusters or granules (Fig. 1644b). Their sites are bounded by walls of disrupted laminae, and they are separated from one another by outwardly arching laminar successions. This differentiation accords with surfaces of some pustules being completely coated by laminar sheets and plates (Fig. 1645b), while others are open to expose arcs of deflected laminae and disrupted cores (Fig. 1645c). The pattern suggests that each pustule is formed of intermittent discharges of mucus from a cell(s) that otherwise secretes secondary shell.

The pustules are comparable to pseudopunctae lacking taleolae, like those of orthotetidines and early strophomenoids (WILLIAMS, 1997, p. 306, fig. 266). Their ultrastructures are strikingly similar, including laminar fragments preserved in the cores of pseudopunctae that may also be capped by entire laminae. Pseudopunctae are assumed to have acted as holdfasts for mantle filaments (WILLIAMS, 1997, p. 311), but there is no morphological evidence of this function for craniid tubercles. The most striking feature of the tubercles is their regular distribution around punctal openings. The periodic secretion of mucus may therefore facilitate the growth of the glycoproteinaceous membranes that separate papillae of outer epithelium occupying punctae from the shell.

SHELL STRUCTURE OF FOSSIL CRANIIDS

The skeletal ultrastructure of craniids has not changed significantly since the earliest record of the group in the Ordovician (Arenig), although it has cumulatively undergone several phases of recrystallization.

Fig. 1640. SEMs of internal surface of primary layer of dorsal valve of *Novocrania anomala* (Müller), Oban, Scotland; surfaces shown in *a* and *b* immersed in phosphate buffer, those in *c* and *d* treated with bleach; *a–b*, general view and detail of granular plates (*gs*) at valve edge with rhombohedral growth banding (*gb*) and linear aggregates of granules (*gl*) aligned parallel with ($\bar{h}$0.1) planes; scale bars: 500 nm, 200 nm; *c*, detail of slatlike rhombohedra (*sa*) composed of linear aggregates of granules (*gl*) with polysaccharide residues (*po*); scale bar: 1 µm; *d*, general view of slats with rhombohedral edges (*sa*); scale bars: 500 nm (Cusack & Williams, 2001).

The antiquity of the living shell structures is confirmed by comparisons of the fabrics of Upper Cretaceous *Crania* and *Isocrania*, the Lower Carboniferous *Crania*? *ryckholtiana* (de Koninck), and the upper Ordovician *Petrocrania* (Cusack & Williams, 2001a). In all these extinct craniids, the primary layer was well developed as a succession of laminar sheets (Fig. 1646c). The laminae are normally degraded on the external surface into radially aligned laths up to 20 µm wide (Fig. 1647.1, 1647.3). In *Petrocrania* the laths usually coalesce distally to form solid lobate edges (Fig. 1647.4), possibly
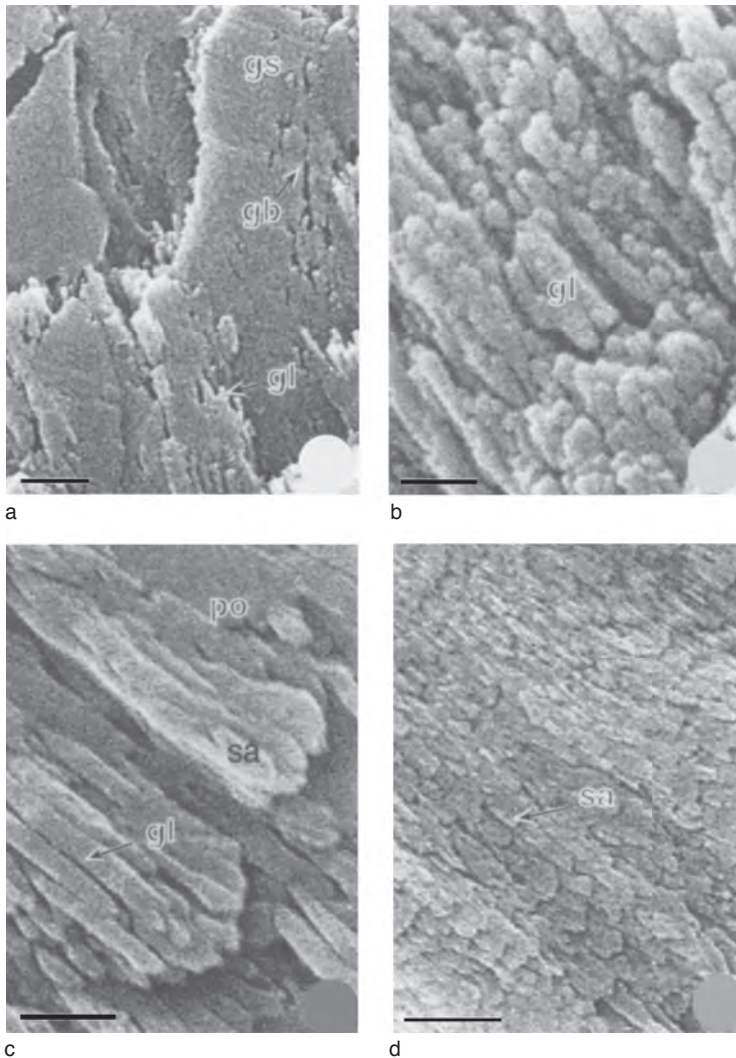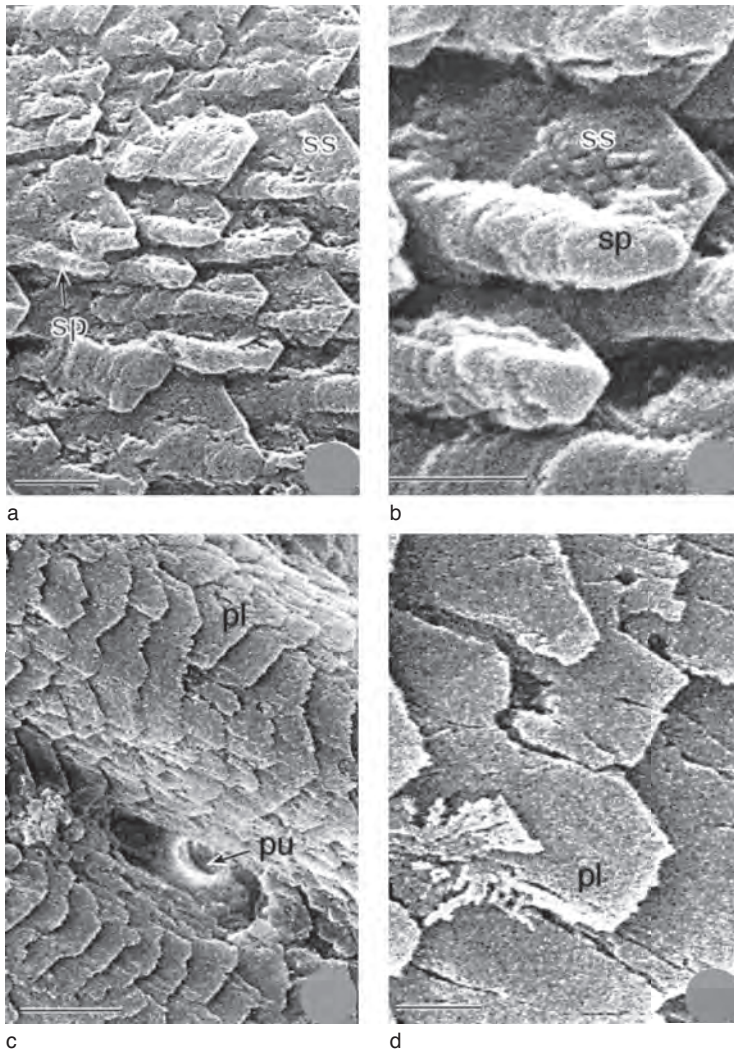
FIG. 1641. SEMs of internal surface of primary layer of dorsal valve of *Novocrania anomala* (MÜLLER), Oban, Scotland; surfaces shown in *a–b,* digested in proteinase-K; *c–d,* treated with bleach; *a–b,* general view and details of slats with rhombohedral edges (*ss*), bearing growth-banded spines (*sp*), one showing the granular texture of growth surface; scale bars: 1 µm and 500 nm; *c–d,* general view and detail of regularly overlapping rhombohedral plates (*pl*) with fretted edges and internal opening of puncta (*pu*); scale bars: 5 µm, 1 µm (Cusack & Williams, 2001).

as a result of recrystallization. Nodular tubercles characterize the internal margins of both valves in *Crania* and *Isocrania* (Fig. 1647.1). They are sporadically present in *Crania* but are a diagnostic feature of the craniid lineage, as they are well developed in the rims of the Ordovician *Orthisocrania* (CUSACK and WILLIAMS, 2001a, pl. 9,*3*) and

consist of successions of laminar sheets as in living *Novocrania*.

The secondary layer of the dorsal valve is invariably developed, and, although internal surfaces are generally obscured by microspar, patches of recrystallized, screw-dislocated rhombohedra survive (Fig. 1646b). A secondary layer that grew spirally was also
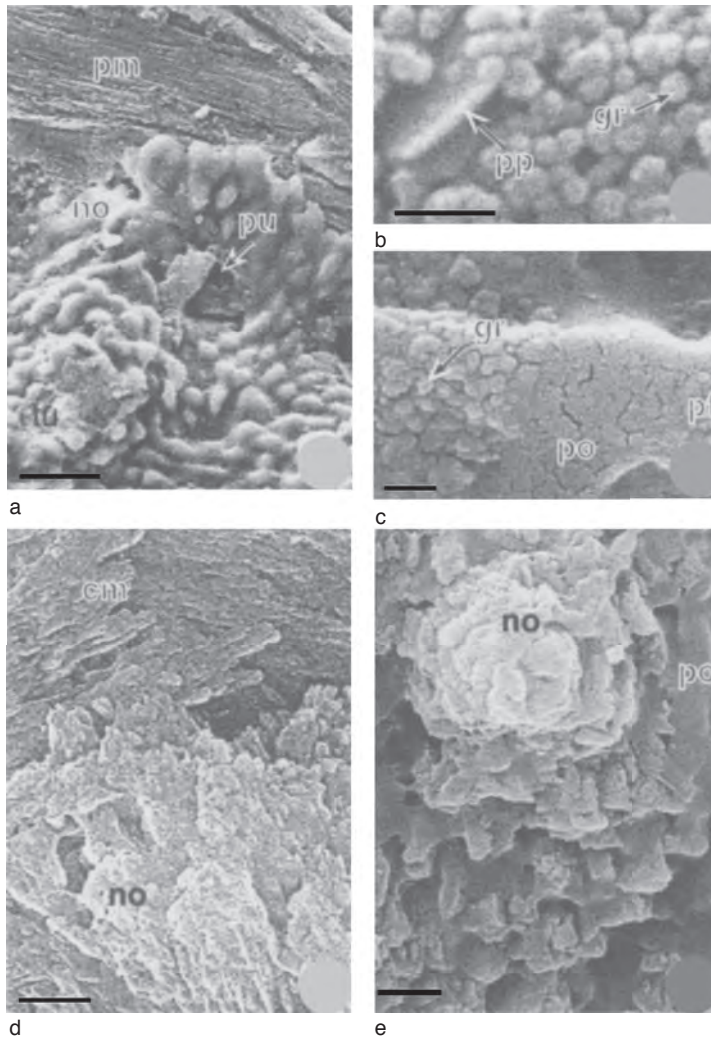
FIG. 1642. SEMs of internal surfaces of ventral valve of *Novocrania anomala* (MÜLLER), Oban, Scotland; surfaces treated with 5% bleach for 6 h except view *c,* which was immersed in phosphate buffer; *a–c,* general view and details of periostracal strip (*pm*) bordering marginal rim, characterized by nodules (*no*), tubercles (*tu*), and punctae (*pu*) and consisting of impersistent concentric folds (*pf*) with coats of calcitic granules (*gr*), rare pinacoidal plates (*pp*), and polysaccharide (*po*); scale bars: 25 μm, 200 nm, 200 nm; *d,* newly formed nodule (*no*) composed of granular plates, secreted on calcitic monolayers (*cm*) of periostracal strip with cleavage lineation almost orthogonal to that of nodule; scale bar: 1 μm; *e,* view of nodule (*no*) showing they are composed of plates (inclined medially) arising from a similarly structured substrate of rhombohedral plates and polysaccharide (*po*); scale bar: 1 μm (Cusack & Williams, 2001).

secreted in the ventral valves of Cretaceous and Carboniferous species (Fig. 1646d, 1647.2). The ventral valve of *Petrocrania,* however, is nothing more than a thin calcitic film, a vestige of an incompletely developed first-formed shell (CUSACK & WILLIAMS,

2001a). At its anterior margin, the shell consists of ill-fitting rhombohedra up to 20 μm long. Medioposteriorly, they are succeeded by calcitic blades disposed as impersistent concentric arcs; posterolaterally, presumably the sites of muscle attachments,
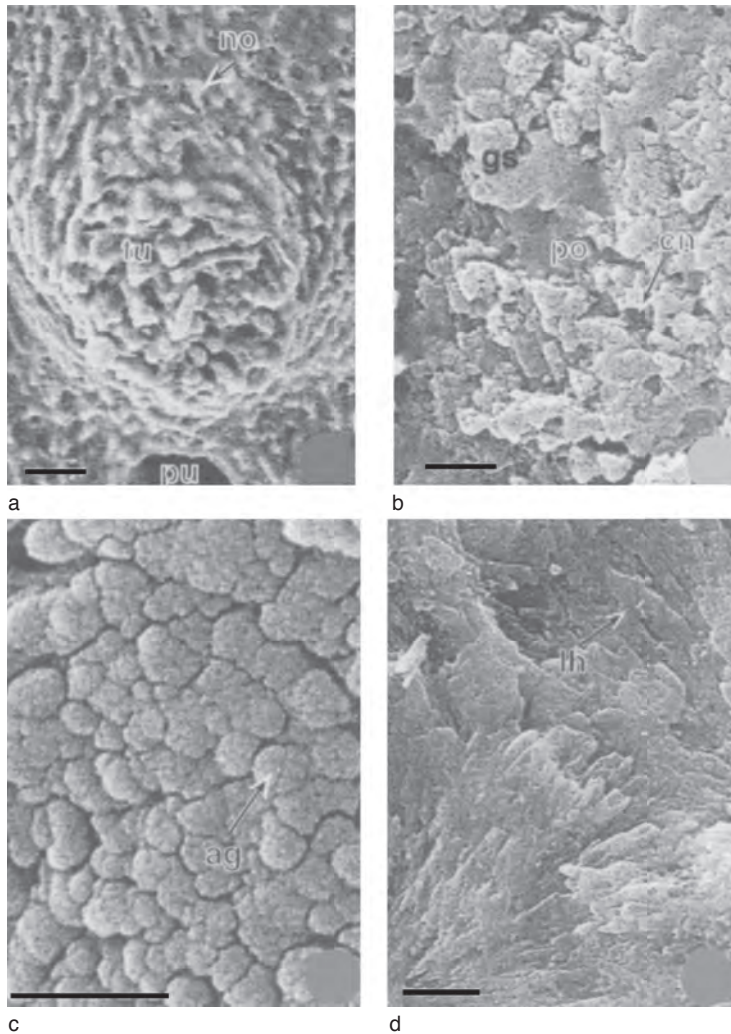
FIG. 1643. SEMs of internal surfaces of ventral valves of *Novocrania anomala* (MÜLLER), Oban, Scotland; *a–b*, after incubation of fracture sections in phosphate buffer, general view of tubercle (*tu*) with a nodular (*no*) and punctate (*pu*) surface and detail of flat-topped surface of tubercle at crest of marginal rim, showing broken granular plates (*gs*), polysaccharides (*po*), and cylindroid cavities (*cn*); scale bars: 25 μm, 1 μm; *c*, coat of granular spherules of calcite (*ag*) on concentrically wrinkled membranous substrate and *d*, details of composite succession of calcitic laths (*lh*); scale bars: 20 and 10 μm respectively (Cusack & Williams, 2001).

the blades overlap like a composite fabric (Fig. 1648).

RECRYSTALLIZATION AND DEGRADATION OF FOSSIL CRANIIDS

Comparative chemicostructural studies of the shells of living *Novocrania* and late Cretaceous *Crania* and *Isocrania* (Fig. 1649)

have established some of the diagnostic features distinguishing between phylogentic and diagenetic changes that affected fossil species (CUSACK & WILLIAMS, 2001a). Apart from the development of a secondary layer in the ventral valves of the Cretaceous craniids, inherent chemicostructural differences are minor. Changes induced by diagenesis, however, are profound but are
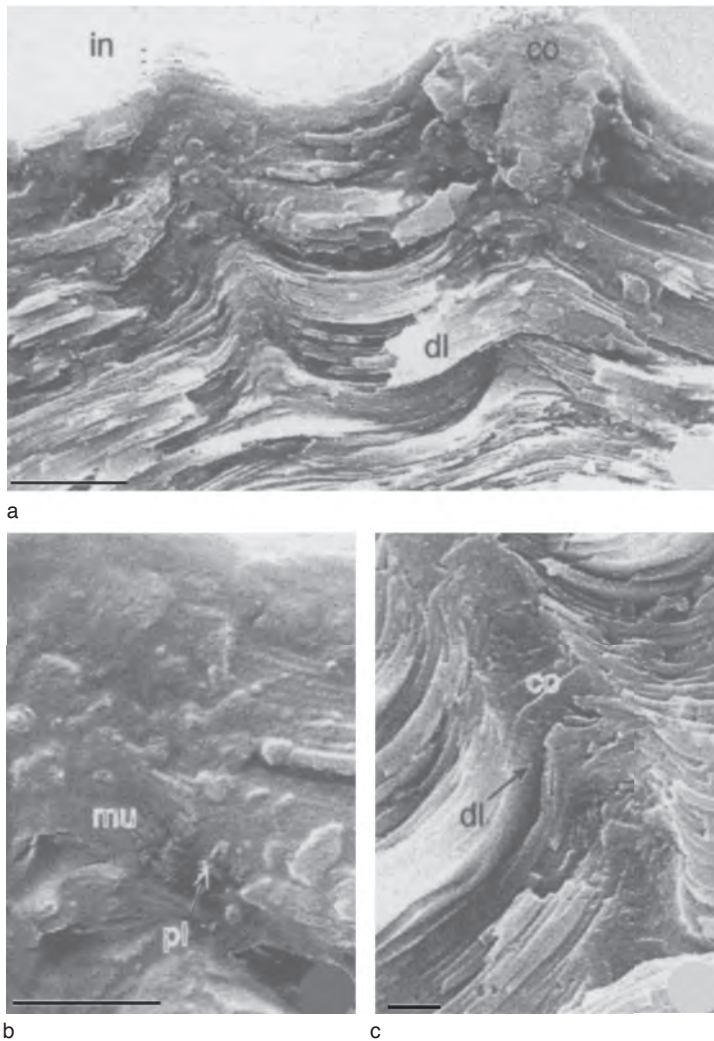
FIG. 1644. SEMs of pustules in dorsal valve of *Novocrania anomala* (MÜLLER), Oban, Scotland, after treatment with proteinase-K; *a–c*, general view and details of two pustules exposed in a fracture section [interior (*in*) to the top] showing core (*co*), composed of fragments of laminae (*pl*) in a polysaccharide (*mu*), bounded by inwardly deflected laminae (*dl*); scale bars: 5 µm, 1 µm, and 1 µm respectively (Cusack & Williams, 2001).

structurally confusing as they commonly result in features similar to those produced by biogenic secretion and resorption. Cavities, intrinsic to internal laminae of the Cretaceous shells, are commonly bounded by mismatched crystal or curved faces and may penetrate several laminae. They are likely to have originated at junction windows and further modified during recrystallization (Fig. 1646b). This would account for

the way cracks (originally junction sutures) radiate from many of them. In contrast tilted rhombohedral depressions (Fig. 1646d) are more likely to be true etch pits that originated with the degradation of the organic axial core of screw dislocations.

Treatment of the Cretaceous shells with bleach and HCl reveals that degradation of intracrystalline polymers took place before the recrystallization of laminae. Laminar
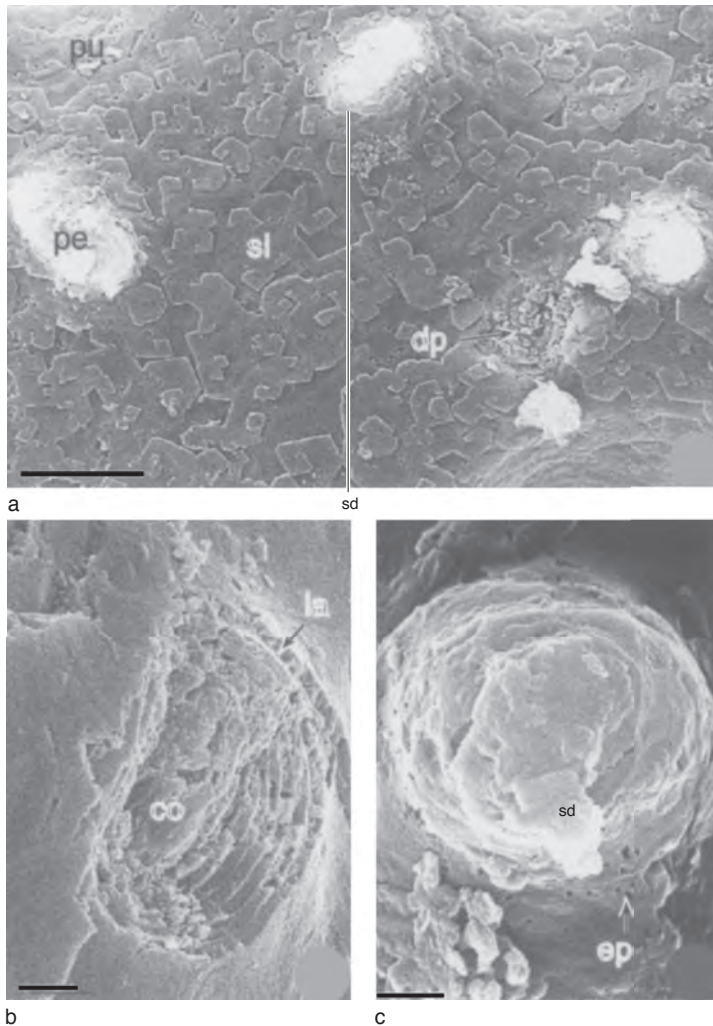
Fɪɢ. 1645. SEMs of pustules in dorsal valve of *Novocrania anomala* (Mᴜʟʟᴇʀ), Oban, Scotland; *a* and *c* immersed in phosphate buffer and *b* digested in proteinase-K; *a,* general view and details of pustules (*pe*) on internal surface of punctate (*pu*), spirally growing laminar secondary layer (*sl*) with entire pustules covered with enzyme-pitted laminae (*ep*) and screw-dislocated plates (*sd*) in view *c* and degraded pustules (*dp*) in *a* and *b* showing polysaccharide-impregnated core (*co*) and successive inwardly deflected laminae (*la*); scale bars: 10 μm, 1 μm, and 1 μm respectively (Cusack & Williams, 2001).

surfaces are free of sectorally distributed cavities, like those induced by bleach in protein-doped rhombohedra of living shells. They become tension cracked and develop curved channels when treated with bleach, however. As these features are not induced by solution in HCl it seems that the volumetric changes that led to tension cracking resulted from the degradation of diffuse organic residues that had been produced and dispersed during the early stages of recrystallization (Fig. 1648).

The Paleozoic cranioids studied by Cᴜsᴀᴄᴋ and Wɪʟʟɪᴀᴍs (2001a) were from nearshore calcareous siltstones and mudstones unaffected by significant geothermal changes or tectonic disturbances. Their shell ultrastructure confirmed that skeletal secretion was
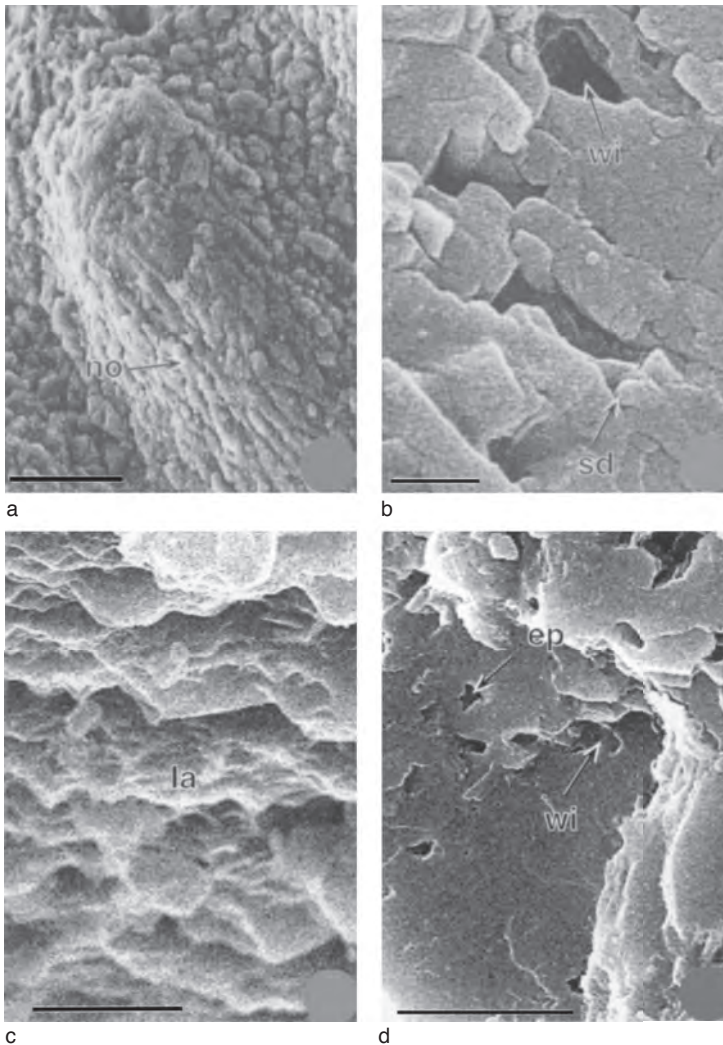
Fig. 1646. SEMs of *a,* internal margin of ventral valve of *Crania craniolaris* (Linnaeus), Upper Cretaceous, Kristianstad, Sweden, and *b,* internal surface of dorsal valves after incubation with bleach (5% v/v) for 6 h; *c–d,* SEMs of fracture sections and internal surfaces within secondary layers of shell of *Isocrania egnabergensis* (Retzius), Upper Cretaceous, Egnaberg, Sweden; *a,* ellipsoidal nodules (*no*) aligned with long axis of tubercle at internal, ventral margin, GLAHM 114 279; scale bar: 50 μm; *b,* internal surfaces within successions of secondary layer (GLAHM 114 280) showing various features of laminae including etch pits, screw dislocated rhombohedra (*sd*), and junction windows (*wi*); scale bar: 1 μm; *c,* detail of fracture section of primary layer of dorsal valve showing sheetlike succession of laminae (*la*); scale bar: 5 μm; *d,* succession of laminar sheets in secondary layer of ventral valve (GLAHM 114 275) with etch pits (*ep*) and junction window (*wi*); scale bar: 10 μm (Cusack & Williams, 2001).

homologous with that of living *Novocrania.* The ultrastructure, however, had been partially obscured by repeated recrystallization that involved changes by pressure solution exploiting the original fabrics. Degrada-

tion of the organic components of the shells reached a steady state in Paleozoic craniids. The residual amino acids derived from the shells of all species are the same suite of the more robust molecules, although their
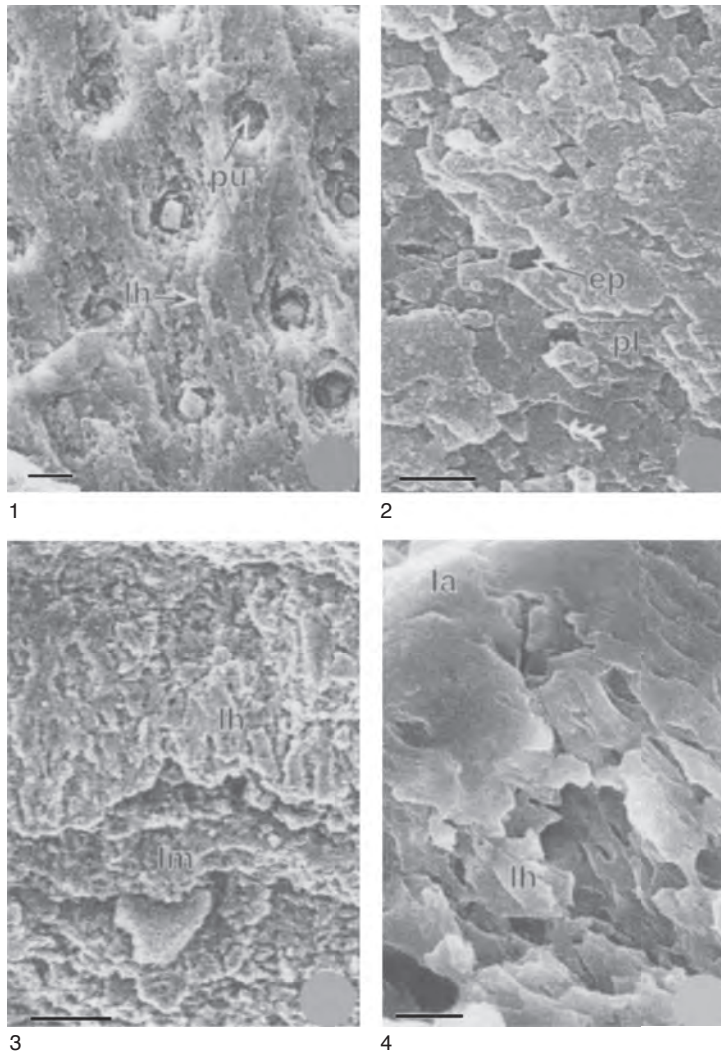
FIG. 1647. SEMs of surfaces and fracture sections of craniid shells; *a, Crania* ? *ryckholtiana* (DE KONINCK), Lower Carboniferous, Scotland; general view and detail of weathered exterior of dorsal valve (NMS 2346) showing punctae (*pu*) and laminae predominantly disposed as laths (*lh*); scale bar: 10 μm; *2*, vertical fracture section of *Rhipidomella* sp. showing etch pits (*ep*) and rhombohedral plates (*pl*) of secondary layer; scale bar: 1 μm; *3*, weathered external surface of dorsal valve of *Petrocrania scabiosa* (HALL), Upper Ordovician, Ohio, GLAHM 114 285, showing laths (*lh*) of lamellae (*lm*); scale bar: 100 μm; *4*, external surface of *Petrocrania scabiosa,* Upper Ordovician, Ohio, GLAHM 114 285, showing laths (*lh*) of primary layer coalescing distally to form a lobate lamella (*la*); scale bar: 5 μm (Cusack & Williams, 2001).

concentrations do not reduce in line with increasing geological age and were probably more closely related to the chemistry of invasive diagenetic fluids. Accordingly, it seems that most of the biochemical degradation of the craniid shell occurred within the last 80 myr, although repeated recrystallization replicated the original biomineral fabric long after it had lost its constraining organic membranes (Fig. 1650).
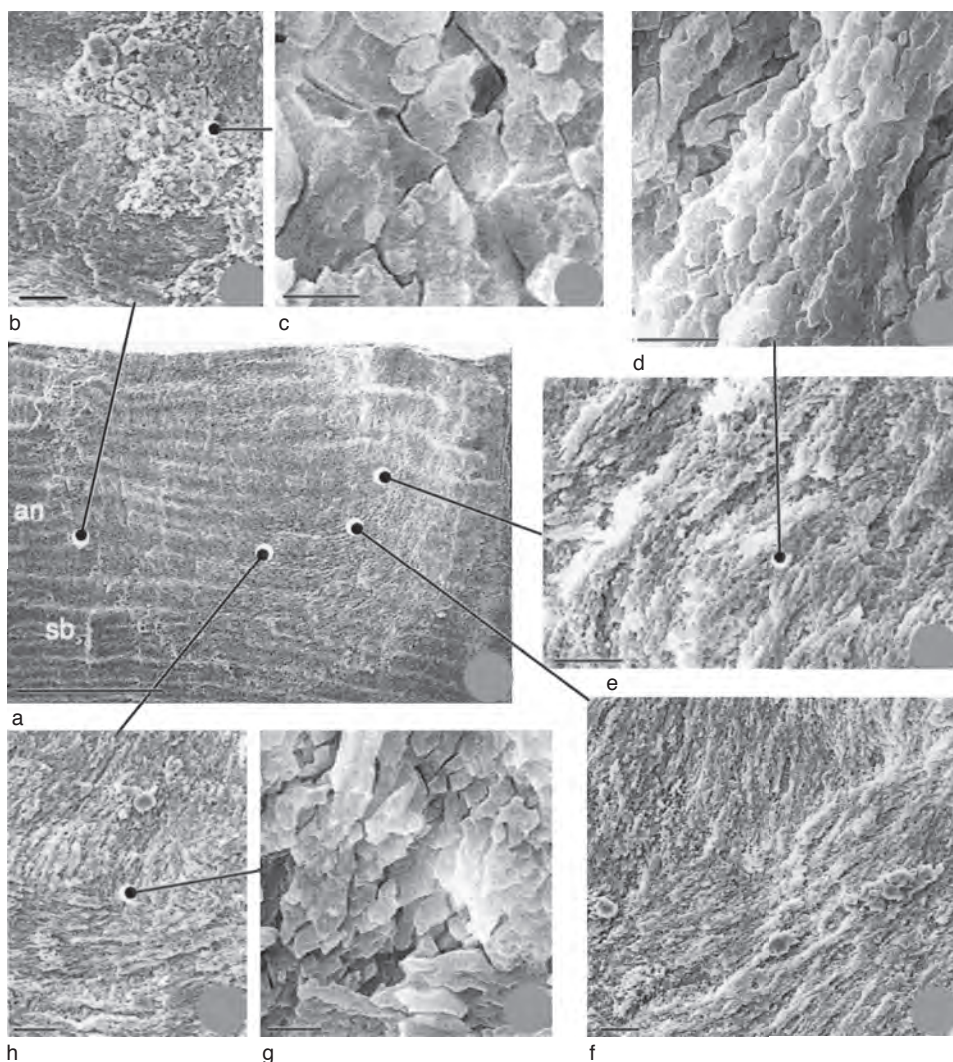
Fig. 1648. Ventral valve (GLAHM 114 284) of *Petrocrania scabiosa* (Hall); *a,* almost complete ventral valve, consisting of calcified film anteriorly (*an*) and thicker body platform posteriorly, cemented on substrate (*sb*) of a *Rafinesquina* shell; scale bar: 1 mm; *b–c*, general view and detail showing irregular boundary of film of overlapping rhombohedral plates at anterior margin; scale bars: 100 µm, 20 µm respectively; *d–e*, detail and general view of posteromedial interior showing overlapping concentric laths composed of rhombohedra, declined toward posterior margin; scale bars: 10 µm, 50 µm respectively; *f–h*, general views and detail showing composite disposition of calcitic laths in posterolateral successions of body platform; scale bars: 100 µm, 10 µm, 100 µm respectively (Cusack & Williams, 2001).

ORGANOCARBONATE FIBROUS SHELL

The fibrous fabric and its cross-bladed (composite) laminar and foliate variants characterize the organocarbonate shell of all rhynchonelliforms, the overwhelmingly dominant brachiopod group since the late Cambrian. The fibrous shell was the first major fabric to be comprehensively investigated (Williams, 1968a). Later studies have tended to be restricted to textural variation (Baker, 1970; Wright, 1970; Gaspard, 1974; Smirnova, 1979) as outlined

FIG. 1649. SEMs of fracture sections and internal surfaces within secondary layers of shell of *Isocrania egnabergensis* (RETZIUS), Upper Cretaceous, Egnaberg, Sweden; *a,* treated with bleach (5% v/v) for 15 h and *b*, dissolved in 0.5% HCl for 1 min; *a*, laminar successions of secondary layer of dorsal valves showing tension cracks (*te*) caused by bleaching, GLAHM 114 281; scale bar: 0.5 μm; *b*, laminae within secondary layer of dorsal valve (GLAHM 114 282) etched by HCl to show enlargement of junction windows (*wi*); scale bar: 1 μm (Cusack & Williams, 2001).
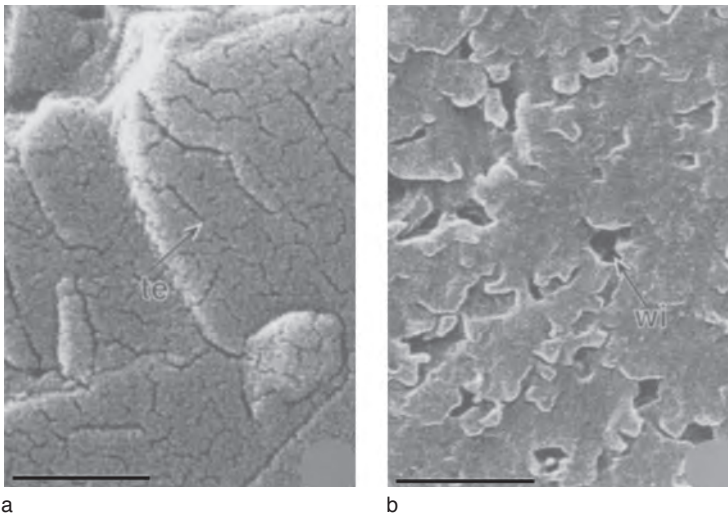
in Volume 1 (WILLIAMS, 1997, p. 280–295). More recently, investigations have concentrated on the chemicostructural accretion of living shells (CUSACK & WILLIAMS, 2001b). They show that, although the intracrystalline, calcifying proteins are more varied than was expected, biomineral accretion is virtually the same in species representing the three extant orders, the Rhynchonellida, Terebratulida, and Thecideida. A deeper understanding of rhynchonelliform secretory regimes has prompted this review of the relationship between the fabrics of living rhynchonellate shells and those that distinguish the shells of extinct groups like the strophomenates and obolellates.

CHEMICOSTRUCTURE OF LIVING RHYNCHONELLATE SHELLS

The rhynchonellide *Notosaria*, the terebratulide *Liothyrella,* and the thecideide *Thecidellina* not only typify the three extant rhynchonellate orders but also the full range of their shell fabric (WILLIAMS,

1997, p. 271–295). The shell of *Notosaria* with its undifferentiated primary and fibrous secondary layers serves as the standard rhynchonellate skeletal succession (WILLIAMS, 1968c, p. 269–270). In contrast, the secondary shell of *Thecidellina* (as in all living thecideides) is virtually suppressed, being restricted to patches on the cardinalia and the valve floors (WILLIAMS, 1973), while the dominant fabric of *Liothyrella* is a prismatic tertiary layer.

The identification of the organic components of the shell and their role in calcification involve some assumptions. In 1965, JOPE reported the presence of amino acids, lipids, and carbohydrates in living (and fossil) rhynchonellate shells. These organic residues, however, were mainly intercrystalline, notably the membranes ensheathing fibers, which had already been identified as glycoproteins by optical and electron microscopic staining techniques. Such membranes serve as substrates, and calcification of the fibers within them is effected by intracrystalline polymers incorporated within the fibers as they grow. These polymers account
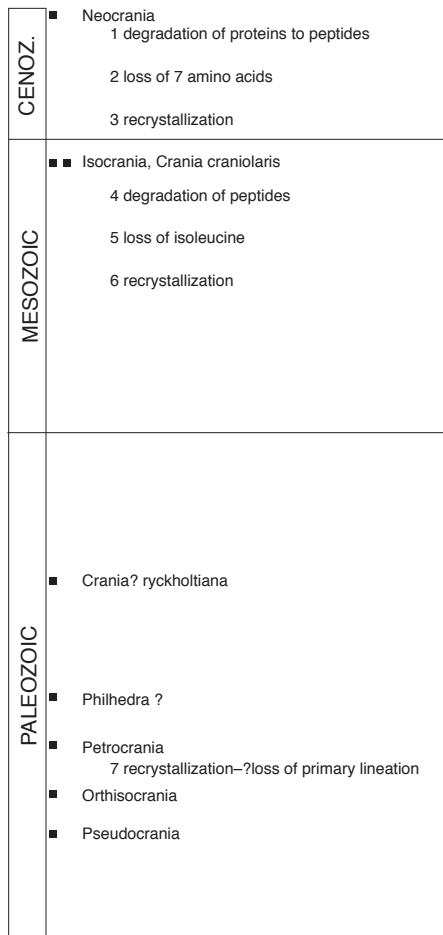
FIG. 1650. Inferred diagenetic changes in chemico-structure of shells of eight cranioid genera, arranged geochronologically and thereby showing relatively short time scale of principal phases of degradation and recrystallization (Cusack & Williams, 2001).

for only 0.3% of shell weight (COLLINS & others, 1991) and are evidently thinly and sporadically distributed. The differential treatment of rhynchonellate shells by degradants such as bleach and enzymes can, however, locate sites of polymer concentrations (doping) within calcitic successions and help to specify the organic components of the primary, secondary, and tertiary layers. The merits of this procedure rest on three assumptions: thecideide shells constitute samples of a universal rhyncho-

nellate primary layer; any differences in the biochemistry of the rhynchonellide and thecideide shells are due to the presence of the secondary layer in rhynchonellides; and differences unique to the terebratulide *Liothyrella* can be attributed to the development of its tertiary layer.

Despite the distinctiveness of their fabrics, the basic biomineral unit of all three layers is structurally the same. It is an organically coated granule of calcite approximately 15–20 nm in diameter and commonly clustering into spherules approximately 50 nm in size. The granules are normally exocytosed to form monolayers that are commonly grouped into laminae (growth bands) up to but rarely exceeding 1 μm thick. Interfaces between laminae are exaggerated by degradants indicating the presence of organic films. As laminae accumulate orthogonal to the secreting plasmalemma, they are differently disposed relative to the isotopic boundaries of the three layers (WILLIAMS, 1997, p. 268). They are virtually flat lying in the primary and tertiary layers but variably inclined in the secondary layer to accord with the slope of the terminal faces of the fibers.

RHYNCHONELLATE PRIMARY LAYER

The rhynchonellate primary layer, as typified by *Notosaria*, can exceed 100 μm in thickness and is composed of granular monolayers aggregating as flat-lying laminae (Fig. 1651a–b). Rare organic inclusions consist of isolated strands approximately 30 nm thick (Fig. 1651a) and amorphous organic blobs within sporadically occurring arcuate grooves (Fig. 1651b). These grooves represent outlying sites of the aborted secretion of incipient membranes and secondary fibers; the blobs are therefore assumed to be glycoproteinaceous residues. The primary layer reacts differently to various degradants. Subtilisin excavates slots between granular laminae (Fig. 1651c–d), leaving amorphous blobs. Each slot evidently represents an organic substrate of a lamina, which
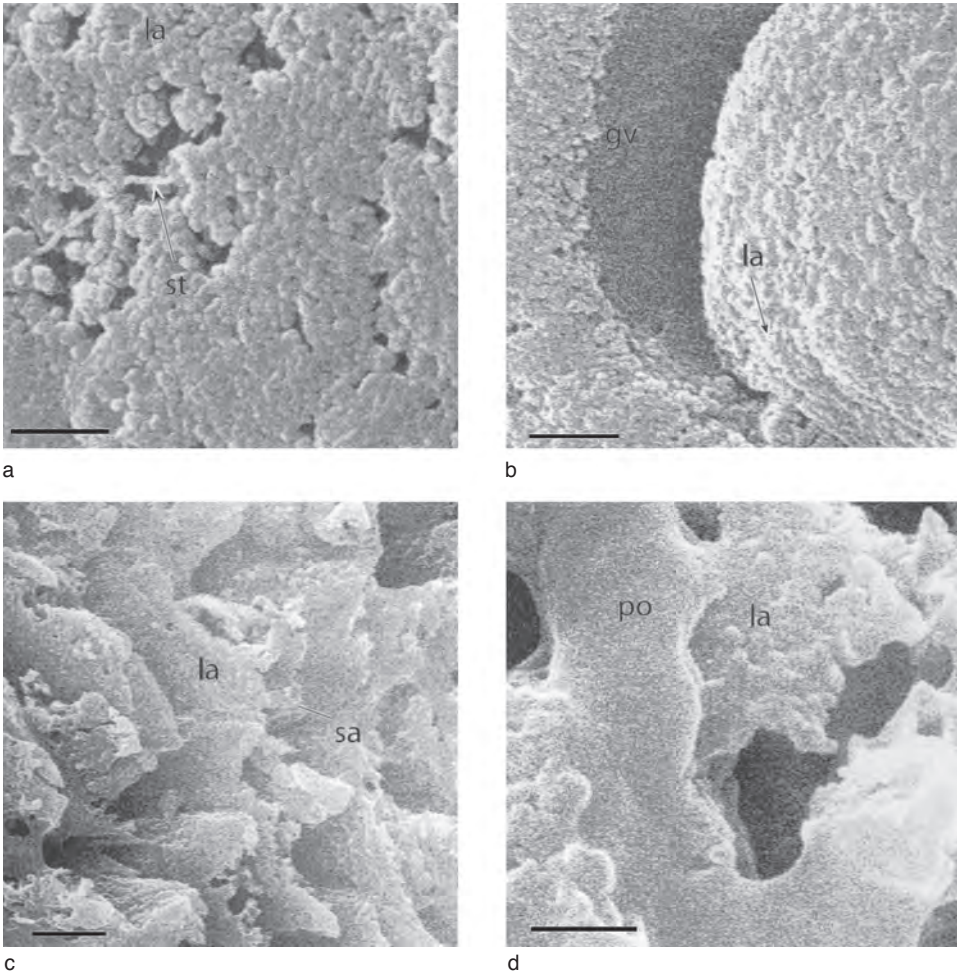
FIG. 1651. Structure of primary layer of *Notosaria nigricans* (SOWERBY), Holocene, New Zealand; *a,* features of near horizontal granular laminae (*la*) including ramifying strands (*st*); *b,* crystallographic continuity between primary and secondary laminae (*la*) present in early-forming fiber behind groove (*gv*) of undegraded glycoproteinaceous membrane; *c,* effects of subtilisin digestion with development of slots (*sa*) by removal of impersistent proteinaceous sheets and *d,* release of amorphous blobs (*po*) of a polysaccharide; *a* and *b* untreated, *c* and *d* digested in subtilisin; scale bars: 0.5, 1.0, 0.5, and 1.0 μm respectively (new).

is composed of protein and presumably an associated polysaccharide remaining as a blob. Both these organic components are degraded by bleach, which virtually destroys the primary layer peripheral to its junction with the secondary layer.

The shell of living thecideides consists almost exclusively of primary layer, because secondary fibers are restricted to isolated patches on the cardinalia and valve floors (WILLIAMS, 1973). The layer is texturally similar to that of *Notosaria,* for it is composed of granular laminae forming horizontal successions (Fig. 1652b), although blocky rhombohedra may also develop (Fig. 1652a). Rhombohedral cleavage, at 200–500 nm intervals, may extend through laminar successions for several micrometers (Fig. 1652c), indicating epitaxial continuity irrespective of the organic components.
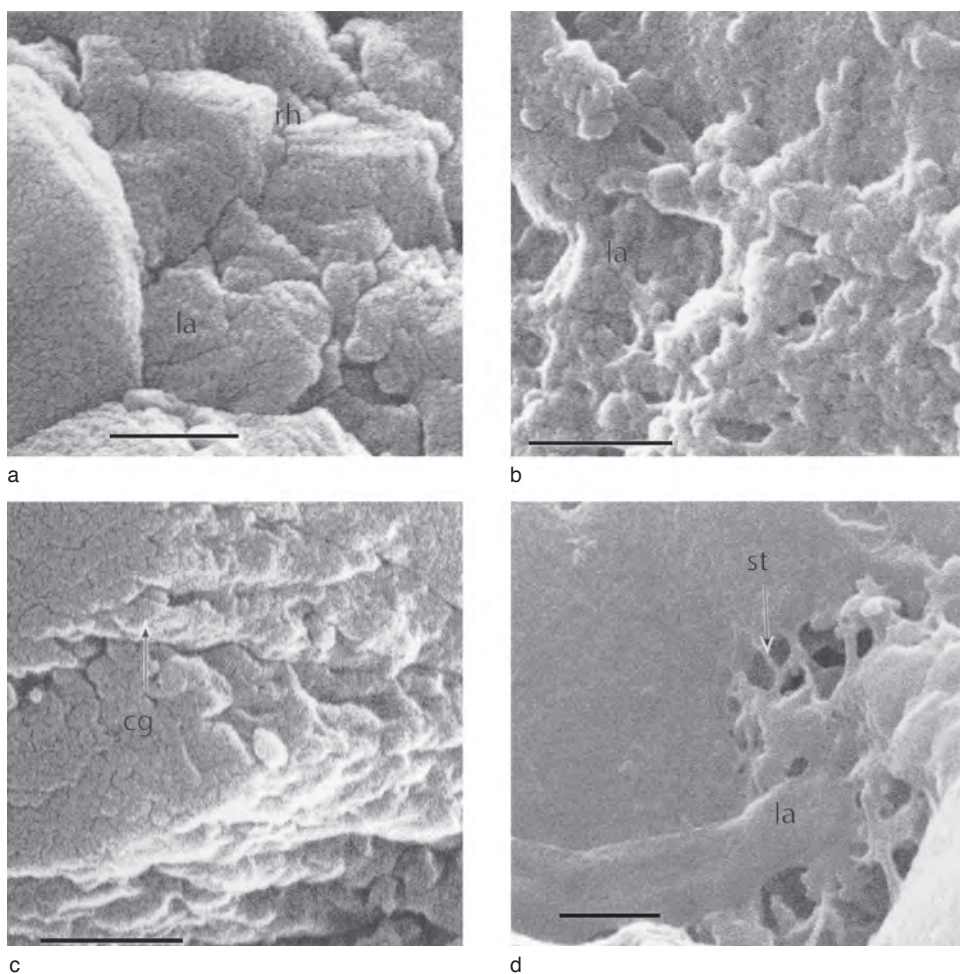
FIG. 1652. Structure of primary layer of *Thecidellina barretti* (DAVIDSON), Holocene, Bahamas; *a,* various features of granular laminae (*la*) including formation of blocky rhombohedra (*rh*); *b,* near horizontal disposition of laminar succession (*la*) in tubercles; *c,* detail of granular layer and cleavage (*cg*); *d,* laminar succession (*la*) with branching strands (*st*); *a* and *c* treated with bleach, *b* and *d* unbleached; scale bars: 0.5 μm (new).

Organic microstructures are rare but include branched strands up to 35 nm thick at laminar interfaces (Fig. 1652d).

RHYNCHONELLATE SECONDARY LAYER

The primary and secondary layers of rhynchonellate shells are structurally distinguishable solely on the interconnected growth of glycoproteinaceous membranes segregating the secondary layer into discrete fibers. Otherwise, the fibers are generally aligned crystallographically not only with one another (Fig. 1653a) but also with the mineral component of the primary layer (Fig. 1652b). The membranes, which act as substrates for a granular coat (Fig. 1653c–d) covering the stalks of forward-growing fibers, are synthesized at the distal and anterior margins of cells where they are exocytosed as a mass of fibrils serving as hemidesmosomes. The proximal and posterior margins of the exposed terminal faces of fibers subtend rhombohedral angles (Fig. 1654c). These
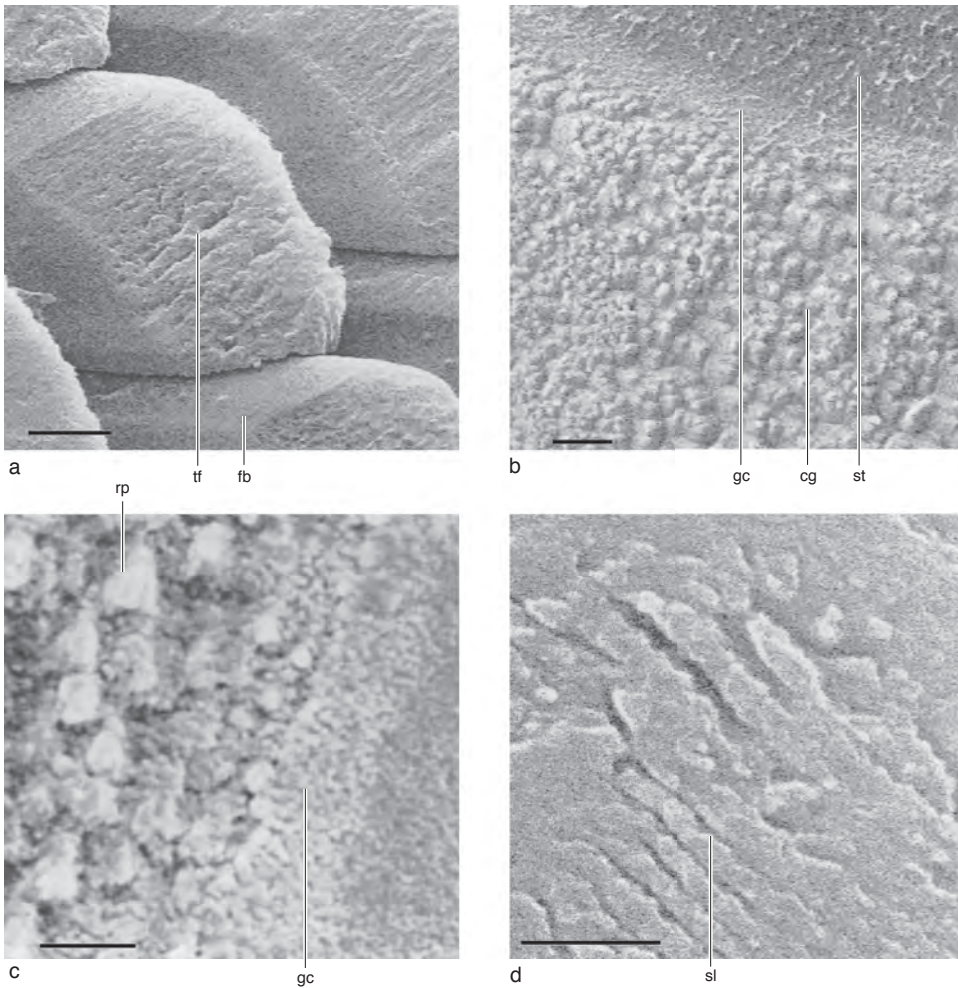
FIG. 1653. Structure of secondary layer of *Notosaria nigricans* (SOWERBY), Holocene, New Zealand; features of fibers (*fb*) and their terminal faces (*tf*) including *a,* crystallographic alignment of cleavage in contiguous fibers, remnants of strands (*st*) associated with an ensheathing membrane and *b–c,* its granular coat (*gc*) bounding cleaved (*cg*) rhombohedral granular plates (*rp*) of a fiber core and *d,* slats (*sl*) aligned with the short diagonal of a (10.4) face of a flat-lying fiber; *a, b, d* treated with bleach, *c* digested in subtilisin; scale bars: 2.5, 1.0, 0.5, and 0.5 μm respectively (new).

angles reveal the essential crystallography of terminal faces that, irrespective of their organic constituents, can be regarded as (10.4) rhombohedral plates constrained from full development by the arcuately disposed membranes being secreted distally. Narrow zones of pits sporadically develop along fiber axes parallel with the boundaries of the terminal faces. The pits mark changes

in the rates of the forward growth of fibers and, as they are exposed after enzymic degradation of ensheathing membranes, they are probably sites of proteinaceous outgrowths (Fig. 1653b).

The cores of fibers, as exposed at their terminal faces, are composed of granular rhombohedral plates (Fig. 1653b–c) with edges (steps) more or less parallel with the
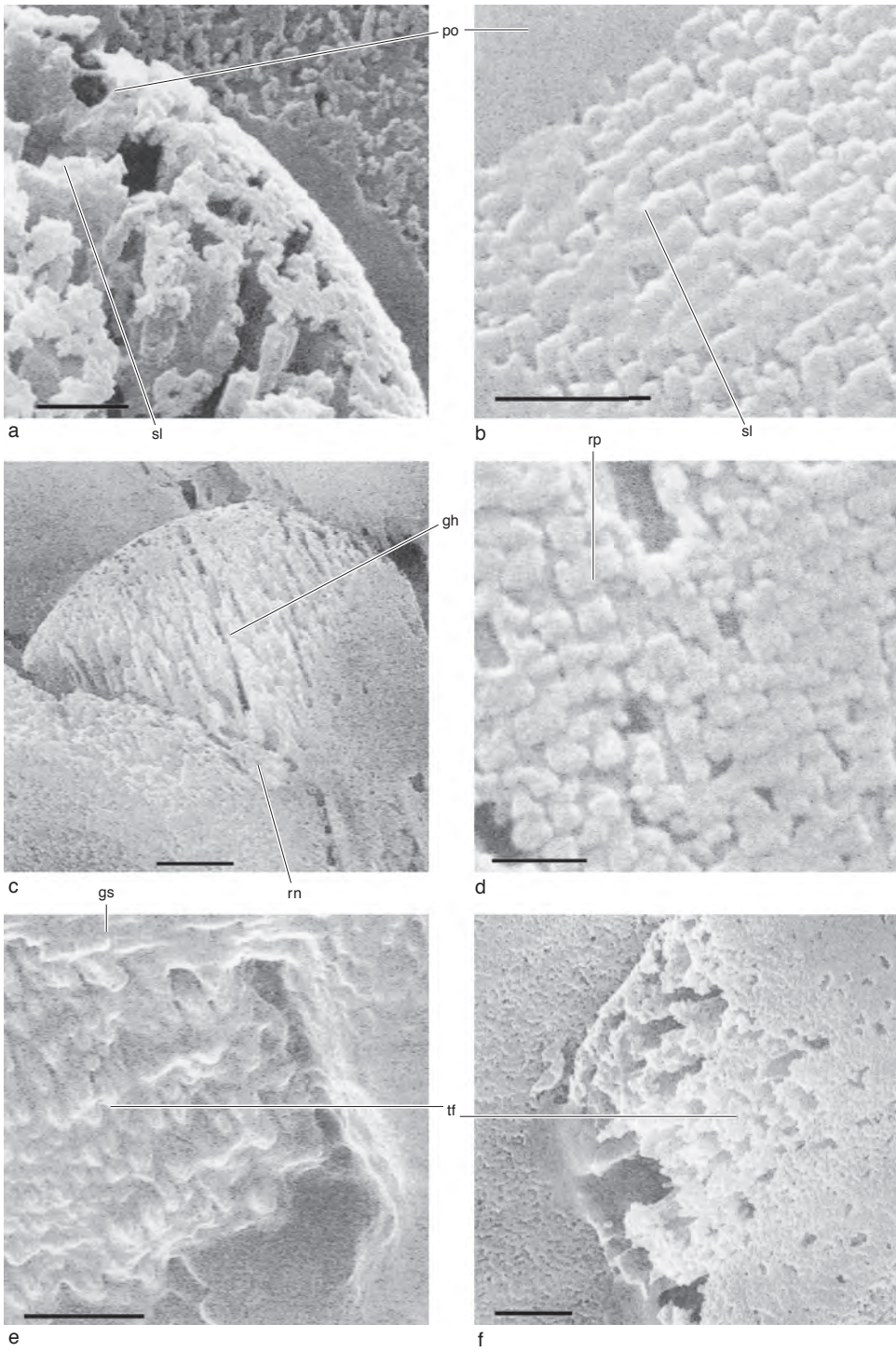
FIG. 1654. *For explanation, see facing page.*

proximal rhombohedral boundaries of the terminal faces. These plates are subparallel with the terminal faces of flat-lying fibers but dip more steeply in the faces of inclined fibers, where they commonly form arrays of rhombohedral tablets up to 2 μm in long diameter (Fig. 1653c). Cleavage develops parallel with both the (01.4) and (1⁻1.4) faces, although one is normally dominant. Degradants sporadically expose grooves delineating slats approximately 150 nm wide on terminal faces (Fig. 1653d).

A typical fiber of *Liothyrella* differs from that of *Notosaria* in being composed mainly of calcitic slats aligned with its long axis (stalk; Fig. 1654a). The slats are secreted as sequences of granular rhombohedral plates (Fig. 1654b, 1654d). They are segregated into bundles by proteinaceous sheets so that pits and gashes are left on the terminal faces and stalks of fibers when digested in enzymes (Fig. 1654c). Some organic residues, however, persist as amorphous blobs (Fig. 1654d) even after treatment with bleach and are identical with those left behind when glycoproteinaceous membranes are digested in enzymes.

RHYNCHONELLATE TERTIARY LAYER

In the transitional zone between the secondary and tertiary layers of *Liothyrella*, fibers become smaller within semiellipsoidal hollows coated with membranes (Fig. 1654f). The earliest secretion of the tertiary layer is marked by an encroachment of horizontally disposed granular sheets of calcite across fibers (Fig. 1654e). The sheets show strong cleavage and fragment as rhombohedral blocks.

The tertiary layer consists of polygonal prisms growing orthogonally to the terminal faces of secondary fibers. The prisms are not ensheathed in membranes but are separated from one another by irregularly developed organic partitions that are also probably glycoproteinaceous according to enzymic treatment. On untreated internal surfaces of the tertiary layer, the partitions are represented by a microstructural valley system delineating gently convex mounds 5–10 μm across (Fig. 1655a). The surface is pierced by micropunctae (GASPARD, 1990) and punctae.

Secretion of the prismatic layer is stratiform with laminae up to 500 nm thick and interleaved with organic substrates (Fig. 1655e). The early stages of laminar secretion are marked by rhombohedral aggregations of granules that may form slatlike arrays approximately 400 nm wide (Fig. 1655d). The slat boundaries tend to have a characteristic alignment for each mound, and sets of slats may form acute angles of 70° or so in contiguous features.

Untreated surfaces of dead shells are commonly indented by flat-bottom pits in a labyrinthine arrangement (Fig. 1655a) and are presumably sites of organic concentrates that have been etched out by postmortem degradation. Such pits in enzymically treated surfaces are greatly enlarged into cavities associated with strong grooves subtending rhombohedral angles with one another (Fig. 1655b–c). Enzymic digestion also exposes outcrops of laminae along the slopes of the mounds (Fig. 1655f). Slopes treated with subtilisin normally retain interleaves of amorphous polymers (Fig. 1655f).

ACCRETION OF LIVING RHYNCHONELLATE SHELLS

The shells of living rhynchonellates are structurally similar in two respects.

FIG. 1654. Structure of secondary layer of *Liothyrella neozelanica* (THOMSON), Holocene, New Zealand; *a–b,* details of fibers including disposition of slats (*sl*) and polysaccharide blobs (*po*) in terminal faces, *c,* gashes (*gh*) representing doped sites on terminal faces of fiber with proximal boundary subtending rhombohedral angle (*rn*), *d,* rhombohedral tablets (*rp*) glued together by polysaccharide in a monolayer array and *e,* encroachment of granular sheets (*gs*) of tertiary layer across slats of terminal face (*tf*) of a fiber with *f,* another incipient fiber in transitional zone of tertiary layer; *b, d* digested in subtilisin, *a, c, f* digested in proteinase-K, *e* untreated; scale bars: 0.5, 0.5, 2.5, 0.2, 1, and 1 μm respectively (new).
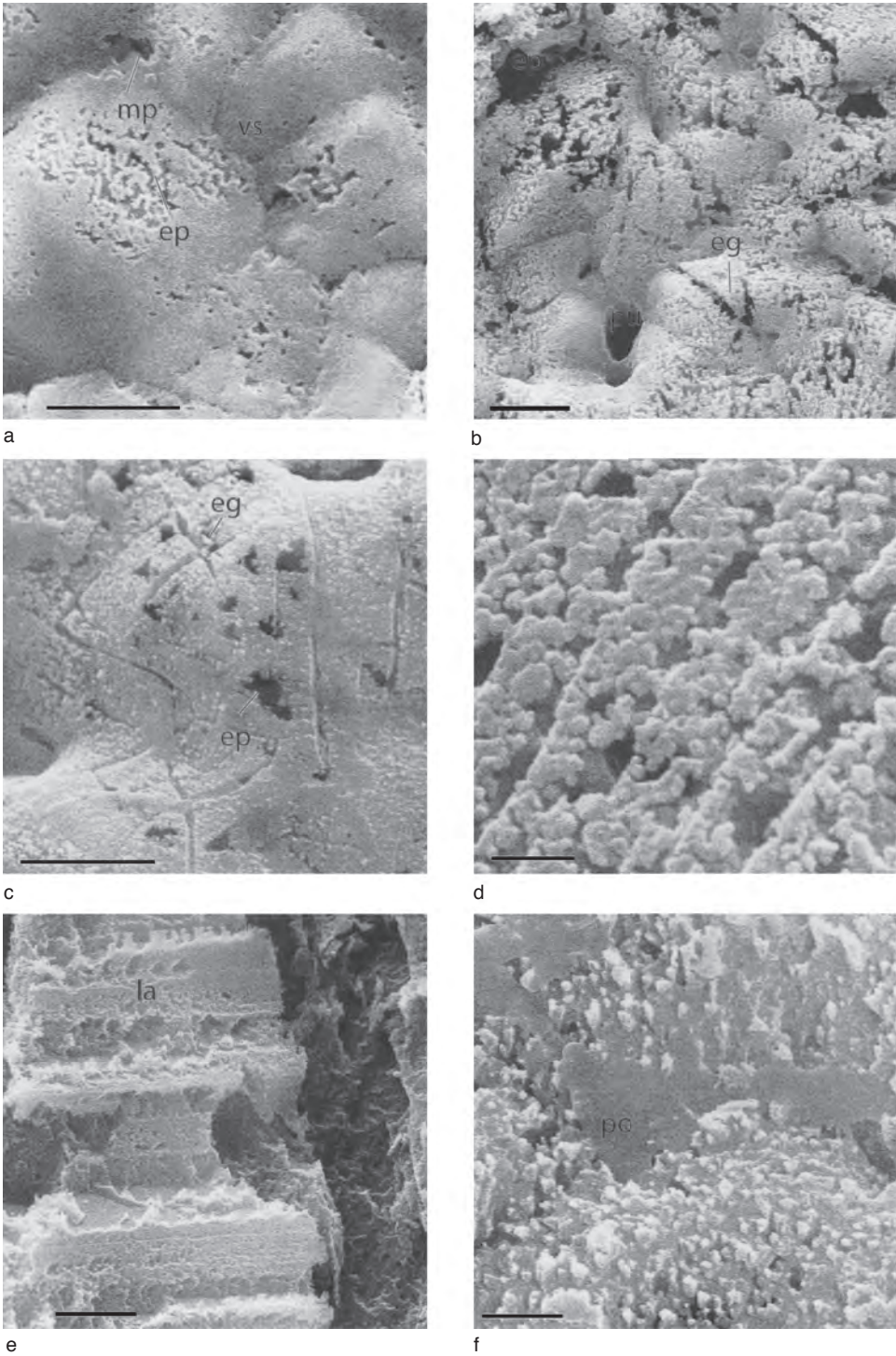
FIG. 1655. *For explanation, see facing page.*

They are composed of granules of calcite approximately 15 nm in size and normally assembled with a rhombohedral motif into monolayers. The monolayers aggregate into laminae of variable thickness that tend to have a crystallographic form that is more or less aligned throughout the shell, irrespective of organic inclusions. One manifestation of this continuity is the way the proximal boundaries of terminal faces of contiguous fibers are virtual sets of aligned (10.4) rhombohedral plates. As laminae grow by granular exocytosis orthogonal to the secreting plasmalemma, any crystallographic realignment is controlled by changing rates of sedimentation that cumulatively effect microtopographic changes in the internal surface of the shell and, therefore, the disposition of the epithelium. This is especially so in the growth of fibers, where the laminae of terminal faces are normally inclined in contrast to their near-horizontal disposition in primary and tertiary layers. In short, many skeletal structural differences characterizing thecideide, rhynchonellide, and terebratulide shells, layer for layer, are related to topographical variation in the internal surfaces of valves.

The precise relationship between the mineral and organic components of the rhynchonellate shell remains elusive. Organic constituents mediate shell growth with certain proteins effecting mineral precipitation and resorption in brachiopods (BROWN, 1998; CUSACK & WILLIAMS, 2001b), mollusks (FALINI & others, 1996), and so on. But the growth of a lamina (or monolayer) is a two-stage process that involves first the precipitation of calcitic units possibly aligned with the substrate fabric and then the binding together of the units into calcitic

sheets. Newly formed primary layers at the margins of *Notosaria* and *Liothyrella* shells become slotted by enzymic digestion, presumably of impersistent proteinaceous membranes, but they are entirely destroyed by bleach. Amorphous organic blobs that appear during enzymic digestion of the glycoproteinaceous sheaths of fibers also occur in primary layers when they are similarly treated. These blobs are assumed to be residues of a polysaccharide that also acts as a glue binding together mineral units into laminae, not just in the primary layer but throughout the shell. Moreover, laminae in the inframarginal, older parts of the primary layer tend to interdigitate and are less prone to disintegration when treated with bleach. This increased durability could result from further polymerization of the polysaccharide matrix (CUSACK & WILLIAMS, 2001b).

In contrast to the ultrastructural conservatism of living rhynchonellate shells, the range of proteins, extracted from intracrystalline residues, is wide with no clear indication of specificity to any particular layer. As the primary, secondary, and tertiary layers are, presumably, structurally homologous throughout fossil and living rhynchonellate shells, it would have been reasonable to expect proteins specific to the primary and tertiary layers to be the dominant molecular weights determined for the thecideide and liothyrellid shells respectively, with proteins characteristic of the secondary layer restricted to *Liothyrella* and especially *Notosaria* where it should be prevalent. No such specificity occurs. Indeed as Figure 1544 suggests, a variety of intracrystalline proteins are likely to be involved in the calcification of each layer of the rhynchonellate shell. Not all of the 21 intracrystalline proteins,

FIG. 1655. Structure of tertiary layer of *Liothyrella neozelanica* (THOMSON), Holocene, New Zealand; *a–c,* internal surfaces of tertiary layer penetrated by micropunctae (*mp*) and punctae (*pu*) showing microtopography of mounds delineated by valley systems (*vs*) with etch pits (*ep*) and etch grooves (*eg*) revealed by *a,* natural degradation of organic constituents and *b–c,* exaggerated by enzymic digestion; scale bars: 10, 10, and 5 μm; *d–f,* details of effects of degradation on slats of fracture section of laminar succession (*la*) and of enzymic digestion on internal surface with laminae exposed in residual polysaccharide (*po*); scale bars: 0.5, 2.5, 1 μm; *a, d* untreated, *b, e* digested in proteinase-K, *c, f* digested in subtilisin (new).

however, necessarily have a calcifying role. One or more molecular weight estimates must represent actinlike strands, sporadically occurring within laminae, that are probably part of a paracrystalline framework strengthening successions. Pits and grooves in rhombohedral arrangements, like those exposed in treated *Liothyrella*, are likely to be sites doped with inclusions of intercrystalline substrates (compare WILLIAMS, CUSACK, & BROWN, 1999). Some intracrystalline proteins could even have arisen by molecular transformation subsequent to the phylogenetic divergence of the terebratulides and the thecideides from their rhynchonellide sister group. Should this be so, the protein chemistry of rhynchonellate shells is presently a less comprehensible guide than ultrastructure to ordinal genealogy.

CHEMICOSTRUCTURAL DIVERSITY OF EARLY RHYNCHONELLIFORM SHELLS

The extinct, organocarbonate-shelled chileate, obolellate, kutorginate, and strophomenate brachiopods are coeval with the early Cambrian rhynchonellates. The groups are morphologically related and probably a monophyly, but each is characterized by a distinctive secondary shell fabric. In attempting to derive these diverse fabrics from an ancestral node, two assumptions have to be made. First, the integument of the ancestral rhynchonelliform did not differ significantly in growth or in layering from that of living species. Secondly, variation in fabric reflects changes in the composition and sites of secretion of polymers acting as substrates for the accretion of relatively uniform, nanometrically sized granules or rhombs of calcite.

The primary layer also plays a crucial role in postulating changes in ancient secretory regimes that could have given rise to diverse secondary fabrics. As it is by definition the first mineralized layer to be secreted on the periostracum, it is invariably present and usually preserved, albeit in a recrystallized state. Indeed, the primary layer is a constant reminder that no mineral accretion can take place without a substrate; and the possible origin of its own substrate, the periostracum, is pertinent to an enquiry into the structural diversity of the rhynchonelliform shell. Presumably, a mucin-based glycocalyx was the precursor to the glycoproteinaceous periostracal substratum (Fig. 1575, 1578) that would have been the ancestral substrate for calcitic accretion in the earliest rhychonelliforms.

In living rhynchonellates, the onset of the fibrous secondary layer is signalled by the secretion of arcuate patches of a glycoproteinaceous membrane on the inner surface of the primary layer (Fig. 1651b). Each patch is secreted by a microvillous anterior arc of an outer epithelial cell (WILLIAMS & others, 1997, fig. 13, p. 20). As the secreting cell advances anteroradially, its patch is extended forward as a semicylindrical strip serving as a substrate for the outer edges of a stack of calcitic laminae (i.e., the fiber) being secreted by the rest of the plasmalemma behind the microvillous arc. This sequence of skeletal secretion by a cell is the same as shell deposition by the mantle where the periostracum is fabricated by the outer mantle lobe marginal to the outer advancing mineralized shell.

The plasmalemmas of outer epithelial cells are closely packed in alternating rows (WILLIAMS, 1997, p. 283). Consequently during continuing secretion by an array of cells, the membranes intermesh to ensheath fibers that are exposed only at their terminal faces. In effect, each cell fabricates a substrate for the granular calcite it secretes. The secretion of its own substrate and mineralized coat is a discrete, spatially ordered event, not a collective one involving an array of cells simultaneously secreting a layer of the same constituent, as when the primary layer is

deposited on the periostracum. Not all linear calcitic structures, however, were secreted discretely with their substrates. Laths and blades, for example, the predominant calcitic structures of the strophomenate secondary shell, would have grown collectively by marginal accretion on an enlarging membranous sheet.

The singularity of the discrete secretory regime, giving rise to the fibrous secondary layer, militates against its having been an ancestral system of shell deposition. The collective secretory regime, on the other hand, is not only the mode of deposition of the primary layer but also of the stratiform shells of the linguliforms, the sister group of the rhynchonelliforms. It is, therefore, reasonable to assume that the fabric of the ancestral secondary shell was stratiform and probably structurally closer to that of an extinct rhynchonelliform group(s) than to the derived fibrous shell of living rhynchonellates. On this assumption, the secondary shell fabrics of the chileates, obolellates, kutorginates, and early strophomenates have been reviewed. As these fabrics are always recrystallized and seldom bear traces of their *in vivo* structure, new studies have been made to supplement published accounts.

The secondary shell fabric of the oldest known strophomenate, the Middle Cambrian *Billingsella*, is stratiform laminar (WILLIAMS, 1970). The basic laminar units are anastomosing calcitic sheets, each approximately 100 nm thick, that are commonly wrinkled into impersistent, radially disposed folds (Fig. 1656a–d). The sheets are interpreted as having originally been membranes coated with calcitic aggregates impregnated with polysaccharides that retained some of their rheological features on polymerization. Sets of sheets occur in close-packed successions, but they are more commonly thickened by the radial folds (8–10 μm wide) and discrete aggregates of radially aligned calcitic tablets or blocky calcite forming impersistent ridges (Fig. 1656e–f).

Although many morphological features distinguishing strophomenates from other rhychonelliforms are homoplastic, the group is probably monophyletic (WILLIAMS & others, 2000b, p. 215). The fabric of the strophomenate secondary shell (except for that of most plectambonitoids) is laminar as in the close-packed laminar sets of *Billingsella* (WILLIAMS, 1997, p. 287–293). The laminar texture, however, is cross bladed, which has an important bearing on changes in the relationship between shell and mantle during strophomenate evolution.

Strophomenate lamination is a collective fabric that was secreted by an array of outer epithelial cells as a recurring succession of a membranous substrate and a nanometrically thick, calcitic coat, sporadically interleaved with laminae thickened by various microstructures. In *Billingsella*, these include radially disposed folds of the calcified substrates and ridges, which would have been aligned more or less orthogonally to the growing margins of successive substrates. In other strophomenate shells, sets of close-packed laminae are also interleaved with thicker laminae mainly composed of tablets. These tablets are cross sections of thickened blades that commonly occur in localized parts of strophomenate shells (Fig. 1657; WILLIAMS, 1997, fig. 251, p. 291). The thickened blades look like the radial folds and ridges of *Billingsella* but are well ordered and differently oriented, being always aligned with the strophomenate cross-bladed fabric. Indeed, a typical section of the strophomenate secondary shell consists of alternating sets of arrays of tablets and laminae representing the transverse and longitudinal sections respectively of ordered successions of laths or blades (Fig. 1658), which is a composite fabric (NEVILLE, 1993).

In effect, cross-bladed lamination is a natural plywood, a helicoidal or pseudoorthogonal composite, consisting of calcified substrates bearing closely spaced laths. The flat laths or blades, being not more
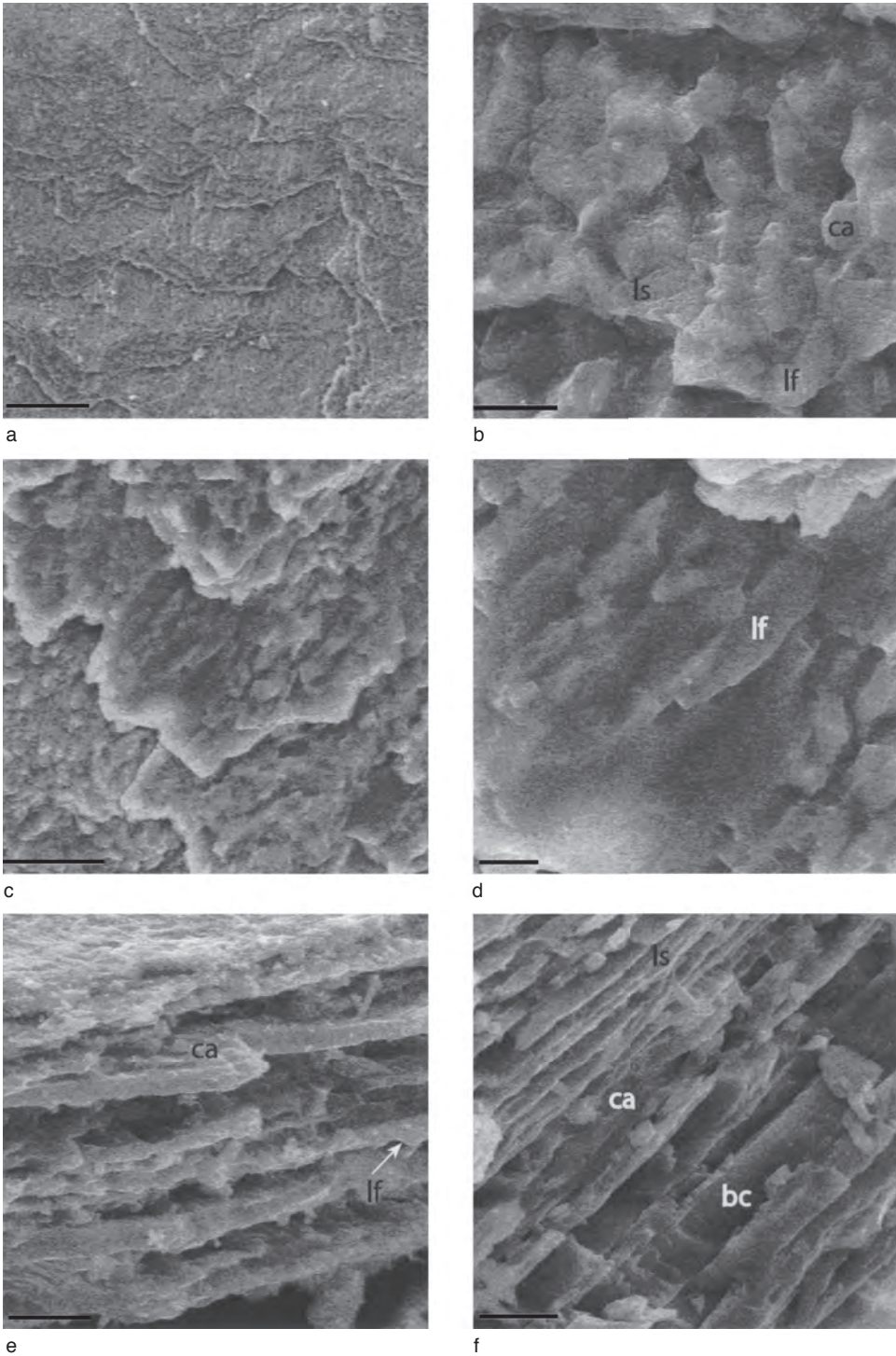
FIG. 1656. *For explanation, see facing page.*

than 6 μm wide, are generally discrete in older strophomenates (Fig. 1657, 1658.1a) and laterally fused into continuous sheets in younger species. They would not have conformed in size or shape to the secreting plasmalemmas of the strophomenate outer epithelium, assuming it to have been the same as in the mantle of living brachiopods. The incremental growth of laths is commonly recorded as transverse growth banding (WILLIAMS, 1997, fig. 250.3, p. 290), and the direction is indicated by the terminal, angular edges of laths (Fig. 1658.1a). Unlike the fibers of the rhynchonellate fabric, however, these growth vectors were only coincidentally orthogonal to the mantle edge of living strophomenates. As in all composite layers, they were determined by the polymeric configuration of the substratal membranes. In effect, the same array of outer epithelial cells secreted a succession of membranes that were so configured as to impose a helicoidal or pseudo-orthogonal lineation on their calcitic coats (Fig. 1658.2). The persistent association of the same array of cells with the laminar succession in the same part of the shell is consistent with the development of pseudopunctal ties between shell and mantle in most of the later strophomenates (WILLIAMS, 1997, p. 305–312).

The composition of the substratal membrane(s) that gave rise to strophomenate composite lamination must have differed from that of the substratal sheaths of rhynchonellate secondary fibers. The organic fibers that determine the fabric of a composite membrane are embedded in a polysaccharide or proteinaceous matrix and may be chitinous or proteinaceous (NEVILLE, 1993, p. 85). There is some
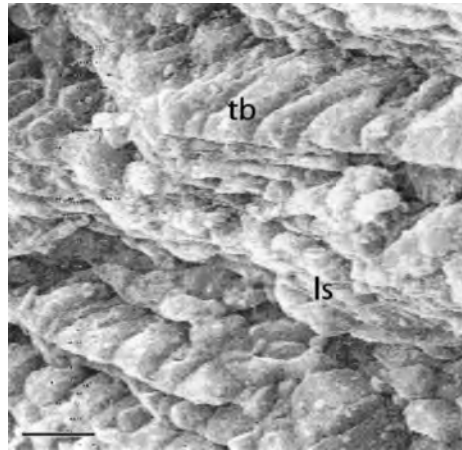

FIG. 1657. Fracture section of dorsal valve of early Ordovician (Arenig) strophomenide, *Hesperinia sinensis* RONG & others, showing thickened (*tb*) and normal sized (*ls*) blades of secondary shell laminae in transverse and longitudinal sections respectively; scale bar: 10 μm (new).

analogous support for the assumption that the membranous substrates, interleaved with strophomenate calcitic laminae, were chitinoproteinaceous, not glycoproteinaceous as in the rhynchonellate secondary layer. Thus, when glycoproteins form collective substrates for calcitic laminae, as in living craniid shells, the fabric is not composite (p. 2513, herein). Moreover, chitin is a common component of the shells of living lingulides and presumably of those linguliforms that were closely related to early rhynchonelliforms.

Attributing the structural difference between the fibrous and laminar secondary shells of rhynchonelliforms to glycoproteinaceous and chitinoproteinaceous membranes respectively, however, seems incompatible with the secondary shell fabric of the

FIG. 1656. Secondary shell structure of *Billingsella lindstromi* (LINNARSSON), Middle Cambrian, Sweden; *a–d,* internal views of fracture surfaces showing exfoliated sheets with anterior margin to bottom lefthand corner (*a–b*) and details of laminar sheets (*ls*) including laminar folds (*lf*) and calcitic aggregates (*ca*); scale bars: 220 μm, 10 μm, 50 μm, and 10 μm respectively; *e–f,* oblique fracture surfaces showing laminar successions with closely grouped laminar sets (*ls*) and thick laminae with laminar folds (*lf*), calcitic aggregates (*ca*), and blocky calcite (*bc*); scale bars: 25 μm and 10 μm respectively (new).
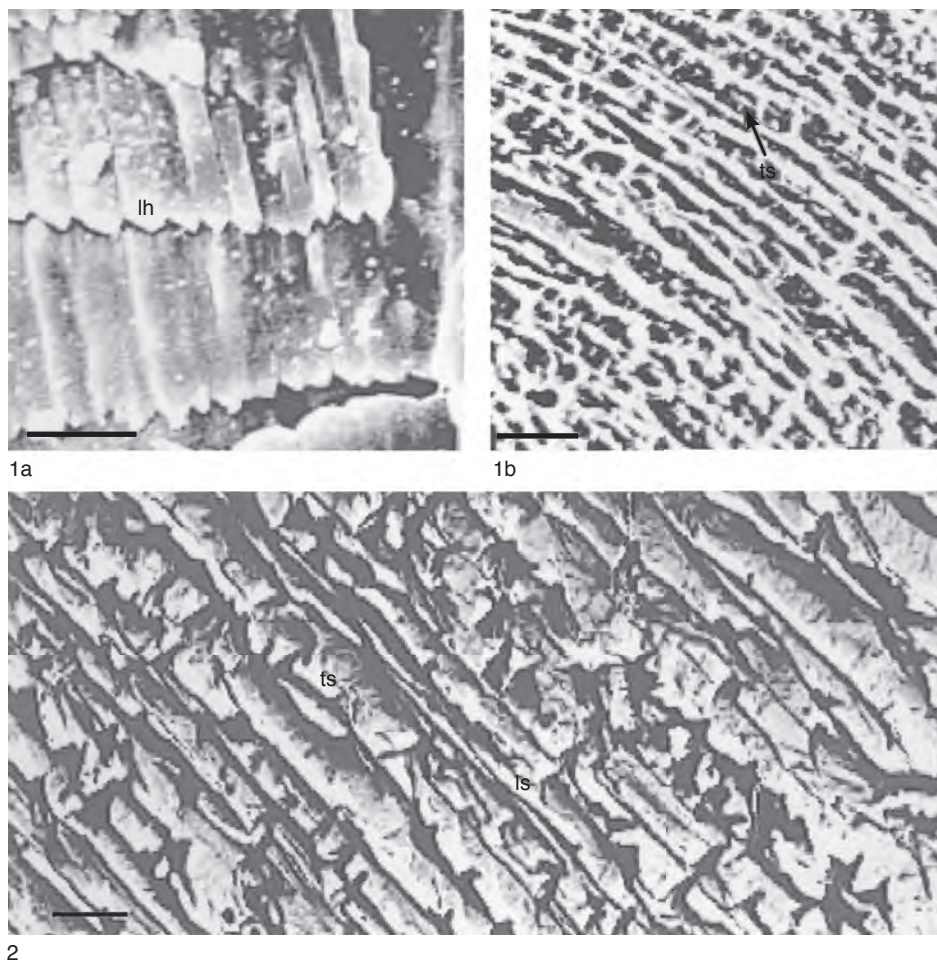
Fig. 1658. Strophomenate secondary shell structures; *1a–b,* exfoliated surface and resin-impregnated section of Upper Ordovician orthotetidine *Gacella insolita* Williams showing laminar laths in planar (*lh*) and transverse (*ts*) and longitudinal views, light bands and crossbars in *1b* represent resin infills and dark areas represent slightly etched laminae; scale bars: 5 μm; *2,* single stage negative replica of slightly etched polished vertical section of resin-impregnated shell of Middle Devonian *Pholidostrophia* sp. cf. *geniculata* Imbrie showing plywood nature of laminar secondary shell with alternating sets of blades in longitudinal (*ls*) and transverse (*ts*) sections; scale bar: 5 μm (new).

strophomenide plectambonitoids, which are probably ancestral to the productide chonetidines. The plectambonitoid fabric is generally regarded as fibrous (Williams, 1997, fig. 252.3–252.4, p. 292), with the implication that the fibers are homologous with the orthodoxly stacked constituents of the rhynchonellate secondary layer (Williams, 1997, fig. 243, p. 284). In fact, as has been shown by Brunton (1972), the

linear structures of the plectambonitoid secondary shell vary from flattened fibers without keels to blades with bevelled sides (Fig. 1659.1a–b). Moreover, the secondary shell structure of the earliest known chonetidines (the late Ordovician *Archaeochonetes*), which is accepted as a typical bladed lamination, is virtually indistinguishable from that of the plectambonitoid *Aegiromena* (Brunton, 1972; Fig. 1659.2–1659.3). Such
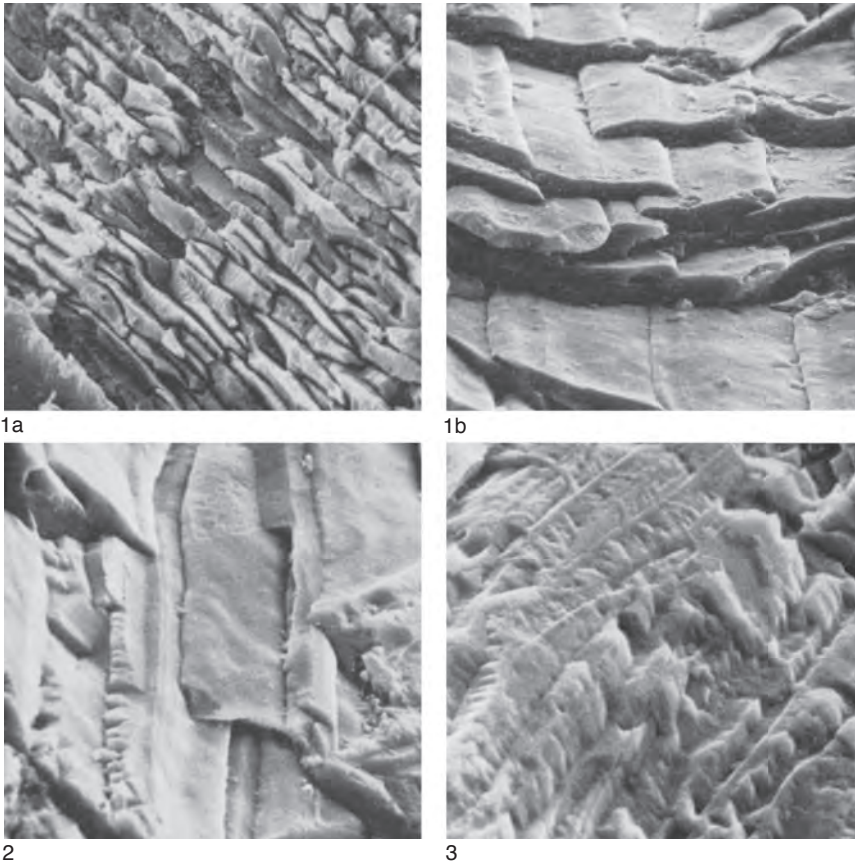
FIG. 1659. Strophomenate secondary shell structures; *1a–b,* lightly etched section and internal fracture surface of shell of Upper Ordovician plectambonitoid *Sowerbyella liliifera* (ÖPIK), showing stacked, flattened fibers, both ×1000; *2–3,* blades or fibers of Upper Ordovician plectambonitoid *Aegiromenia aquila* (BARRANDE) and Upper Ordovician chonetidines *Archaeochonetes primigenius* (TWENHOFEL) showing similarity in structure and stacking; ×1200, ×1000 respectively (Brunton, 1972).

a close relationship suggests that membranous substrates of the same composition were present in both secondary shells and are unlikely to have been chitin, which is absent from the shells of living rhynchonelliforms (and craniiforms). Whether these particular textural features indicate that the plectambonitoid fibrous fabric evolved independently of the rhynchonellate fabric will be considered later.

The composite fabric of the later strophomenides has evidently been derived from two sources. The basic constituent of the composite fabric of billingsellides (including orthotetidines and triplesiidines) and strophomenoids is a lath or blade that evolved from laminar folds as ridges as in those of the *Billingsella* shell. The basic constituent of the composite fabric of productides, on the other hand, was a flat, plectambonitoid fiber. The billingsellid ridge or blade had much in common with folii, and the plectambonitoid fiber had much in common with the rhynchonellate fibers. Both derived constituents grew on collective membranous substrates.

The presumed fabrics of the secondary shells of the three other early rhynchonelliform groups were first described more
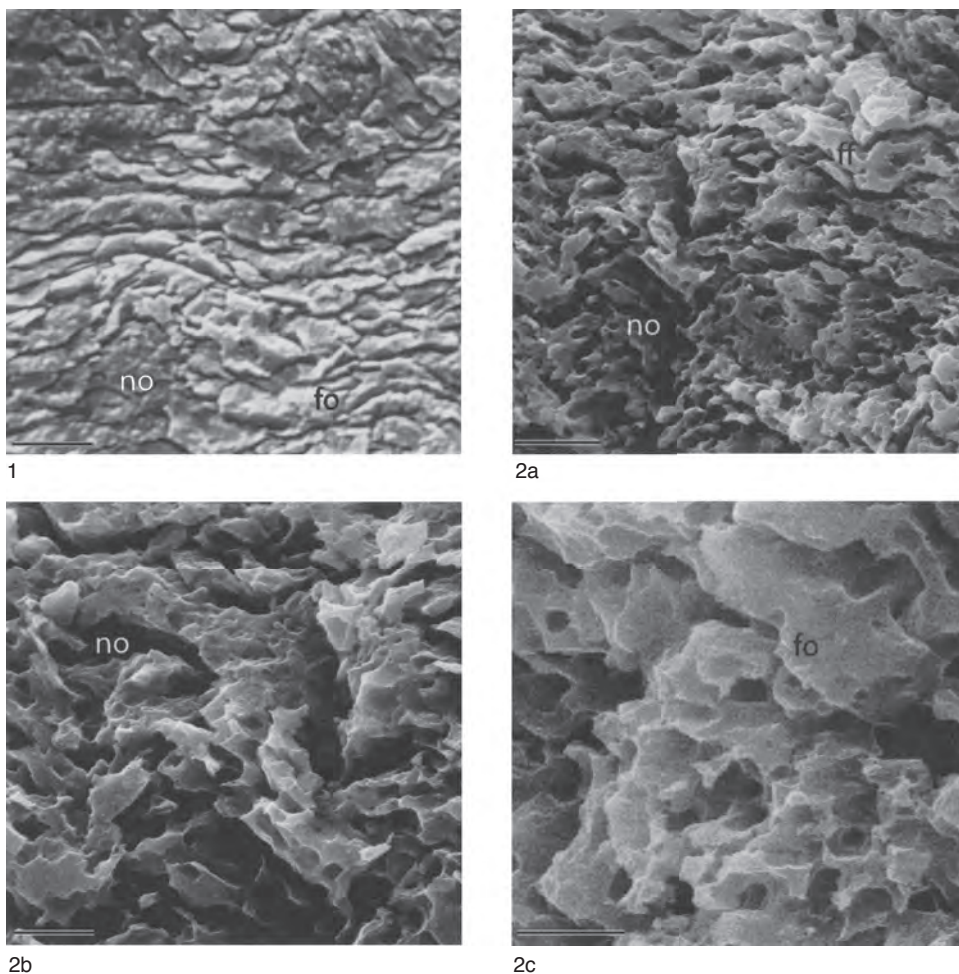
FIG. 1660. Secondary shell structure of *1, Trematobolus pristinus bicostatus* and *2a–c, Obolella* sp., Lower Cambrian, Rassokha River Basin, eastern Siberia; *1*, polished and slightly etched section showing folii (*fo*) disposed around nodules (*no*); scale bar: 25 µm; *2a–c*, fracture sections showing nodules (*no*) are composed largely of successive, hemispherical to semi-ellipsoidal layers of folded folii (*ff*) (*2a–b* with external shell surface to top of micrographs), and *2c*, detail of slightly etched, folded folii (*fo*); scale bars: 10 µm, 5 µm, and 5 µm respectively (new).

than thirty years ago, but they are rarely preserved and there has been some doubt about their textural authenticity. All three groups, the chileates, kutorginates, and obolellates, are restricted to the Lower and Middle Cambrian, although the chileates are tentatively regarded as being ancestral to the post-Cambrian dictyonellidines, whose secondary shells are disputably fibrous or aragonitic (HOLMER, 2000, p. 196). Recent work has clarified textural details of all three fabrics and has led to reinterpretations of their structures in the living state.

The obolellate secondary shell was first described as laminar and was homologized with the screw-dislocated lamination of living craniids (WILLIAMS & WRIGHT, 1970, p. 45). The relative coarseness of the laminae and their lenticularity in cross section, however, later prompted their redefinition as folii that had been sheathed by membranes in the living state, like rhynchonellate fibers
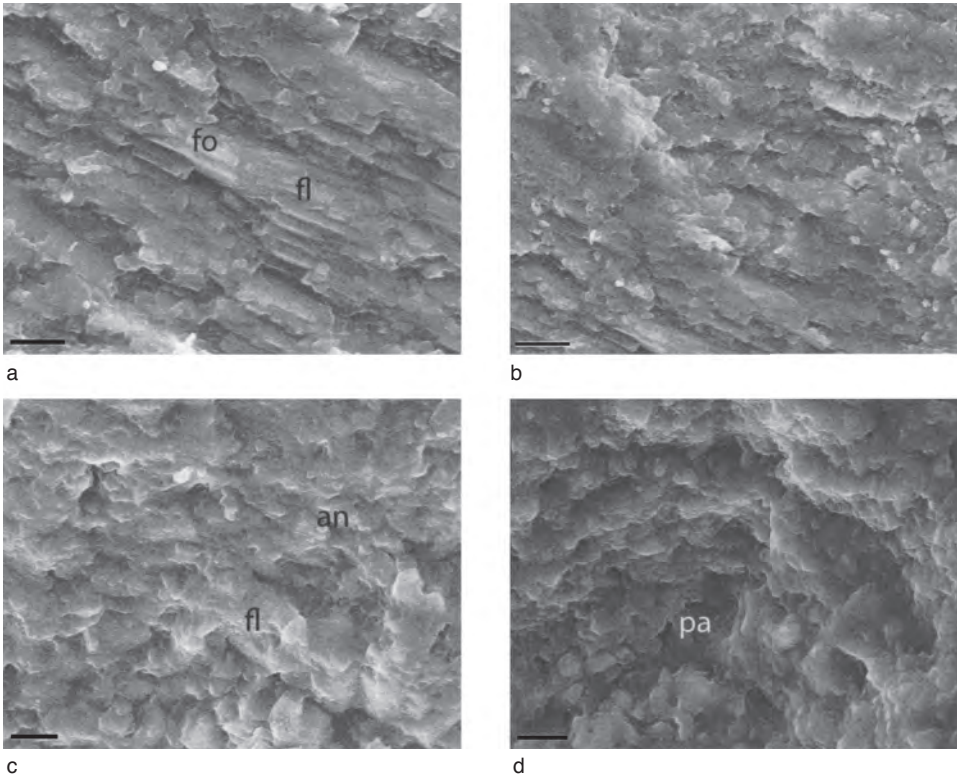
Fig. 1661. Secondary shell structure of chileate *Kotujella calva* Andreeva, Lower Cambrian, Rassokha River Basin, eastern Siberia; slightly etched fracture sections of ventral valve with external surface beyond top right corner of micrographs; *a–b,* succession of sets of folii (*fo*), some forming lenses (*fl*); scale bars: 20 µm; *c–d,* views of junction of anastomosing sets of folii (*an*) and puncta (*pa*) with frequent lenses of folii (*fl*); scale bars: 25 and 10 µm respectively (new).

(Williams, 1997, p. 286). The obolellide secondary shell fabric (Fig. 1660) is neither tabular in the manner of craniid laminae nor lenticular in cross section like rhynchonellate fibers. The fabric is laminar in the sense of having been secreted collectively, but the constituent plates are wrinkled into folds with wavelengths of approximately 5 µm. It seems appropriate therefore to recognize the distinctiveness of the obolellide fabric by continuing to describe it as foliate. The rheological state of *in vivo* folii is reflected in the way they form successive sheets composing the so-called nodules that occur in hexagonal-packed arrays throughout the shell and have been interpreted as hollows accommodating impersistent secretion bodies or as tempo-

rary sites of mantle muscle ties (Williams & Wright, 1970, pl. 15,*4–6;* fig. 16).

The fabrics of the secondary shell of chileates and kutorginates were initially interpreted as having been fibrous in the living state with the chileate (*Kotujella*) shell also being punctate (Williams, 1968b, p. 487). Recent studies of *Kotujella*, however, indicate that its secondary shell (Fig. 1661) is composed of anastomosing sheets less than 300 nm thick, commonly occurring in sets approximately 25 µm thick, which may look like oblique sections of fibers but are structurally closer to foliate sets. The folii are not wrinkled but may be variably differentiated into lenticular tablets or occasional laths. The fabric of the kutorginate
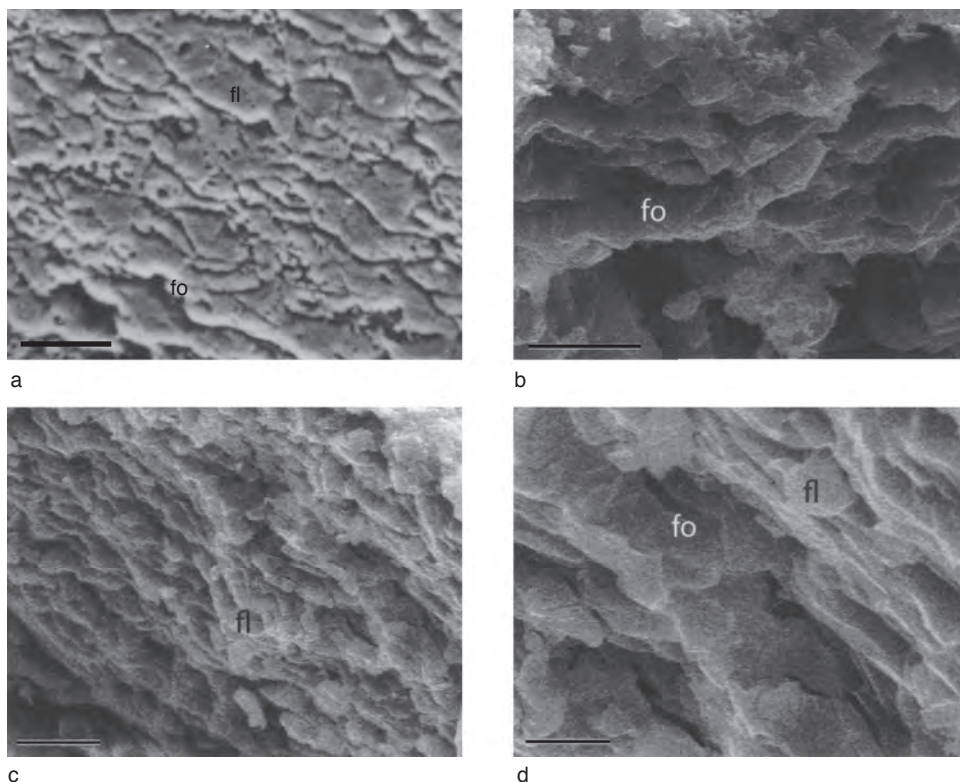
Fig. 1662. Secondary shell structure of kutorginate *Narynella ferganenis* (Andreeva), Lower Cambrian, Uzbekistan: *a*, polished and etched section showing succession of lenticular (*fl*) and laminar (*fo*) folii; scale bars: 10 μm; *b–d,* fracture sections showing foliate sets with slip planes developed on surfaces of folii that also enlarge into lenses (*fl*); scale bars: 20 μm, 25 μm, and 10 μm (new).

shell is also unlikely to have been fibrous in the living state. Sections of the nisusioid *Narynella* show horizons of ordered lenticles simulating fibers and interleaved with laminar sets (Fig. 1662). The lenticles are commonly composed of slip planes that are assumed to reflect recrystallized lamination in Mesozoic craniids (Cusack & Williams, 2001a, p. 890). In short, the kutorginate secondary shell appears to be laminar, but with lenticles instead of laths and blades as in strophomenates. Both the wrinkled folii of chileates and lenticular folii of kutorginates could have been sheathed in membranes in the manner of a fiber. Both folii and their enclosing membranes, however, would still

have been secreted collectively on membranous substrates as in laminar successions. In effect, the foliate fabric could have been transitional between the laminar and fibrous rhynchonelliform fabrics and ancestral to both or either. A relationship that presently best fits a phylogenetic model for the brachiopod phylum as a whole is considered in the Conclusions section, p. 2518 below (see also Williams & Carlson, p. 2822, herein, and Carlson, p. 2878, herein).

In attempting to ascertain the evolution of the rhynchonelliform secondary shell, the phylogeny of the brachiopod phylum as a whole has to be taken into account. Seven morphological and anatomical features,

which have long been recognized in extinct as well as living groups as key aspects of the brachiopod body plan, have been used with five characteristics of the secondary shell (Tables 34–35) to construct a phylogenetic tree for the eight brachiopod classes. The choice of *Micrina* as an outgroup accords with the assumed derivation of brachiopods from halkieriids (WILLIAMS & HOLMER, 2002). The resultant cladogram (Fig. 1663) is a feasible representation of brachiopod phylogeny. Among several novel features, it shows that the most dramatic transformations affecting the morphology of the brachiopod and the chemicostructure of its shell were out of phase and supports a rhynchonelliform ancestry for the craniates.

The morphological and anatomical evidence identifies lingulates as the sister group of all other brachiopods, including the paterinates that, with their strophic hinge lines, adductor and diductor musculature, and gonadal sacs in saccate mantle canal systems, are the stem group of rhynchonelliforms. Morphological evidence also identifies the three extinct rhynchonelliform classes, the chileates, kutorginates and obolellates, and the craniiforms as the most derived of the organocarbonate-shelled brachiopods. In passing, it is noteworthy that the three rhynchonelliform groups are characterized by apertures in their ventral valves that could have accommodated holdfasts as well as delthyrial openings for pedicles. A vestigial homologue of such a holdfast may initiate the cementation of the ventral valve of living craniids. This phylogenetic reconstruction also shows that the straight gut of craniates is a derived rather than an inherited ancestral state.

The most dramatic transformation in the chemicostructural differentiation of the brachiopod shell was the change from an organophosphatic to an organocarbonate composition (Fig. 1664 and Tables 36–37). The change included the replacement of apatite by calcite and the loss of GAGs and chitin from the greatly reduced organic content of carbonate shells. These changes distinguished the carbonate-shelled ancestor of the rhynchonelliforms (and craniiforms) from its paterinate sister group. The secondary layer of this ancestral calcitic shell was probably secreted collectively as a predominately foliate succession, but with glycoproteinaceous membranes serving as substrates for sporadically deposited laminae as well as the folii.

The transformation(s) leading to the secretion of the rhynchonellate fibrous secondary shell was little more than a switch from a collective epithelial secretion of folii and laminae on glycoproteinaceous sheets to a discrete cellular deposition of fibers on their glycoproteinaceous strips that intermeshed to form sheaths. The derivation of the secondary shell fabrics of strophomenates, the sister group of the rhynchonellates, was more complicated. The composite laminar fabric of later strophomenates convergently evolved from the coarse laminae of billingselloids (and strophomenoids) and the flat fibers of the plectambonitoids. As the strophomenates were probably monophyletic, the dual origin of the composite fabric needs clarification. Our assumptions are that the billingselloid lamination is closer to the fabric of the stem-group rhynchonelliforms, and that the plectambonitoid fibers developed later, independently of the fibrous secondary shell of rhynchonellates.

Tabular lamination is a fabric unique to craniate shells. In living craniids, it succeeds a primary layer that is also unique because it is inwardly differentiated into laths, laminae, and tablets with polysaccharide substrates. Now that the craniates can be feasibly derived from an early rhychonelliform, an alternative interpretation of their shell successions is tenable. The laths and laminae of the inner primary layer could really be vestiges of a foliate-derived secondary layer and the spirally growing tabular laminar succession, a novel tertiary layer (see also CARLSON, p. 2878, herein, for a different perspective on brachiopod phylogeny).
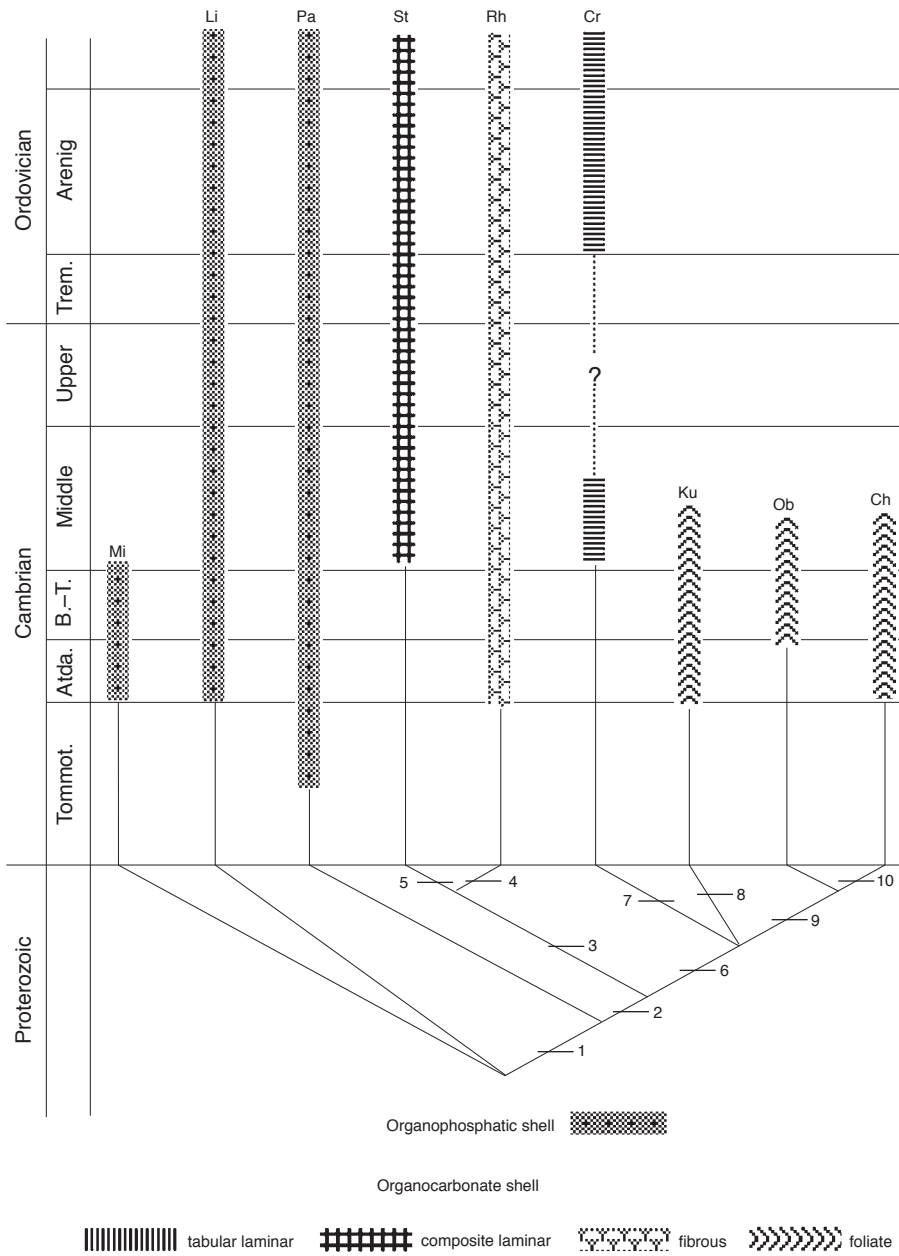
FIG. 1663. *For explanation, see facing page.*

TABLE 34. List of character states used in the cladogram of Figure 1663 to illustrate a possible origin of the diverse fabrics of the mature secondary shell of early rhynchonelliforms and craniiforms (new).

Morphology and anatomy
    1. Valve relationship   separated (0), conjoined (1), articulated (2), strophic (3), astrophic (4)
    2. Dentition   no teeth (0), ventral denticles (1), by hinge margins (2), deltidiont (3), cyrtomatodont (4)
    3. Gut disposition   straight (0), longitudinal U-bend (1), transverse U-bend (2)
    4. Gonadal sacs   absent (0), present (1)
    5. Principal muscle systems   unknown (0), obliques (1), dispersed adductors (and weak diductors) (2), adductors and diductors (3), quadripartite adductors (4)
    6. Pedicle   absent (0), ventral body wall (1), holdfast (2), rudiment (3)

Shell chemicostructure
    7. Shell composition   organophosphatic (0), organocarbonate (1)
    8. Secondary shell   stratiform (0), tabular laminar (1), composite laminar (2), foliate (3), fibrous (4)
    9. Secretory regime   collective (0), discrete (1)
    10. Chitin & GAGs   absent (0), present (1)
    11. Canaliculate system   absent (0), present (1)

TABLE 35. Matrix of 11 characters described in Table 34 and 8 designated classes of Brachiopoda (new).

	[11 12345678901]
Micrina	000?0000011
Lingulates	10101100011
Paterinates	10113100010
Craniates	10014(02)11000
Chileates	10112213000
Obolellates	(12)1102213(01)00
Kutorginates	22113213000
Strophomenates	3311311(24)(01)00
Rhynchonellates	(34)(34)(12)1(13)314100

FIG. 1663. Chart showing evolution of main fabrics of secondary shells of Cambro-Ordovician brachiopods with presumed halkieriide *Micrina* (*Mi*) as sister group; 8 brachiopod classes are lingulates (*Li*), paterinates (*Pa*), strophomenates (*St*), rhynchonellates (*Rh*), craniates (*Cr*), kutorginates (*Ku*), obolellates (*Ob*), and chileates (*Ch*). Cladogram (not to geological time scale) is a 50% majority-rule consensus of 4 trees generated by a PAUP heuristic search (10 stepwise additions) of 11 character states (Table 34) and matrix (Table 35). The numbered transformations are: *1*, loss of canaliculate system and acquisition of basic rhynchonelliform characters including development of diductor-adductor muscle system and gonadal sacs in mantles; *2*, loss of the organophosphatic, stratiform shell with GAGs and chitin and its replacement by an organocarbonate foliate shell; *3*, development of articulating shells with teeth and sockets and a fibrous fabric with a discrete secretory regime; *4*, differentiation of pedicles from apical rudiments; *5*, development of composite lamination; *6*, development of holdfasts, other than pedicles, breaching ventral valves; *7*, development of straight gut and tabular lamination and loss of diductor muscles; *8*, development of articulating hinge margins; *9*, comparatively weak differentiation of diductor-adductor muscle system; *10*, development of ventral denticles (new).

craniide

tabular laminar

kutorginate

foliate

obolellate

foliate

rhynchonellate

fibrous

strophomenate

bladed laminar

chileate

micrina

columnar

siphonotretide

acrotretide

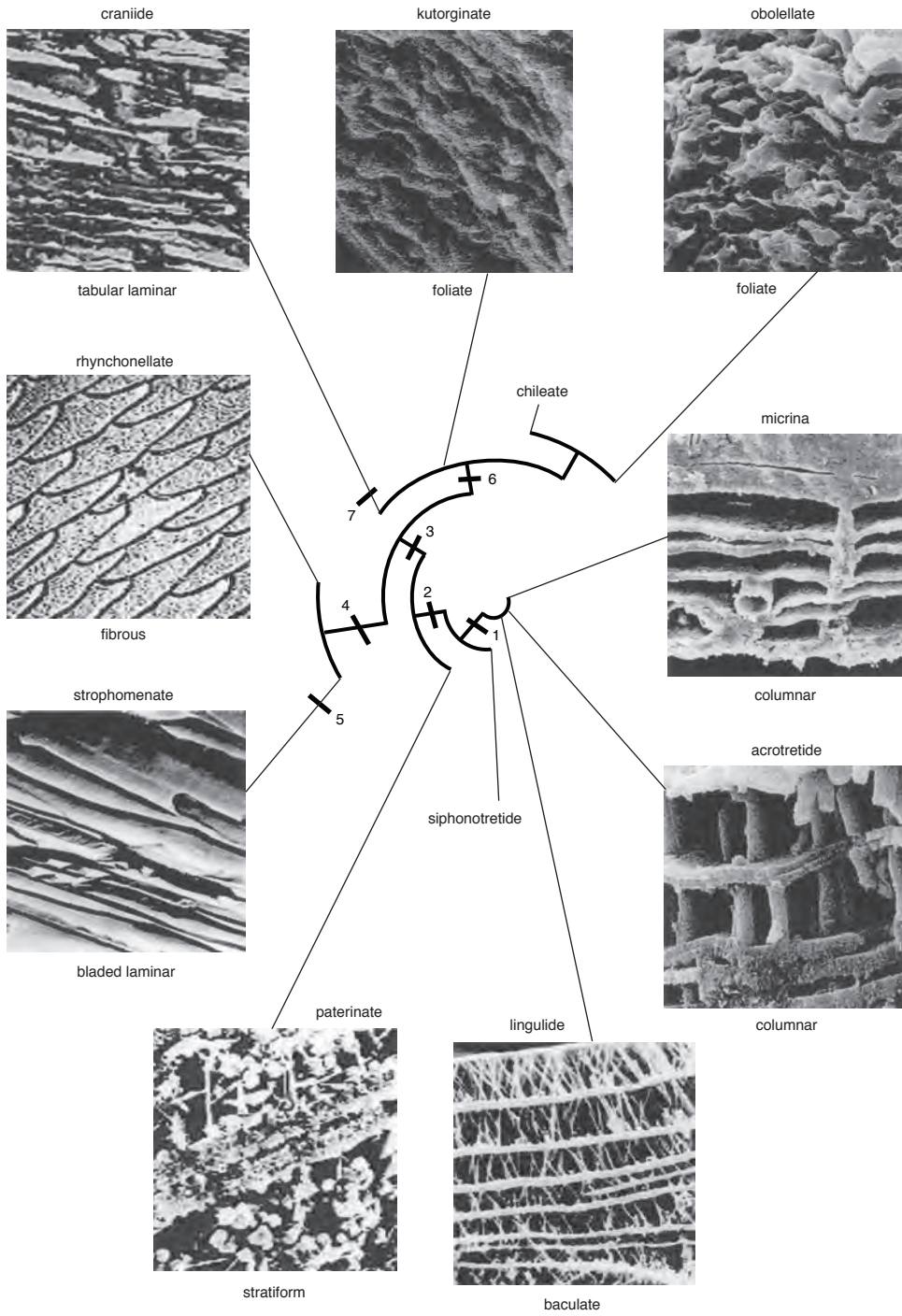columnar

paterinate

stratiform

lingulide

baculate

FIG. 1664. *For explanation, see facing page.*

TABLE 36. List of character states used in circle cladogram of Figure 1664 to illustrate a possible evolution of brachiopod secondary shell (new).

Body plan features
    1. Valve disposition   separated (0), conjoined (1), articulated (2), strophic (3), astrophic (4)
    2. Dentition   no teeth (0), variable denticles (1), by hinge margins (2), deltidiont (3),
         cyrtomatodont (4)
    3. Gut disposition   straight (0), longitudinal U-bend (1), transverse U-bend (2)
    4. Gonadal mantle sacs   absent (0), present (1)
    5. Principal muscle systems   unknown (0), obliques (1), dispersed adductors (and weak diductors)
         (2), adductors and diductors (3), quadripartite adductors (4)
    6. Pedicle   absent (0), ventral body wall (1), holdfast (2), rudiment (3), within ventral
         valve (4)
Shell chemicostructure
    7. Shell composition   organophosphatic (0), organocarbonate (1)
    8. Calcitic secondary shell   phosphatic (0), tabular laminar (1), composite laminar (2), foliate (3),
         fibrous (4)
    9. Secretory regime   collective (0), discrete (1)
    10. GAGs and chitin   absent (0), present (1)
    11. Canaliculate system   absent (0), present (1)
    12. Phosphatic secondary shell   calcitic (0), stratiform (1), columnar (2), baculate (3)
    13. Setigerous tubes   absent (0), present (1), other (2)
    14. GAGs chambers   absent (0), poorly developed (1), well developed (2)

TABLE 37. Matrix of 14 characters described in Table 36 and 11 listed taxa representing presumed halkieriide *Micrina* (as outgroup) and all 8 classes of Brachiopoda (new).

	[11111 12345678901234]
Micrina	000?0000011212
Lingulates	10101100011302
Paterinates	10113100010101
Craniates	10014(02)11000000
Chileates	10112213000000
Obolellates	(12)1102213(01)00000
Kutorginates	22113213000000
Strophomenates	3311311(24)(01)00000
Rhynchonellates	(34)(34)(12)1(13)314100000
Acrotretides	10101100011202
Siphonotretides	10101400010121

Fig. 1664. Circle cladogram representing 50% majority-rule consensus of 8 trees generated by PAUP heuristic search (10 stepwise additions) of character states (Table 36) and matrix (Table 37) that illustrates derivation of 7 main fabrics of secondary shells (in transverse sections) of halkieriide *Micrina* (columnar, with a column and setigerous tubes to left, ×130); acrotretide *Prototreta* (columnar sets, ×850); lingulide *Schizotreta* (baculate sets, ×800); the paterinates *Cryptotreta* (stratiform with poorly developed GAGs chambers, ×800); strophomenate *Strophomena* (cross-bladed laminar, ×1500); rhynchonellate terebratulide *Macandrevia* (fibrous, ×3800); craniide *Novocrania* (tabular laminar, ×7000); kutorginate *Narynella* (foliate, ×350); obolellate *Obolella* (foliate, ×100). The most important transformations that affected the brachiopod shell structure and body plan were *1,* loss of organic canaliculate framework and well-developed GAGs chambers with columns or baculi; *2,* development of rhynchonelliform body plan; *3,* replacement of organophosphatic, stratiform shell with GAGs and chitin by organocarbonate shell with foliate secondary layer; *4,* development of fibrous secondary shell; *5,* development of composite (cross-bladed) laminar secondary shell; *6,* development of holdfast; *7,* development of tabular laminar secondary shell (new).

CONCLUSIONS

Research since 1995 has overturned many of the long-held assumptions on the chemicostructure of the living and fossil brachiopod shell. The biochemistry of the living shell is more complex than pioneer investigations indicated. There is an unexpectedly wide range of polysaccharides and especially of proteins, which presently obscures identification of standard calcifying agents even within ordinal groups of brachiopods. Progress, however, has been made in determining the modes of association of intercrystalline as well as intracrystalline polymers within the mineral constituents, while analyses of the organic residues of fossilized shells have refined the geological time scale of polymeric degradation.

The mineralogy of the shell can no longer be regarded as exclusively apatitic or calcitic. The juvenile shell of organophosphatic discinids has been composed of siliceous tablets for over 400 myr, contrary to the belief that shell secretion within a life cycle has never involved more than one crystalline component. Indeed, there is evidence to suggest that many Paleozoic lingulates had calcitic juvenile and apatitic mature shells, which refutes the general opinion that these two mineral phases have always been mutually exclusive in the brachiopod secretory regime. The main fabrics of the mineral components of the shell are now known and have been traced throughout geological time. Their configuration in relation to the organic constituents of living shells is reasonably well understood, which has aided in the identification of extinct fabrics despite repeated recrystallization.

Any attempt at understanding the evolution of the brachiopod shell entails chemicostructural comparisons of living and fossilized exoskeletons. Changes in the organic and mineral components of the shell, however, begin in the postmortem stages of subfossilization and proceed at different rates and to different degrees of profundity. As has been shown, the disparities in these changes become so great in geologic time as to prompt their consideration separately. Even so, the nature of the more degradable organic contents can usually be inferred from the microstructures of the more enduring mineral components.

Brachiopod shells, like all other biominerals, are organic-inorganic composites. A range of organic components has been extracted from brachiopod shells, including amino acids (Walton, Cusack, & Curry, 1993; Cusack & others, 2000), proteins (Cusack & others, 1992; Cusack, 1996; Williams, Cusack, & Buckman, 1998; Lévêque & others, 2004), carbohydrates (Collins & others, 1991; Brown, 1998), and lipids (Clegg, 1993; McClintock, Slattery, & Thayer, 1993; Williams, Cusack, & Brunton, 1998; Cobabe & Ptak, 1999). The high organic content determined by loss on ignition (LOI) experiments (e.g., 2.5 wt% and 5 wt% for the dorsal valves of *Terebratulina retusa* and *Novocrania anomala* respectively [England, 2005]) and the relatively low protein concentrations of 0.8 μmoles intracrystalline EDTA-soluble amino acid/g shell of *T. retusa* and *N. anomala* respectively (Cusack & others, 2000) suggest that, although soluble proteins are extremely important in biomineral formation (Addadi & others, 1990; Belcher & others, 1996; Falini & others, 1996; Cusack, Walton, & Curry, 1997; Cusack & others, 2000), in brachiopods a large proportion of the organic components comprise fibrous proteins such as in *Discinisca tenuis* where the soluble protein fraction only accounts for about 0.016% of the total shell protein (Williams, Cusack, & others, 1998). Other major organic components are lipids (Clegg, 1993; McClintock, Slattery, & Thayer, 1993) and carbohydrates (Collins & others, 1991). Indeed, many brachiopod shell proteins are glycosylated (Williams, Cusack, & Brunton, 1998; Lévêque & others, 2004).

The organic components occupy various locations within the shell. Some of these organic polymers occur in intracrystalline

positions, requiring complete dissolution of the mineral for their extraction. Others occur in membranes between laminae and in sheaths surrounding fibers (intercrystalline). Intercrystalline polymers trapped within the skeletal frame by crystal growth are termed paracrystalline, e.g., doped sites in craniiform laminae (WILLIAMS, CUSACK, & BROWN, 1999) or surrounding the apatite granules in spherules in *Lingula* (WILLIAMS, CUSACK, & MACKAY, 1994). Polymeric secretions also occur as large bodies within successions. Examples of these are the glycosaminoglycans (GAGs) chambers within linguliforms (CUSACK & WILLIAMS, 1996) and pustules that are vertical inclusions of mucins in craniiforms (CUSACK & WILLIAMS, 2001a). In rhynchonelliforms, polymeric secretions are likely to have occurred in the pseudopunctae evident in fossil strophomenides (WILLIAMS, HOLMER, & CUSACK, 2004).

In polymeric extractions, no distinction is made between primary and secondary shell except for thecideidides where only primary layer is present. Studies by the authors revealed about ten proteins in the molecular weight range of 6 kDa to 46 kDa in *Lingula anatina* (WILLIAMS, CUSACK, & MACKAY, 1994), two of which are glycosylated (LÉVÊQUE & others, 2004). In addition, GAGs were present throughout the shell of *L. anatina,* as a pervading isotropic gel and chitin was also evident, associated with proteins (WILLIAMS, CUSACK, & MACKAY, 1994). The discinoid succession is similar to that of lingulids with protein-coated francolite granules aggregated as spherules supported by proteinaceous and chitinous nets in GAGs (WILLIAMS, CUSACK, & BRUNTON, 1998). In *Discinisca tenuis*, proteins in the molecular weight range 6.5 to 100 kDa were extracted, one of which (13 kDa) is glycosylated (WILLIAMS, CUSACK, & BRUNTON, 1998). *Novocrania anomala* contains an intralaminar glycosylated 60kDa protein as well as a 44kDa protein that is incorporated into calcite tablets during growth by screw dislocation (WILLIAMS, CUSACK, & BROWN, 1999). In a small survey

of intracrystalline shell proteins from species representing all extant rhynchonellate orders, 21 proteins of different molecular weight were identified from shells of six species that yielded sufficient protein extractions for reliable analyses (CUSACK & WILLIAMS, 2001b). Protein profiles range from three in *Notosaria nigricans* (20, 43, and 53 kDa) to six in *Liothyrella mediterranea* (28, 36, 40, 52, 60, and 107 kDa). Although five of these occur in the shells of more than one species, there is no evidence of proteins being specific to one layer. The chemicostructural differentiation of the rhynchonellate shell, as typified by living species of three ordinal groups, is less straightforward than their phylogenetic relationships and ultrastructures suggest.

Polysaccharides are present as intracrystalline cement of basic mineral units of craniiforms and rhynchonelliforms and possibly in coatings of granules in linguliforms. Polysaccharides occur as membranes of β-chitin in linguliforms, glycoproteinaceous sheets in craniiforms, and sheaths in rhynchonelliforms. In *Novocrania anomala*, the soluble extract has typically 0.75 µg carbohydrate per gram of shell (BROWN, 1998). Polysaccharides degrade during fossilization, possibly within Tertiary times. Although chitin is an extremely tough polysaccharide, even it is degraded in Cretaceous *Credolingula,* although ultrastructural casts of its fabric survive. Periostracum of late Cretaceous *Sellithyris* survives (GASPARD, 1982), most likely because it is a case of protein and carbohydrate sclerotization.

Methods employed for protein extraction from brachiopod shells preclude analyses of water-insoluble, intercrystalline, and paracrystalline proteins but include water-soluble proteins. This group of proteins exerts a very significant influence on the control of biomineral formation in other systems such as bivalve mollusks where soluble proteins control the polymorph of calcium carbonate produced (BELCHER & others, 1996; FALINI & others, 1996). The only work done on brachiopod insoluble proteins has been with traditional

cytological staining or imaging using freeze-dried demineralized sections (JAMES & others, 1992). Although investigation of intracrystalline proteins of rhynchonellate brachiopods revealed that it is difficult to generalize about protein profiles in brachiopods, in many species and indeed in all three subphyla, a protein of around 40kDa is often present. Further characterization of this protein is required to determine whether this is the same protein in all instances or a coincidence of molecular weight. There are broad distinctions in amino acid composition between the three subphyla. Organocalcitic brachiopod shells have very high concentrations of glycine, with the exception of craniids, as demonstrated by *Novocrania anomala,* which also has a higher aspartic acid and glutamic acid content, in common with *Notosaria nigricans* (Fig. 1539 herein; WALTON, CUSACK, & CURRY, 1993). Organophosphatic brachiopod shells have lower glycine content and higher alanine content than the organocalcitic brachiopod shells. There are also differences in amino acid composition within the phyla. WILLIAMS, CUSACK, and BRUNTON (1998) compared the amino acid content of two species of lingulid, *Lingula anatina* and *Glottidia pyramidata* with four species of discinids, *Discinisca tenuis*, *Discinisca lamellosa*, *Discina striata,* and *Pelagodiscus atlanticus*. Although lingulids have a higher organic content than discinids, discinids have greater amino acid content (WILLIAMS, CUSACK, & BRUNTON, 1998). Differences in amino acid composition are also apparent with the shells of lingulids containing higher concentrations of acidic amino acids (glutamic acid and aspartic acid) than those of discinids, with an average of 21.1 mole% in lingulids compared to 14.5 mole% in discinids. The concentra-

tion of basic amino acids (lysine, histidine, and arginine) is lower in lingulids (mean 9.1 mole%) than in discinids (mean 13.2 mole%). Glycine occurs in high concentrations in lingulids and discinids, with average values of 19.6 mole% and 24.4 mole% respectively. Alanine occurs in similarly high concentrations (23 mole%) in lingulid and discinid shells (WILLIAMS, CUSACK, & BRUNTON, 1998). The amino acid compositions of *L. anatina* and *G. pyramidata* are very similar (CUSACK & WILLIAMS, 1996; WILLIAMS, CUSACK, & BRUNTON, 1998), although comparisons of more species begin to differentiate *Lingula* from *Glottidia* (see Fig. 1536 herein). Within the discinids, the greatest difference in amino acid composition occurs in *P. atlanticus,* where glycine and alanine occur in much lower concentrations and arginine and threonine in much higher concentrations (WILLIAMS, CUSACK, & BRUNTON, 1998; see also Fig. 1536 herein).

In fossil brachiopod shells, the remaining amino acid content in some cases appears to reflect some of the original composition; e.g., the high concentration of glutamic acid, glycine, and alanine in Carboniferous *Lingula squamiformis* shells; amino acids that are also present in high concentrations in living *Lingula anatina* shells (CUSACK & WILLIAMS, 1996). However, expanding the survey of amino acids in fossil brachiopod shells reveals the tendency for the survival of similar suites of amino acids, the acidic amino acids possibly surviving by interaction with the carbonate or apatite matrix and the survival of the structurally simple, more robust amino acids. The fact that proteins are so information rich and relate directly to the DNA means that they are rich sources of information relating to evolutionary changes in living species genealogies. The

low concentration of soluble proteins in brachiopod shells makes this difficult to achieve, however. The rapid diagenetic degradation of shell proteins rules out the use of proteins as a phylogenetic tool for fossil species genealogies.

STRUCTURAL EVOLUTION OF MATURE SHELLS

The structural differentiation of the juvenile shell of living and fossil brachiopods has already been described. As their secretion differs from that of mature shells and results in different structures, juvenile shells will not be further considered. Moreover, the primary and secondary (and the variant tertiary) layers of the mature shell have also been structurally distinct throughout the geological record. Indeed, the differences are so striking as to merit separate reviews of their fabrics.

Despite the invariable recrystallization of fossilized primary layers, it is safe to assume that their fabrics have never differed significantly from those characterizing living species of the three subphyla. The primary layers of the linguliforms (WILLIAMS, CUSACK, & MACKAY, 1994, p. 241; CUSACK, WILLIAMS, & BUCKMAN, 1999, p. 806) and rhynchonelliforms (CUSACK & WILLIAMS, 2001b, p. 19) have always been virtual pastes of apatitic granules in GAGs and calcitic granules in polysaccharides respectively, lining the periostracum and serving as a mineralized substrate for the succeeding secondary shell. Only the primary layer of living craniids (CUSACK & WILLIAMS, 2001a, p. 882), with its inner succession of calcitic granules and tablets aggregated into laminae of laths, differs from the fine undifferentiated lamination that commonly characterizes the linguliform and rhynchonelliform primary layer (as well as the outermost succession of the craniiforms).

In contrast to the limited structural variation of the primary layer, the fabrics of the secondary shell of living species are diverse, due to the development of intricate successions of anastomosing membranes that divide the mineralized part of the shell into distinctive units. Such mineralized structures also recrystallize during fossilization, but they are frequently converted into casts of the original structures even in nanometric detail. These mineralized records show that the fabric of the oldest known brachiopods was equally diverse with some surviving to the present day.

ACKNOWLEDGMENTS

STABLE OXYGEN AND CARBON ISOTOPES IN EXTANT BRACHIOPOD SHELLS: KEYS TO DECIPHERING ANCIENT OCEAN ENVIRONMENTS

David Parkinson and Maggie Cusack

[University of Glasgow]

BACKGROUND

For over half a century the stable oxygen and carbon isotope ratios of fossilized shells of calcite brachiopods have been used to provide a record of environmental conditions in the ancient oceans in which they lived. The hypothesis that the abundance of the ^{18}O isotope in biogenic carbonates could be used as a proxy for the temperature of the seawater in which they were formed was first proposed by Urey (1947). The application of oxygen isotope paleothermometry became possible through the development of the stable isotope abundance mass spectrometer, pioneered by Nier (1940, 1947). Incorporating modifications by McKinney and others (1950) and a reproducible method for producing carbon dioxide (CO_2) from carbonates by digestion in phosphoric acid (H_3PO_4) at a constant temperature, McCrea (1950) significantly improved precision for measuring relative stable isotope abundances. Results of such analyses are reported by the standard delta (δ) notation in parts per thousand relative to the international standards Pee Dee Belemnite (PDB) and more recently Vienna PDB (VPDB) (for explanation see Coplen, 1995; Gonfiantini, Stichler, & Rozanski, 1995; Hoefs, 1997; Koch, 1998).

Construction of carbonate paleotemperature scales, which determined the relationship between temperature and oxygen isotope fractionation in carbonate water systems, has enabled $^{18}O/^{16}O$ ratio to be employed as a proxy indicator of fluctuations in the temperature of ancient oceans (McCrea, 1950; Epstein & others, 1951, 1953). The first practical paleotemperature equation was that of Epstein and others (1953):

T (^{o}C) = 16.5-4.3($\delta^{18}O_{calcite} - \delta^{18}O_{seawater}$) + 0.14($\delta^{18}O_{calcite} - \delta^{18}O_{seawater}$)^2

Palaeotemperatures, which are more correctly called isotopic temperatures (Rye & Sommer, 1980), can be extrapolated from the $\delta^{18}O$ value of carbonate relative to the international standards PDB or VPDB when the $\delta^{18}O$ of ambient seawater (relative to the international standards SMOW or VSMOW) is also known (For explanation of international standards see Gonfiantini, Stichler, & Rozanski, 1995). Similarly, the expected range of oxygen isotope equilibrium can be calculated if the measured seawater temperature range of ambient seawater is available.

The equation of Epstein and others (1953), based on biogenic calcium carbonate, agrees well with relations based on laboratory-synthesized calcite (e.g., O'Neil, Clayton, & Mayeda, 1969), suggesting that at least certain taxa (e.g., mollusks) precipitate shells in oxygen isotopic equilibrium with the water. Disequilibrium fractionation, termed vital effect (Urey & others, 1951), has been demonstrated in many taxa, however (Compston, 1960; Keith & Weber, 1965; Weber & Raup, 1966; Weber & Woodhead, 1970; Erez, 1978; Swart, 1983; Gonzalez & Lohmann, 1985; Rosenberg, Hughes, & Tkachuck, 1988; McConnaughey, 1989a, 1989b; Ortiz & others, 1996; Böhm & others, 2000).

In a recent study Adkins and others (2003) proposed an alternative mechanism to explain these observed variations. Adkins

and others (2003, p. 1130) proposed that vital effects observed in deep sea corals were the result of "a thermodynamic response to a biologically induced pH gradient in the calcifying region." Notwithstanding the mechanism, it is clear that stable isotope variation does occur in some biogenic carbonates. CARPENTER and LOHMANN (1995) maintained that if other calcareous marine organisms display vital effects, then there are too few data to confidently claim that brachiopods exhibit a unique characteristic. Thus, to ensure accurate determination of isotopic temperatures in fossil brachiopod specimens, isotopic studies are required on modern specimens.

Skeletal carbonates also record the carbon isotopic composition of dissolved inorganic carbon (DIC) in the ocean. This is a proxy for carbon cycling on local and global scales (VEIZER, FRITZ, & JONES, 1986; BRUCKSCHEN & VEIZER, 1997; VEIZER & others, 1999).

Brachiopods are considered to be exceptionally suitable for isotopic studies of ancient ocean temperatures and carbon cycling because the phylum is ubiquitous and continuous throughout the fossil record, spanning from Cambrian to Recent. In addition, most brachiopod species have shells composed of low-magnesium calcite (LMC). This is the most stable form of skeletal carbonate and the most resilient to diagenetic alteration (e.g., LOWENSTAM, 1961; AL-ASSAM & VEIZER, 1982; BRAND, 1989a).

BRACHIOPOD ISOTOPE RESEARCH

The first published research into the relative abundance of ^{18}O and ^{13}C stable isotopes in fossilized brachiopod shells was probably that of UREY and others (1951) in an investigation of paleotemperatures derived from fossil organisms extracted from Upper Cretaceous chalk of England, Denmark, and the southeastern United States. It was concluded that the temperature record within the shells of the brachiopods

studied had been destroyed, possibly by diffusion of material into the open structure of the shell. A more detailed study using brachiopods and crinoids from the Devonian and Permian by COMPSTON (1960) also observed diagenetic alteration and only the Permian brachiopods retained the original $^{18}O/^{16}O$ composition. As with UREY and others (1951) it was concluded that alteration was due to impregnation of the shell structure by diagenetic calcite. This study also raised the possibility that brachiopods could exert some phylogenetic control over the carbon isotope fractionation, an issue that is commonly referred to as biological fractionation or vital effect.

LOWENSTAM (1961) was the first to test whether brachiopod shells were precipitated in oxygen isotope equilibrium with ambient seawater and thus were reliable materials for measuring isotopic temperatures. That influential study (LOWENSTAM, 1961) was based on the analyses of extant articulated brachiopod shells from a variety of different taxa collected from locations with different environmental conditions and latitudes around the world. The specimens came from the Marshall Islands in the Pacific, Bermuda, Barbados, California, New Zealand, the Mediterranean, and Alaska. Bottom water samples were collected from the sea at the same locations as the specimens and analyzed to determine the local ^{18}O content of the seawater. Temperatures derived from the equation of EPSTEIN and others (1953) agreed with measured seawater temperatures, leading LOWENSTAM (1961) to conclude that brachiopods precipitate their shell material in oxygen isotopic equilibrium with ambient seawater. Based on this foundation, LOWENSTAM (1961) compared data from modern brachiopod shells with fossil samples from the Pliocene, Cretaceous, Permian, and Carboniferous. Only samples that retained the original ultrastructure were used and comparisons made between the $^{18}O/^{16}O$ and $SrCO_3$ and $MgCO_3$ contents of the extant species. Where the relationship

was compatible, it was concluded that the isotope signal remained intact.

The conclusion of Lowenstam (1961) that brachiopods precipitate skeletal calcite in equilibrium with ambient seawater was widely accepted. Workers studying paleoenvironments were confident that oxygen isotope analyses of fossil brachiopod shells provided an accurate record of ancient ocean temperatures, and any biological effects were minimal. It was also generally accepted that care must be taken when selecting fossil specimens for analysis, however, to make sure that the original calcite is unaltered by diagenetic processes. Trace element analysis and cathodoluminescence are commonly used to identify suitable samples. The theories and methods of these procedures have been discussed in detail (Veizer, 1983a, 1983b; Popp, Anderson, & Sandberg, 1986b; Rush & Chafetz, 1990; Mii & Grossman, 1994; Wenzel & Joachimski, 1996; Samtleben & others, 2001).

Confidence in the analytical techniques, together with the abundance of brachiopod remains in the fossil record, has led to stable isotope analyses of fossil brachiopod shells being employed over the last 40 years in many extensive and detailed paleoenvironmental investigations covering periods ranging throughout the Phanerozoic. Veizer, Fritz, and Jones (1986) used trace element and isotope determinations from 319 brachiopod fossils spanning the Ordovician through to the Permian in order to establish evidence for change in the chemical composition of Paleozoic oceans. Similarly, Popp, Anderson, and Sandberg (1986a, 1986b) analyzed brachiopods from Paleozoic limestones. Examples of other notable paleoenvironmental works involving isotopic analyses of brachiopods include: Brand (1989a), Devonian–Carboniferous; Brand (1989b), Carboniferous; Marshall and Middleton (1990), Late Ordovician; Grossman, Mii, and Yancey (1991, 1993), Carboniferous; Quing and Veizer (1994) Ordovician; Wenzel and Joachimski (1996),

Silurian; Veizer and others (1999), Phanerozoic; Wenzel, Lécuyer, and Joachimski (2000), Silurian; Mii and Grossman (1994), Carboniferous; and Stanton, Jeffery, and Ahr (2002), Carboniferous. Despite the widespread use of brachiopod shells in isotopic studies of Paleozoic and younger sedimentary rocks, uncertainties still exist in the factors controlling the oxygen and especially carbon isotopic compositions of brachiopod shells.

THE EQUILIBRIUM DEBATE

Underpinning the use of stable isotope determinations from brachiopod shells for environmental investigations is the conclusion of Lowenstam (1961) that brachiopod shells are secreted in oxygen isotopic equilibrium with ambient seawater. Lepzelter, Anderson, and Sandberg (1983) supported this supposition with a small study of $^{18}O/^{16}O$ ratios in several Recent species, which were considered representative of extant brachiopods. The study concurred with the finding of Lowenstam (1961) in that covariance between $\delta^{18}O$ and $\delta^{13}C$ was not observed, and the study concluded that brachiopod shells are precipitated in equilibrium with ambient seawater. The only detraction from this position noted by Lepzelter, Anderson, and Sandberg (1983) was in the case of specimens taken from cold-water habitats where isotopic disequilibrium was reported.

The first suggestion that variations in oxygen isotope ratios observed in disparate, but contemporary brachiopod genera collected from the same location could be due to biological rather than diagenetic effects was made by Popp, Anderson, and Sandberg (1986a). The implication of this is that brachiopods could precipitate shell calcite out of isotopic equilibrium as a result of vital effects. Despite this possibility, however, little was done to test the reliability of stable isotopes in brachiopod shells as recorders of seawater temperature until Carpenter and Lohmann (1995).

CARPENTER and LOHMANN (1995) investigated $\delta^{18}O$ and $\delta^{13}C$ values in a range of extant brachiopods, using 44 specimens originating from a variety of environments and latitudes (Antarctica, United States, New Zealand, Japan and Palau in the Pacific; Norway, Canada, South Africa and Curacao, and Sicily). Their study examined intraspecimen, interspecimen, intraspecies, and interspecies isotopic variations using shell material extracted from a variety of areas differentiated by shell ultrastructure (e.g., external primary and internal secondary layers) and also from different morphological features of the secondary shell layer (i.e., hinge, foramen, brachidium, muscle scars). Direct measurements of seawater $\delta^{18}O$ ($\delta^{18}O_{water}$) were only available from one location. Therefore, it was necessary to calculate $\delta^{18}O_{water}$ from salinity information available from the National Oceanic and Atmospheric Administration (NOAA) and National Oceanographic Data Center (NODC) databases using the $\delta^{18}O_{water}$–salinity relationship described in BROECKER (1989).

In all cases, the primary layer and areas of the secondary layer that form specialized morphological structures showed a high degree of covariance between $\delta^{18}O$ and $\delta^{13}C$. The reasons suggested are metabolic (vital effects) or kinetic effects, either during the hydroxylation of CO_2 or as a result of rapid calcite precipitation or possibly a combination of some or all of these factors. CARPENTER and LOHMANN (1995) advised against the use of these parts of the shell for investigations employing ancient brachiopods. The nonspecialized areas of the secondary layer close to the anterior margin, however, were less fractionated and therefore closer to equilibrium. There were two exceptions to this trend. 1) *Thecidellina* sp., which have no clearly defined secondary shell structure and are mainly comprised of primary layer calcite (WILLIAMS, 1973). Measurements from *Thecidellina* were frequently isotopically heavier than equilibrium. 2) As was

the case with the cold-water brachiopods of LEPZELTER, ANDERSON, and SANDBERG (1983), *Stethothyris* sp. from Antarctica, were considerably depleted relative to expected oxygen isotope equilibrium values.

The data of CARPENTER and LOHMANN (1995) show little evidence of carbon isotopic equilibrium as defined by ROMANEK, GROSSMAN, and MORSE (1992). Values of $\delta^{13}C$ were nearly always lower than the expected range.

MARSHALL and others (1996) studied the isotopic compositions of extant brachiopods from Antarctica. This study highlighted the uncertainties of determining meaningful oxygen isotope values from very low-temperature habitats to use as proxy indicators of seawater temperatures. The paleotemperature equations for biogenic carbonates (EPSTEIN & others, 1953) is based on carbonates precipitated between 7 °C and 30 °C. In contrast, the inorganic calcite–water fractionation curve (O'NEIL, CLAYTON, & MAYEDA, 1969; FRIEDMAN & O'NEIL, 1977) employed by CARPENTER and LOHMANN (1995) is based on equilibrium exchange experiments from 200–700 °C and precipitation experiments at 0 °C and 25 °C. Thus, the data represent a wider temperature range. MARSHALL and others (1996) further point out that, at very low temperatures, the lines for the two equations diverge, leaving no adequate method for determining oxygen isotope equilibrium at very low temperatures. Notwithstanding these difficulties, MARSHALL and others (1996) argue that the ~2‰ range of $\delta^{18}O$ values, which signifies a range of temperatures of around 8 °C, is difficult to justify given the very narrow seasonal variation in the Antarctic. This level of variation cannot be explained solely by problems with the paleotemperature scales.

Since CARPENTER and LOHMANN (1995) opened the equilibrium debate, four studies from temperate waters have considered the issue. BUENING and SPERO (1996) analyzed four specimens of the extant brachiopod *Laqueus californianus* collected near the

California coast. They were able to identify El Niño warming events and concluded that the [18]O content of the brachiopod shell is a useful recorder of environmental change in temperate waters.

Two other investigations were conducted with extant brachiopods collected from the Lacepede Shelf, southern Australia. Rahimpour-Bonab, Bone, and Moussavi-Harami (1997) investigated stable isotopes in the shells of extant gastropods, bivalves, and brachiopods. Ten brachiopod specimens were used, but the species were not specified. The results suggested that the gastropod and bivalve shells had $\delta^{18}O$ values in equilibrium with ambient seawater, whereas brachiopod shells were enriched in [18]O relative to equilibrium. Rahimpour-Bonab, Bone, and Moussavi-Harami (1997) also observed a high degree of carbon and oxygen isotopic covariance, which they suggest was indicative of vital effects, resulting in disequilibrium precipitation. Working with samples from the same location, James, Bone, and Kyser (1997) analyzed 48 extant brachiopods from 4 terebratulid species. The brachiopods were grab sampled, allowing differentiation between specimens from discrete parts of the shelf. Disregarding the recommendations of Carpenter and Lohmann (1995) on the grounds that primary layer calcite accounted for less than 6% of the bulk, James, Bone, and Kyser (1997) analyzed samples of whole shells. Their results distinguished between specimens collected in areas of the Lacepede Shelf influenced by seasonal upwelling of colder water and those not. The conclusion of the study was that the $\delta^{18}O$ content of the brachiopod shell did in general reflect equilibrium with ambient seawater.

Curry and Fallick (2002) added to the controversy when they reported different [18]O values from the dorsal (1.06‰) and ventral (0.58‰) valves of the articulated brachiopod *Calloria inconspicua* from the Otago Shelf in New Zealand. This observation was corroborated in the same study using well-preserved fossil specimens of *C. inconspicua* extracted from upper Pleistocene deposits from the Wanganui Basin, North Island, New Zealand (Curry, 1999).

In a recent compilation, Brand and others (2003) combined extensive new and published data to assess $\delta^{18}O$ equilibrium in extant brachiopods. For equilibrium, the authors required that 75% of temperatures calculated from brachiopod shell carbonate fall within the measured seawater temperature range. Given this and the fact that, in many cases, measured seawater temperatures are wide ranging, there are still many analyses that fail their test and have ambiguous or disequilibrium results.

Clearly, there is still much controversy surrounding brachiopods and their ability to precipitate their shells in isotopic equilibrium with ambient seawater. It could be that the diversity of extant brachiopods with a variety of ecologies, environments, shell structures, and biomineralization regimes leads to many of the conflicting data. Understanding stable isotope distribution within living brachiopods is vital to deciphering the signal from fossil specimens and improving the resolution of paleoenvironmental investigations.

Parkinson and others (2005) sought to shed light on the situation in a large systematic study of extant brachiopods taken from a variety of environments and latitudes. In all cases, the brachiopods were collected alive. The specimens represented all extant groups of calcite-precipitating brachiopods, as defined by Williams and others (1996). The species analyzed in the Parkinson and others (2005) study are shown in Table 38. Parkinson and others (2005) examined the shell structures of each group to determine differences in ultrastructure. The inarticulated craniids had a thin acicular calcite primary (outer) layer overlying a secondary layer composed of laminar sheets of calcite (Williams & Wright, 1970; Williams, 1997). The articulated terebratulids and rhynchonellids also have acicular primary layers but fibrous secondary layers (Williams, 1968, 1997). The one exception was from the genus *Liothyrella*, a terebratulid whose

TABLE 38. Brachiopods included in isotope survey of PARKINSON and others (2005). Members of subphylum Craniiformea are inarticulated and those of subphylum Rhynchonelliformea are articulated (new).

Subphylum	Order	Suborder	Species	Location
Craniiformea	Craniida		*Novocrania anomala*	Scotland, UK
			Neoancistrocrania norfolki	South Pacific Ocean
Rhynchonelliformea	Rhynchonellida		*Notosaria nigricans*	New Zealand
	Terebratulida	Terebratulidina	*Terebratulina retusa*	Scotland, UK
			Laqueus rubellus	Japan
			Liothyrella neozelanica	New Zealand
			Liothyrella uva	Antarctica
			Calloria inconspicua	New Zealand
			Neothyris lenticularis	New Zealand
			Terebratella sanguinea	New Zealand
			Terebratalia transversa	Puget Sound, USA
	Thecideida		*Thecidellina barretti*	Jamaica

secondary layer is underlain by a tertiary succession of prismatic calcite (WILLIAMS, 1968, 1997). Thecideidine brachiopods are small articulated species that showed little secondary layer development and were composed of granular primary layer material (WILLIAMS, 1968, 1973, 1997).

PARKINSON and others (2005) used samples from the primary and secondary layers and in the case of *Liothyrella* the tertiary layer for stable oxygen and carbon analysis. The secondary and tertiary layer samples included material from nonspecialized as well as specialized areas that form readily identifiable morphological features (i.e. the cardinal process, loop, and muscle scars from the dorsal valves; pedicle foramen, teeth, and muscle scars from the ventral valves).

Carbon and oxygen isotopic compositions of the primary layer of terebratulids (e.g., Fig. 1665) showed a positive correlation, with a tendency for both isotopes to be depleted in the heavy isotope relative to the secondary layer. This was consistent with the findings of CARPENTER and LOHMANN (1995) and AUCLAIR, JOACHIMSKI, and LÉCUYER (2003) and is likely to result from kinetic fractionation, which can be the result of higher growth rates (M^{c}CONNAUGHEY, 1989a, 1989b; M^{c}CONNAUGHEY & others, 1997). In brachiopods, the primary layer is only precipitated from the edge of the mantle as the shell enlarges and is precip-

itated relatively faster than the secondary layer (RUDWICK, 1970). In all terebratulids other than *T. retusa,* $\delta^{18}O$ values for the primary layer fall outside the range expected for equilibrium with ambient seawater. These temperatures were calculated using measured seawater temperatures and $\delta^{18}O$, with the paleotemperature equation recommended by ANDERSON and ARTHUR (1983), a modification of the original equation of EPSTEIN and others (1953). The rhynchonellid, *N. nigricans* in contrast showed no correlation between $\delta^{18}O$ and $\delta^{13}C$, and the $\delta^{18}O$ values fell within the expected range for isotopic equilibrium with ambient seawater.

With the exception of *L. uva*, the fibrous secondary or prismatic tertiary material of the terebratulids and rhynchonellid did not display a correlation between $\delta^{18}O$ and $\delta^{13}C$ (PARKINSON & others, 2005). In *T. transversa*, samples from the teeth and pedicle foramen were not in $\delta^{18}O$ equilibrium with ambient seawater, but all other secondary-tertiary layer samples were, regardless of the specialization in the areas of the shell they were extracted. PARKINSON and others (2005) did not find any significant variation between the dorsal and ventral valves as reported by CURRY and FALLICK (2002). PARKINSON and others (2005) report the least variation in the nonspecialized material, however, which produced isotopic temperatures close to the mean measured
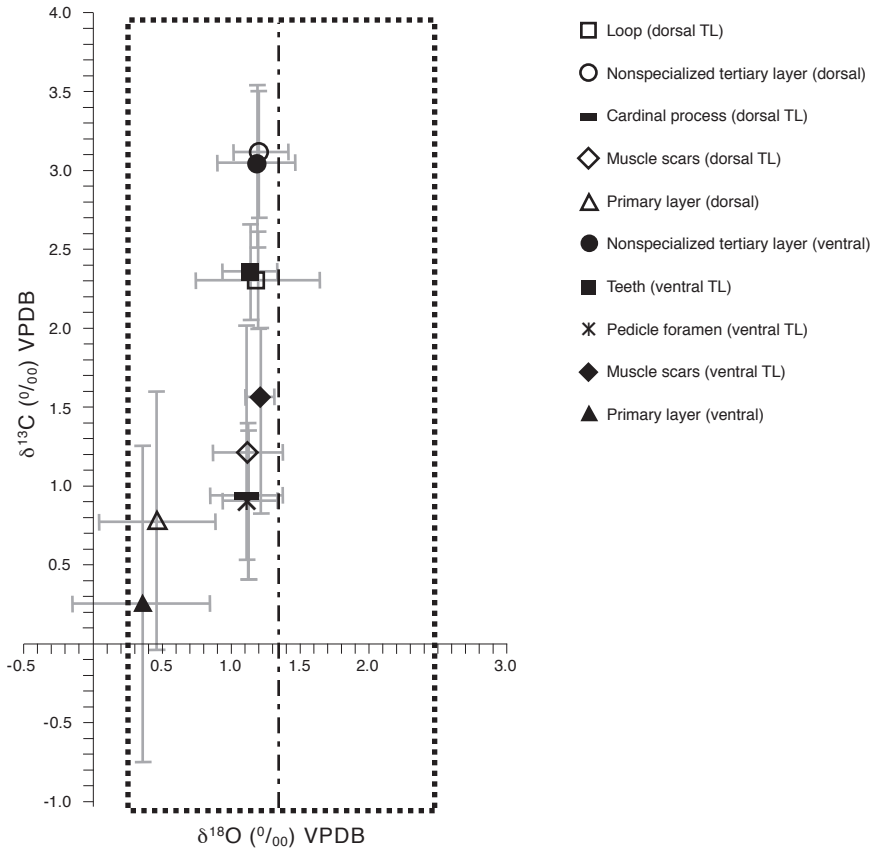
Fig. 1665. δ18O–δ13C crossplot of *Liothyrella neozelanica* including all areas analyzed from both dorsal and ventral valves; *data points* represent mean values; *error bars* indicate 1σ; *dotted box* indicates oxygen isotope equilibrium parameters, with mean value indicated by *dashed line; TL,* tertiary layer (Parkinson & others, 2005).

annual temperatures for ambient seawater. *L. uva* specimens from Antarctica had a strong positive correlation between δ18O and δ13C in the tertiary layer, with many of the δ18O values not in equilibrium with ambient seawater. This concurs with the observations of LEPZELTER, ANDERSON, and SANDBERG (1983), CARPENTER and LOHMANN (1995), and MARSHALL and others (1996) for brachiopods in very cold environments. Examination of the *L. uva* shells under a scanning electron microscope revealed that the tertiary succession in the shells of *Liothyrella* sp. (MACKINNON & WILLIAMS, 1974; WILLIAMS, 1997) was poorly formed, and fibrous secondary material dominated (PARKINSON & others, 2005). The implica-

tions are a possible link between abnormal shell growth and isotopic disequilibrium in brachiopod shells living in extreme environments. The thecideidine brachiopod *T. barretti* produced very consistent δ18O and δ13C values. It was not in isotopic equilibrium with ambient seawater, however, producing cooler isotopic temperatures than the measured range.

The δ13C values from the secondary-tertiary layers of the articulated brachiopods (PARKINSON & others, 2005) were variable, although not correlated with δ18O (Fig. 1665). They fall into palpable groups, however, dependent on the specialization of the area of the sample material (Fig. 1666–1667). The observed pattern, summa-
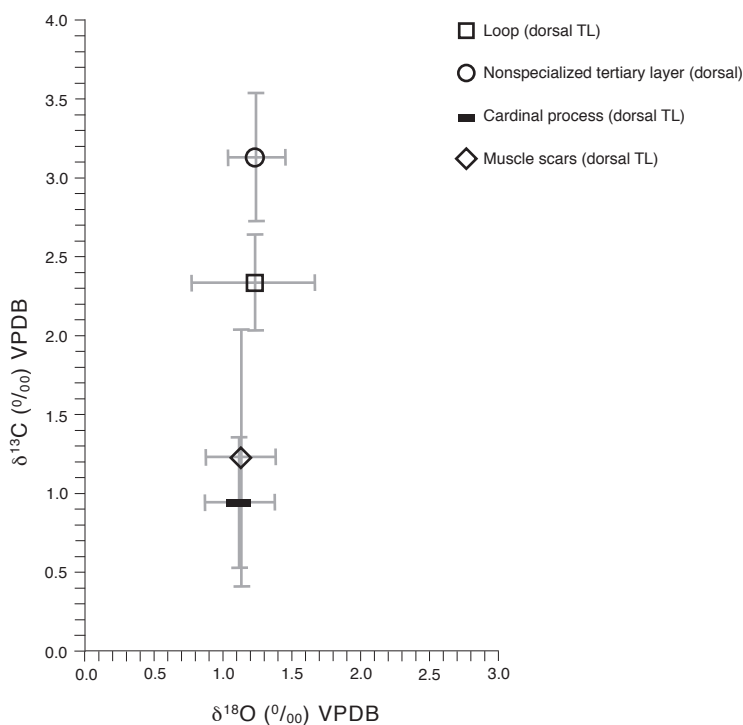
FIG. 1666. δ¹⁸O–δ¹³C crossplot of *Liothyrella neozelanica* dorsal valves; *data points* represent mean values; *error bars* indicate 1σ; *TL,* tertiary layer (new).

rized in Figure 1668, was independent of geographical location. The highest values were at the anterior of the valves, with the lowest values being recorded at the posterior. Although PARKINSON and others (2005) did not provide data for δ¹³C equilibrium, it is inconceivable that all the areas of the secondary layer are in carbon isotopic equilibrium with the seawater. The conclusion was that the brachiopods may be controlling the incorporation of ¹³C as a result of metabolic prioritization.

The inarticulated craniids displayed few discernable patterns. The primary layer of *N. anomala* was depleted in both isotopes and offset relative to the laminar secondary layer. Although some δ¹⁸O values were in equilibrium, the distribution of both δ¹⁸O and δ¹³C was erratic, producing some extreme values. *N. norfolki* had no separation between different areas of the shell in

terms of δ¹⁸O and δ¹³C. No δ¹⁸O values were in isotopic equilibrium with ambient seawater.

While the majority of the paleothermometry studies on brachiopods have concentrated on calcite-shelled species, recent evidence indicates that while the phosphate in lingulid valves is not an accurate recorder of seawater oxygen isotope ratio, the carbonate component of the francolite may be used in paleothermometry (RODLAND & others, 2003).

IMPLICATIONS FOR USE IN PALEOENVIRONMENTAL INVESTIGATIONS

Stable isotope analyses of extant brachiopods are important because specimens can be collected from locations where the ambient environmental conditions can be
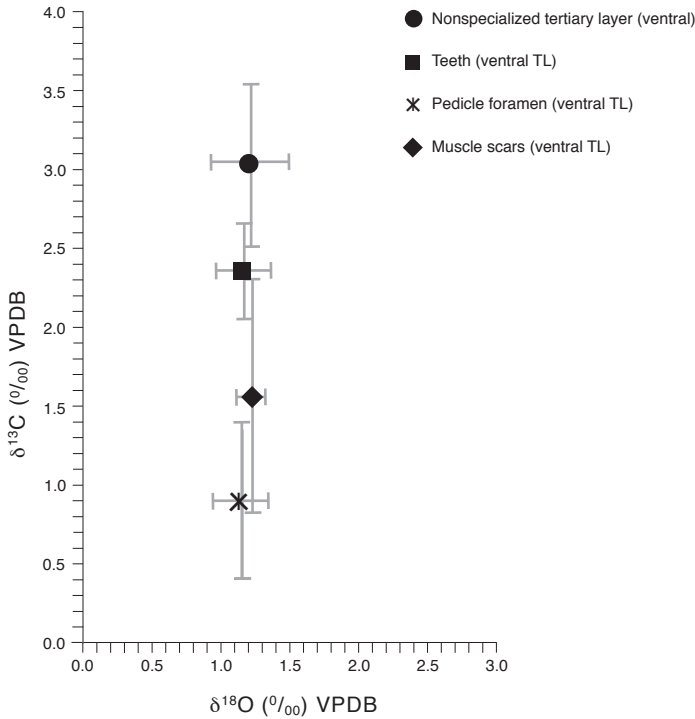
FIG. 1667. $\delta^{18}O - \delta^{13}C$ crossplot of *Liothyrella neozelanica* ventral valves; *data points* represent mean values; *error bars* indicate 1σ; *TL,* tertiary layer (new).

measured. Studying the isotopic composition of extant brachiopod shells increases understanding of the limitations when using stable isotope determinations from fossil shells in paleoenvironmental investigations. Recent isotopic studies of extant brachiopods (e.g., CARPENTER & LOHMANN, 1995; AUCLAIR, JOACHIMSKI, & LÉCUYER, 2003; BRAND & others, 2003; PARKINSON & others, 2005) have shown that the oxygen isotope composition of brachiopods frequently records ambient seawater temperatures accurately. All the studies concur that the primary layer is usually in disequilibrium and should not be used. Notwithstanding the success reported by BUENING and SPERO (1996), seasonal profiling, which can only be

effectively carried out on the outside of the shell where growth lines are visible, may be unreliable in modern brachiopod shells. This is not the case in all ancient brachiopods, however (MII & GROSSMAN, 1994). The

	Dorsal Valve	Ventral Valve
	Nonspecialized	Nonspecialized
	Loop	Teeth
	Muscle scar	Muscle scar
	Cardinal process	Pedicle foramen

FIG. 1668. Trend of $\delta^{13}C$ within secondary shell layer of modern terebratulid and rhynchonellid brachiopods; general trend applies irrespective of geographical location (Parkinson & others, 2005).

secondary layer generally yields $\delta^{18}O$ values at or near equilibrium. Some precautions should be taken during sampling, however. Auclair, Joachimski, and Lécuyer (2003) observed that the upper portion of the secondary layer (i.e., immediately adjacent to the primary layer) is not in oxygen isotopic equilibrium, and only material close to the internal surface should be used. Carpenter and Lohmann (1995) and Parkinson and others (2005) reported that areas of the secondary layer, which form specialized morphological features, may be depleted in some species.

There are disequilibrium effects in the oxygen isotopic composition of some brachiopod groups. The Craniida show wide variation in $\delta^{18}O$ values (Carpenter & Lohmann, 1995; Brand & others, 2003; Parkinson & others, 2005). The craniids have a secondary layer composed of laminar sheets. It is possible that the biomineralization regime that produces this kind of ultrastructure could be related to the level of fluctuation in $\delta^{18}O$ values. Until there is a better understanding of the relationship between shell structure and oxygen isotope composition it is advisable to avoid fossil shells with this type of ultrastructure. The situation of the Thecideidina is uncertain, with oxygen isotope equilibrium noted by Brand and others (2003) and the contrary by Carpenter and Lohmann (1995) and Parkinson and others (2005).

Studies of extant brachiopods from cold-water environments have all found difficulty in producing meaningful environmental interpretations (e.g., Lepzelter, Anderson, & Sandberg, 1983; Carpenter & Lohmann, 1995; Marshall & others, 1996; Parkinson & others, 2005).

Incorporation of carbon isotopes into brachiopod shells is little understood and there is no consensus of opinion in the literature. There is evidence for metabolic effects (e.g., Buening & Spero, 1996; Auclair, Joachimski, & Lécuyer, 2003; Parkinson & others, 2005), but the mechanisms are unclear. If $\delta^{13}C$ values are to be useful proxies for environmental conditions, detailed physiological investigations are required.

Recent investigations of the stable isotope compositions of extant brachiopods have provided valuable insight into their usefulness as paleoenvironmental proxies. The potential resolution of future studies using fossil shells is therefore improved. Further research is required to increase the quality of understanding of the environmental information recorded in brachiopod shells.

ACKNOWLEDGMENTS